AWARD NUMBER: W81XWH-14-1-0464

TITLE: The Roles of Primary Cilia in Cardiovascular System

PRINCIPAL INVESTIGATOR: Surya Nauli

CONTRACTING ORGANIZATION: Chapman University
Orange, CA 92618-1908

REPORT DATE: October 2016

TYPE OF REPORT: Annual

PREPARED FOR: U.S. Army Medical Research and Materiel Command
Fort Detrick, Maryland 21702-5012

REPORT DOCUMENTATION PAGE

Form Approved
OMB No. 0704-0188

1. REPORT DATE	**2. REPORT TYPE**	**3. DATES COVERED**
October 2016	Annual	15 Sep 2015 - 14 Sep 2016

4. TITLE AND SUBTITLE
The Roles of Primary Cilia in Cardiovascular System

5a. CONTRACT NUMBER

5b. GRANT NUMBER
W81XWH-14-1-0464

5c. PROGRAM ELEMENT NUMBER

6. AUTHOR(S)
Surya Nauli

E-Mail: Nauli@chapman.edu

5d. PROJECT NUMBER

5e. TASK NUMBER

5f. WORK UNIT NUMBER

7. PERFORMING ORGANIZATION NAME(S) AND ADDRESS(ES)

Chapman University
9401 Jeronimo Road
Irvine, CA 92618-1908

8. PERFORMING ORGANIZATION REPORT NUMBER

9. SPONSORING / MONITORING AGENCY NAME(S) AND ADDRESS(ES)

U.S. Army Medical Research and Materiel Command
Fort Detrick, Maryland 21702-5012

10. SPONSOR/MONITOR'S ACRONYM(S)

11. SPONSOR/MONITOR'S REPORT NUMBER(S)

12. DISTRIBUTION / AVAILABILITY STATEMENT

Approved for Public Release; Distribution Unlimited

13. SUPPLEMENTARY NOTES

14. ABSTRACT

Hypertension and aneurysm are a prevalent problem in our society. Because the risk of these vascular diseases is too important to ignore, our studies are designed to provide exciting and original concepts to examine the etiologies of hypertension and aneurysm with regard to mechanosensory organelles (primary cilia). Especially within polycystic kidney disease, untreated hypertension can worsen kidney function. Aneurysm rupture in PKD patients also remains a devastating complication that often could result in stroke and death. Our studies therefore aim at investigating new ideas in understanding hypertension and aneurysm formation in PKD.

15. SUBJECT TERMS

16. SECURITY CLASSIFICATION OF:			**17. LIMITATION OF ABSTRACT**	**18. NUMBER OF PAGES**	**19a. NAME OF RESPONSIBLE PERSON**
					USAMRMC
a. REPORT	**b. ABSTRACT**	**c. THIS PAGE**	Unclassified	90	**19b. TELEPHONE NUMBER** *(include area code)*
Unclassified	Unclassified	Unclassified			

Table of Contents

Page

1. INTRODUCTION:

Polycystic kidney disease (PKD) is characterized by formation of fluid-filled cysts in both kidneys. PKD patients will eventually have renal failure, with subsequent dialysis or renal transplant. The genes mutated in PKD include Pkd1 and Pkd2, encoded for polycystin-1 and polycystin-2, respectively. Many studies have shown that the baseline circulating NO is much lower in PKD patients. This suggests possible vascular dysfunction. The purpose of our research is to investigate cilia function in the vascular endothelial cells. More important, hypertension has been a critically important risk factor for cardiovascular diseases in PKD patients, which occur early in these individuals, compared to their age-matched cohorts, and still remains the most frequent cause of mortality even when their renal function is still normal. With our expertise and tools available in our laboratory, we thus hypothesize that cilia in the cilia play crucial and important roles in regulating PKD pathology. Specifically, we will provide the first insights into physiological functions and cellular pathways of primary cilia in vasculatures and in PKD.

2. KEYWORDS:

Cardiovascular, cilia, ciliopathy, ciliotherapy, endothelia, epithelia, polycystic kidney disease, polycystin-1, polycystin-2, primary cilia

3. ACCOMPLISHMENTS:

Major Goals

The main goal of the project is to determine the roles of primary cilia in PKD. This goal is divided into two major subaims, and our Statement of Work (SOW) is as follow.

Aim 1 (months 1-30). We will study mechanosensory function of endothelial cilia in hypertension.
Aim 1.1 (months 1-12): We will measure blood pressure in cilium mutant mice in vivo.
Aim 1.2 (months 13-30): We will examine signaling mechanisms of cilia & their effects on blood pressure.

Aim 2 (months 7-36). We will study mechanosensory function of endothelial cilia in vascular aneurysm.
Aim 2.1 (months 7-20): We will quantify aneurysm formation in cilium mutant mice in vivo.
Aim 2.2 (months 20-36): We will identify signaling mechanisms of cilia & their consequence on aneurysm.

Accomplishments

<u>Aim 1.1 (months 1-12): Measurement of blood pressure</u>

In our first year, we have measured the systolic and diastolic blood pressure by non-invasive blood pressure system - tail cuff method with the aid of a computerized system (CODA system, Kent Scientific, Connecticut, USA). Measurements were performed at the baseline 3-times per week for 2 weeks after previous 3 days of training for each mouse. On each day of blood pressure measurement, 2 sets of 18 measurements were obtained including three measurements of training or acclimation. The measurements were averaged for each mouse with at least three mice for each genotype. All animals were tested by an investigator blinded to the genotypes of the animals. The data from the tail cuff method was also verified with limited studies with a more invasive, surgically implanted telemetry probe (data not shown).

When blood pressure was monitored in our mutant mice, *Survivin* knockout mice surprisingly did not show an elevated blood pressure (**Figure 1**). However, *Pkd1* and *Tg737* mice were hypertensive. Supporting this view, patients with PKD have a significantly greater chance to develop hypertension than general population.

Part of Aim 1 was to set up mouse models for Aim 2. To generate vascular-specific knockout, we have used and confirmed *PdgfβCre* and *Tie2Cre* mice (**Figure 2**). Briefly, one-week old pups were injected intra-peritoneally with 62.5 µg of 50 µL polyinosinic:polycytidylic ribonuceic acid (pI:pC) every day for five consecutive days. *Tie2Cre* or *PdgfβCre* mouse was bred with *Gt(ROSA)26Sor* (*Rosa26*) mouse, resulting in either *PdgfβCre•Rosa26* or *Tie2Cre•Rosa26* genotype. The *Rosa26* mouse was used as a control. These 3 mouse groups were induced to activate Cre which acts on *Rosa26* allele. The *Rosa26* genetic background is used as a reporter system to verify and validate the efficiency of the *Cre* mice. The *Rosa26* includes its inducible fluorescence reporter system; i.e. all endothelia lining the vasculatures have red fluorescence (non-induced). The red fluorescence will be replaced with green fluorescence upon *Cre* recombinant (induction). Abdominal aortas were isolated, stained with nuclear marker (blue), and imaged for their green/red fluorescence (**Figure 2a**). Quantitation analysis of vascular-lining endothelia indicates high efficacy of both *PdgfbCre* and *Tie2Cre* backgrounds to delete a specific gene in vascular lining endothelia (**Figure 2b**). N=4 for each genotype and treatment.

Figure 1

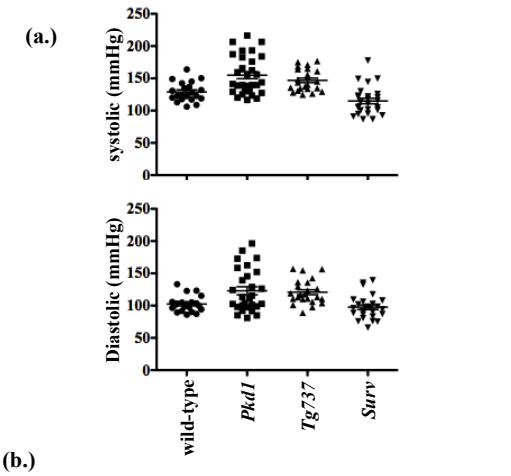

(b.)

	systolic (mmHg)	diastolic (mmHg)	N
wild-type	128±9	102±7	3
Pdgfbcre:Pkd1$^{flox/flox}$	150±19*	120±21*	4
Tie2Cre:Tg737$^{flox/flox}$	147±10*	120±11*	3
Pdgfβcre:Surv$^{flox/flox}$	114±13	99±13	3
** significant different from wild-type control*			

Figure 1. Blood pressure was measured in wild-type and conditional *Pkd1*, *Tg737*, and *Survivin* (*Sur*) mice for a 2-week period (***a***). The averaged measurements of blood pressure during this 2-week period were tabulated (***b***).

Figure 2

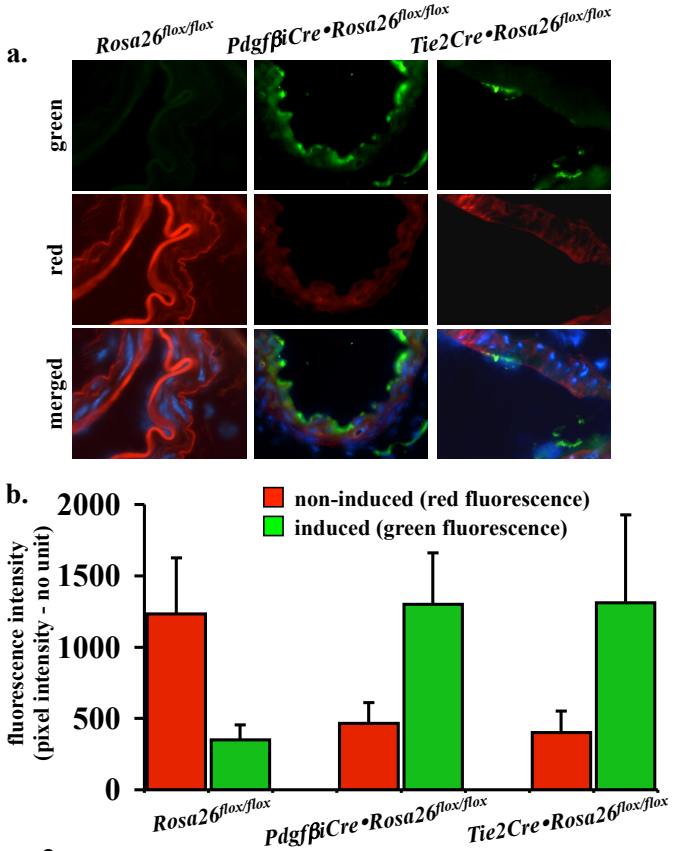

Figure 2. Both *Tie2Cre* and *PdgfβCre* models had high efficiency in gene deletion to turn vascular endothelia from red to green fluorescence.

Aim 1.2 (months 13-30): Examine signaling mechanisms of cilia

To identify if formation of ciliary signaling was regulated by GM3S, Bicc-1 or PC2, we generated knockdown cell lines for the respective genes (*St3gal5*, *Bicc-1* or *Pkd2*). We tested knockdown efficiencies of these genes using four different knockdown sequences (**Figure 3**). In the case of *Bicc-1*, we used both chemical siRNA transfection and shRNA viral infection approaches. All stably knockdown cell lines were verified for their corresponding protein expressions, and *Bicc-1* #B, *St3gal5* #D, and *Pkd2* #D shRNA knockdown cell lines were selected for further studies. Because the shRNA expression was tagged with fluorescence GFP, we confirmed the stability of the shRNA integration in these knockdown cell lines after several passages by immunefluorescence microscopy and flow-cytometry.

We next examined if Bicc-1 and PC2 regulated overall expression of GM3S. To understand the global effect of the knockdown genes at the cell level, we performed immunoblot studies to understand the interrelationship between the ciliary and cytoplasmic proteins. In particular, Bicc-1, GM3S and PC2 have been detected at the cell body. miRNA-17 (Mir-17) was included in this experiment, because Mir-17 has been known to modulate PC2 and Bicc-1. Our studies indicated while knockdown of *Mir-17* induced Bicc-1 expression level, knockdown of *Bicc-1*, *St3gal5*, or *Pkd2* could have an effect on the global expression of each other (**Figure 4**).

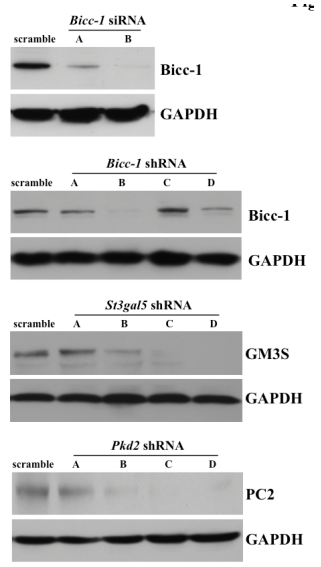

Figure 3. Knockdown efficiency was \ examined with silencing different regions of each gene, and siRNA was also tested as an earlier approach. Total cell lysate from scramble (control) and various siRNAs or shRNA-GFP lentivirus sequences (A, B, C, D) of each gene were analyzed.

Aim 2.1 (months 7-20): Quantify aneurysm formation

Compared to normal tissue , karyotyping data of a single renal epithelium from PKD patients showed an abnormal ploidy. We consistently observed an astonishingly high abnormality in the genetic composition in the samples acquired from PKD patients. We recently showed that survivin is down-regulated in *Pkd*-derived mouse vascular endothelia. We therefore examined survivin expression levels in our patients' samples. All freshly isolated kidney samples from PKD patients consistently show a down-regulation in survivin expression.

Because *Survivin* knockout mouse dies at 4.5 days *post coitum*, we crossed *survivin-flox* mouse with kidney-specific *Cre* mouse (*Mx1Cre*). We also performed UUO surgery as a renal injury model to examine the relationship between renal injury and cyst formation. We inactivated survivin (*Mx1Cre:Survivin*$^{flox/flox}$) in one-week old mice and analyzed the cystic kidney phenotypes in five-week and three-month old mice. At five-weeks old, the effects of *Survivin* knockout were most apparent in injury model, in which the UUO kidneys were bulged and filled with fluid. Kidneys from three-month-old *Mx1Cre:Survivin*$^{flox/flox}$ mice showed

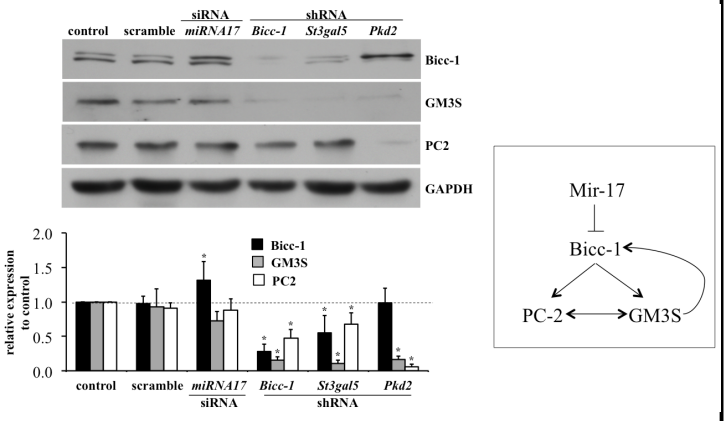

Figure 4. To examine if there is any interrelationship between the proteins located in the cilia, protein expressions were analyzed in wild-type (control), scramble, *miRNA17*, *st3gal5*, *Bicc-1* and *Pkd2* knockdown cells. A flow diagram shows the proposed mechanistic pathway for the identified ciliary proteins. Asterisks denote significant difference between groups.

severe gross anatomical kidney defects. Cross-section analysis further showed that inactivation of *survivin* at one-week old was sufficient to induce kidney cyst formation at five-weeks old, although it was not as severe as those with UUO surgery. Histology analysis using standard H&E and fluorescent lectin staining confirmed a gross structure abnormality in *Survivin* knockout kidney, especially in the injury model, compared to wild-type age-matched kidneys undergoing the same surgery. Survivin inactivation resulted in a progressively more severe cystic kidney phenotype in older mice.

The occurrence of aneurysm represents a major risk factor for morbidity and mortality associated with PKD. To examine whether *Survivin* knockout would result in aneurysm, we induced aneurysm formation in endothelial-specific *Survivin* knockout (*PdgfβCre:Survivin*$^{flox/flox}$) mice. These mice were later sacrificed to measure the aorta diameter at the site of the aneurysm surgery. Unlike wild-type mice, in which aorta diameter was only slightly enlarged following aneurysm surgery, *Survivin* knockout mice displayed a gross aortic aneurysm similar to that of *PdgfβCre:Pkd1*$^{flox/flox}$, *Pkd2*$^{+/-}$ or *Tg737*$^{Orpk/Orpk}$ mice following aneurysm surgery (**Figure 5**). Histological analysis of the cross sections further confirmed a marked arterial enlargement and aneurysm formation at the site of surgery from *PdgfβCre:Survivin*$^{flox/flox}$, *PdgfβCre:Pkd1*$^{flox/flox}$, *Pkd2*$^{+/-}$, and *Tg737*$^{Orpk/Orpk}$ mice. Surprisingly, the *Pkd2*$^{+/-}$ mice also demonstrated a high propensity for aneurysm formation. Our data clearly indicated that similar to *Pkd1*, *Pkd2* or *Tg737* inactivation, *Survivin* knockout resulted in aneurysm formation. We next categorized the aneurysm types according to the classification by Daugherty[16]. Regardless of the genotypes, the mutant mice consistently showed a more severe grade than the wild-type mice. Taken together, we proposed that vascular and kidney phenotypes of PKD may share a similar cellular mechanism through survivin.

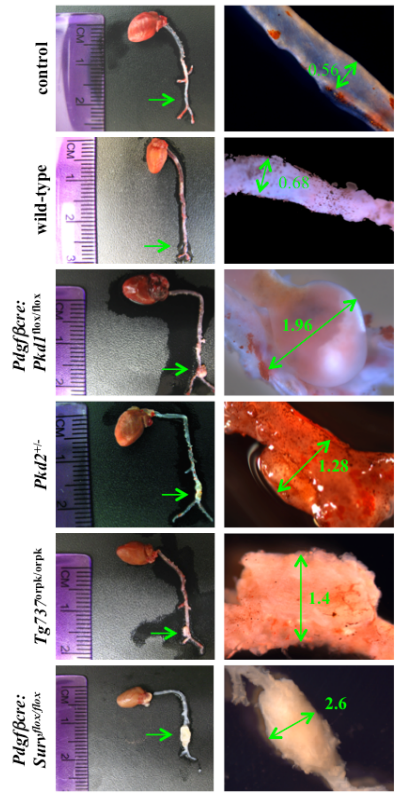

Figure 5. Aneurysm formation is an extra-renal phenotype of PKD. Aneurysm surgery was performed in mice at two months old that were sacrificed at three months of age. The aortas were isolated and their diameters were measured at the surgical site. Unlike wild-type, *Pdgfβcre:Survivin*$^{flox/flox}$ mice show a severe aneurysm induction to a similar extent shown in *Pdgfβcre:Pkd1*$^{flox/flox}$, *Pkd2*$^{+/-}$, and *Tg737*$^{orpk/orpk}$ mice.

To examine the mechanism by which survivin down-regulation contributes to cystic kidney and vascular aneurysm, we performed live-cell imaging on renal epithelial. As expected, we observed a symmetric division in normal epithelial cell. Although survivin knockdown epithelium committed to enter cell division, severe cytokinesis defect was observed, resulting in failure to exit mitosis properly. This, in turn, led to polyploidy formation with cytomegaly and multi-nucleated phenotypes. Similar studies were performed on vascular endothelial cells. Likewise, similar observations were obtained in control and survivin knockdown endothelia.

Oriented cell division dictates the maintenance of renal tubule diameter during tubular lengthening. Defects in this process will trigger renal tubular enlargement and cyst formation in *Pkd* rodent models. We thus examined this possibility in *Survivin* mouse. Unlike kidney sections from wild-type mice in which normal cell division orientation was parallel to the axis of kidney tubules, kidney sections from *Survivin* knockout mice (*Mx1Cre:Survivin*$^{flox/flox}$) revealed abnormal cell division and orientation pattern. Both mitotic misorientation and abnormal cell division were very apparent in the *Survivin* knockout mice, particularly following UUO surgery. Abnormal cell divisions include enlarged nucleus, multi-nucleated cells, or asymmetric mitosis. Our data further strengthened the argument that survivin shared a similar cellular mechanism as previously reported in polycystic kidney models.

Aim 2.2 (months 20-36): Identify signaling mechanisms of cilia

Our effort to identify signaling mechanism on aneurysm has just been started. Due to some troubleshooting, we are not able to share our progress at this time.

Training and Professional Development

The project will continue to be part of our research-training program for two postdoctoral fellows and one graduate student. All of our trainees will continue working on the proposed studies, and results of their studies will be presented in conferences, such as FASEB meeting. This is an important meeting for our trainees to demonstrate their research productivity. We meet one on one in my office regularly to discuss any technical problems that may have arisen from their experiments. All trainees also participate in our laboratory meeting. All are expected to present their research progress in our laboratory meeting.

In addition, the Postdoctoral Research Committee and Graduate Committee will also evaluate the productivity of our postdoctoral fellows and graduate student, respectively. For most of the technical skills and methods, they will be trained within our laboratory and our surrounding laboratories. For more specialized skills, we will encourage them to attend various workshops. All trainees are recommended and student is required to the following courses.

- PHS601- Research Ethics and Regulations
- PHS 614- Biologics
- PHS 636- Proteomics

Results Dissemination

No outreach activity was attempted. Relevant results have been published and/or deposited into the National Library of Medicine.

1. Liu T, Jin X, Prasad RM, Sari Y, **Nauli SM**. Three types of ependymal cells with intracellular calcium oscillation are characterized by distinct cilia beating properties. J Neurosci Res. 2014 Sep;92(9):1199-204. [PMID:24811319]
2. Muntean BS, Jin X, Williams FE, **Nauli SM**. Primary cilium regulates CaV1.2 expression through Wnt signaling. J Cell Physiol. 2014 Dec;229(12):1926-34. [PMID:24700505]
3. Atkinson KF, Kathem SH, Jin X, Muntean BS, Abou-Alaiwi WA, Nauli AM, **Nauli SM**. Dopaminergic signaling within the primary cilia in the renovascular system. Front Physiol. 2015 Apr 16;6:103. [PMID:25932013]
4. Mohieldin AM, Zubayer HS, Al Omran AJ, Saternos HC, Zarban A, **Nauli SM**, AbouAlaiwi WA. Vascular Endothelial Primary Cilia: Mechanosensation and Hypertension. Curr Hypertens Rev. 2015 Jun 30 [In Press; PMID:26122329]
5. Atkinson KF, **Nauli SM**. pH sensors and ion Transporters: Potential therapeutic targets for acid-base disorders. International Journal of Pharma Research & Review. 2016 March 01; 5(3):51-58.
6. Kathem SH, AbouAlaiwi WA, Zi X, **Nauli SM**. Capillary Endothelia from Two ADPKD Patients are Polyploidy. Annals of clinical cytology and Pathology. 2016 April 25; 2(2):1022.
7. Grimes DT, Keynton JL, Buenavista MT, Jin X, Patel SH, Kyosuke S, Vibert J, Williams DJ, Hamada H, Hussain R, **Nauli SM**, Norris DP. Genetic Analysis Reveals a Hierarchy of Interactions between Polycystin-Encoding Genes and Genes Controlling Cilia Function during Left-Right Determination. PLoS Genet. 2016 Jun 6;12(6):e1006070.

8. **Nauli SM**, Pala R, Kleene SJ. Calcium channels in primary cilia. Curr Opin Nephrol Hypertens. 2016 Sep;25(5):452-8.
9. Doerr N, Wang Y, Kipp KR, Liu G, Benza JJ, Pletnev V, Pavlov TS, Staruschenko A, Mohieldin AM, Takahashi M, **Nauli SM**, Weimbs T. Regulation of Polycystin-1 Function by Calmodulin Binding. PLoS One. 2016 Aug 25;11(8):e0161525.

Future Goal

Our goal for next funding year is to wrap-up Aim 1.2 and to initiate Aim 2.2.

4. IMPACT:

Impact on the discipline

Primary cilia are sensory organelles that extend from the cell surface and sense extracellular signals. Endothelial primary cilia protruding from the inner surface of blood vessel walls sense changes in blood flow and convert this mechanosensation into an intracellular biochemical/molecular signal, which triggers a cellular response. Endothelial cilia dysfunction may contribute to the impairment of this response and thus be directly implicated in the development of vascular abnormalities such as hypertension as seen in our PKD animal models. The completion of this project may present primary cilia as a novel therapeutic target for vascular hypertension.

Impact on other disciplines

Although our project is directed to lower blood pressure in patients with PKD, it may apply to a general population with hypertension. The completion of our project may serve as a proof of comcept for targeted-clinical therapy on primary cilia as a novel mechanism in general hypertensive patients.

Impact on technology transfer

Nothing to Report at this time.

Impact on society

Nothing to Report.

5. CHANGES AND PROBLEMS:

Nothing to Report.

6. PRODUCTS:

1. Liu T, Jin X, Prasad RM, Sari Y, **Nauli SM**. Three types of ependymal cells with intracellular calcium oscillation are characterized by distinct cilia beating properties. J Neurosci Res. 2014 Sep;92(9):1199-204. [PMID:24811319]
2. Muntean BS, Jin X, Williams FE, **Nauli SM**. Primary cilium regulates CaV1.2 expression through Wnt signaling. J Cell Physiol. 2014 Dec;229(12):1926-34. [PMID:24700505]
3. Atkinson KF, Kathem SH, Jin X, Muntean BS, Abou-Alaiwi WA, Nauli AM, **Nauli SM**. Dopaminergic signaling within the primary cilia in the renovascular system. Front Physiol. 2015 Apr 16;6:103. [PMID:25932013]
4. Mohieldin AM, Zubayer HS, Al Omran AJ, Saternos HC, Zarban A, **Nauli SM**, AbouAlaiwi WA. Vascular Endothelial Primary Cilia: Mechanosensation and Hypertension. Curr Hypertens Rev. 2015 Jun 30 [In Press; PMID:26122329]
5. Atkinson KF, **Nauli SM**. pH sensors and ion Transporters: Potential therapeutic targets for acid-base disorders. International Journal of Pharma Research & Review. 2016 March 01; 5(3):51-58.
6. Kathem SH, AbouAlaiwi WA, Zi X, **Nauli SM**. Capillary Endothelia from Two ADPKD Patients are Polyploidy. Annals of clinical cytology and Pathology. 2016 April 25; 2(2):1022.
7. Grimes DT, Keynton JL, Buenavista MT, Jin X, Patel SH, Kyosuke S, Vibert J, Williams DJ, Hamada H, Hussain R, **Nauli SM**, Norris DP. Genetic Analysis Reveals a Hierarchy of Interactions between Polycystin-Encoding Genes and Genes Controlling Cilia Function during Left-Right Determination. PLoS Genet. 2016 Jun 6;12(6):e1006070.
8. **Nauli SM**, Pala R, Kleene SJ. Calcium channels in primary cilia. Curr Opin Nephrol Hypertens. 2016 Sep;25(5):452-8.
9. Doerr N, Wang Y, Kipp KR, Liu G, Benza JJ, Pletnev V, Pavlov TS, Staruschenko A, Mohieldin AM, Takahashi M, **Nauli SM**, Weimbs T. Regulation of Polycystin-1 Function by Calmodulin Binding. PLoS One. 2016 Aug 25;11(8):e0161525.

7. PARTICIPANTS:

Individuals

Name:	*Kimberly Atkinson*
Project Role:	*Postdoctoral Fellow*
Researcher Identifier (e.g. ORCID ID):	*N/A*
Nearest person month worked:	*~9*
Contribution to Project:	*Dr. Atkinson has been working on the in vivo mouse model.*
Funding Support:	*This award*

Name:	*Pala Rajasekharreddy*
Project Role:	*Postdoctoral Fellow*
Researcher Identifier (e.g. ORCID ID):	*N/A*
Nearest person month worked:	*~6*
Contribution to Project:	*Dr. Rajasekharreddy has been working on the in vitro assay.*
Funding Support:	*This award*

Name:	*Rinzhin Sherpa*
Project Role:	*Graduate Student*
Researcher Identifier (e.g. ORCID ID):	*N/A*
Nearest person month worked:	*~9*
Contribution to Project:	*Mr. Sherpa has been working on the in vivo mouse model and in vitro cilia measurement.*
Funding Support:	*This award*

Change in Other Supports or Key Personnel

Nothing to Report

Partner Organization

Nothing to Report

8. SPECIAL REPORTING REQUIREMENTS:

Not applicable

9. APPENDICES:

See Below

Journal of Neuroscience Research 92:1199–1204 (2014)

Three Types of Ependymal Cells With Intracellular Calcium Oscillation Are Characterized by Distinct Cilia Beating Properties

Tongyu Liu, Xingjian Jin, Rahul M. Prasad, Youssef Sari, and Surya M. Nauli*

Department of Pharmacology, University of Toledo, Toledo, Ohio

Ependymal cells are multiciliated epithelial cells that line the ventricles in the adult brain. Abnormal function or structure of ependymal cilia has been associated with various neurological deficits. For the first time, we report three distinct ependymal cell types, I, II, and III, based on their unique ciliary beating frequency and beating angle. These ependymal cells have specific localizations within the third ventricle of the mouse brain. Furthermore, neither ependymal cell types nor their localizations are altered by aging. Our high-speed fluorescence imaging analysis reveals that these ependymal cells have an intracellular pacing calcium oscillation property. Our study further shows that alcohol can significantly repress the amplitude of calcium oscillation and the frequency of ciliary beating, resulting in an overall decrease in volume replacement by the cilia. Furthermore, the pharmacological agent cilostazol could differentially increase cilia beating frequency in type II, but not in type I or type III, ependymal cells. In summary, we provide the first evidence of three distinct types of ependymal cells with calcium oscillation properties.

Key words: cilia; cerebrospinal fluid; calcium

Cilia are generally classified as solitary nonmotile and bundled motile organelles (Abou Alaiwi et al., 2009a; Nauli et al., 2011). Motile and nonmotile cilia have been implicated in fundamental processes of development and disease. Motile cilia can be found in the ependymal cells, forming a lining in the brain ventricles and central canal of the spinal cord. Ependymal cells are ciliated, simple cuboidal, epithelium-like glial cells that move cerebrospinal fluid (CSF) along the ventricles (Del Bigio, 1995). Abnormal ependymal cilia result in hydrocephalus induced by anomalous flow of CSF (Banizs et al., 2005; Baas et al., 2006; Wodarczyk et al., 2009; Tissir et al., 2010).

Ependymal cells also play an important role in regulating pluripotent neural stem cells (Rietze et al., 2001). Beating of ependymal cilia is required for normal CSF flow, which functions as a guide for specific directional migration of new neurons (Sawamoto et al., 2006). The coupling between ependymal cilia beating and hydrodynamic forces has been proposed to regulate planar cell polarity during development or stroke (Guirao et al., 2010; Mirzadeh et al., 2010; Devaraju et al., 2013). In addition, ependymal cilia play major roles in CSF dynamics, cerebral fluid balance, secretion, toxin metabolism, and many other functions (Genzen et al., 2009; Appelbe et al., 2013). Although ependymal cells regulate CSF flow, which regulates many neuronal processes, different types of ependymal cells have not been distinguished. We show here, based on the cilia beating frequency and beating angle, that ependymal cells can be distinctly categorized into three types. Furthermore, each type of ependymal cell is uniquely localized within the ventricle.

MATERIALS AND METHODS

All animal experiments were approved by the University of Toledo's Institutional Animal Care and Use Committee (IACUC). The wild-type mice were euthanized with carbon dioxide for 5 min. After craniotomy, the whole brain was removed. The sagittal slice was dissected with a thickness of about 100 μm and was immediately embedded in Dulbecco's modified Eagle's medium (DMEM; Cellgro Corning Life Sciences-Mediatech, Manassas, VA) at 39°C in the presence of 95%/5% O_2/CO_2 mixture.

Immunofluorescence Microscopy

The brain slice was fixed in phosphate buffer containing 3% paraformaldehyde and 2% sucrose for 10 min. Mouse primary antibody antiacetylated α-tubulin was used at a dilution of 1:5,000 (Sigma, St. Louis, MO). The brain slice was

Additional Supporting Information may be found in the online version of this article.

Contract grant sponsor: NIH, contract grant number: DK080640; Contract grant sponsor: DOD, contract grant number: PR130153; Contract grant sponsor: University of Toledo.

*Correspondence to: Surya M. Nauli, PhD, Department of Pharmacology, University of Toledo, MS 1015, Health Education Building, Room 274, 3000 Arlington Ave., Toledo, OH 43614.
E-mail: surya.nauli@utoledo.edu

Received 15 January 2014; Revised 7 April 2014; Accepted 7 April 2014

Published online 9 May 2014 in Wiley Online Library (wileyonlinelibrary.com). DOI: 10.1002/jnr.23405

incubated in primary antibody solution overnight. Secondary antibody fluorescein anti-mouse IgG was used at a dilution of 1:500 (Vector Laboratories, Burlingame, CA), and the brain slice was incubated with secondary antibody solution for 1 hr. Before observation under a TiU fluorescent microscopy (Nikon, Tokyo, Japan), the section was dyed with DAPI for 5 min (Abou Alaiwi et al., 2014).

Measurement of Cilia Beating Frequency

The prepared brain slice was kept in a customized glass-bottom plate covered with 500 μl DMEM containing 2% B27 at 39°C. In some cases, 0.25% ethanol was added to the media. The video of cilia beating was captured with a TiU high-resolution differentiation interference contrast microscope. The capture rate of the video was 5 msec for a minimum of 1 sec (200 frames per sec).

Measurement of Fluid Movement and Volume Replacement

Because of the transparency of the buffer solution, we used 200-nm latex beads (Molecular Probes, Eugene, OR) to help analyze speed in the solution movement. The velocity of fluid movement was calculated by tracing one single nanobead flowing across the third ventricle wall. The overall fluid volume moved by ependymal cilia was calculated with the following formula: volume replacement (μm^3/stroke) = fluid movement velocity (μm^3/sec)/cilia beating frequency (stroke/sec).

Calcium Signal Recording

To record cytosolic calcium oscillation, the brain slice was incubated with 20 μg/ml fluo-2 (TEFLabs, Austin, TX) for 30 min at 39°C. The tissue was then transferred to a glass-bottom plate covered with 500 μl DMEM containing 2% B27 (Gibco, Rockville, MD) at 39°C. In some cases, 0.25% ethanol was added to the media. The video of calcium oscillation was recorded at a capture rate of 5 msec for a minimum of 1 sec (200 frames per sec), with excitation and emission wavelengths of 488 nm and 515 nm, respectively.

RESULTS

Ependymal Cells Can Be Classified Into Three Types Based on Their Cilia Beating Frequency

We cut the mouse brain in a sagittal plane to enhance our observation of the entire third ventricle. To verify our high-resolution differential interference contrast and fluorescence microscope systems, we examined the presence of ependymal cilia in the third ventricle (Fig. 1). Ependymal cilia were confirmed with a ciliary marker, acetylated-α-tubulin. Although in the control permeabilized brain no fluid movement was observed in nonbeating ependymal cilia (Supp. Info. Movie 1), we could observe the direction of fluid movement via oil ink in a freshly prepared brain ex vivo (Supp. Info. Movie 2).

We next attempted to quantify the cilia beating frequency. Based on our observation of individual ependymal cells from 87 independent experiments, we were surprised to notice that there were wide variations in the beating frequencies of ependymal cilia (Fig. 2). We could accurately assign each ependymal cell to one of three classifications depending on its ciliary beating. Type I ependymal cells

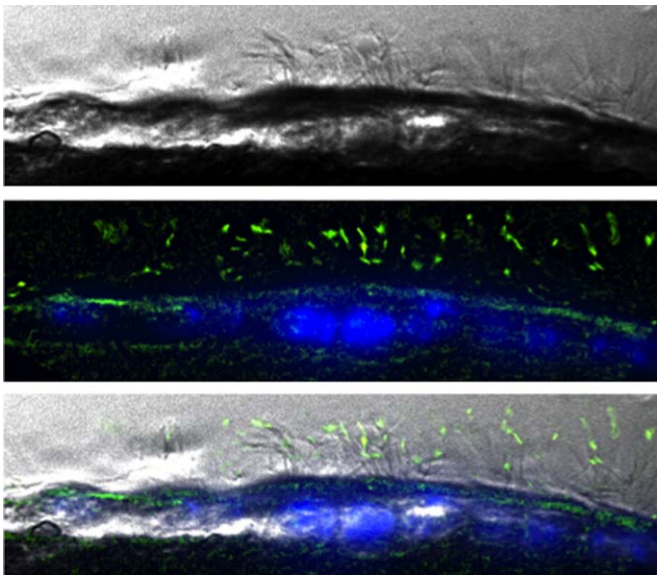

Fig. 1. The presence of ependymal cilia in mouse brain. Shown here are ependymal cells from the third ventricle of a mouse brain. The brain section was stained with anti-acetylated-α-tubulin, a ciliary marker (green), and counterstained with DAPI, a nucleus marker (blue). Individual differential interference contrast (**top**), fluorescence (**middle**), and merged (**bottom**) images are shown. [Color figure can be viewed in the online issue, which is available at wileyonlinelibrary.com.]

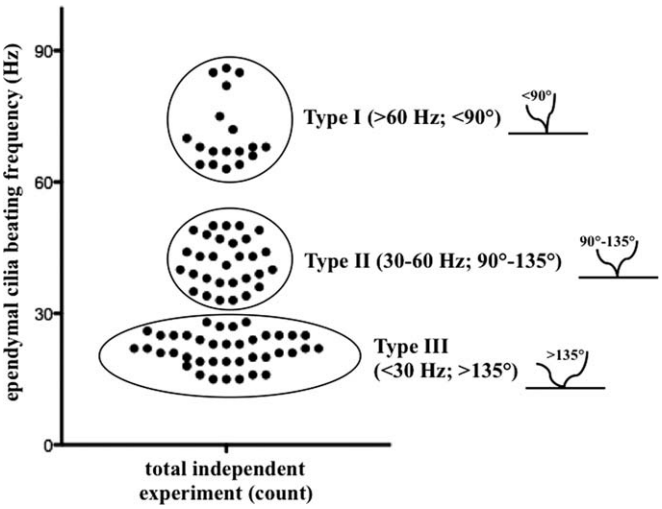

Fig. 2. Categories of ependymal cells in mouse brain. Based on a total of 87 independent experiments or preparations (represented as dots), ependymal cells could be classified into three types (grouped within circle or oval lines). Type I ependymal cilia had the highest beating frequency (>60 Hz), with a ciliary beating angle of less than 90°. Type II ependymal cilia had a medium beating frequency (30–60 Hz), with a ciliary beating angle between 90° and 135°. Type III ependymal cilia had the slowest beating frequency (<30Hz), with a ciliary beating angle of greater than 135°. The cartoon on the right depicts the beating angles of ependymal cilia.

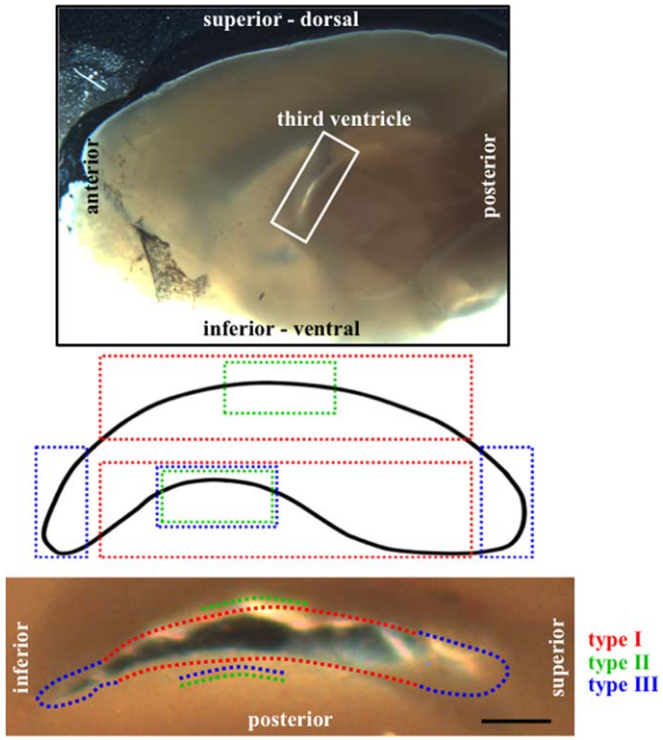

Fig. 3. Differential ependymal cell types and localization. Based on the ependymal cilia beating frequency, different ependymal cell types were enriched at certain locations within the third ventricle. A freshly cut brain section was imaged to show the third ventricle region (**top**). The cartoon (**middle**) and brain section (**bottom**) of the third ventricle depict localizations of different ependymal cells from a sagittal view. Scale bar = 30 μm. [Color figure can be viewed in the online issue, which is available at wileyonlinelibrary.com.]

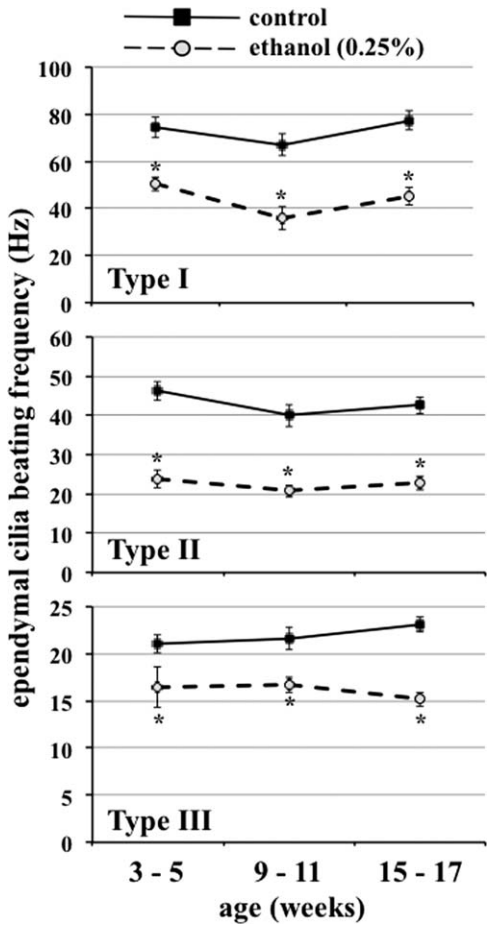

Fig. 4. Ependymal cilia beating frequency in different mouse age groups. All types of ependymal cilia in control and alcohol-treated mouse third ventricles were studied at different ages. Although beat frequency of ependymal cilia was not affected by age, acute alcohol treatment significantly decreased cilia beating frequency in all types of ependymal cells. At least three independent preparations were used for each ependymal cell type and age group.

had the highest beating frequency (>60Hz) and had a beating angle of less than 90° (Supp. Info. Movie 3). Type II ependymal cells had a medium beating frequency (30–60 Hz) and had a beating angle between 90° and 135° (Supp. Info. Movie 4). Type III ependymal cells had the slowest beating frequency (<30 Hz) and had a beating angle of more than 135° (Supp. Info. Movie 5).

To understand the difference in localizations among these ependymal cells, we mapped the distributions of ependymal cell types within the third ventricle (Fig. 3). Our mapping analysis indicated that type I cells were widely distributed along the ventricle walls, but they were absent at both inferior and superior corners of the third ventricle. Type II cells were observed mainly on the anterior wall of the ventricle, but they could also be found at the posterior wall of the ventricle. Type III cells were distributed almost exclusively in the inferior and superior corners of the third ventricle. Of note is that we could find all three cell types at the lower wall of the third ventricle.

Cilia Beating Frequency Is Age Independent in Third Ventricles

Because ependymal cilia have been proposed to move CSF to support migration of various substances (Banizs et al., 2005; Sawamoto et al., 2006), we next sought to understand the role of aging in ependymal cilia beating. Mice were grouped according to age: 3–5 weeks, 9–11 weeks, and 15–17 weeks. The data indicate that we could distinctively classify the ependymal cilia beating into three types regardless of the age groups (Fig. 4). More importantly, there was no evidence that age was a factor in regulating ependymal cilia beating.

Ependymal Cilia Beating Can Be Repressed by Ethanol

To confirm further that our classification of ependymal cells was valid and consistent, we preformed chemical screening on the cilia beating frequency. Ethanol at a concentration of 0.25% provided us with the most consistent changes in ependymal cilia beating. The data indicated that ethanol repressed ependymal cilia beating regardless of the age group (Fig. 4). Most importantly, ethanol repressed

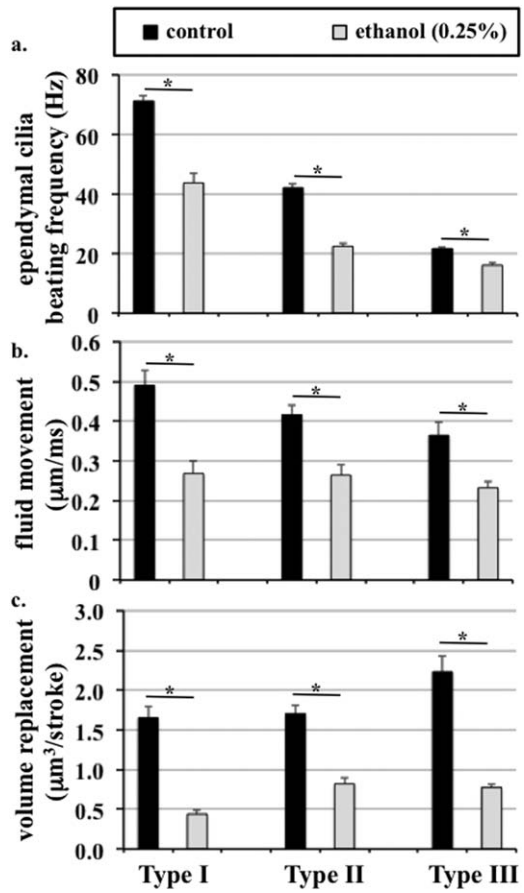

Fig. 5. Effects of alcohol on the dynamics of mouse third ventricle. The ex vivo brain slice was incubated without (control) or with (ethanol) alcohol for 5 min. **a:** Compared with control, alcohol treatment significantly decreased cilia beating frequency. **b:** This resulted in a decrease in fluid movement, as indicated by speed of fluid movement surrounding the ependymal cilia. **c:** Further calculation of the volume replacement and cilia beating indicated that, compared with control, alcohol significantly decreased volume replacement for each stroke of cilia beating. This indicates that alcohol not only decreases the frequency of ependymal cilia beating but also reduces the efficiency of each cilia stroke. At least 10 independent preparations were used for each ependymal cell type and treatment group.

ependymal cilia beating (Fig. 5a), resulting in a significant decrease in fluid movement velocity around ependymal cilia (Fig. 5b). Because of the transparency of the fluid media, we used nanobeads to guide us in measuring the speed of the fluid movement (Supp. Info. Movie 6). Given the fluid movement velocity, we estimated the volume replacement for each stroke of cilia beating efficiency. Our calculation indicated that ethanol not only repressed cilia beating frequency but also decreased the efficiency of ependymal cilia to move fluid per each stroke (Fig. 5c).

Calcium Signaling by Ependymal Cilia Can Be Altered by Alcohol

Fluid-shear stress resulting from fluid movement above a layer of cells can generate intracellular calcium signaling (Abou Alaiwi et al., 2009b; Jin et al., 2013). We therefore examined the calcium signaling within the third ventricle (Fig. 6a). As expected, we did not see any apparent calcium oscillation in fixed brain sections (Supp. Info. Movie 7). In the absence (Supp. Info. Movie 8) or presence (Supp. Info. Movie 9) of ethanol, however, calcium oscillation was observed on ependymal cells. The frequency of calcium oscillation was not changed either by mock (PBS or control) or by ethanol treatment (Fig. 6b). Although the frequency of calcium signal in each ependymal cell type was unchanged, the amplitude of calcium signal was significantly repressed in the ethanol group compared with the control groups of each of the corresponding ependymal cell types (Fig. 6c).

DISCUSSION

We report here for the very first time that there are three distinct types of ependymal cells uniquely and specifically positioned within the third ventricle. We classified them based on their cilia beating frequency as type I (>60Hz), type II (30–60 Hz), and type III (<30 Hz). The beat frequency for each type of ependymal cilia is age independent. We also report here that ependymal cells are characterized by calcium oscillations, the frequency and amplitude of which are the same in all ependymal cell types. Our chemical testing indicates that alcohol has a profound effect on the beating frequency of the ependymal cilia, resulting in a significant decrease in fluid movement and volume replacement. Although alcohol did not change the frequency of calcium oscillation in the ependymal cells, the amplitude of calcium oscillation was significantly repressed.

Even with the advancement in the technology of high-speed digital imaging (Lechtreck et al., 2009), there has been no report on different types of ependymal cells. We thus believe that our study is the first to identify distinct ependymal cilia, which is fundamentally important to gain basic understanding of ependymal physiology. For example, many substances that are known to alter cilia beating (Sisson et al., 1991; Sisson, 1995) may fail to show an effect in ependymal cells, especially when ependymal cells are randomly analyzed (Smith et al., 2013). To validate our point further, 1% ethanol was reported to have no effect on the beating frequency of ependymal cilia (Smith et al., 2013). After we classified the ependymal cilia into three types, however, our data clearly showed that ethanol as low as 0.25% had a definitive effect on ependymal cilia beating frequency.

Our study also revealed a unique aspect of calcium signaling in ependymal cells. It was previously thought that cardiac myocytes were the only cells that naturally have a pacing calcium oscillation. We used a florescence high-speed digital imaging system to demonstrate that, like myocytes, ependymal cells also have an oscillating intracellular calcium pattern. The frequency and amplitude of this calcium oscillation are similar among all three types of ependymal cells, indicating that the calcium may reflex functional states rather than types of the ependymal

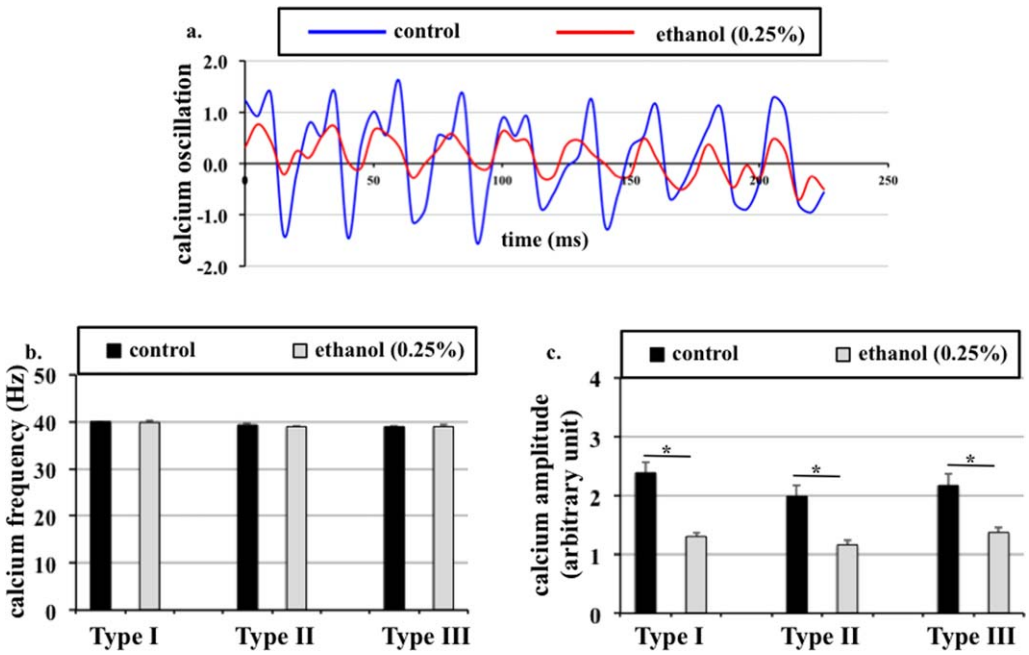

Fig. 6. Effects of alcohol on calcium oscillation in mouse brain ependymal cells. After being loaded with calcium indicator fluo-2, the ex vivo brain slice was incubated without (control) or with (ethanol) alcohol for 5 min. **a:** Intracellular calcium of ependymal cells was measured every 5 msec, as indicated by the representative blue and red lines. **b:** There was no difference in calcium oscillation frequency between control and alcohol-treated groups. **c:** However, the amplitude of calcium oscillation was significantly repressed in alcohol-treated groups compared with control groups in all types of ependymal cells. At least five independent preparations were used for each ependymal cell type and treatment group. [Color figure can be viewed in the online issue, which is available at wileyonlinelibrary.com.]

cells. Furthermore, the frequencies of ciliary beating and calcium oscillation on ependymal cells might not be associated with one another. Consistent with this idea, an ethanol-induced decrease in ciliary beating frequency did not alter the frequency of calcium oscillation.

Despite the fact that the characteristics of cilia beating are very different among these three types of ependymal cilia, it is important to note that our understanding of these cells is just starting to unfold. For example, cilostazol could differentially increase cilia beating frequency in type II but not in type I or type III cells (Supp. Info. Fig. 1). Cilostazol is a specific inhibitor for phosphodiesterase-3, an enzyme that metabolizes cAMP to AMP, and it also regulates intracellular calcium (Kawanabe et al., 2012). It has been known that cAMP and calcium could regulate cilia beating frequency (Nguyen et al., 2001; Monkkonen et al., 2008; Genzen et al., 2009), but the differential effect of cilostazol and many other pharmacological agents requires further in-depth study to advance our understanding of the molecular and cellular biology of different ependymal cell types.

It is also worth mentioning that, among the three types of ependymal cells, type III cells were the most efficient at moving fluid volume with each ciliary stroke. Although their frequency of ciliary beating was the slowest, type III cells had the largest angle of stroke. The angle of stroke might therefore contribute significantly to moving fluid volume. However, it is important to mention that ciliary beat frequency was also a critical contributing factor in moving fluid volume, as seen with the ethanol treatment. Treatment with ethanol decreased fluid replacement significantly, primarily because of a slowing of ciliary beating.

Alcohol can produce a variety of detrimental effects in the central nervous system, leading to a wide range of impairments. Within minutes of alcohol consumption, the alcohol in the CSF reaches the same level as that in the blood (Kiianmaa and Virtanen, 1978; Agapejev et al., 1992; Huang and Huang, 2007). However, the effect of alcohol on each type of ependymal cell had never before been examined, although abnormal ependymal cilia are associated with ventricle enlargement associated with hydrocephalus (Banizs et al., 2005; Baas et al., 2006; Wodarczyk et al., 2009; Tissir et al., 2010). Consistent with this notion, the brains of alcoholics are known to have an increase in the size of the ventricles, causing hydrocephalus ex vacuo (de la Monte, 1988). The use of 0.25% of ethanol in our study was within the range of alcohol levels in the CSF as observed in humans and various animal models (Kiianmaa and Virtanen, 1978; Agapejev et al., 1992; Huang and Huang, 2007). Thus, our study also reflects a serious clinical implication in alcohol abusive behavior with regard to ventricle-lining ependymal cells, in addition to providing fundamental basic

scientific understanding of ependymal cilia and calcium signaling.

ACKNOWLEDGMENTS

We thank Charisse Montgomery for her editing service. T. Liu's work partially fulfilled the requirements for a Master's degree in Pharmacology.

REFERENCES

Abou Alaiwi WA, Lo ST, Nauli SM. 2009a. Primary cilia: highly sophisticated biological sensors. Sensors 9:7003–7020.

Abou Alaiwi WA, Takahashi M, Mell BR, Jones TJ, Ratnam S, Kolb RJ, Nauli SM. 2009b. Ciliary polycystin-2 is a mechanosensitive calcium channel involved in nitric oxide signaling cascades. Circ Res 104: 860–869.

Abou Alaiwi WA, Muntean BS, Ratnam S, Joe B, Liu L, Booth RL, Rodriguez I, Herbert BS, Bacallao RL, Fruttiger M, Mak TW, Zhou J, Nauli SM. 2014. Survivin-induced abnormal ploidy contributes to cystic kidney and aneurysm formation. Circulation 126:660–675.

Agapejev S, Vassilieff I, Curi PR. 1992. Alcohol levels in cerebrospinal fluid and blood samples from patients under pathological conditions. Acta Neurol Scand 86:496–500.

Appelbe OK, Bollman B, Attarwala A, Triebes LA, Muniz-Talavera H, Curry DJ, Schmidt JV. 2013. Disruption of the mouse Jhy gene causes abnormal ciliary microtubule patterning and juvenile hydrocephalus. Dev Biol 382:172–185.

Baas D, Meiniel A, Benadiba C, Bonnafe E, Meiniel O, Reith W, Durand B. 2006. A deficiency in RFX3 causes hydrocephalus associated with abnormal differentiation of ependymal cells. Eur J Neurosci 24: 1020–1030.

Banizs B, Pike MM, Millican CL, Ferguson WB, Komlosi P, Sheetz J, Bell PD, Schwiebert EM, Yoder BK. 2005. Dysfunctional cilia lead to altered ependyma and choroid plexus function, and result in the formation of hydrocephalus. Development 132:5329–5339.

de la Monte SM. 1988. Disproportionate atrophy of cerebral white matter in chronic alcoholics. Arch Neurol 45:990–992.

Del Bigio MR. 1995. The ependyma: a protective barrier between brain and cerebrospinal fluid. Glia 14:1–13.

Devaraju K, Barnabe-Heider F, Kokaia Z, Lindvall O. 2013. FoxJ1-expressing cells contribute to neurogenesis in forebrain of adult rats: evidence from in vivo electroporation combined with piggyBac transposon. Exp Cell Res 319:2790–2800.

Genzen JR, Yang D, Ravid K, Bordey A. 2009. Activation of adenosine A2B receptors enhances ciliary beat frequency in mouse lateral ventricle ependymal cells. Cerebrospinal Fluid Res 6:15.

Guirao B, Meunier A, Mortaud S, Aguilar A, Corsi JM, Strehl L, Hirota Y, Desoeuvre A, Boutin C, Han YG, Mirzadeh Z, Cremer H, Montcouquiol M, Sawamoto K, Spassky N. 2010. Coupling between hydrodynamic forces and planar cell polarity orients mammalian motile cilia. Nat Cell Biol 12:341–350.

Huang CM, Huang RH. 2007. Ethanol inhibits the sensory responses of cerebellar granule cells in anesthetized cats. Alcoholism Clin Exp Res 31:336–344.

Jin X, Mohieldin AM, Muntean BS, Green JA, Shah JV, Mykytyn K, Nauli SM. 2013. Cilioplasm is a cellular compartment for calcium signaling in response to mechanical and chemical stimuli. Cell Mol Life Sci doi: 10.1007/s00018-013-1483-1.

Kawanabe Y, Takahashi M, Jin X, Abdul-Majeed S, Nauli AM, Sari Y, Nauli SM. 2012. Cilostazol prevents endothelin-induced smooth muscle constriction and proliferation. PloS One 7:e44476.

Kiianmaa K, Virtanen P. 1978. Ethanol and acetaldehyde levels in cerebrospinal fluid during ethanol oxidation in the rat. Neurosci Lett 10: 181–186.

Lechtreck KF, Sanderson MJ, Witman GB. 2009. High-speed digital imaging of ependymal cilia in the murine brain. Methods Cell Biol 91: 255–264.

Mirzadeh Z, Han YG, Soriano-Navarro M, Garcia-Verdugo JM, Alvarez-Buylla A. 2010. Cilia organize ependymal planar polarity. J Neurosci 30:2600–2610.

Monkkonen KS, Hirst RA, Laitinen JT, O'Callaghan C. 2008. PACAP27 regulates ciliary function in primary cultures of rat brain ependymal cells. Neuropeptides 42:633–640.

Nauli SM, Haymour HS, AbouAlaiwi WA, Lo ST, Nauli AM. 2011. Primary cilia are mechanosensory organelles in vestibular tissues. mechanosensitivity and mechanotransduction. In: Kamkin A, Kiseleva I, editors. Mechanosensitivity and mechanotransduction. New York: Springer. Chapter 14.

Nguyen T, Chin WC, O'Brien JA, Verdugo P, Berger AJ. 2001. Intracellular pathways regulating ciliary beating of rat brain ependymal cells. J Physiol 531:131–140.

Rietze RL, Valcanis H, Brooker GF, Thomas T, Voss AK, Bartlett PF. 2001. Purification of a pluripotent neural stem cell from the adult mouse brain. Nature 412:736–739.

Sawamoto K, Wichterle H, Gonzalez-Perez O, Cholfin JA, Yamada M, Spassky N, Murcia NS, Garcia-Verdugo JM, Marin O, Rubenstein JL, Tessier-Lavigne M, Okano H, Alvarez-Buylla A. 2006. New neurons follow the flow of cerebrospinal fluid in the adult brain. Science 311: 629–632.

Sisson JH. 1995. Ethanol stimulates apparent nitric oxide-dependent ciliary beat frequency in bovine airway epithelial cells. Am J Physiol 268: L596–L600.

Sisson JH, Tuma DJ, Rennard SI. 1991. Acetaldehyde-mediated cilia dysfunction in bovine bronchial epithelial cells. Am J Physiol 260:L29–L36.

Smith CM, Radhakrishnan P, Sikand K, O'Callaghan C. 2013. The effect of ethanol and acetaldehyde on brain ependymal and respiratory ciliary beat frequency. Cilia 2:5.

Tissir F, Qu Y, Montcouquiol M, Zhou L, Komatsu K, Shi D, Fujimori T, Labeau J, Tyteca D, Courtoy P, Poumay Y, Uemura T, Goffinet AM. 2010. Lack of cadherins Celsr2 and Celsr3 impairs ependymal ciliogenesis, leading to fatal hydrocephalus. Nat Neurosci 13:700–707.

Wodarczyk C, Rowe I, Chiaravalli M, Pema M, Qian F, Boletta A. 2009. A novel mouse model reveals that polycystin-1 deficiency in ependyma and choroid plexus results in dysfunctional cilia and hydrocephalus. PloS One 4:e7137.

Journal of Cellular Physiology

Primary Cilium Regulates CaV1.2 Expression Through Wnt Signaling

BRIAN S. MUNTEAN,[1] XINGJIAN JIN,[2] FREDERICK E. WILLIAMS,[2] AND SURYA M. NAULI[1,2]*

[1]*Department of Medicinal and Biological Chemistry, The University of Toledo, Toledo, Ohio*

[2]*Department of Pharmacology, The University of Toledo, Toledo, Ohio*

Primary cilia are sensory organelles that provide a feedback mechanism to restrict Wnt signaling in the absence of endogenous Wnt activators. Abnormal Wnt signaling has been shown to result in polycystic kidney disease (PKD) although the exact mechanism has been debated. Previously, we reported that the calcium channel CaV1.2 functions in primary cilia. In this study, we show that CaV1.2 expression level is regulated by Wnt signaling. This occurs through modulation of mitochondrial mass and activity resulting in increased reactive oxygen species which generate oxidative DNA lesions. We found that the subsequent cellular DNA damage response triggers increased CaV1.2 expression. In the absence of primary cilia where Wnt signaling is upregulated, we found that CaV1.2 is overexpressed as a compensatory mechanism. We show for the first time that CaV1.2 knockdown in zebrafish results in classic primary cilia defects including renal cyst formation, hydrocephalus, and left-right asymmetry defects. Our study shows that suppressed Wnt signaling prevents CaV1.2 expression ultimately resulting in PKD phenotypes. Thus, CaV1.2 expression is tightly regulated through Wnt signaling and plays an essential sensory role in primary cilia necessary for cellular homeostasis.

J. Cell. Physiol. 229: 1926–1934, 2014.

Wnt signaling is an important regulator of cellular development and proliferation. In the absence of Wnt ligands, a complex consisting of Axin, adenomatous polyposis coli (APC), and glycogen synthase kinase 3β (GSK3β) induces β-catenin for ubiquitylation by SCF E3 ligases and eventual proteasomal degradation (Aberle et al., 1997). Wnt signal transduction occurs when secreted Wnt ligands bind Frizzled receptors resulting in phosphorylation of LRP5/6. The Axin-APC-GSK3β complex is then recruited to LRP5/6 at the cell membrane which prevents β-catenin from being degraded. The accumulated β-catenin translocates to the nucleus and activates transcription of Wnt target genes (Muntean et al., 2012).

Primary cilia are non-motile sensory organelles present as a single copy on most differentiated cells in the body. Calcium signaling through primary cilium is essential for renal epithelial homeostasis (Nauli et al., 2003; Jin et al., 2013). Cilia extend from the cell surface through the basal body via intraflagellar transport (Moyer et al., 1994). The most common pathologies resulting from cilia dysfunction include polycystic kidney (Wilson, 2004), hypertension (Nauli et al., 2008; AbouAlaiwi et al., 2009), aneurysm (Aboualaiwi et al., 2013), hydrocephalus (Carter et al., 2012), and left-right asymmetry defects (Norris, 2012).

Abnormal Wnt signaling has also been linked to polycystic kidney disease (PKD) (Lancaster et al., 2009). For example, increased cytosolic and nuclear β-catenin accumulation has been shown in various cilia mutant cells (Gerdes et al., 2007; Lancaster et al., 2011). Thus, primary cilia are thought to provide a feedback mechanism that restricts Wnt signaling in the absence of appropriate ligands (Gerdes et al., 2007; Lancaster et al., 2009, 2011).

We recently showed that voltage-gated L-type calcium channel CaV1.2 localized to primary cilia in renal epithelia (Jin et al., 2013). Because Wnt signaling has also been reported to modulate mitochondrial physiology (Yoon et al., 2010), we hypothesized that primary cilia play a role in Wnt regulation of mitochondria through CaV1.2. We show that although CaV1.2 is not required for cilia formation, Wnt increases mitochondria mass and activity in CaV1.2 deficient renal epithelial cells. This increases mitochondria reactive oxidative species (ROS) and DNA damage, resulting in PKD phenotypes. Thus, our study suggests that primary cilia may play a role in CaV1.2 expression level through Wnt regulation of mitochondria.

Materials and Methods

The experimental use of zebrafish was approved by The University of Toledo's Institutional Animal Care and Use Committee (IACUC). The use of lentiviral components was approved by the Institutional Biosafety Committee of The University of Toledo.

Cell culture

Immortalized mouse renal epithelial wild-type and *Tg737*$^{orpk/orpk}$ cells were cultured in Dulbecco's Modified Eagle Medium (Corning Cellgro) supplemented with 10% fetal bovine serum (HyClone Laboratories, Logan, Utah) and 1% penicillin/streptomycin (Corning Cellgro) at 39°C in 5% CO_2, as previously described (Aboualaiwi et al., 2013). Prior to experiments, cells were treated with 100 ng/ml recombinant Wnt3a (R&D Systems, Minneapolis, MN) for 3 days and serum starved for 24 h.

RNAi knockdown cells

shRNA lentiviral vectors specific to *Cacna1c* (*Origene*; pGFP-C-shLenti clone ID: TL500242) were transfected into HEK293T cells. Viral supernatants were collected after 48 h, centrifuged, and passed through a 0.45 μm filter. Cells were then spin-inoculated with pseudoviral particles containing 8 μg/ml polybrene at 2,500 rpm for 30 min at 30°C and then cultured for up to 1 week. CaV1.2 knockdown was verified through Western blot analysis.

Brian S. Muntean and Xingjian Jin contributed equally to this work.

* Correspondence to: Surya M. Nauli, Department of Pharmacology, The University of Toledo, MS 1015, Health Education Building; Room 274, 3000 Arlington Ave, Toledo, OH 43614.
E-mail: surya.nauli@utoledo.edu

Manuscript Received: 20 January 2014
Manuscript Accepted: 1 April 2014

Accepted manuscript online in Wiley Online Library (wileyonlinelibrary.com): 2 April 2014.
DOI: 10.1002/jcp.24642

TABLE 1. shRNA sequences

Descriptions	Sequences
Scrambled control	5′-TGACCACCCTGACCTACGGCGTGCAGTGC-3′
Cacna1c	5′-TCAGAAGTGCCTCACTGTTCTCGTGACCT-3′

Stable knockdown cell lines were obtained through puromycin selection. The following shRNA sequences were used (Table 1).

Immunostaining studies

Cells were grown to confluence on collagen-coated glass coverslips and differentiated in serum-free media for 24 h. Cells were then fixed in 4% paraformaldehyde in PBS containing 2% sucrose, permeabilized in 10% triton X-100, incubated sequentially with primary followed by secondary antibodies for 1 h each, and finally mounted on a slide with DAPI hard set mounting media (Vector Laboratories, Burlingame, CA). The following primary antibody dilutions were used: acetylated-α-tubulin 1:10,000 (Sigma-Aldrich, St. Louis, MO) and CaV1.2 1:50 (Alomone Labs, Jerusalem, Israel). Anti-mouse Texas Red and anti-rabbit FITC fluorescent conjugated secondary antibodies were used at 1:500 (VectorLabs).

Mitochondrial studies

MitoTracker Green FM and MitoTracker Red CMXRos (Cell Signaling Technology) were incubated with cells at 100 nM for 30 min at 37°C. MitoSOX (Life Technologies) was incubated with cells at 5 μM for 10 min at 37°C. After staining, cells were washed three times with PBS and analyzed immediately through microscopy or flow cytometry. For microscopic analysis, cells were grown on custom glass-bottom cell culture plates and imaged under a Nikon Eclipse TE2000-U microscope controlled by MetaMorph software with a 100× objective lens. For flow cytometry studies, cells were detached with trypsin, washed, and analyzed.

DNA damage assessment

Oxidative DNA lesions were detected with an 8-oxoguanine antibody (Santa Cruz). Detached cells were fixed in 4% formaldehyde for 10 min at 37°C and permeabilized in ice-cold 90% methanol for 30 min on ice. After washing with PBS, cells were incubated in PBS containing anti-8-oxoguanine antibody (1:50), 0.5% Tween-20, and 5% FBS for 1 h. Cells were washed and incubated in PBS containing anti-mouse Texas Red antibody (1:500), 0.5% Tween-20, and 5% FBS for 1 h. Cells were then washed and analyzed with flow cytometer.

Mitochondrial DNA and mRNA measurement

Total cellular DNA was obtained using the DNeasy Blood & Tissue Kit (Qiagen) and used for detection with PCR primers listed below to quantify the nuclear (*18S rRNA*) to mitochondrial DNA (*Coi*) ratio as described (Brown and Clayton, 2002; Bai et al., 2004). Total cellular RNA was obtained using TRIzol (Life Technologies) and reverse transcribed to cDNA using the High-Capacity cDNA Reverse Transcription Kit (Applied Biosystems). PCR detection of expression genes was performed using the primers listed below comparing mitochondrial encoded oxidative phosphorylation genes (*ATP5γ1* and *CytC*) to nuclear encoded *β-Actin* as described (Yoon et al., 2010) (Table 2).

Western blot analysis

Cells were scraped from culture plates in the presence of RIPA buffer supplemented with Complete Protease Inhibitor (Roche,

TABLE 2. Primer sequences

Descriptions	Sequences
Coi F	5′-GCCCCAGATATAGCATTCCC-3′
Coi R	5′-GTTCATCCTGTTCCTGCTCC-3′
18S rRNA F	5′-TAGAGGGACAAGTGGCGTTC-3′
18S rRNA R	5′-CGCTGAGCCAGTCAGTGT-3′
ATP5γ1 F	5′-AGTTGGTGTGGCTGGATCA-3′
ATPγ1 R	5′-GCTGCTTGAGAGATGGGTTC-3′
CytC F	5′-GGAGGCAAGCATAAGACTGG-3′
CytC R	5′-TCCATCAGGGTATCCTCTCC-3′
β-actin F	5′-TGTTACCAACTGGGACGACA-3′
β-actin R	5′-GGGGTGTTGAAGGTCTCAAA-3’

New York, NY), incubated on ice with frequent vortexing, and centrifuged. Supernatants were subjected to protein quantification and PAGE on 6–10% SDS gels followed by wet transfer to PVDF membranes and detection using β-catenin 1:1,000, CaV1.2 1:200, NF-κB p65 1:200, and GAPDH 1:1,000 (Cell Signaling Technology, Danvers, MA).

Zebrafish

Adult wild-type AB zebrafish were obtained from the Zebrafish International Resource Center (Eugene, OR) and used for breeding. Embryos were injected with 1 mM antisense translation blocking morpholino oligos (MO; GeneTools) at the 1–2 cell stage. Zebrafish embryos were then cultured at 28.5°C in sterile egg water (Muntean et al., 2010). The following MO sequences were used: *control MO:* 5′-CCT CTT ACC TCA GTT ACA ATT TAT A-3′, *cav1.2 MO:* 5′-ACA TGT TTT TGC TTT CAT TTA CCA T-3′, *pkd2 MO:* 5′-AGG ACG AAC GCG ACT GGA GCT CAT C-3′. Knockdown of CaV1.2 was verified through Western blot analysis. Briefly, zebrafish embryos were dechorionated at 28 h postfertilization and homogenized in RIPA buffer to obtain protein extracts. Western was performed on 50 μg total protein using CaV1.2 (1:200) and GAPDH (1:1,000) antibodies.

Histological examination was used to measure renal cyst formation and hydrocephalus at 3 days postfertilization. Embryos were fixed in a PBS solution containing 4% paraformaldehyde and 2% sucrose overnight at 4°C, dehydrated through an ethanol gradient, and embedded in JB4 resin (Polysciences, Inc., Warrington, PA) as specified in manufacturer's protocol. A Reichert Jung microtome was used to cut 5 μm sections which were subsequently hematoxylin and eosin stained. Heart looping was assessed at 48 h postfertilization by positioning zebrafish on their dorsal axis and recording heart beat to reveal the respective relative locations of the atrium and the ventricle.

Data analysis

Data are reported as the mean ± standard error of the mean. All image analysis was performed using ImageJ. All flow cytometry data were analyzed with BD Accuri C6 software and were presented without any compensation gating. All data were analyzed using IBM SPSS Statistics Version 21 software by performing the student *t*-test for two group comparison or ANOVA test followed by Tukey's post-test for three or more group comparison. Statistical significance is reported with a statistical power greater than 0.8 at $P < 0.05$.

Results

CaV1.2 is not required for primary cilia assembly

We recently reported that the voltage gated L-type calcium channel CaV1.2 localized to primary cilia in bovine LLCPK cells (Jin et al., 2013). We performed immunostaining to verify this finding in mouse renal epithelial cells (Fig. 1). The mouse *Tg737*$^{orpk/orpk}$ cell line contains a hypomorphic mutation in an intraflagellar transport gene (*Ift88*) that is required for cells

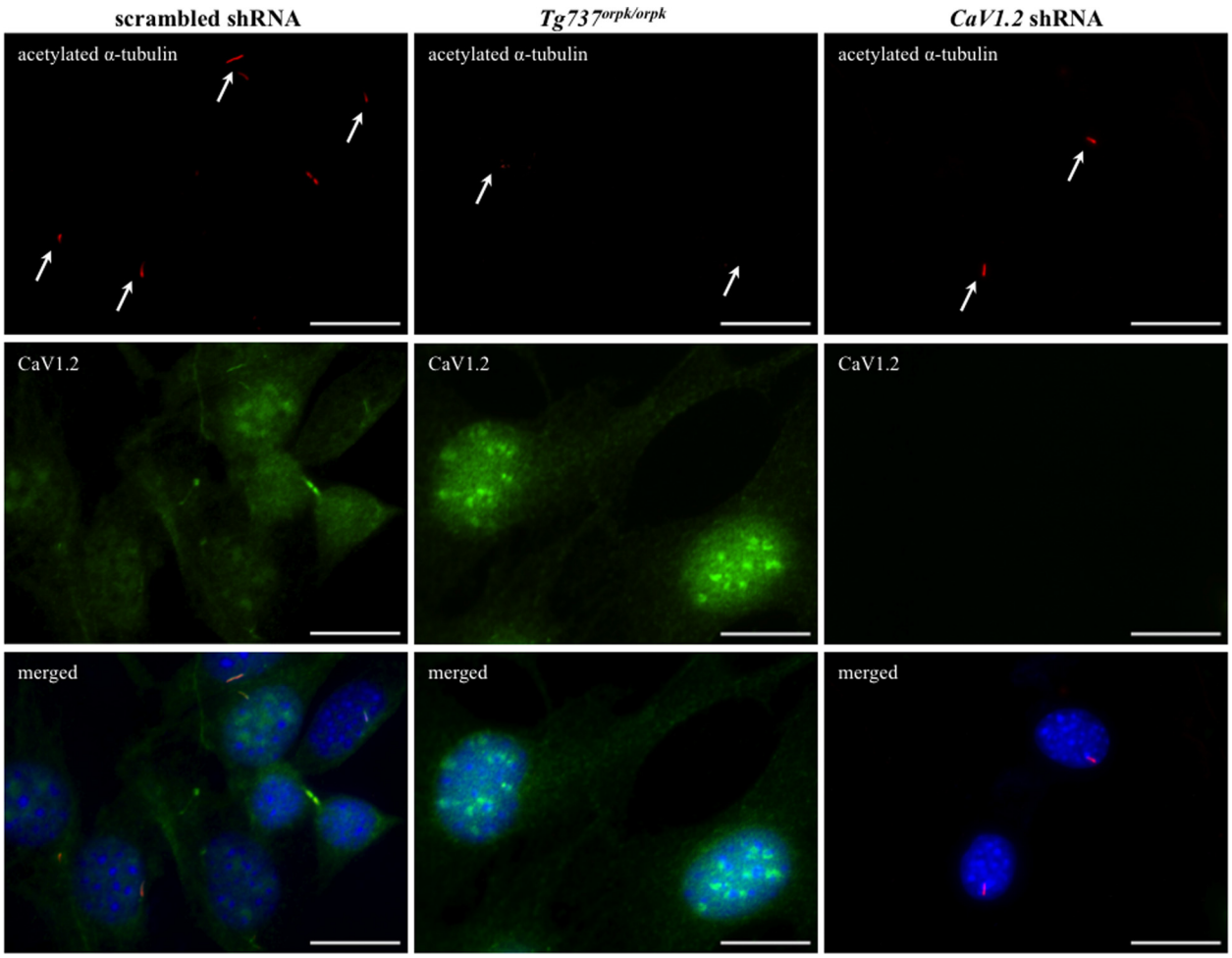

Fig. 1. Localization of CaV1.2 to renal epithelial cilia is not required for primary cilia assembly. Immunofluorescence revealed that CaV1.2 localized to primary cilia in renal epithelial cells (scrambled shRNA) when compared with cilia-deficient cells (Tg737$^{orpk/orpk}$). The presence of primary cilia was confirmed in CaV1.2 shRNA cells. Acetylated-α-tubulin was used as a ciliary marker. Arrow indicates the presence of primary cilium, except in cilia-deficient cells. Bar = 20 μm.

to assemble primary cilia (Moyer et al., 1994). Thus, the *Tg737*$^{orpk/orpk}$ system is a well-established model for studying cells without longer primary cilia, as verified through our immunostaining. We next asked if CaV1.2 played a role in primary cilia assembly. We generated a stable CaV1.2 shRNA knockdown mouse renal epithelial cell line and immunostaining studies revealed that primary cilia were similar to that of scrambled shRNA.

Wnt3a induces mitochondrial biogenesis in CaV1.2-deficient but not cilia-deficient cells

Wnt signaling has recently been reported to regulate mitochondrial physiology (Yoon et al., 2010). To assess mitochondrial mass, cells were stained with Mito Tracker Green (MTG) and observed live using fluorescence microscopy. When treated with recombinant Wnt3a, mitochondrial mass increased (Fig. 2a). However, the mitochondrial mass in *Tg737*$^{orpk/orpk}$ cells was unchanged after Wnt3a treatment. We next performed this experiment in CaV1.2 shRNA cells and the results were similar to that of the scrambled control. To quantify these findings, MTG fluorescence was recorded using flow cytometry which confirmed our fluorescent observation (Fig. 2b). Our MTG studies were further validated using a common technique by comparing mitochondrial DNA (*Coi*) to nuclear DNA (*18S rRNA*) (Brown and Clayton, 2002; Bai et al., 2004). As expected, Wnt3a did indeed statistically increase mitochondrial biogenesis in scrambled and CaV1.2 shRNA but not in *Tg737*$^{orpk/orpk}$ cells (Fig. 2c). Our immunofluorescence study showed that Wnt3a did not alter CaV1.2 localization to cilia (Table 3).

Wnt3a increases mitochondrial activity in CaV1.2-deficient cells while decreasing activity in cilia-deficient cells

We next asked if Wnt3a would have an effect on mitochondrial oxidative phosphorylation (activity) in *Tg737*$^{orpk/orpk}$ cells. Similar to before, we stained cells with Mito Tracker Red (MTR). Unlike MTG, MTR staining is dependent on the mitochondrial membrane potential (Poot and Pierce, 2001; Pendergrass et al., 2004). Therefore, increased staining

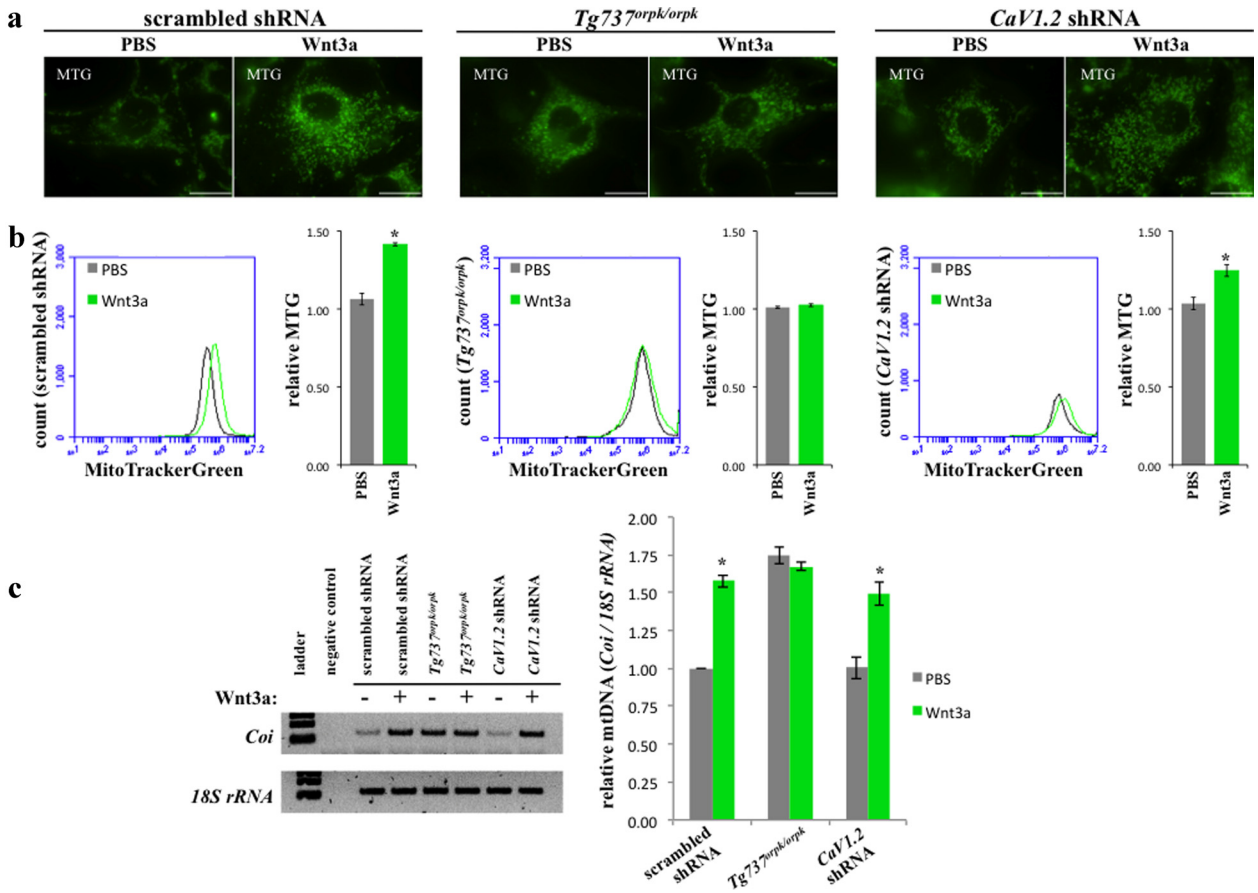

Fig. 2. Wnt3a induces mitochondrial biogenesis in CaV1.2 shRNA but not Tg737$^{orpk/orpk}$ cells. a: Mitochondrial mass was assessed by staining cells with Mito Tracker Green. Wnt3a was found to induce mitochondrial mass in scrambled and CaV1.2 shRNA cells but had no effect on Tg737$^{orpk/orpk}$ when examined using fluorescence microscopy (bar = 20 μm). b: Results were quantified using flow cytometry. c: Mitochondrial DNA was measured using PCR by taking the ratio of a mitochondrial gene (Coi) to a nuclear gene (18S rRNA) (N = 3).

correlates to increased oxidative phosphorylation. As expected, Wnt3a increased MTR staining in scrambled and CaV1.2 shRNA cells when observed using fluorescence microscopy (Fig. 3a). However, mitochondrial activity decreased in *Tg737*$^{orpk/orpk}$ cells. We again quantified our findings using flow cytometry (Fig. 3b). Wnt3a significantly increased mitochondrial activity in scrambled and CaV1.2 shRNA while significantly decreasing activity in *Tg737*$^{orpk/orpk}$ cells. To verify these results, we compared expression of two key mitochondrial encoded oxidative phosphorylation genes (ATP Synthase 5γ1 and Cytochrome *c*) relative to that of nuclear encoded β-actin (Fig. 3c).

TABLE 3. CaV1.2 ciliary localization

	% CaV1.2 localization to cilia	N
PBS (control)		
Scramble shRNA	91.1	45
Tg737$^{orpk/orpk}$	91.7	36
CaV1.2 shRNA	0.0	41
Wnt3a (100 ng/ml)		
Scramble shRNA	90.4	52
Tg737$^{orpk/orpk}$	92.3	39
CaV1.2 shRNA	0.0	46

Wnt3a increases ROS and DNA damage in CaV1.2-deficient but not in cilia-deficient cells

An inevitable consequence of oxidative phosphorylation is the generation of reactive oxygen species (ROS) (Boveris et al., 1972; Boveris and Chance, 1973). MitoSOX is a cell permeable red fluorescent indicator specific for mitochondrial ROS. We therefore stained cells with MitoSOX and observed a significant increase in mitochondrial ROS in scrambled and CaV1.2 shRNA after treatment with Wnt3a (Fig. 4a). A significant decrease in staining was observed in *Tg737*$^{orpk/orpk}$ cells (Fig. 4b). Genomic DNA can be damaged by ROS to form DNA lesions resulting from mismatched repairs (Kasai et al., 1984). Thus, we quantified the levels of 8-Oxoguanine, a common DNA lesion formed by mismatched Adenine (Kasai, 1997). Treatment with Wnt3a was found to increase 8-Oxoguanine in scrambled and CaV1.2 shRNA while no change was observed in *Tg737*$^{orpk/orpk}$ cells (Fig. 4c).

Cilia modulates Wnt signaling to regulate CaV1.2 expression

As previously reported, Wnt3a treatment induced β-catenin expression in all cells (Aberle et al., 1997). We confirmed this in our system, including in *Tg737*$^{orpk/orpk}$ and CaV1.2 shRNA cells (Fig. 5). Consistent with previous study (Corbit et al., 2008),

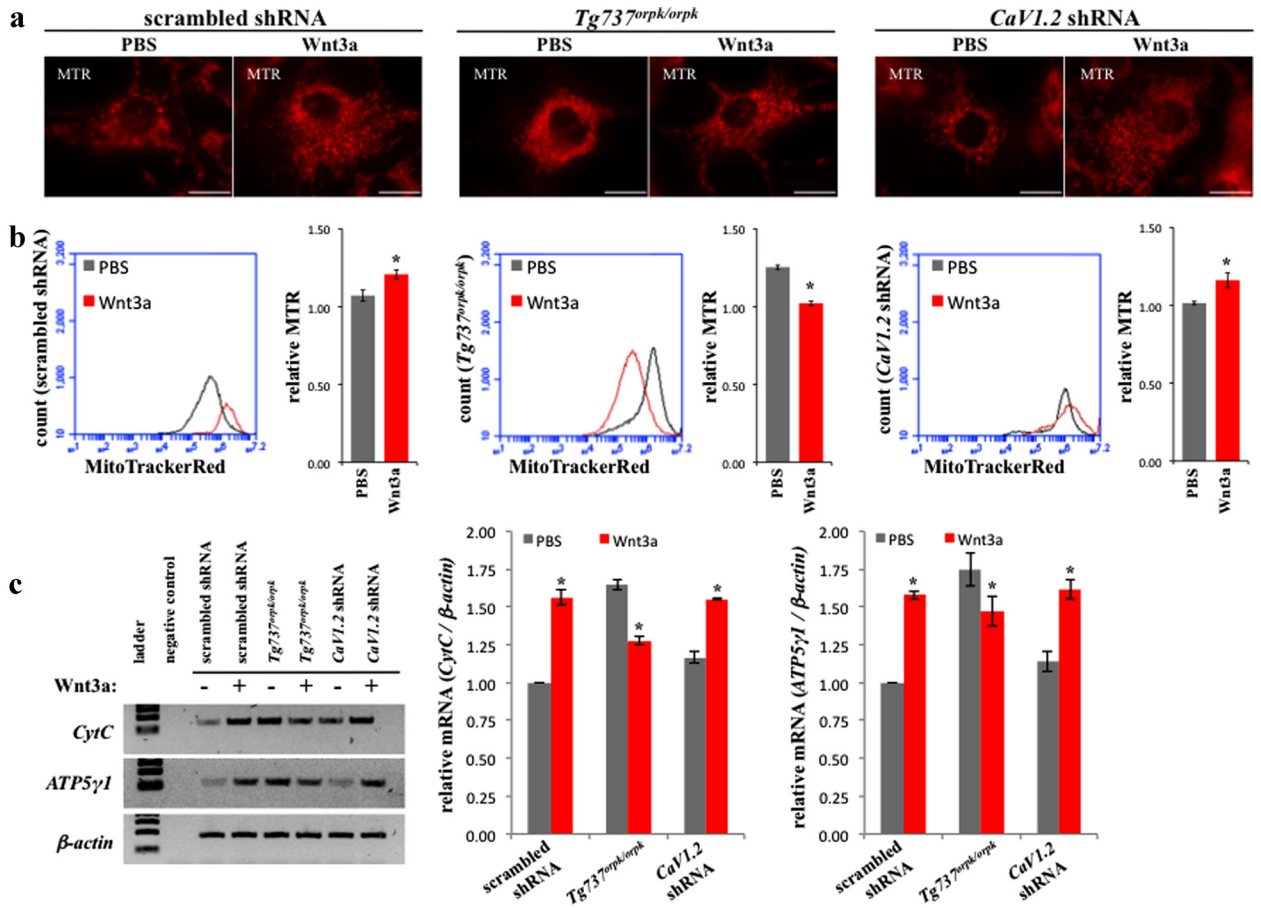

Fig. 3. Wnt3a increases mitochondrial activity in CaV1.2 shRNA but decreasing activity in Tg737$^{orpk/orpk}$ cells. a: Mitochondrial oxidative phosphorylation was used to indicate activity through Mito Tracker Red staining. Wnt3a was found to increase oxidative phosphorylation in scrambled and CaV1.2 shRNA cells while decreasing oxidative phosphorylation in Tg737$^{orpk/orpk}$ when examined using fluorescence microscopy (bar = 20 μm). b: Results were quantified using flow cytometry. c: Two mitochondrial mRNAs encoded oxidative phosphorylation genes (CytC and ATP5γ1) were measured using PCR normalized to nuclear encoded β-actin (N = 3).

Tg737$^{orpk/orpk}$ cells showed a higher basal level of β-catenin than control. Further, Wnt3a treatment increased CaV1.2 expression in scrambled shRNA while decreasing CaV1.2 in *Tg737$^{orpk/orpk}$* cells. Of note is that CaV1.2 expression was not detectable in CaV1.2 shRNA cells, confirming knockdown of CaV1.2 in our stable cell line.

The DNA damage response (DDR) is a cellular mechanism to recover from DNA lesions, such as 8-Oxoguanine (Kasai et al., 1984; Jackson and Bartek, 2009). One arm of this cell survival pathway is the activation of nuclear factor κB p65 (NFκB p65) (Janssens and Tschopp, 2006). Through Western blot analysis, we also found that Wnt3a induced NFκB p65 expression in scrambled and CaV1.2 shRNA (Fig. 5). On the other hand, *Tg737$^{orpk/orpk}$* cells expressed a high basal level of NFκB p65 which decreased in response to Wnt3a. In addition, CaV1.2 expression was found to correlate with NFκB p65.

CaV1.2 knockdown zebrafish develop PKD phenotypes

We have shown that CaV1.2 localizes to primary cilia and have now elucidated the mechanism by which CaV1.2 expression is regulated in renal epithelial cells. To assess the biological significance of CaV1.2 expression, we used antisense morpholinos to knockdown CaV1.2 in zebrafish. Knockdown of the ciliary calcium channel polycystin-2 in zebrafish has been reported to result in PKD phenotypes including renal cyst formation, hydrocephalus, and left-right asymmetry (Obara et al., 2006). Our study showed that knockdown of *pkd2* increased CaV1.2 expression (Fig. 6). This slight increase in CaV1.2 was significant compared to the control morpholino. Interestingly, similar phenotypes were observed in CaV1.2 morpholino (*cav1.2 MO*) zebrafish. Compared with a non-specific control morpholino (*control MO*) injection, *cav1.2 MO* zebrafish developed renal cysts (Fig. 7a), hydrocephalus (Fig. 7b) and various heart-looping defects (Fig. 7c). As generally accepted (Bakkers, 2011), left-right asymmetry was assessed by measuring the relative position of the cardiac atrium and ventricle with respect to the dorsal axis (Supplemental Movie 1).

Discussion

Non-motile primary cilia have been found to play a critical role in Wnt signaling by restricting β-catenin accumulation. Overexpression of polycystin-1 (a ciliary signaling receptor) inhibits GSK3β and stabilizes β- catenin (Kim et al., 1999).

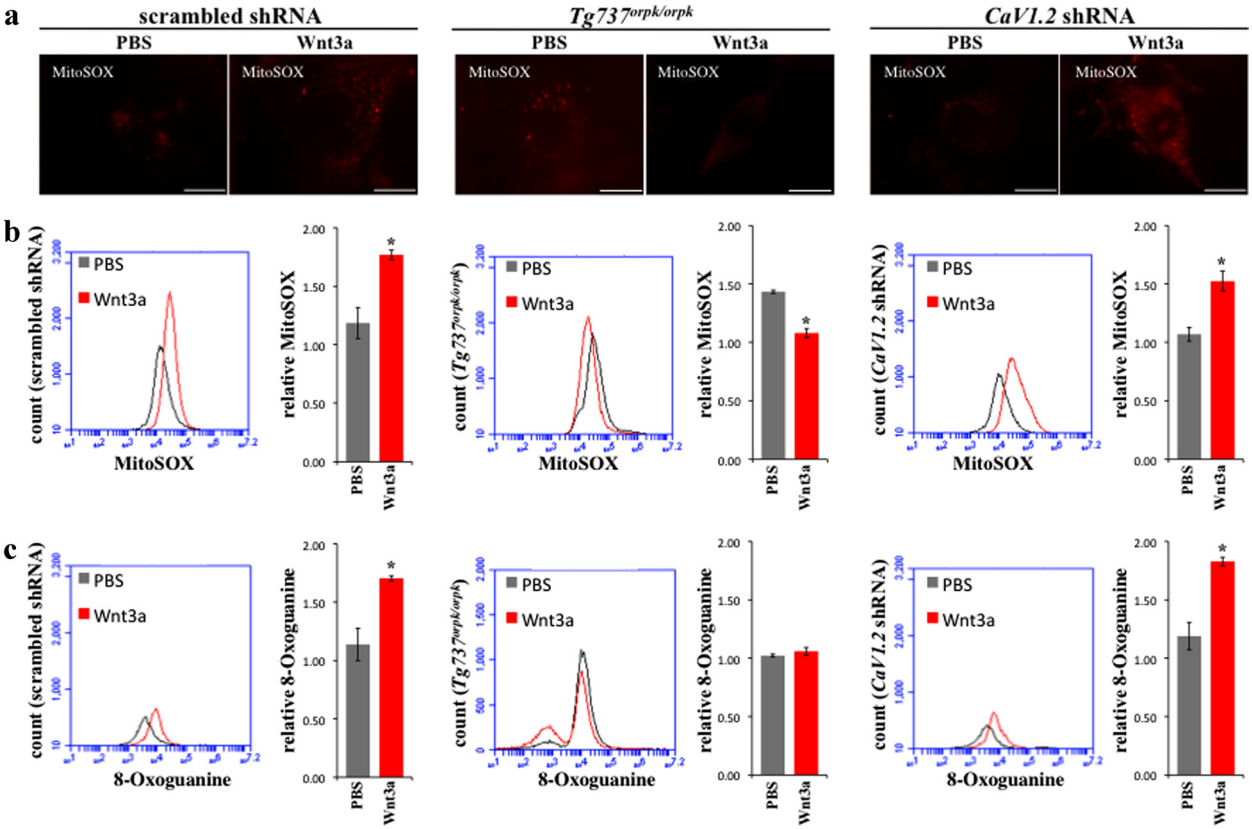

Fig. 4. Wnt3a increases ROS and DNA damage in CaV1.2 shRNA but not in Tg737$^{orpk/orpk}$ cells. a: Mitochondrial ROS was assessed by staining cells with MitoSOX. Wnt3a was found to increase ROS in scrambled and CaV1.2 shRNA cells while decreasing ROS in Tg737$^{orpk/orpk}$ when examined using fluorescence microscopy (bar = 20 μm). b: Results were quantified using flow cytometry. c: Wnt3a increased formation of the oxidative DNA lesion 8-Oxoguanine in scrambled and CaV1.2 shRNA cells but had no effect on Tg737$^{orpk/orpk}$ cells (N = 3).

Polycystin-2 (encoded by *Pkd2*) is calcium channel forming protein found in primary cilia. In *Pkd2*$^{-/-}$ embryos, cilia length was found to be decreased while β-catenin was upregulated (Kim et al., 2009). Interestingly, transgenic mice overexpressing β-catenin also developed cystic kidneys (Saadi-Kheddouci et al., 2001). Further, LRP6$^{-/-}$ (a component of the Wnt receptor complex) mouse embryos die in utero with cystic kidneys (Pinson et al., 2000). Thus, primary cilia and Wnt signaling play a crucial role in PKD (Corbit et al., 2008).

Given that Wnt signaling also modulates mitochondrial physiology (Yoon et al., 2010), we examined the role of cilia in regards to mitochondria. *Tg737*$^{orpk/orpk}$ contains an intron insertion at the 3′ end of the intraflagellar transport 88 (*Ift88*) gene which results in a hypomorphic mutation that prevents ciliogenesis (Moyer et al., 1994). We used *Tg737*$^{orpk/orpk}$ cells as a model for a cilia-deficient system. Through immunostaining, we confirmed the absence of cilia in *Tg737*$^{orpk/orpk}$ cells compared with control (Fig. 1). The voltage-gated L-type calcium channel CaV1.2 also localized to primary cilia. We generated a stable CaV1.2 shRNA cell line and observed no changes in primary cilia compared with control. Further, treatment with Wnt3a had no effect on cilia number or length in scrambled or CaV1.2 shRNA cells (data not shown). Thus, CaV1.2 does not seem to play a role in ciliogenesis.

Mitochondrial biogenesis, oxidative phosphorylation, and generation of reactive oxidative species (ROS) were increased in response to Wnt3a in control renal epithelial cells (Figures 2–4). The elevated levels of oxidative stress increased the formation of DNA lesions and the cellular DNA damage response (DDR). An interesting aspect of this response was an increase in expression of CaV1.2 (Fig. 5). In CaV1.2 knockdown cells, Wnt3a induced a similar effect on mitochondria and DDR. This data suggests that CaV1.2 is a downstream effector in regard to Wnt signaling. In cilia-deficient cells, Wnt3a was unable to induce mitochondrial biogenesis and decreased mitochondrial activity, ROS production, and DDR. CaV1.2 was found to be overexpressed in cilia-deficient cells as a compensatory mechanism; however, its expression decreased following Wnt3a treatment. Therefore, cilia length plays a role in regulating CaV1.2 expression through modulation of Wnt signaling.

Defective primary cilia, indicated by either depletion of key ciliary proteins or fundamental changes in structure/length, results in PKD phenotypes (Wilson, 2004). Here we show that CaV1.2 is a biologically significant ciliary protein. In the absence of CaV1.2 in zebrafish (Fig. 6), PKD phenotypes including renal cyst formation, hydrocephalus, and left-right asymmetry defects were observed (Fig. 7). Moreover, CaV1.2 was found to be overexpressed in *pkd2* knockdown zebrafish. This is intriguing given that both CaV1.2 and PC2 are calcium channel forming proteins in the primary cilium, which further suggests a role for CaV1.2 in PKD pathogenesis. Therefore, CaV1.2 not only localizes to renal epithelial primary cilia, but it is also required for cilia function.

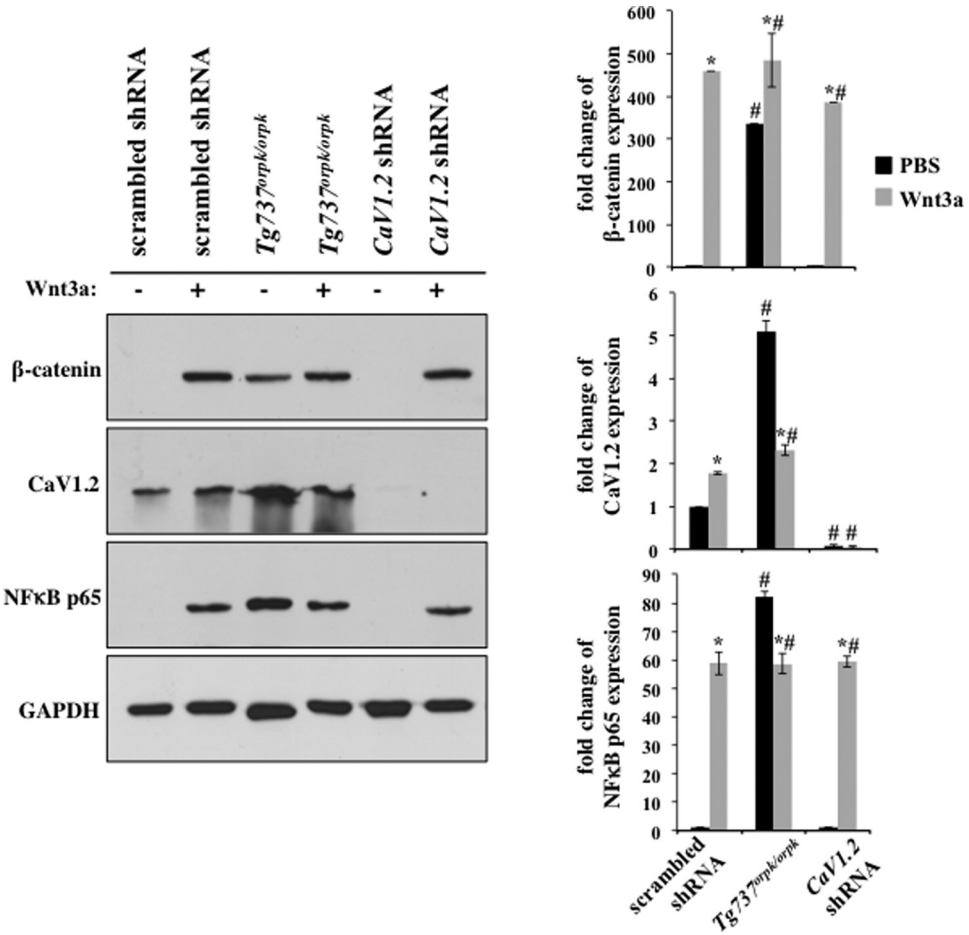

Fig. 5. Cilia modulates Wnt signaling to regulate CaV1.2 expression. Western blotting was performed on cellular protein extracts. Wnt3a treatment increased β-catenin accumulation in all cells, however, Tg737$^{orpk/orpk}$ cells displayed high basal levels of β-catenin. NF-κB p65 was blotted as a readout for DNA damage response (DDR) to ROS induced DNA lesions. Wnt3a induced NF-κB p65 expression in scrambled and CaV1.2 shRNA cells but decreased NF-κB p65 in Tg737$^{orpk/orpk}$ cells. CaV1.2 was overexpressed in Tg737$^{orpk/orpk}$ cells. Wnt3a treatment induced CaV1.2 expression in scrambled shRNA while decreasing expression in Tg737$^{orpk/orpk}$ cells. Data normalized to GAPDH for analysis (N = 3). Asterisks indicate significant difference from the corresponding control group ($P < 0.05$). # signs denote significant difference from the corresponding scrambled shRNA group ($P < 0.05$).

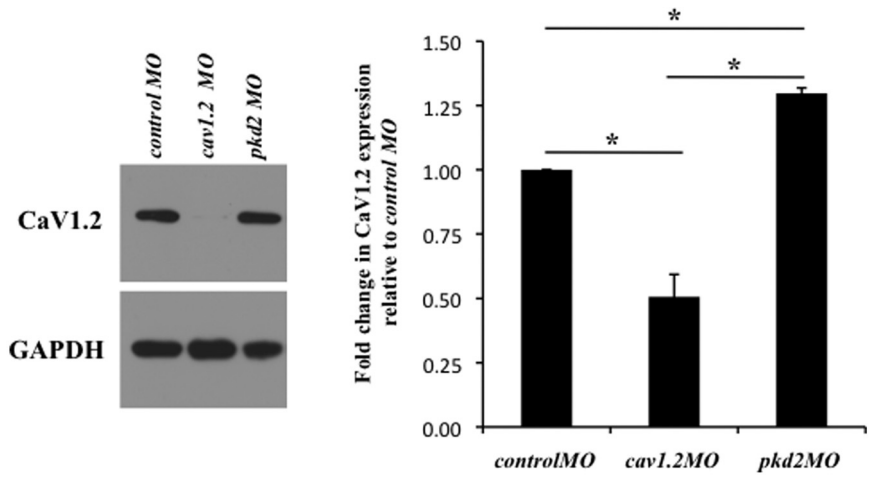

Fig. 6. pkd2 knockdown increases CaV1.2 expression in zebrafish. Embryonic zebrafish protein extracts were obtained at 28 h postfertilization. Western blotting showed that cav1.2MO effectively reduced CaV1.2 expression compared with controlMO. pkd2MO zebrafish were used to further verify morpholino specificity. Results were quantified through one-way ANOVA with Tukey post-test. Statistical significance is reported with a mean difference at the 0.05 level and denoted with an asterisk (N = 3).

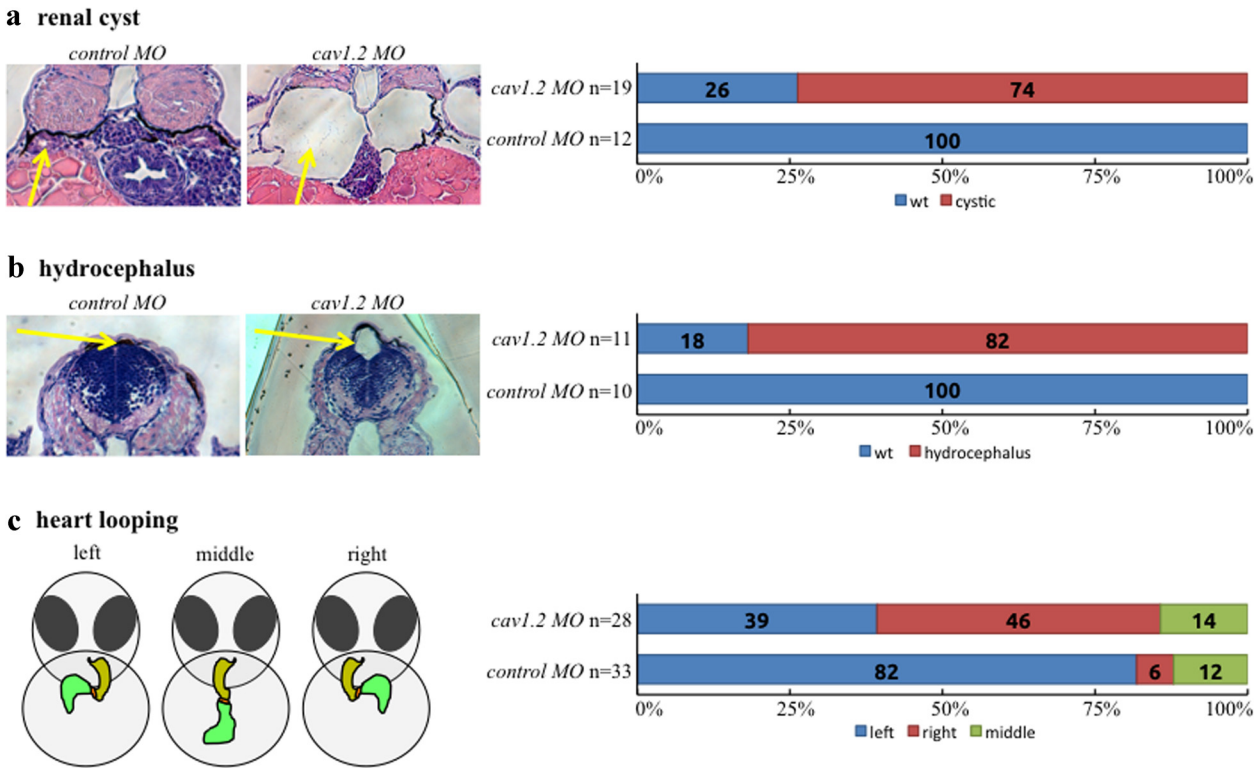

Fig. 7. CaV1.2 knockdown zebrafish develop renal cysts, hydrocephalus, and left-right asymmetry defects. CaV1.2 was knocked down in zebrafish (cav1.2 MO) using morpholino microinjection and compared to a scrambled control morpholino (control MO) to assess phenotypes. Renal cyst formation (a) and hydrocephalus (b) were measured at 3 days postfertilization through standard H&E staining as indicated by arrows. Left-right asymmetry was determined by measuring heart looping (c) at 2 days postfertilization under live microscopy.

Although it has been known that abnormal Wnt signaling leads to renal cyst formation (Lancaster et al., 2009), the underlying mechanism has been unclear. One proposed explanation is that Wnt signaling regulates renal cell proliferation and planar cell polarity to maintain renal tubule homeostasis (Happe et al., 2009). Our present study further suggests that cilia regulate Wnt signaling which ultimately controls CaV1.2 expression. Therefore, in the absence of CaV1.2, ciliary function is compromised leading to formation of renal cysts. In addition, our study also shows a previously unrecognized relationship between primary cilia and mitochondrial function. Overall, we propose that Wnt3a induces β-catenin accumulation in a cilia-dependent manner. This in turn increases mitochondrial biogenesis, oxidative phosphorylation, and generation of ROS that cause genomic DNA damage. The DDR triggers NFκB p65 expression ultimately resulting in increased CaV1.2 expression.

Acknowledgments

This work was supported in part by DOD PR130153 and NIH DK080640.

Literature Cited

Aberle H, Bauer A, Stappert J, Kispert A, Kemler R. 1997. Beta-catenin is a target for the ubiquitin-proteasome pathway. EMBO J 16:3797–3804.

AbouAlaiwi WA, Takahashi M, Mell BR, Jones TJ, Ratnam S, Kolb RJ, Nauli SM. 2009. Ciliary polycystin-2 is a mechanosensitive calcium channel involved in nitric oxide signaling cascades. Circ Res 104:860–869.

Aboualaiwi WA, Muntean BS, Ratnam S, Joe B, Liu L, Booth RL, Rodriguez I, Herbert BS, Bacallao RL, Fruttiger M, Mak TW, Zhou J, Nauli SM. 2013. Survivin-induced abnormal ploidy contributes to cystic kidney and aneurysm formation. Circulation.

Bai RK, Perng CL, Hsu CH, Wong LJ. 2004. Quantitative PCR analysis of mitochondrial DNA content in patients with mitochondrial disease. Ann NY Acad Sci 1011:304–309.

Bakkers J. 2011. Zebrafish as a model to study cardiac development and human cardiac disease. Cardiovasc Res 91:279–288.

Boveris A, Chance B. 1973. The mitochondrial generation of hydrogen peroxide. General properties and effect of hyperbaric oxygen. Biochem J 134:707–716.

Boveris A, Oshino N, Chance B. 1972. The cellular production of hydrogen peroxide. Biochem J 128:617–630.

Brown TA, Clayton DA. 2002. Release of replication termination controls mitochondrial DNA copy number after depletion with 2′,3′-dideoxycytidine. Nucleic acids Res 30:2004–2010.

Carter CS, Vogel TW, Zhang Q, Seo S, Swiderski RE, Moninger TO, Cassell MD, Thedens DR, Keppler-Noreuil KM, Nopoulos P, Nishimura DY, Searby CC, Bugge K, Sheffield VC. 2012. Abnormal development of NG2+PDGFR-alpha+ neural progenitor cells leads to neonatal hydrocephalus in a ciliopathy mouse model. Nat Med 18:1797–1804.

Corbit KC, Shyer AE, Dowdle WE, Gaulden J, Singla V, Chen MH, Chuang PT, Reiter JF. 2008. Kif3a constrains beta-catenin-dependent Wnt signalling through dual ciliary and non-ciliary mechanisms. Nat Cell Biol 10:70–76.

Gerdes JM, Liu Y, Zaghloul NA, Leitch CC, Lawson SS, Kato M, Beachy PA, Beales PL, DeMartino GN, Fisher S, Badano JL, Katsanis N. 2007. Disruption of the basal body compromises proteasomal function and perturbs intracellular Wnt response. Nat Genet 39:1350–1360.

Happe H, Leonhard WN, van der Wal A, van de Water B, Lantinga-van Leeuwen IS, Breuning MH, de Heer E, Peters DJ. 2009. Toxic tubular injury in kidneys from Pkd1-deletion mice accelerates cystogenesis accompanied by dysregulated planar cell polarity and canonical Wnt signaling pathways. Hum Mol Genet 18:2532–2542.

Jackson SP, Bartek J. 2009. The DNA-damage response in human biology and disease. Nature 461:1071–1078.

Janssens S, Tschopp J. 2006. Signals from within: The DNA-damage-induced NF-kappaB response. Cell Death Differ 13:773–784.

Jin X, Mohieldin AM, Muntean BS, Green JA, Shah JV, Mykytyn K, Nauli SM. 2013. Cilioplasm is a cellular compartment for calcium signaling in response to mechanical and chemical stimuli. Cell Mol Life Sci.

Kasai H. 1997. Analysis of a form of oxidative DNA damage, 8-hydroxy-2′-deoxyguanosine, as a marker of cellular oxidative stress during carcinogenesis. Mutat Res 387:147–163.

Kasai H, Tanooka H, Nishimura S. 1984. Formation of 8-hydroxyguanine residues in DNA by X-irradiation. Gann 75:1037–1039.

Kim E, Arnould T, Sellin LK, Benzing T, Fan MJ, Gruning W, Sokol SY, Drummond I, Walz G. 1999. The polycystic kidney disease 1 gene product modulates Wnt signaling. J Biol Chem 274:4947–4953.
Kim I, Ding T, Fu Y, Li C, Cui L, Li A, Lian P, Liang D, Wang DW, Guo C, Ma J, Zhao P, Coffey RJ, Zhan Q, Wu G. 2009. Conditional mutation of Pkd2 causes cystogenesis and upregulates beta-catenin. J Am Soc Nephrol 20:2556–2569.
Lancaster MA, Louie CM, Silhavy JL, Sintasath L, Decambre M, Nigam SK, Willert K, Gleeson JG. 2009. Impaired Wnt-beta-catenin signaling disrupts adult renal homeostasis and leads to cystic kidney ciliopathy. Nat Med 15:1046–1054.
Lancaster MA, Schroth J, Gleeson JG. 2011. Subcellular spatial regulation of canonical Wnt signalling at the primary cilium. Nat Cell Biol 13:700–707.
Moyer JH, Lee-Tischler MJ, Kwon HY, Schrick JJ, Avner ED, Sweeney WE, Godfrey VL, Cacheiro NL, Wilkinson JE, Woychik RP. 1994. Candidate gene associated with a mutation causing recessive polycystic kidney disease in mice. Science 264:1329–1333.
Muntean BS, Horvat CM, Behler JH, Aboualaiwi WA, Nauli AM, Williams FE, Nauli SM. 2010. A comparative study of embedded and anesthetized zebrafish in vivo on myocardiac calcium oscillation and heart muscle contraction. Front Pharmacol 1:139.
Muntean BS, Jin X, Nauli SM. Chapter 9: Primary cilia are mechanosensory organelles with chemosensory roles. Mechanosensitivity and mechanotransduction. ISBN: 978-994-007-2003-2009.
Nauli SM, Alenghat FJ, Luo Y, Williams E, Vassilev P, Li X, Elia AE, Lu W, Brown EM, Quinn SJ, Ingber DE, Zhou J. 2003. Polycystins 1 and 2 mediate mechanosensation in the primary cilium of kidney cells. Nat Genet 33:129–137.
Nauli SM, Kawanabe Y, Kaminski JJ, Pearce WJ, Ingber DE, Zhou J. 2008. Endothelial cilia are fluid shear sensors that regulate calcium signaling and nitric oxide production through polycystin-1. Circulation 117:1161–1171.
Norris DP. 2012. Cilia, calcium and the basis of left-right asymmetry. BMC Biol 10:102.
Obara T, Mangos S, Liu Y, Zhao J, Wiessner S, Kramer-Zucker AG, Olale F, Schier AF, Drummond IA. 2006. Polycystin-2 immunolocalization and function in zebrafish. J Am Soc Nephrol 17:2706–2718.
Pendergrass W, Wolf N, Poot M. 2004. Efficacy of MitoTracker Green and CMXrosamine to measure changes in mitochondrial membrane potentials in living cells and tissues. Cytometry A 61:162–169.
Pinson KI, Brennan J, Monkley S, Avery BJ, Skarnes WC. 2000. An LDL-receptor-related protein mediates Wnt signalling in mice. Nature 407:535–538.
Poot M, Pierce RH. 2001. Analysis of mitochondria by flow cytometry. Methods Cell Biol 64:117–128.
Saadi-Kheddouci S, Berrebi D, Romagnolo B, Cluzeaud F, Peuchmaur M, Kahn A, Vandewalle A, Perret C. 2001. Early development of polycystic kidney disease in transgenic mice expressing an activated mutant of the beta-catenin gene. Oncogene 20:5972–5981.
Wilson PD. 2004. Polycystic kidney disease. N Engl J Med 350:151–164.
Yoon JC, Ng A, Kim BH, Bianco A, Xavier RJ, Elledge SJ. 2010. Wnt signaling regulates mitochondrial physiology and insulin sensitivity. Genes Dev 24:1507–1518.

Supporting Information

Additional supporting information may be found in the online version of this article at the publisher's web-site.

Journal of Cellular Physiology

Primary Cilium Regulates CaV1.2 Expression Through Wnt Signaling

BRIAN S. MUNTEAN,[1] XINGJIAN JIN,[2] FREDERICK E. WILLIAMS,[2] AND SURYA M. NAULI[1,2]*

[1]*Department of Medicinal and Biological Chemistry, The University of Toledo, Toledo, Ohio*

[2]*Department of Pharmacology, The University of Toledo, Toledo, Ohio*

Primary cilia are sensory organelles that provide a feedback mechanism to restrict Wnt signaling in the absence of endogenous Wnt activators. Abnormal Wnt signaling has been shown to result in polycystic kidney disease (PKD) although the exact mechanism has been debated. Previously, we reported that the calcium channel CaV1.2 functions in primary cilia. In this study, we show that CaV1.2 expression level is regulated by Wnt signaling. This occurs through modulation of mitochondrial mass and activity resulting in increased reactive oxygen species which generate oxidative DNA lesions. We found that the subsequent cellular DNA damage response triggers increased CaV1.2 expression. In the absence of primary cilia where Wnt signaling is upregulated, we found that CaV1.2 is overexpressed as a compensatory mechanism. We show for the first time that CaV1.2 knockdown in zebrafish results in classic primary cilia defects including renal cyst formation, hydrocephalus, and left-right asymmetry defects. Our study shows that suppressed Wnt signaling prevents CaV1.2 expression ultimately resulting in PKD phenotypes. Thus, CaV1.2 expression is tightly regulated through Wnt signaling and plays an essential sensory role in primary cilia necessary for cellular homeostasis.

J. Cell. Physiol. 229: 1926–1934, 2014.

Wnt signaling is an important regulator of cellular development and proliferation. In the absence of Wnt ligands, a complex consisting of Axin, adenomatous polyposis coli (APC), and glycogen synthase kinase 3β (GSK3β) induces β-catenin for ubiquitylation by SCF E3 ligases and eventual proteasomal degradation (Aberle et al., 1997). Wnt signal transduction occurs when secreted Wnt ligands bind Frizzled receptors resulting in phosphorylation of LRP5/6. The Axin-APC-GSK3β complex is then recruited to LRP5/6 at the cell membrane which prevents β-catenin from being degraded. The accumulated β-catenin translocates to the nucleus and activates transcription of Wnt target genes (Muntean et al., 2012).

Primary cilia are non-motile sensory organelles present as a single copy on most differentiated cells in the body. Calcium signaling through primary cilium is essential for renal epithelial homeostasis (Nauli et al., 2003; Jin et al., 2013). Cilia extend from the cell surface through the basal body via intraflagellar transport (Moyer et al., 1994). The most common pathologies resulting from cilia dysfunction include polycystic kidney (Wilson, 2004), hypertension (Nauli et al., 2008; AbouAlaiwi et al., 2009), aneurysm (Aboualaiwi et al., 2013), hydrocephalus (Carter et al., 2012), and left-right asymmetry defects (Norris, 2012).

Abnormal Wnt signaling has also been linked to polycystic kidney disease (PKD) (Lancaster et al., 2009). For example, increased cytosolic and nuclear β-catenin accumulation has been shown in various cilia mutant cells (Gerdes et al., 2007; Lancaster et al., 2011). Thus, primary cilia are thought to provide a feedback mechanism that restricts Wnt signaling in the absence of appropriate ligands (Gerdes et al., 2007; Lancaster et al., 2009, 2011).

We recently showed that voltage-gated L-type calcium channel CaV1.2 localized to primary cilia in renal epithelia (Jin et al., 2013). Because Wnt signaling has also been reported to modulate mitochondrial physiology (Yoon et al., 2010), we hypothesized that primary cilia play a role in Wnt regulation of mitochondria through CaV1.2. We show that although CaV1.2 is not required for cilia formation, Wnt increases mitochondria mass and activity in CaV1.2 deficient renal epithelial cells. This increases mitochondria reactive oxidative species (ROS) and DNA damage, resulting in PKD phenotypes. Thus, our study suggests that primary cilia may play a role in CaV1.2 expression level through Wnt regulation of mitochondria.

Materials and Methods

The experimental use of zebrafish was approved by The University of Toledo's Institutional Animal Care and Use Committee (IACUC). The use of lentiviral components was approved by the Institutional Biosafety Committee of The University of Toledo.

Cell culture

Immortalized mouse renal epithelial wild-type and *Tg737*$^{orpk/orpk}$ cells were cultured in Dulbecco's Modified Eagle Medium (Corning Cellgro) supplemented with 10% fetal bovine serum (HyClone Laboratories, Logan, Utah) and 1% penicillin/streptomycin (Corning Cellgro) at 39°C in 5% CO_2, as previously described (Aboualaiwi et al., 2013). Prior to experiments, cells were treated with 100 ng/ml recombinant Wnt3a (R&D Systems, Minneapolis, MN) for 3 days and serum starved for 24 h.

RNAi knockdown cells

shRNA lentiviral vectors specific to *Cacna1c* (*Origene*; pGFP-C-shLenti clone ID: TL500242) were transfected into HEK293T cells. Viral supernatants were collected after 48 h, centrifuged, and passed through a 0.45 μm filter. Cells were then spin-inoculated with pseudoviral particles containing 8 μg/ml polybrene at 2,500 rpm for 30 min at 30°C and then cultured for up to 1 week. CaV1.2 knockdown was verified through Western blot analysis.

Brian S. Muntean and Xingjian Jin contributed equally to this work.

* Correspondence to: Surya M. Nauli, Department of Pharmacology, The University of Toledo, MS 1015, Health Education Building; Room 274, 3000 Arlington Ave, Toledo, OH 43614.
E-mail: surya.nauli@utoledo.edu

Manuscript Received: 20 January 2014
Manuscript Accepted: 1 April 2014

Accepted manuscript online in Wiley Online Library (wileyonlinelibrary.com): 2 April 2014.
DOI: 10.1002/jcp.24642

TABLE 1. shRNA sequences

Descriptions	Sequences
Scrambled control	5′-TGACCACCCTGACCTACGGCGTGCAGTGC-3′
Cacna1c	5′-TCAGAAGTGCCTCACTGTTCTCGTGACCT-3′

Stable knockdown cell lines were obtained through puromycin selection. The following shRNA sequences were used (Table 1).

Immunostaining studies

Cells were grown to confluence on collagen-coated glass coverslips and differentiated in serum-free media for 24 h. Cells were then fixed in 4% paraformaldehyde in PBS containing 2% sucrose, permeabilized in 10% triton X-100, incubated sequentially with primary followed by secondary antibodies for 1 h each, and finally mounted on a slide with DAPI hard set mounting media (Vector Laboratories, Burlingame, CA). The following primary antibody dilutions were used: acetylated-α-tubulin 1:10,000 (Sigma-Aldrich, St. Louis, MO) and CaV1.2 1:50 (Alomone Labs, Jerusalem, Israel). Anti-mouse Texas Red and anti-rabbit FITC fluorescent conjugated secondary antibodies were used at 1:500 (VectorLabs).

Mitochondrial studies

MitoTracker Green FM and MitoTracker Red CMXRos (Cell Signaling Technology) were incubated with cells at 100 nM for 30 min at 37°C. MitoSOX (Life Technologies) was incubated with cells at 5 μM for 10 min at 37°C. After staining, cells were washed three times with PBS and analyzed immediately through microscopy or flow cytometry. For microscopic analysis, cells were grown on custom glass-bottom cell culture plates and imaged under a Nikon Eclipse TE2000-U microscope controlled by MetaMorph software with a 100× objective lens. For flow cytometry studies, cells were detached with trypsin, washed, and analyzed.

DNA damage assessment

Oxidative DNA lesions were detected with an 8-oxoguanine antibody (Santa Cruz). Detached cells were fixed in 4% formaldehyde for 10 min at 37°C and permeabilized in ice-cold 90% methanol for 30 min on ice. After washing with PBS, cells were incubated in PBS containing anti-8-oxoguanine antibody (1:50), 0.5% Tween-20, and 5% FBS for 1 h. Cells were washed and incubated in PBS containing anti-mouse Texas Red antibody (1:500), 0.5% Tween-20, and 5% FBS for 1 h. Cells were then washed and analyzed with flow cytometer.

Mitochondrial DNA and mRNA measurement

Total cellular DNA was obtained using the DNeasy Blood & Tissue Kit (Qiagen) and used for detection with PCR primers listed below to quantify the nuclear (*18S rRNA*) to mitochondrial DNA (*Coi*) ratio as described (Brown and Clayton, 2002; Bai et al., 2004). Total cellular RNA was obtained using TRIzol (Life Technologies) and reverse transcribed to cDNA using the High-Capacity cDNA Reverse Transcription Kit (Applied Biosystems). PCR detection of expression genes was performed using the primers listed below comparing mitochondrial encoded oxidative phosphorylation genes (*ATP5γ1* and *CytC*) to nuclear encoded *β-Actin* as described (Yoon et al., 2010) (Table 2).

Western blot analysis

Cells were scraped from culture plates in the presence of RIPA buffer supplemented with Complete Protease Inhibitor (Roche,

TABLE 2. Primer sequences

Descriptions	Sequences
Coi F	5′-GCCCCAGATATAGCATTCCC-3′
Coi R	5′-GTTCATCCTGTTCCTGCTCC-3′
18S rRNA F	5′-TAGAGGGACAAGTGGCGTTC-3′
18S rRNA R	5′-CGCTGAGCCAGTCAGTGT-3′
ATP5γ1 F	5′-AGTTGGTGTGGCTGGATCA-3′
ATPγ1 R	5′-GCTGCTTGAGAGATGGGTTC-3′
CytC F	5′-GGAGGCAAGCATAAGACTGG-3′
CytC R	5′-TCCATCAGGGTATCCTCTCC-3′
β-actin F	5′-TGTTACCAACTGGGACGACA-3′
β-actin R	5′-GGGGTGTTGAAGGTCTCAAA-3’

New York, NY), incubated on ice with frequent vortexing, and centrifuged. Supernatants were subjected to protein quantification and PAGE on 6–10% SDS gels followed by wet transfer to PVDF membranes and detection using β-catenin 1:1,000, CaV1.2 1:200, NF-κB p65 1:200, and GAPDH 1:1,000 (Cell Signaling Technology, Danvers, MA).

Zebrafish

Adult wild-type AB zebrafish were obtained from the Zebrafish International Resource Center (Eugene, OR) and used for breeding. Embryos were injected with 1 mM antisense translation blocking morpholino oligos (MO; GeneTools) at the 1–2 cell stage. Zebrafish embryos were then cultured at 28.5°C in sterile egg water (Muntean et al., 2010). The following MO sequences were used: *control MO:* 5′-CCT CTT ACC TCA GTT ACA ATT TAT A-3′, *cav1.2 MO:* 5′-ACA TGT TTT TGC TTT CAT TTA CCA T-3′, *pkd2 MO:* 5′-AGG ACG AAC GCG ACT GGA GCT CAT C-3′. Knockdown of CaV1.2 was verified through Western blot analysis. Briefly, zebrafish embryos were dechorionated at 28 h postfertilization and homogenized in RIPA buffer to obtain protein extracts. Western was performed on 50 μg total protein using CaV1.2 (1:200) and GAPDH (1:1,000) antibodies.

Histological examination was used to measure renal cyst formation and hydrocephalus at 3 days postfertilization. Embryos were fixed in a PBS solution containing 4% paraformaldehyde and 2% sucrose overnight at 4°C, dehydrated through an ethanol gradient, and embedded in JB4 resin (Polysciences, Inc., Warrington, PA) as specified in manufacturer's protocol. A Reichert Jung microtome was used to cut 5 μm sections which were subsequently hematoxylin and eosin stained. Heart looping was assessed at 48 h postfertilization by positioning zebrafish on their dorsal axis and recording heart beat to reveal the respective relative locations of the atrium and the ventricle.

Data analysis

Data are reported as the mean ± standard error of the mean. All image analysis was performed using ImageJ. All flow cytometry data were analyzed with BD Accuri C6 software and were presented without any compensation gating. All data were analyzed using IBM SPSS Statistics Version 21 software by performing the student *t*-test for two group comparison or ANOVA test followed by Tukey's post-test for three or more group comparison. Statistical significance is reported with a statistical power greater than 0.8 at $P < 0.05$.

Results

CaV1.2 is not required for primary cilia assembly

We recently reported that the voltage gated L-type calcium channel CaV1.2 localized to primary cilia in bovine LLCPK cells (Jin et al., 2013). We performed immunostaining to verify this finding in mouse renal epithelial cells (Fig. 1). The mouse *Tg737*$^{orpk/orpk}$ cell line contains a hypomorphic mutation in an intraflagellar transport gene (*Ift88*) that is required for cells

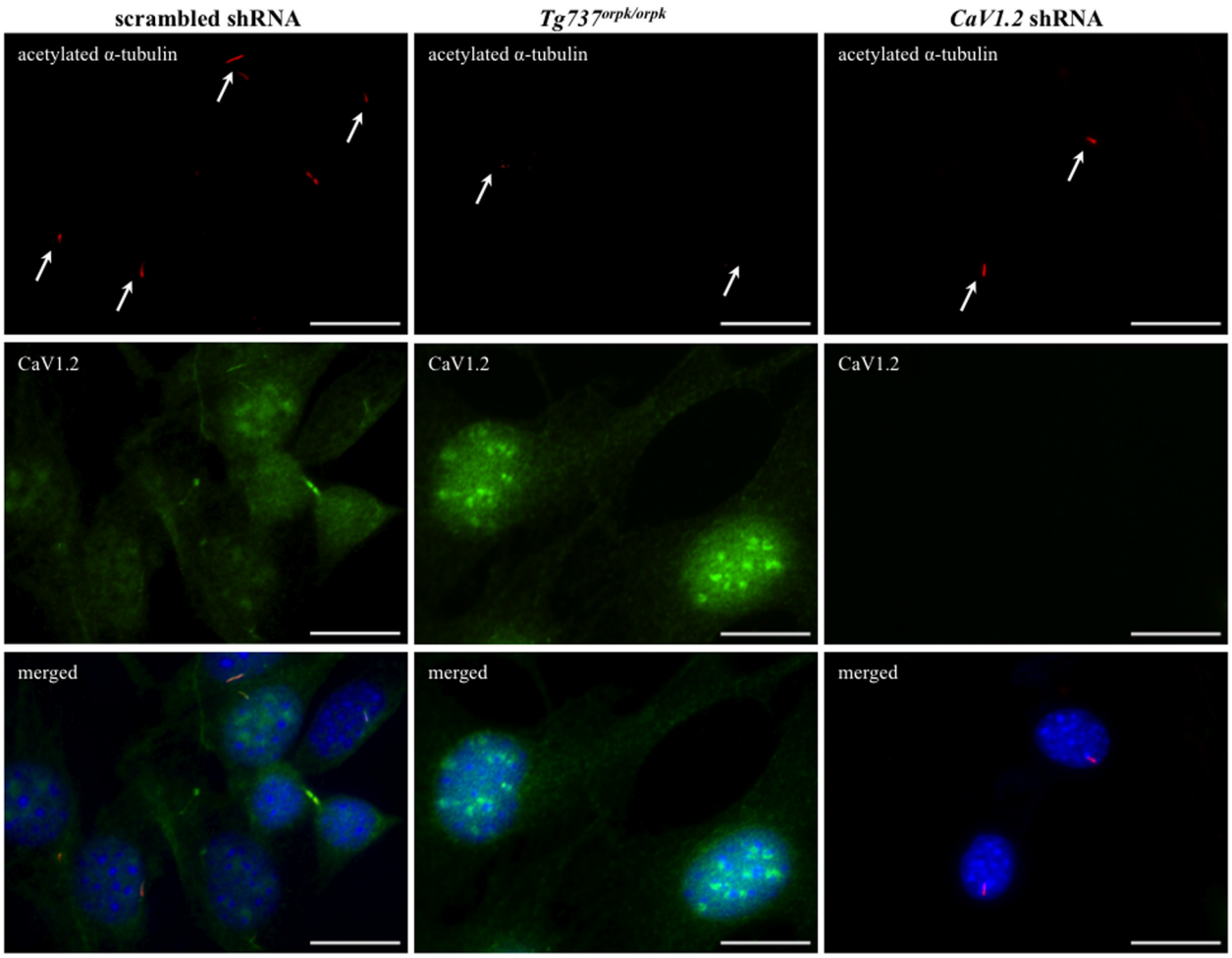

Fig. 1. Localization of CaV1.2 to renal epithelial cilia is not required for primary cilia assembly. Immunofluorescence revealed that CaV1.2 localized to primary cilia in renal epithelial cells (scrambled shRNA) when compared with cilia-deficient cells (Tg737$^{orpk/orpk}$). The presence of primary cilia was confirmed in CaV1.2 shRNA cells. Acetylated-α-tubulin was used as a ciliary marker. Arrow indicates the presence of primary cilium, except in cilia-deficient cells. Bar = 20 μm.

to assemble primary cilia (Moyer et al., 1994). Thus, the *Tg737*$^{orpk/orpk}$ system is a well-established model for studying cells without longer primary cilia, as verified through our immunostaining. We next asked if CaV1.2 played a role in primary cilia assembly. We generated a stable CaV1.2 shRNA knockdown mouse renal epithelial cell line and immunostaining studies revealed that primary cilia were similar to that of scrambled shRNA.

Wnt3a induces mitochondrial biogenesis in CaV1.2-deficient but not cilia-deficient cells

Wnt signaling has recently been reported to regulate mitochondrial physiology (Yoon et al., 2010). To assess mitochondrial mass, cells were stained with Mito Tracker Green (MTG) and observed live using fluorescence microscopy. When treated with recombinant Wnt3a, mitochondrial mass increased (Fig. 2a). However, the mitochondrial mass in *Tg737*$^{orpk/orpk}$ cells was unchanged after Wnt3a treatment. We next performed this experiment in CaV1.2 shRNA cells and the results were similar to that of the scrambled control. To quantify these findings, MTG fluorescence was recorded using flow cytometry which confirmed our fluorescent observation (Fig. 2b). Our MTG studies were further validated using a common technique by comparing mitochondrial DNA (*Coi*) to nuclear DNA (*18S rRNA*) (Brown and Clayton, 2002; Bai et al., 2004). As expected, Wnt3a did indeed statistically increase mitochondrial biogenesis in scrambled and CaV1.2 shRNA but not in *Tg737*$^{orpk/orpk}$ cells (Fig. 2c). Our immunofluorescence study showed that Wnt3a did not alter CaV1.2 localization to cilia (Table 3).

Wnt3a increases mitochondrial activity in CaV1.2-deficient cells while decreasing activity in cilia-deficient cells

We next asked if Wnt3a would have an effect on mitochondrial oxidative phosphorylation (activity) in *Tg737*$^{orpk/orpk}$ cells. Similar to before, we stained cells with Mito Tracker Red (MTR). Unlike MTG, MTR staining is dependent on the mitochondrial membrane potential (Poot and Pierce, 2001; Pendergrass et al., 2004). Therefore, increased staining

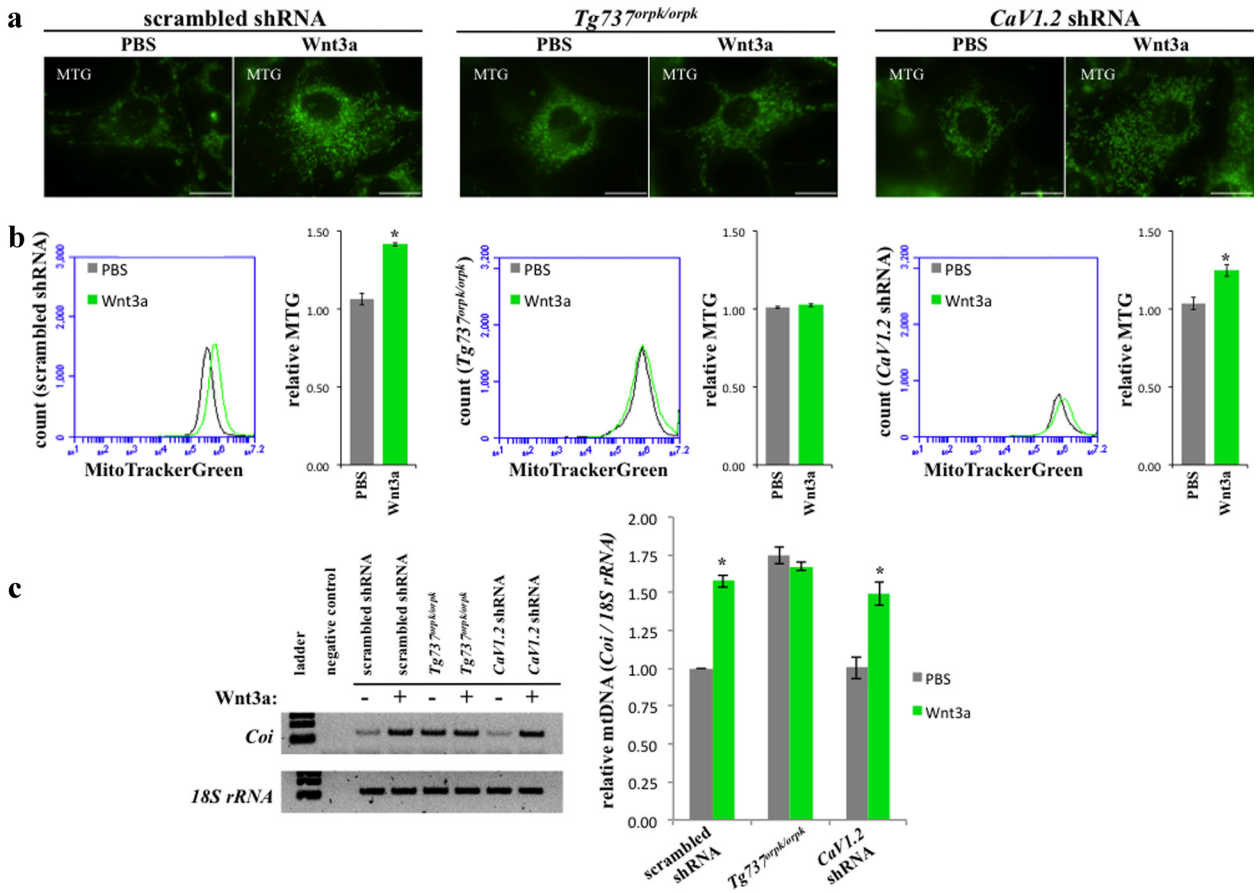

Fig. 2. Wnt3a induces mitochondrial biogenesis in CaV1.2 shRNA but not Tg737$^{orpk/orpk}$ cells. a: Mitochondrial mass was assessed by staining cells with Mito Tracker Green. Wnt3a was found to induce mitochondrial mass in scrambled and CaV1.2 shRNA cells but had no effect on Tg737$^{orpk/orpk}$ when examined using fluorescence microscopy (bar = 20 μm). b: Results were quantified using flow cytometry. c: Mitochondrial DNA was measured using PCR by taking the ratio of a mitochondrial gene (Coi) to a nuclear gene (18S rRNA) (N = 3).

correlates to increased oxidative phosphorylation. As expected, Wnt3a increased MTR staining in scrambled and CaV1.2 shRNA cells when observed using fluorescence microscopy (Fig. 3a). However, mitochondrial activity decreased in *Tg737*$^{orpk/orpk}$ cells. We again quantified our findings using flow cytometry (Fig. 3b). Wnt3a significantly increased mitochondrial activity in scrambled and CaV1.2 shRNA while significantly decreasing activity in *Tg737*$^{orpk/orpk}$ cells. To verify these results, we compared expression of two key mitochondrial encoded oxidative phosphorylation genes (ATP Synthase 5γ1 and Cytochrome *c*) relative to that of nuclear encoded β-actin (Fig. 3c).

TABLE 3. CaV1.2 ciliary localization

	% CaV1.2 localization to cilia	N
PBS (control)		
Scramble shRNA	91.1	45
Tg737$^{orpk/orpk}$	91.7	36
CaV1.2 shRNA	0.0	41
Wnt3a (100 ng/ml)		
Scramble shRNA	90.4	52
Tg737$^{orpk/orpk}$	92.3	39
CaV1.2 shRNA	0.0	46

Wnt3a increases ROS and DNA damage in CaV1.2-deficient but not in cilia-deficient cells

An inevitable consequence of oxidative phosphorylation is the generation of reactive oxygen species (ROS) (Boveris et al., 1972; Boveris and Chance, 1973). MitoSOX is a cell permeable red fluorescent indicator specific for mitochondrial ROS. We therefore stained cells with MitoSOX and observed a significant increase in mitochondrial ROS in scrambled and CaV1.2 shRNA after treatment with Wnt3a (Fig. 4a). A significant decrease in staining was observed in *Tg737*$^{orpk/orpk}$ cells (Fig. 4b). Genomic DNA can be damaged by ROS to form DNA lesions resulting from mismatched repairs (Kasai et al., 1984). Thus, we quantified the levels of 8-Oxoguanine, a common DNA lesion formed by mismatched Adenine (Kasai, 1997). Treatment with Wnt3a was found to increase 8-Oxoguanine in scrambled and CaV1.2 shRNA while no change was observed in *Tg737*$^{orpk/orpk}$ cells (Fig. 4c).

Cilia modulates Wnt signaling to regulate CaV1.2 expression

As previously reported, Wnt3a treatment induced β-catenin expression in all cells (Aberle et al., 1997). We confirmed this in our system, including in *Tg737*$^{orpk/orpk}$ and CaV1.2 shRNA cells (Fig. 5). Consistent with previous study (Corbit et al., 2008),

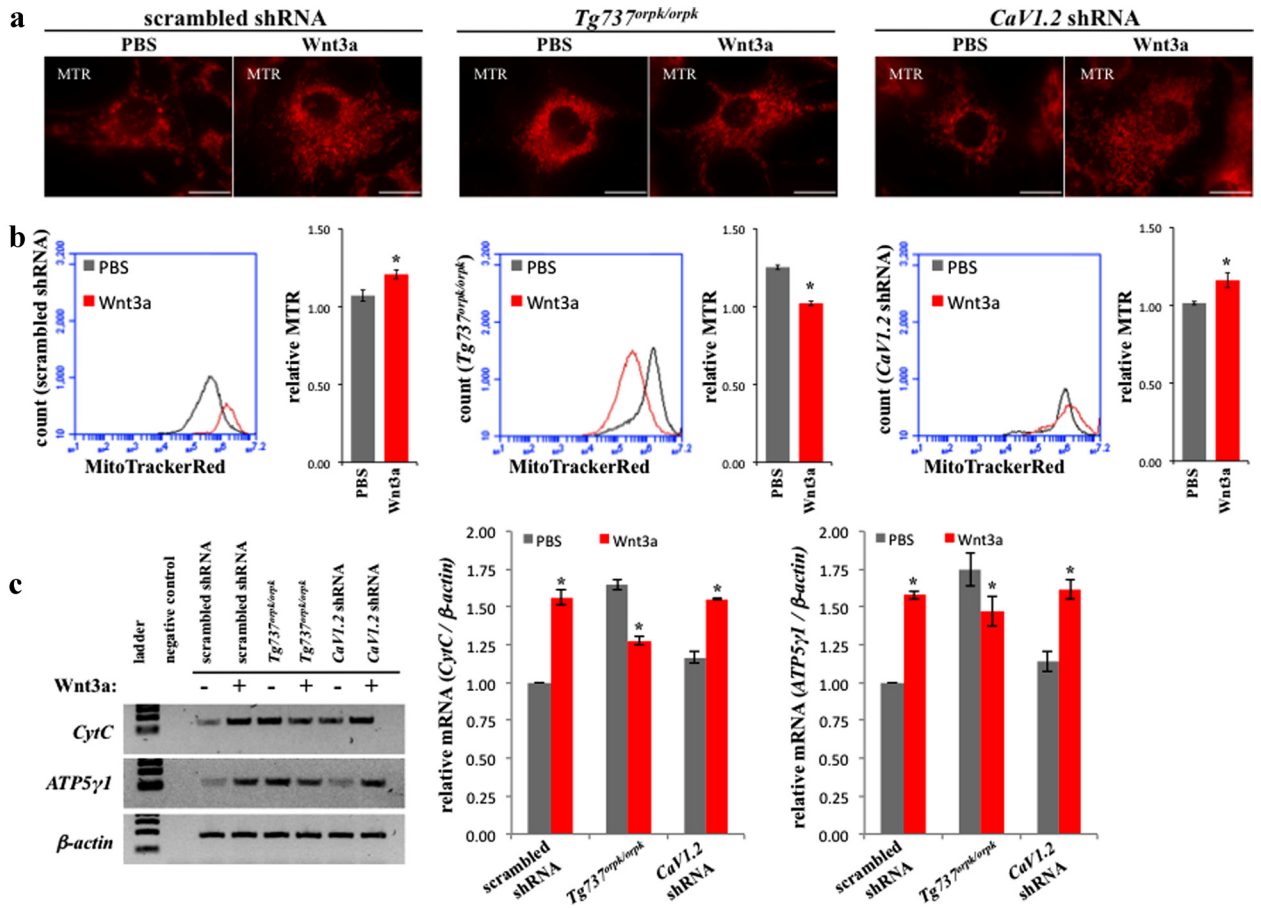

Fig. 3. Wnt3a increases mitochondrial activity in CaV1.2 shRNA but decreasing activity in Tg737$^{orpk/orpk}$ cells. a: Mitochondrial oxidative phosphorylation was used to indicate activity through Mito Tracker Red staining. Wnt3a was found to increase oxidative phosphorylation in scrambled and CaV1.2 shRNA cells while decreasing oxidative phosphorylation in Tg737$^{orpk/orpk}$ when examined using fluorescence microscopy (bar = 20 μm). b: Results were quantified using flow cytometry. c: Two mitochondrial mRNAs encoded oxidative phosphorylation genes (CytC and ATP5γ1) were measured using PCR normalized to nuclear encoded β-actin (N = 3).

Tg737$^{orpk/orpk}$ cells showed a higher basal level of β-catenin than control. Further, Wnt3a treatment increased CaV1.2 expression in scrambled shRNA while decreasing CaV1.2 in *Tg737$^{orpk/orpk}$* cells. Of note is that CaV1.2 expression was not detectable in CaV1.2 shRNA cells, confirming knockdown of CaV1.2 in our stable cell line.

The DNA damage response (DDR) is a cellular mechanism to recover from DNA lesions, such as 8-Oxoguanine (Kasai et al., 1984; Jackson and Bartek, 2009). One arm of this cell survival pathway is the activation of nuclear factor κB p65 (NFκB p65) (Janssens and Tschopp, 2006). Through Western blot analysis, we also found that Wnt3a induced NFκB p65 expression in scrambled and CaV1.2 shRNA (Fig. 5). On the other hand, *Tg737$^{orpk/orpk}$* cells expressed a high basal level of NFκB p65 which decreased in response to Wnt3a. In addition, CaV1.2 expression was found to correlate with NFκB p65.

CaV1.2 knockdown zebrafish develop PKD phenotypes

We have shown that CaV1.2 localizes to primary cilia and have now elucidated the mechanism by which CaV1.2 expression is regulated in renal epithelial cells. To assess the biological significance of CaV1.2 expression, we used antisense morpholinos to knockdown CaV1.2 in zebrafish. Knockdown of the ciliary calcium channel polycystin-2 in zebrafish has been reported to result in PKD phenotypes including renal cyst formation, hydrocephalus, and left-right asymmetry (Obara et al., 2006). Our study showed that knockdown of *pkd2* increased CaV1.2 expression (Fig. 6). This slight increase in CaV1.2 was significant compared to the control morpholino. Interestingly, similar phenotypes were observed in CaV1.2 morpholino (*cav1.2 MO*) zebrafish. Compared with a non-specific control morpholino (*control MO*) injection, *cav1.2 MO* zebrafish developed renal cysts (Fig. 7a), hydrocephalus (Fig. 7b) and various heart-looping defects (Fig. 7c). As generally accepted (Bakkers, 2011), left-right asymmetry was assessed by measuring the relative position of the cardiac atrium and ventricle with respect to the dorsal axis (Supplemental Movie 1).

Discussion

Non-motile primary cilia have been found to play a critical role in Wnt signaling by restricting β-catenin accumulation. Overexpression of polycystin-1 (a ciliary signaling receptor) inhibits GSK3β and stabilizes β- catenin (Kim et al., 1999).

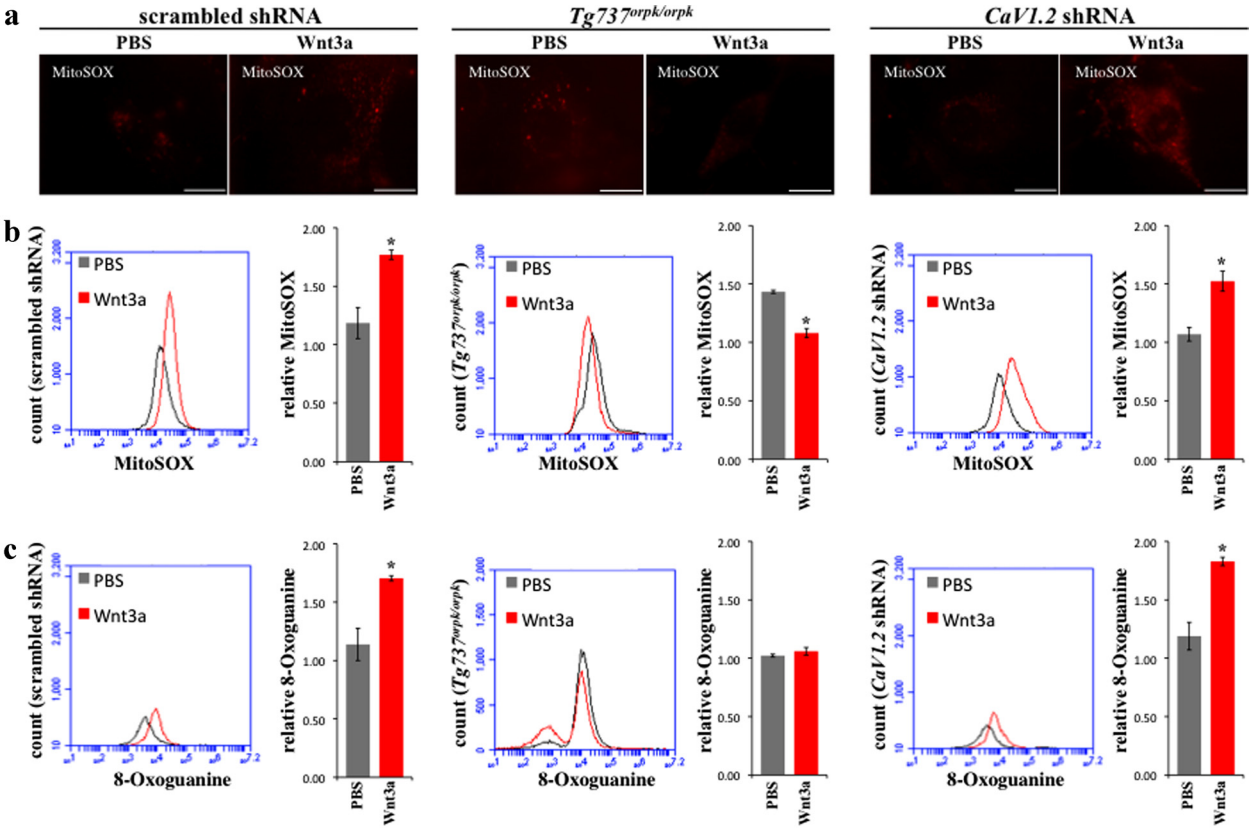

Fig. 4. Wnt3a increases ROS and DNA damage in CaV1.2 shRNA but not in Tg737$^{orpk/orpk}$ cells. a: Mitochondrial ROS was assessed by staining cells with MitoSOX. Wnt3a was found to increase ROS in scrambled and CaV1.2 shRNA cells while decreasing ROS in Tg737$^{orpk/orpk}$ when examined using fluorescence microscopy (bar = 20 μm). b: Results were quantified using flow cytometry. c: Wnt3a increased formation of the oxidative DNA lesion 8-Oxoguanine in scrambled and CaV1.2 shRNA cells but had no effect on Tg737$^{orpk/orpk}$ cells (N = 3).

Polycystin-2 (encoded by *Pkd2*) is calcium channel forming protein found in primary cilia. In *Pkd2*$^{-/-}$ embryos, cilia length was found to be decreased while β-catenin was upregulated (Kim et al., 2009). Interestingly, transgenic mice overexpressing β-catenin also developed cystic kidneys (Saadi-Kheddouci et al., 2001). Further, LRP6$^{-/-}$ (a component of the Wnt receptor complex) mouse embryos die in utero with cystic kidneys (Pinson et al., 2000). Thus, primary cilia and Wnt signaling play a crucial role in PKD (Corbit et al., 2008).

Given that Wnt signaling also modulates mitochondrial physiology (Yoon et al., 2010), we examined the role of cilia in regards to mitochondria. *Tg737*$^{orpk/orpk}$ contains an intron insertion at the 3′ end of the intraflagellar transport 88 (*Ift88*) gene which results in a hypomorphic mutation that prevents ciliogenesis (Moyer et al., 1994). We used *Tg737*$^{orpk/orpk}$ cells as a model for a cilia-deficient system. Through immunostaining, we confirmed the absence of cilia in *Tg737*$^{orpk/orpk}$ cells compared with control (Fig. 1). The voltage-gated L-type calcium channel CaV1.2 also localized to primary cilia. We generated a stable CaV1.2 shRNA cell line and observed no changes in primary cilia compared with control. Further, treatment with Wnt3a had no effect on cilia number or length in scrambled or CaV1.2 shRNA cells (data not shown). Thus, CaV1.2 does not seem to play a role in ciliogenesis.

Mitochondrial biogenesis, oxidative phosphorylation, and generation of reactive oxidative species (ROS) were increased in response to Wnt3a in control renal epithelial cells (Figures 2–4). The elevated levels of oxidative stress increased the formation of DNA lesions and the cellular DNA damage response (DDR). An interesting aspect of this response was an increase in expression of CaV1.2 (Fig. 5). In CaV1.2 knockdown cells, Wnt3a induced a similar effect on mitochondria and DDR. This data suggests that CaV1.2 is a downstream effector in regard to Wnt signaling. In cilia-deficient cells, Wnt3a was unable to induce mitochondrial biogenesis and decreased mitochondrial activity, ROS production, and DDR. CaV1.2 was found to be overexpressed in cilia-deficient cells as a compensatory mechanism; however, its expression decreased following Wnt3a treatment. Therefore, cilia length plays a role in regulating CaV1.2 expression through modulation of Wnt signaling.

Defective primary cilia, indicated by either depletion of key ciliary proteins or fundamental changes in structure/length, results in PKD phenotypes (Wilson, 2004). Here we show that CaV1.2 is a biologically significant ciliary protein. In the absence of CaV1.2 in zebrafish (Fig. 6), PKD phenotypes including renal cyst formation, hydrocephalus, and left-right asymmetry defects were observed (Fig. 7). Moreover, CaV1.2 was found to be overexpressed in *pkd2* knockdown zebrafish. This is intriguing given that both CaV1.2 and PC2 are calcium channel forming proteins in the primary cilium, which further suggests a role for CaV1.2 in PKD pathogenesis. Therefore, CaV1.2 not only localizes to renal epithelial primary cilia, but it is also required for cilia function.

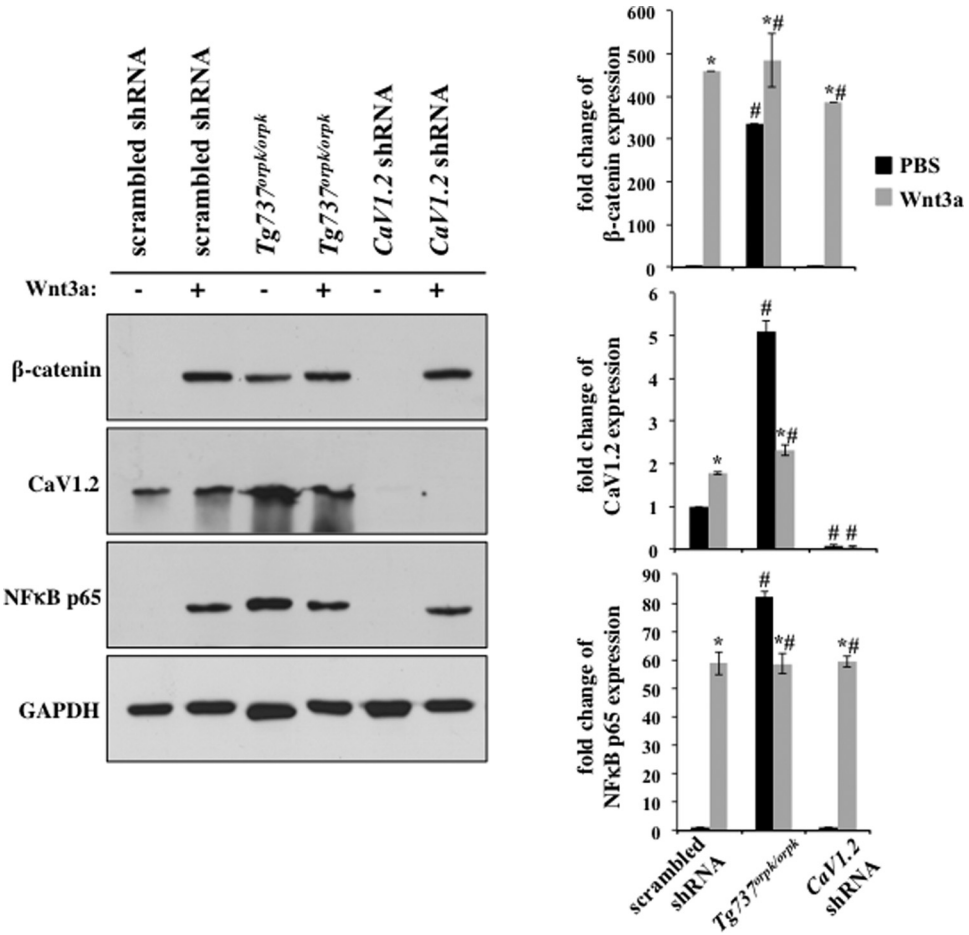

Fig. 5. Cilia modulates Wnt signaling to regulate CaV1.2 expression. Western blotting was performed on cellular protein extracts. Wnt3a treatment increased β-catenin accumulation in all cells, however, Tg737$^{orpk/orpk}$ cells displayed high basal levels of β-catenin. NF-κB p65 was blotted as a readout for DNA damage response (DDR) to ROS induced DNA lesions. Wnt3a induced NF-κB p65 expression in scrambled and CaV1.2 shRNA cells but decreased NF-κB p65 in Tg737$^{orpk/orpk}$ cells. CaV1.2 was overexpressed in Tg737$^{orpk/orpk}$ cells. Wnt3a treatment induced CaV1.2 expression in scrambled shRNA while decreasing expression in Tg737$^{orpk/orpk}$ cells. Data normalized to GAPDH for analysis (N = 3). Asterisks indicate significant difference from the corresponding control group ($P < 0.05$). # signs denote significant difference from the corresponding scrambled shRNA group ($P < 0.05$).

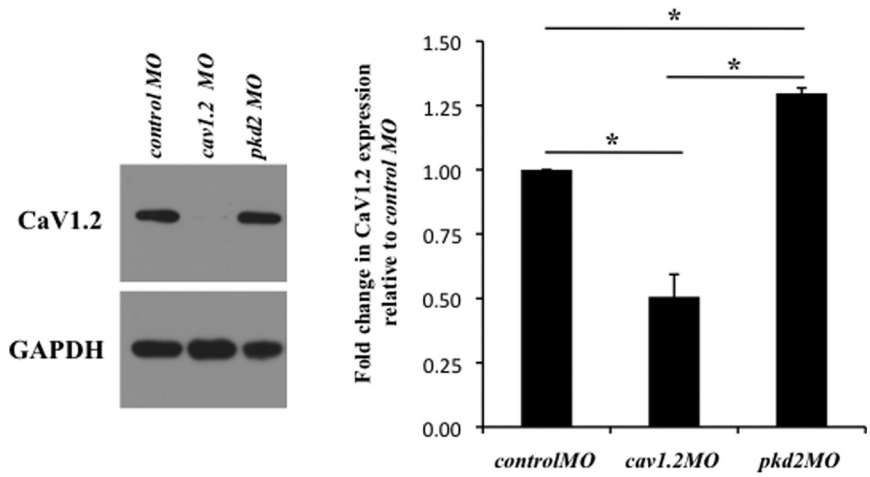

Fig. 6. pkd2 knockdown increases CaV1.2 expression in zebrafish. Embryonic zebrafish protein extracts were obtained at 28 h postfertilization. Western blotting showed that cav1.2MO effectively reduced CaV1.2 expression compared with controlMO. pkd2MO zebrafish were used to further verify morpholino specificity. Results were quantified through one-way ANOVA with Tukey post-test. Statistical significance is reported with a mean difference at the 0.05 level and denoted with an asterisk (N = 3).

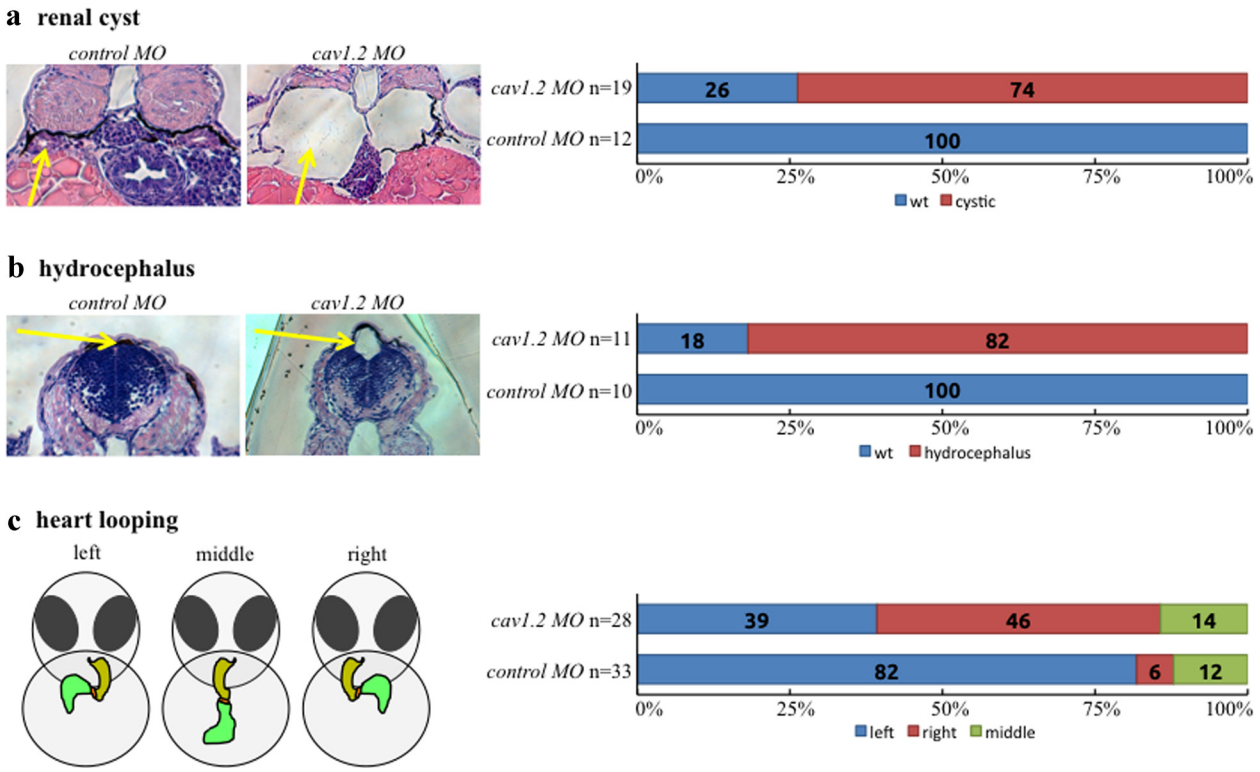

Fig. 7. CaV1.2 knockdown zebrafish develop renal cysts, hydrocephalus, and left-right asymmetry defects. CaV1.2 was knocked down in zebrafish (cav1.2 MO) using morpholino microinjection and compared to a scrambled control morpholino (control MO) to assess phenotypes. Renal cyst formation (a) and hydrocephalus (b) were measured at 3 days postfertilization through standard H&E staining as indicated by arrows. Left-right asymmetry was determined by measuring heart looping (c) at 2 days postfertilization under live microscopy.

Although it has been known that abnormal Wnt signaling leads to renal cyst formation (Lancaster et al., 2009), the underlying mechanism has been unclear. One proposed explanation is that Wnt signaling regulates renal cell proliferation and planar cell polarity to maintain renal tubule homeostasis (Happe et al., 2009). Our present study further suggests that cilia regulate Wnt signaling which ultimately controls CaV1.2 expression. Therefore, in the absence of CaV1.2, ciliary function is compromised leading to formation of renal cysts. In addition, our study also shows a previously unrecognized relationship between primary cilia and mitochondrial function. Overall, we propose that Wnt3a induces β-catenin accumulation in a cilia-dependent manner. This in turn increases mitochondrial biogenesis, oxidative phosphorylation, and generation of ROS that cause genomic DNA damage. The DDR triggers NFκB p65 expression ultimately resulting in increased CaV1.2 expression.

Acknowledgments

This work was supported in part by DOD PR130153 and NIH DK080640.

Literature Cited

Aberle H, Bauer A, Stappert J, Kispert A, Kemler R. 1997. Beta-catenin is a target for the ubiquitin-proteasome pathway. EMBO J 16:3797–3804.

AbouAlaiwi WA, Takahashi M, Mell BR, Jones TJ, Ratnam S, Kolb RJ, Nauli SM. 2009. Ciliary polycystin-2 is a mechanosensitive calcium channel involved in nitric oxide signaling cascades. Circ Res 104:860–869.

Aboualaiwi WA, Muntean BS, Ratnam S, Joe B, Liu L, Booth RL, Rodriguez I, Herbert BS, Bacallao RL, Fruttiger M, Mak TW, Zhou J, Nauli SM. 2013. Survivin-induced abnormal ploidy contributes to cystic kidney and aneurysm formation. Circulation.

Bai RK, Perng CL, Hsu CH, Wong LJ. 2004. Quantitative PCR analysis of mitochondrial DNA content in patients with mitochondrial disease. Ann NY Acad Sci 1011:304–309.

Bakkers J. 2011. Zebrafish as a model to study cardiac development and human cardiac disease. Cardiovasc Res 91:279–288.

Boveris A, Chance B. 1973. The mitochondrial generation of hydrogen peroxide. General properties and effect of hyperbaric oxygen. Biochem J 134:707–716.

Boveris A, Oshino N, Chance B. 1972. The cellular production of hydrogen peroxide. Biochem J 128:617–630.

Brown TA, Clayton DA. 2002. Release of replication termination controls mitochondrial DNA copy number after depletion with 2′,3′-dideoxycytidine. Nucleic acids Res 30:2004–2010.

Carter CS, Vogel TW, Zhang Q, Seo S, Swiderski RE, Moninger TO, Cassell MD, Thedens DR, Keppler-Noreuil KM, Nopoulos P, Nishimura DY, Searby CC, Bugge K, Sheffield VC. 2012. Abnormal development of NG2+PDGFR-alpha+ neural progenitor cells leads to neonatal hydrocephalus in a ciliopathy mouse model. Nat Med 18:1797–1804.

Corbit KC, Shyer AE, Dowdle WE, Gaulden J, Singla V, Chen MH, Chuang PT, Reiter JF. 2008. Kif3a constrains beta-catenin-dependent Wnt signalling through dual ciliary and non-ciliary mechanisms. Nat Cell Biol 10:70–76.

Gerdes JM, Liu Y, Zaghloul NA, Leitch CC, Lawson SS, Kato M, Beachy PA, Beales PL, DeMartino GN, Fisher S, Badano JL, Katsanis N. 2007. Disruption of the basal body compromises proteasomal function and perturbs intracellular Wnt response. Nat Genet 39:1350–1360.

Happe H, Leonhard WN, van der Wal A, van de Water B, Lantinga-van Leeuwen IS, Breuning MH, de Heer E, Peters DJ. 2009. Toxic tubular injury in kidneys from Pkd1-deletion mice accelerates cystogenesis accompanied by dysregulated planar cell polarity and canonical Wnt signaling pathways. Hum Mol Genet 18:2532–2542.

Jackson SP, Bartek J. 2009. The DNA-damage response in human biology and disease. Nature 461:1071–1078.

Janssens S, Tschopp J. 2006. Signals from within: The DNA-damage-induced NF-kappaB response. Cell Death Differ 13:773–784.

Jin X, Mohieldin AM, Muntean BS, Green JA, Shah JV, Mykytyn K, Nauli SM. 2013. Cilioplasm is a cellular compartment for calcium signaling in response to mechanical and chemical stimuli. Cell Mol Life Sci.

Kasai H. 1997. Analysis of a form of oxidative DNA damage, 8-hydroxy-2′-deoxyguanosine, as a marker of cellular oxidative stress during carcinogenesis. Mutat Res 387:147–163.

Kasai H, Tanooka H, Nishimura S. 1984. Formation of 8-hydroxyguanine residues in DNA by X-irradiation. Gann 75:1037–1039.

Kim E, Arnould T, Sellin LK, Benzing T, Fan MJ, Gruning W, Sokol SY, Drummond I, Walz G. 1999. The polycystic kidney disease 1 gene product modulates Wnt signaling. J Biol Chem 274:4947–4953.
Kim I, Ding T, Fu Y, Li C, Cui L, Li A, Lian P, Liang D, Wang DW, Guo C, Ma J, Zhao P, Coffey RJ, Zhan Q, Wu G. 2009. Conditional mutation of Pkd2 causes cystogenesis and upregulates beta-catenin. J Am Soc Nephrol 20:2556–2569.
Lancaster MA, Louie CM, Silhavy JL, Sintasath L, Decambre M, Nigam SK, Willert K, Gleeson JG. 2009. Impaired Wnt-beta-catenin signaling disrupts adult renal homeostasis and leads to cystic kidney ciliopathy. Nat Med 15:1046–1054.
Lancaster MA, Schroth J, Gleeson JG. 2011. Subcellular spatial regulation of canonical Wnt signalling at the primary cilium. Nat Cell Biol 13:700–707.
Moyer JH, Lee-Tischler MJ, Kwon HY, Schrick JJ, Avner ED, Sweeney WE, Godfrey VL, Cacheiro NL, Wilkinson JE, Woychik RP. 1994. Candidate gene associated with a mutation causing recessive polycystic kidney disease in mice. Science 264:1329–1333.
Muntean BS, Horvat CM, Behler JH, Aboualaiwi WA, Nauli AM, Williams FE, Nauli SM. 2010. A comparative study of embedded and anesthetized zebrafish in vivo on myocardiac calcium oscillation and heart muscle contraction. Front Pharmacol 1:139.
Muntean BS, Jin X, Nauli SM. Chapter 9: Primary cilia are mechanosensory organelles with chemosensory roles. Mechanosensitivity and mechanotransduction. ISBN: 978-994-007-2003-2009.
Nauli SM, Alenghat FJ, Luo Y, Williams E, Vassilev P, Li X, Elia AE, Lu W, Brown EM, Quinn SJ, Ingber DE, Zhou J. 2003. Polycystins 1 and 2 mediate mechanosensation in the primary cilium of kidney cells. Nat Genet 33:129–137.
Nauli SM, Kawanabe Y, Kaminski JJ, Pearce WJ, Ingber DE, Zhou J. 2008. Endothelial cilia are fluid shear sensors that regulate calcium signaling and nitric oxide production through polycystin-1. Circulation 117:1161–1171.
Norris DP. 2012. Cilia, calcium and the basis of left-right asymmetry. BMC Biol 10:102.
Obara T, Mangos S, Liu Y, Zhao J, Wiessner S, Kramer-Zucker AG, Olale F, Schier AF, Drummond IA. 2006. Polycystin-2 immunolocalization and function in zebrafish. J Am Soc Nephrol 17:2706–2718.
Pendergrass W, Wolf N, Poot M. 2004. Efficacy of MitoTracker Green and CMXrosamine to measure changes in mitochondrial membrane potentials in living cells and tissues. Cytometry A 61:162–169.
Pinson KI, Brennan J, Monkley S, Avery BJ, Skarnes WC. 2000. An LDL-receptor-related protein mediates Wnt signalling in mice. Nature 407:535–538.
Poot M, Pierce RH. 2001. Analysis of mitochondria by flow cytometry. Methods Cell Biol 64:117–128.
Saadi-Kheddouci S, Berrebi D, Romagnolo B, Cluzeaud F, Peuchmaur M, Kahn A, Vandewalle A, Perret C. 2001. Early development of polycystic kidney disease in transgenic mice expressing an activated mutant of the beta-catenin gene. Oncogene 20:5972–5981.
Wilson PD. 2004. Polycystic kidney disease. N Engl J Med 350:151–164.
Yoon JC, Ng A, Kim BH, Bianco A, Xavier RJ, Elledge SJ. 2010. Wnt signaling regulates mitochondrial physiology and insulin sensitivity. Genes Dev 24:1507–1518.

Supporting Information

Additional supporting information may be found in the online version of this article at the publisher's web-site.

Send Orders for Reprints to reprints@benthamscience.ae

Current Hypertension Reviews, 2015, *11*, 000-000

Vascular Endothelial Primary Cilia: Mechanosensation and Hypertension

Ashraf M. Mohieldin[2,#], Hossain Saad Md Zubayer[1,#], Alzahra J. Al Omran[1], Hannah C. Saternos[1], Ali Zarban[1], Surya M. Nauli[3] and Wissam A. AbouAlaiwi[1,*]

[1]*Department of Pharmacology, University of Toledo Health Science Campus, Toledo, OH, USA;* [2]*Department of Medicinal & Biological Chemistry, University of Toledo Health Science Campus, Toledo, OH, USA;* [3]*Department of Biomedical & Pharmaceutical Sciences, Chapman University Rinker Health Science campus, Irvine, CA, USA*

W.A. AbouAlaiwi

Abstract: Primary cilia are sensory organelles that extend from the cell surface and sense extracellular signals. Endothelial primary cilia protruding from the inner surface of blood vessel walls sense changes in blood flow and convert this mechanosensation into an intracellular biochemical/ molecular signal, which triggers a cellular response. Primary endothelial cilia dysfunction may contribute to the impairment of this response and thus be directly implicated in the development of vascular abnormalities such as hypertension and aneurysms. Using both *in vitro* techniques as well as *in vivo* animal models, we and others have investigated fluid flow mechanosensory functions of endothelial cilia in cultured cells, animal models and autosomal dominant polycystic kidney disease (ADPKD) patients. More in-depth studies directed at identification of the mechanisms of fluid flow sensing will further enhance our knowledge of cilia-dependent vascular pathology. Although the current treatments aimed at treating the cardiovascular symptoms in ADPKD patients successfully slowed the progression of cyst growth, there is growing evidence which suggests that drugs which interfere with primary cilia function or structure could reduce cardiovascular complications in ADPKD. This review is to summarize the most recent studies on primary endothelial cilia function in the vascular system and to present primary cilia as a novel therapeutic target for vascular hypertension.

Keywords: Cardiovascular, cell division, fluid-shear, hypertension, primary cilia.

INTRODUCTION

It has been over a century since primary cilia have been visualized, but the study of their sensory role is, comparatively, a new field [1]. Like other cellular organelles i.e. nucleus, Golgi bodies, mitochondria etc. cilia can be considered as a separate entity and have the following specialized functions:

- Mechanosensation [2-4].
- Shear-stress sensation [5-7].
- Nodal flow generation [8-10].
- Nodal flow sensation [11, 12].
- Osmosensation [13-15].
- Chemosensation [16-19].
- Light sensation [20-22].
- Smell sensation [23, 24].
- Gravitational sensation [25].
- Developmental regulation [26-28].
- Fluid clearance [29, 30].
- Sperm motility [31-33].
- Fluid transportation [34-36].
- Oocyte transportation [37, 38].
- Sound-wave sensation [39-41].

In order to study a cilium, it must be divided into five distinct structural blocks – the ciliary membrane, the soluble compartment, the axoneme, the ciliary tip and the basal body complex (Fig. **1a**). The primary ciliary membrane has a distinct lipid bilayer composition and is continuous with the cell membrane at the transition fiber. It houses various membrane mechanosensory receptors, ligand-activated chemoreceptors and ion channels to support mechanosensation, chemosensation and ion influx in response to extracellular stimuli. The soluble or matrix compartment also called the cilioplasm is composed of fluid materials to support signaling activities. The axoneme, which emanates from the basal body, is composed of nine pairs of microtubules forming heterodimer structure. Apart from delivering cellular components in and out of the ciliary shaft, it plays a significant role in maintaining a long ciliary structure. The ciliary tip contains specialized proteins, but

*Address correspondence to this author at the Department of Pharmacology; MS 1015, The University of Toledo, College of Pharmacy and Pharmaceutical Sciences, Health Education building; Room 282E, 3000 Arlington Ave, Toledo, OH 43614; Tel: 419-383-1949; Fax: 419-383-1909;
E-mail: Wissam.Abou-Alaiwi@UToledo.Edu

[#]Hossain Saad Md Zubayer and Ashraf M. Mohieldin contributed equally to this work.

1573-4021/15 $58.00+.00

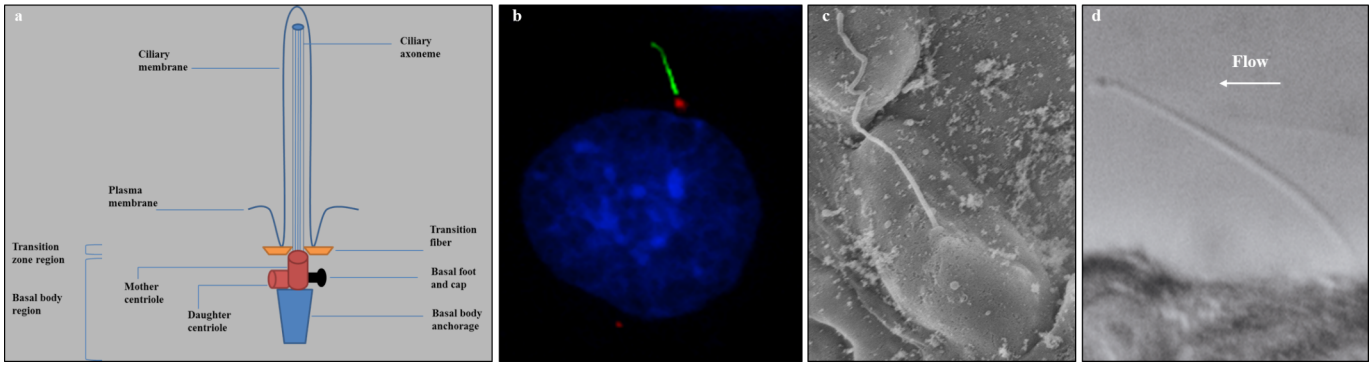

Fig. (1). Mechanosensory cilium. A primary cilium is a cellular organelle extending from the apical surface of many cell types. The mechanosensory cilia act as antennas to receive and transmit extracellular fluid-shear stress into cellular biochemical signals. **(a)** A cilium is composed of a ciliary membrane, a soluble matrix, a ciliary axoneme, and a basal body complex. The *ciliary membrane* contains various sensory proteins. The *soluble matrix* contains many regulatory proteins that are involved in signal transduction networks. The *ciliary axoneme* is surrounded by the nine pairs of microtubules that are thought to control the length of a cilium. The *basal body complex* is the anchoring point for axonemal microtubules. (**b**) Primary cilia found on the surface of endothelial cells can be localized by a simple immunostaining experiment using antibody against acetylated α-tubulin (green) to label primary cilia and pericentrin (red) to label centriole or basal body. The nucleus is counterstained with DAPI to label DNA. (**c**) Mouse primary epithelial cilia can be studied *in vivo* by scanning electron microscopy (SEM) to reveal kidney epithelial cilia protruding from the surface of kidney epithelial cells towards the lumen of kidney tubules. (**d**) Primary cilia are sensory organelles that sense fluid-shear stress on the apical surface of cells. Fluid flow that produces enough drag-force on the cells will bend sensory cilia. Part of this figure is reproduced from [152].

their roles are still unknown. The basal body complex is composed of the mother and daughter centrioles connected by rootlets and emanate from the basal body anchorage. The mother centriole is the basal body from which the cilium protrudes [42].

Primary Cilia is a term commonly used to denote "9+0" non-motile cilia. These have nine parallel doublet microtubules (denoted by '9') and a central pair of microtubule is absent within the central sheath (denoted by '0'). Length of a primary cilium can vary from 2-50 μM and it has a diameter of approximately 0.25 μM [42]. Primary cilia are found on several mammalian cell types i.e. endothelia (Fig. **1b**) [43-46], epithelia (Fig. **1c**) [47-49], neurons [50-53], osteoblasts [54-56], fibroblasts and others [57-59]. Thus, abnormal ciliary proteins and/or abnormal ciliary function can be associated with various pathological conditions collectively known as ciliopathies; which include polycystic kidney disease (PKD), nephronophthisis, bardet biedl syndrome, left-right asymmetry defect, oral facial syndrome, obesity, hypertension and others [60]. Primary cilia can be activated by bending through perfusing cells with fluid-shear stress (Fig. **1d**) or by mechanical stress [61]. Bending cilia by apical fluid perfusion with physiologically relevant flow rate [2, 62] or by suction through a micropipette [63] can activate primary cilia. Consequently, mechanosensory ciliary proteins such as polycystin-1 [5], polycystin-2 [7], transient receptor potential-4 [64], fibrocystin [65], and probably many others convert this mechanical force into an intracellular biochemical signal [66, 67].

PRIMARY ENDOTHELIAL CILIA AS BLOOD PRESSURE SENSORS

The control of the circulatory system depends largely on the mechanical properties of blood vessels in both normal and pathological conditions. The continuous change in blood vessel diameter triggered by contraction and relaxation of vascular smooth muscle cells is important for normal blood flow [68-71].

Different blood vessels are subjected to changes in blood pressure as well as changes in the hemodynamic forces which induce distinct responses within the vascular tree and allows for tissue perfusion. Resistant arteries have the most influence on blood flow and they are subjected to the continuous effect of blood flow and pressure. An increase in blood pressure induces a vasoconstriction known as the myogenic tone, which facilitates the action of the sympathetic nervous system [72]. When transmural blood pressure increases, vessel diameter is reduced [73-75]; while faster flow velocity (shear stress) increases blood vessel diameter [74, 76, 77]. Vascular endothelial cells lining the inner wall of blood vessels can sense changes in blood flow and pressure and convert these mechanical changes into changes of smooth muscle tone [74, 78].

The pulsatile nature of blood flow through the vasculature exerts different types of mechanical forces such as shear stress, cyclic strains and hydrostatic pressure that can impact the physiology of the blood vessel wall. Being the inner most layer and in direct contact with blood flow, the endothelial cell layer bears the most frictional forces induced by the flow of blood. Though these forces are practically impossible to differentiate *in vivo*, they can be distinguished from one another in *in vitro* and *ex vivo* studies [79-81]. In this review, we will focus on shear stress which is the most studied mechanical force in cilia research.

We have previously demonstrated the presence as well as the function of endothelial primary cilia as fluid mechanosensor *in vitro* in mouse aortic endothelial cells, *ex*

vivo in isolated mouse arteries and *in vivo* in mouse models as well as in blood vessels from human patients [5, 7]. The presence as well as the size of primary endothelial cilia varies with respect to the level of fluid shear stress or fluid turbulence. For example, blood vessels with relatively low fluid shear stress have longer cilia while blood vessels with high fluid shear stress are devoid of cilia or have shorter cilia simply due to the inability of cilia to tolerate high levels of shear stress, which could induce its disassembly. Consequently, the ciliary mechanosensory function in those areas of high fluid shear stress could be minimized or substituted by other vessel components such as the glycocalyx [82]. Sensory proteins localized to primary endothelial cilia such as polycystins can detect any sudden increase in blood pressure or shear stress inside the blood vessel [5, 7]. This in turn, leads to the influx of calcium ions to the cilioplasm followed by an increase in intracellular calcium concentration. As a result, primary cilia enable cells to translate this extracellular fluid mechanics into a complex intracellular signaling cascade. This signaling cascade eventually leads to the activation of endothelial nitric oxide synthase (eNOS), an endothelial enzyme that synthesizes nitric oxide gas. Nitric oxide diffuses from endothelial cells to the surrounding smooth muscle cells and promotes vasodilation [83-85]. Both polycystin-1 and polycystin-2, an 11 transmembrane protein with a long extracellular domain and a cation channel with 6 transmembrane domains, respectively are expressed in the endothelial and vascular smooth muscle cells of all major blood vessels [86]. We previously reported the loss of response to fluid-shear stress in mouse endothelial cells with *knockdown* or *knockout* of *PKD2* [7]. In addition to the mouse data, polycystin-2 null endothelial cells generated from *PKD2* patients that do not show polycystin-2 in the cilia are unable to sense fluid flow. Therefore, mutations in both *PKD1* and *PKD2* have been shown to contribute to hypertension [87], in part by the failure to convert an increase in mechanical blood flow into cellular NO biosynthesis [5, 7]. In summary, by sensing any increase in fluid shear stress, primary cilia can activate different cellular mechanisms in order to lower total peripheral resistance and consequently, blood pressure.

It is crucial to discern the physiological mechanism behind mechanosensory role of primary cilia in order to clearly understand the correlation between primary cilia abnormalities and cardiovascular pathology and in particular hypertension. A new mechanism has been proposed that involves polycystin-1 and polycystin-2 [5, 7]. Endothelial cells without primary cilia were isolated from $Tg737^{Orpk/Orpk}$ mice to examine the mechanosensory role of primary cilia. In addition and to confirm the role of polycystin-1 and polycystin-2 as mechanosensory proteins, endothelial cells were collected from PKD mice and ADPKD human patients. Polycystins are absent in the cilia of these cells and present in *Tg737* mice cells, but localized at the base of the "stubby" primary cilia. Different magnitudes of fluid shear stress were applied to these cells. Though shear induced cytosolic calcium was increased in normal endothelial cells, diseased artery and mutant endothelial cells did not show any calcium response to fluid shear stress [5, 7]. To verify cilia function specifically against fluid shear stress, a new technique involving artery perfusion in glass capillary was utilized [7, 88]. It was observed that though cilia react normally when other mechanical stimuli are applied, response to fluid shear stress is highly altered.

To dissect the molecular mechanisms downstream of cilia function, different biochemical and pharmacological inhibitors were used in these studies to block downstream molecular targets in endothelial cells. When EGTA is used to block extracellular calcium, both cytosolic calcium and nitric oxide production was inhibited. In addition, L-NAME (N^G-nitro-L-arginine methylester), an eNOS inhibitor, was found to block shear induced nitric oxide synthesis but not cytosolic calcium increase. This indicates the necessity of extracellular calcium influx for the downstream generation of nitric oxide. To examine calcium dependent mechanism of nitric oxide biosysnthesis, calphostin C, a PKC inhibitor and W7, a calmodulin antagonist were employed. Results showed that PKC and calmodulin function downstream of calcium pathway and blocking either of these will inhibit nitric oxide synthesis. When pharmacological blockers Akt inhibitor II, LY-294,002, and wortmannin were applied, role of Akt was confirmed in shear induced nitric oxide production. These studies in addition to others demonstrate an interaction between mechanosensory polycystin-1 and poylycystin-2 and that absence of this interaction results in disturbance of localization of polycystin-2 to primary cilia and hence, disturb ciliary functions. In summary, these studies lead us to propose that, after sensing fluid shear stress, polycystin-1 interacts with and activates polycystin-2, a calcium channel which induces an intracellular calcium influx. This is followed by activation of PKC and formation of calcium-calmodulin complex. Our data also indicate that Akt/PKB is also involved in regulation of eNOS activation and the generation of nitric oxide in response to fluid shear (Fig. **2a** and **b**).

ROLE OF PRIMARY CILIA IN THE CARDIO-VASCULAR SYSTEM

Despite its well-known and demonstrated function as a mechanosensory organelle in the cardiovascular system, the role of primary cilia in this system is still a widely debated topic. Recent studies have successfully demonstrated the presence of primary cilia throughout the cardiovascular system. Primary cilia have been observed in endocardia [6, 89], arterial endothelia [2, 7], venous endothelia [90], corneal endothelia [44, 46], arterial smooth muscle cells [91] and airway smooth muscle cells [92].

Primary Cilia and Heart Development

Recent studies have demonstrated an important role of cardiac primary cilia in harmonizing heart development, and defects in these cilia are associated with inherited heart disease. Different types of cilia are present in different chambers throughout heart development to control cardiogenesis. For example, sensory nodal cilia play an important role in regulating signaling mechanisms essential for the establishment of left-right asymmetry, a process for regulating heart morphogenesis. In addition, primary cilia are present on the surface of cardiomyocytes during heart development and houses different receptor complexes which coordinate various signaling mechanisms that are important

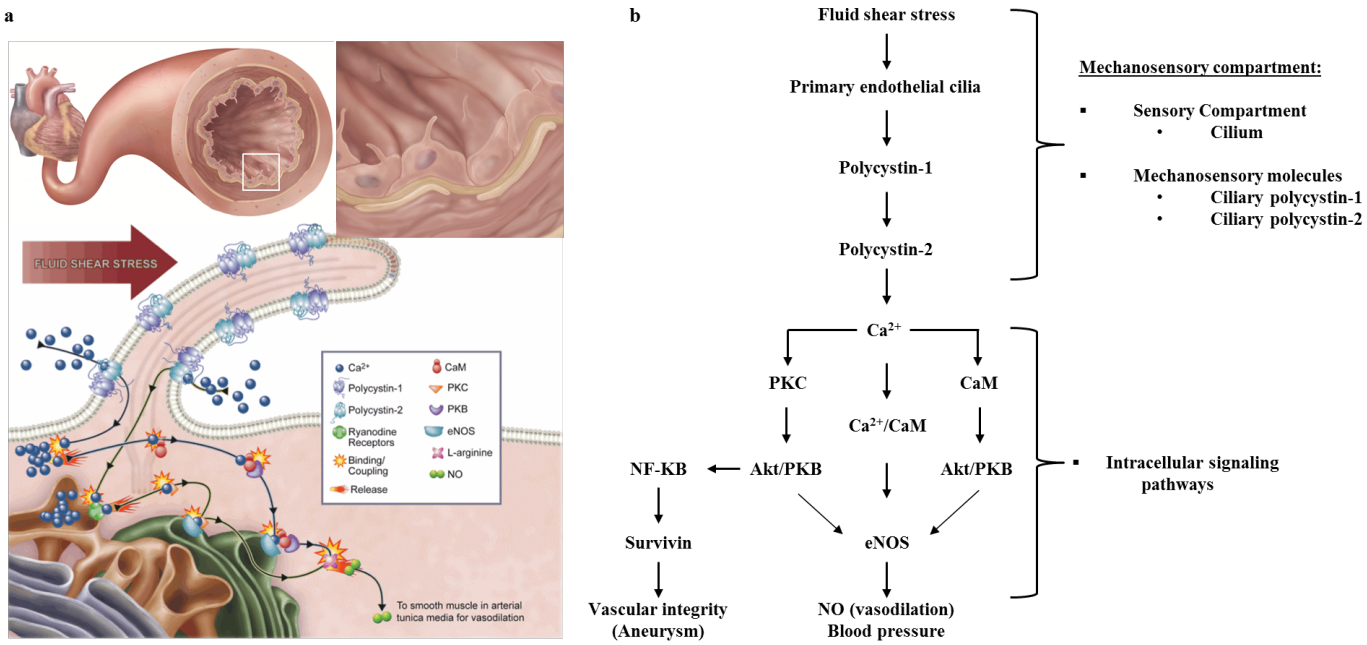

Fig. (2). Endothelial primary cilia as regulators of blood pressure through nitric oxide production and vascular architecture through survivin. (**a** and **b**) Nitric oxide synthesis and survivin expression depend on the presence of functional sensory cilia housing sensory complex, polycystin-1 and polycystin-2. Bending of primary endothelial cilia by fluid flow activates polycystin complex and initiates a series of intracellular signaling cascades resulting in the synthesis and release of NO gas, which vasodilates smooth muscles in the vasculature. These intracellular signaling cascades includes calcium influx, calcium-calmodulin, protein kinase C, Akt/PKB and eNOS. Survivin downregulation is involved in aneurysm formation. Fluid shear stress induced the activation of polycystin-1/2 complex followed by increase in intracellular calcium influx. Akt and NF-κB are downstream effectors of PKC pathway in regulating flow-induced survivin expression. The increase in p-NF-κB expression is accompanied by an increase in survivin expression, which is critical for normal endothelial cell division and consequently vascular integrity. Modified from [152, 153] with permission.

for proper heart morphogenesis and development. Cilia mutants have been characterized by heart developmental defects such as ventricular and atrial septum defects, myocardial wall disorganization and thinning and double-outlet right ventricles due to mutations in *pkd1* or *pkd2*, the causative genes of ADPKD [93]. Moreover, knockout mice of cilia structural genes such as *ift88* and *kif3a* are also characterized by severe cardiac phenotypes such as hypoplasia of the endocardial cushions, reduction in ventricular trabeculation and enlarged pericardium [94]. This suggests that these cardiac phenotypes could be contributed mainly by ciliary dysfunction and that primary cardiac cilia are critical for normal heart development. More importantly, dysfunctional cilia are associated with congenital heart disease. Several ciliopathies such as nephronophthisis (NPHP), Meckel syndrome (MKS), Bardet-Biedl syndrome (BBS), and Joubert syndrome (JBTS) are usually associated with cardiac defects such as septum defects and aortic stenosis [95].

Cardiac development is controlled by complex regulatory networks of both inductive and inhibitory signals from both the heart as well as the surrounding tissue which coordinate different stages of heart development. An example is the Hedgehog (Hh) signaling pathway which regulates the L-R asymmetry in vertebrates and promotes the activation of several transcription factors involved in various cellular mechanisms during tissue homeostasis and development. It has been shown that primary cilia can regulate the Hh signaling pathway in several cell types by functioning as a unique compartment for the continuous turnover of Hh signaling components. As a result, defects in primary cilia assembly and consequently Hh signaling components turnover can lead to a variety of developmental pathologies including congenital heart defects [96]. Another example of a signaling network which plays a critical role during heart development is the TGFβ/Bone Morphogenic Protein (BMP) network. It has been recently shown that primary cilia can regulate the canonical TGFβ signaling network through the activation of transcription factors Smad2/3 [97]. Furthermore, it has been shown that the TGFβ ligand, TGFβ-1 can stimulate the differentiation of stem cells into cardiomyocytes and that *Tg737*$^{Orpk/Orpk}$ mouse embryonic fibroblasts are characterized by diminished TGFβ activity, suggesting a direct role of cardiac primary cilia in regulating TGFβ signaling during cardiomyogenesis. Taken together, these studies prompted us to speculate that primary cilia may function as signaling hubs facilitating the cross-talk between the different signaling networks that regulate heart development.

Primary Endothelial Cilia and Vascular Architecture

The morphology and function of blood vessels are continuously altered in response to blood flow which is mainly detected by the vascular endothelium. An aneurysm

is a balloon-like bulge in the wall of blood vessels. Studies on both ADPKD patients and animal models indicate that polycystins are essential for normal blood vessel's structure and development [98]. Aneurysm formation is one of the deadliest vascular abnormalities in PKD patients. The occurrence of aneurysm represents a major risk factor for morbidity and mortality associated with PKD [99]. Mice with *Pkd* mutations develop hemorrhages and aneurysms [100]. Vascular aneurysms are associated with tissue remodeling due to abnormal proliferation of the endothelial cell layers in response to complex hemodynamic changes in fluid shear stress [101]. We recently demonstrated that aneurysm formation is more severe in *survivin, pkd1* and *Tg737* vascular-specific knockout (*PdgfβCre:Survivin* $^{flox/flox}$, *PdgfβCre:Pkd1* $^{flox/flox}$ and *PdgfβCre:Tg737* $^{flox/flox}$) mice than in wild type mice [102]. An abnormality of primary cilia structure (polaris) or function (polycystin-1) is associated with downregulation of survivin expression, which is associated with abnormal mitotic events in endothelial cells [103]. This is turn can lead to abnormal cytokinesis triggered by polyploidy formation and ultimately contributes to vascular aneurysm [102]. Thus, the inability of primary endothelial cilia to respond to fluid shear stress can contribute to the exacerbation of aneurysm formation in these mice models.

Protein Kinase C (PKC) and Akt are downstream signaling messengers of primary cilia. Studies on endothelial cells have verified that survivin expression following cilia activation is regulated by PKC, Akt and Nuclear Factor-κB (NF-κB). Akt is downstream of PKC and can regulate NF-κB, which is known to regulate survivin expression. Taken all the above together, we propose a Cilia-PKC-Akt-NF-κB pathway involved in survivin expression and cell division regulation [102, 104-107]. All in all, the inability of mechanosensory cilia to detect fluid shear stress is associated with down-regulation of survivin leading to abnormal cytokinesis triggered by polyploidy formation and finally contributing to vascular aneurysm (Fig. **2b**) [102].

Primary Cilia in Corneal Endothelium

The corneal endothelium located beneath the anterior chamber of the eye is orchestrated into a two-dimensional layer of hexagonal cells and plays critical role in maintaining corneal transparency. The presence of primary cilia in the corneal endothelium has been demonstrated in various mammalian species [44]. In humans, corneal endothelial cilia protruding into the anterior chamber of the eye have similar structure to the "9+0" primary cilia, but their function remains somehow unclear, although evidence for an osmoregulatory or a chemosensory function exists. Moreover, it has been postulated that primary cilia of the mouse corneal endothelium play key role towards proper morphogenesis of the characteristic hexagonal shape or pattern of the corneal endothelium during development and disassemble following tissue homeostasis during adult stage pointing towards a role of corneal endothelial primary cilium in corneal endothelial development [108].

More importantly, a link between primary cilia and intraocular pressure regulation has been recently demonstrated through studying a rare X-linked congenital syndrome known as pediatric glaucoma or Lowe syndrome [109]. It has been previously shown that the *Oculocerebrorenal syndrome of Lowe* (*OCRL*) gene encoding an inositol polyphosphate 5- phosphatase, which is mutated in Lowe syndrome is involved in vesicle trafficking to the primary cilium [110]. More recently, a potential role of primary cilia in the trabecular meshwork which regulates intraocular pressure in the eye has been demonstrated. In this study, it was shown that primary cilia are important sensors of intraocular pressure changes and that in glaucoma, defective trabecular meshwork cells have shortened primary cilia due to increased intraocular pressure and fluid flow [109]. Consequently, this shortening is associated with increased expression of TNFα, TGFβ and GLI1 genes. Primary cilia response to increased intraocular pressure is mainly mediated through interaction between OCRL and transient receptor potential vanilloid 4 (TRPV4), a ciliary mechanosensory channel. Although these findings significantly advance the current understanding of how intraocular pressure is regulated, they provide further evidence and support for our proposed role of primary endothelial cilia as both blood pressure sensor and regulator.

Primary Cilia and Vascular Smooth Muscle Cell Function

Vascular smooth muscle cells (VSMCs) localized in the medial layer of the arterial wall play critical roles in maintaining and regulating blood vessel tone, blood pressure and blood flow [111]. VSMCs express a unique group of proteins with specialized contractile functions and have very low proliferative profile during adult stages. The environment in which VSMCs reside is mainly composed of collagen and elastic fibers as extracellular matrix (ECM) components. Normally, VSMCs are not exposed directly to fluid shear stress simply because the inner lining endothelial cell layer provide the contacting surface with blood flow and consequently shields the VSMC layer. However, in cases of endothelial cell layer injury or denudation, VSMCs become directly exposed to fluid shear stress levels similar to the endothelial cell layer in intact vascular regions. It is critical to understand the mechanisms by which VSMCs sense and transduce the stimuli of shear stress into intracellular biochemical signals which allows better understanding of vascular disease. Studies reviewing the effects of fluid shear stress on VSMCs revealed the presence of shear specific mechanosensors such as cell membrane-related receptors, cell surface glycocalyx, ion channels and integrins as well as the presence of shear-specific secondary signaling messengers such as NO, Ca^{+2} and MAPKs. These messengers in turn regulate the expression of shear-responsive genes which control various VSMCs responses such as proliferation, differentiation, apoptosis and migration.

A sensory role of primary cilia in VSMCs similar to its role in several other cellular systems has not been demonstrated until recently [112]. It has been shown that primary cilia are localized to VSMCs in a preferentially oriented pattern with respect to the artery axis as well as to the ECM and they house mechanosensory proteins that are responsive to ECM proteins and to cell-ECM interaction. These initial observations suggest a mechanochemical

sensory role of VSMCs primary cilia in the vasculature. In addition, primary cilia on the surface of VSMCs may act as fluid mechanosensors regulating intracellular Ca^{+2} influx and VSMCs migration in response to fluid shear stress. Primary cilia and cell surface glycocalyx are both displaced in response to fluid flow and affect cell surface receptors as well as integrins. Both cell contraction and migration requires disassembly of integrin-mediated focal adhesion [113]. Therefore, it remains to be discovered if VSMCs primary cilia can sense interstitial flow and play a role in controlling VSMCs contraction and migration. In addition, VSMCs *in vivo* are exposed to other hemodynamic forces such as stretch, and pressure at the same time, which may act in concert to regulate mechanosensitive signaling pathways controlling vascular function and disease. In summary, it is safe to assume that if VSMCs' primary cilia function or structure is perturbed, it will contribute to vascular disease and hypertension.

HYPERTENSION AND HUMAN ADPKD

ADPKD is an example of a ciliopathy or a genetic disorder resulting from the abnormal function and/or structure of primary cilia. Even with successful renal transplant or replacement therapy, patients with ADPKD eventually die due to cardiovascular complications, including hypertension, aneuryms, aortic root dilation, dissection, vascular ectasia, mitral valve prolapse and abnormal function of the microvascular bed [99, 114-116], heart failure and congestive heart disease [115-121]. Aside from the kidney phenotype, the frequencies of phenotypic manifestations in patients with ciliopathy include congestive heart failure/hypertension (78%), hepatic cysts (75%), diverticulosis (70%), ovarian cysts (40%), cardiac valve disorders (25%), inguinal hernias (15%) and intracranial aneurysms (10%) [107]. Our group is one of the first to report cilia function using mouse models and patient samples to explain cystic kidney phenotypes [2, 122] and to report cilia function in nitric oxide (NO) biosynthesis [5, 123]. Plasma concentration of the vasodilator nitric oxide has been found to be lowered in ADPKD patients compared to healthy volunteers [124]. This demonstrates a strong link between endothelial dysfunction and ADPKD. Another study reported similar results where the level of ADMA (asymmetric dimethylarginine), a marker of an inhibitor of nitric oxide synthase, was found to be elevated in PKD patients [125].

The correlation between hypertension and kidney volume occurs in the early childhood stages of ADPKD. The development of hypertension in ADPKD patients is associated with increased renal volume as well as increased left ventricular mass index. Similarly, it has also been suggested that high blood pressure can advance cyst growth [126, 127]. Interestingly, hypertension appears in children before they confront any significant reduction in glomerular filtration rate or development of ADPKD [128, 129]. Now that ADPKD is strongly correlated with dysfunction of ciliary proteins and/or abnormal cilia structure [2, 130, 131], this prompted us to propose that, endothelial dysfunction in ADPKD patients may be attributed to the inability of primary endothelial cilia to sense fluid-shear stress, or to an anomaly in any other downstream signaling mechanism. Taken together, this suggests that the pathogenesis of hypertension is a risk factor of endothelial primary cilia dysfunction at least partially independent from kidney function in ADPKD.

On the other hand, renal cyst enlargement in ADPKD adults has been ascribed to contribute in part to hypertension. Enlargement of renal cysts leads to the stimulation of both circulating as well as the intrarenal renin-angiotensin-aldosterone system (RAAS) system due to the compression of the cyst-adjacent parenchyma on the renal vasculature resulting in areas of renal ischemia and vascular changes [132, 133]. Activation of RAAS in PKD has been substantiated in both clinical studies [134] and murine models [135, 136]. Other components of the RAAS, including angiotensinogen, angiotensin converting enzyme (ACE), angiotensin II receptor and angiotensin II peptide have also been detected in cysts and dilated tubules in ADPKD kidneys [137]. In addition to hypertension, angiotensin contributes significantly to cyst growth and expansion, increased endothelin levels, fibrosis and increased sympathetic activity. Sympathetic activity can stimulate RAAS and angiotensin can stimulate sympathetic nervous system as well [138, 139]. Moreover, activation of the RAAS has been found in normotensive and hypertensive PKD patients, regardless of their blood pressure and renal function [140]. Not surprisingly, the high levels of circulating angiotensin II in PKD patients have been shown to contribute to the development of vascular hypertrophy, which is further implicated in vascular remodeling [141]. The effect of blockage of the renin-angiotensin-aldosterone system with Angiotensin Converting Enzyme inhibitors (ACE-I) and angiotensin receptor antagonists on renal volume and kidney function is discussed in the next section. A study involving eleven kidney transplant cases of hypertensive PKD patients accounted an improved blood pressure in only six patients [142]. Another report demonstrated that PKD patients with hypertension continue to show cardiovascular complications after renal transplantation [143]. These studies clearly suggest that, though kidney transplantation is beneficial for improving some cardiovascular issues, it is not sufficient to control hypertension in PKD patients. Whether hypertension contributes to diminished renal function or deteriorated kidney function exacerbates hypertension is still a debated topic that warrants further discussion and there is a wide scope of more research to clearly understand the cause and effect phenomenon undergoing in this case.

AVAILABLE AND ONGOING TREATMENT OPTIONS FOR CARDIOVASCULAR DISEASES IN ADPKD

A recent review involving 1877 ADPKD patients' records showed that the use of antihypertensive therapy in ADPKD patients have been increased from 32% in 1991 to 62% in 2008. A similar increase in the use of RAAS inhibitors was also reported (from 7 % to 42 %) [144]. But given that cardiovascular complications are the most

common cause of death in ADPKD patients, it is justified that researches are going on to a greater extent for innovation of novel therapeutics.

Alike regular hypertensive patients, reduced salt and caffeine intake, smoking cessation, regular exercise, and optimal water consumption have been suggested and found beneficial in hypertensive PKD patients [145, 146]. Pathophysiology of hypertension in this disease suggests the usefulness of ACE inhibitors. ACE-I enalapril is found to control blood pressure but it has a consistent antiproteinuric effect [133]. In a different study, 3% of patients displayed a reversible increase in serum creatinine after initiation of ACE-I use [147, 148]. So, ACE-Is should be used cautiously in ADPKD patients. The RAAS based pathophysiology of hypertension foretells the effectiveness of Angiotensin Receptor Blockers (ARBs). A randomized trial compared candesartan (ARB) with amlodipine (calcium channel blocker) and both were found equally effective in controlling blood pressure in PKD patients [149]. However, there is no other study exhibiting similar outcome and should be explored further. Dual blockade of RAAS with ACE-Is and ARBs has also been suggested and being tested in two clinical trials [150]. The most recent release of the results of the HALT study among 558 hypertensive participants with ADPKD revealed that the combination of lisinopril, an ACE-I and telmisartan, an ARB did not significantly alter the rate of increase in total kidney volume in the early stages of ADPKD. However, they indicated that aggressive blood-pressure control might slow kidney cyst growth and reduce left-ventricular-mass index compared to normal blood pressure control [151]. Beta-blockers (metoprolol, atenolol) and calcium channel blockers (amlodipine) are found to be effective in controlling hypertension in PKD patients. Though metoprolol did not alter glomerular filtration rate (GFR) or urinary albumin excretion, effects of atenolol on kidney function is still unknown. Calcium channel blockers are not recommended for use as a first line therapy in PKD patients, as this may cause a significant reduction in GFR. Theoretically, diuretics are recommended in PKD patients only as an additional therapy with ACE-Is as diuretics activate RAAS. Moreover, patients treated with diuretics showed increased urinary excretion of proteins [150].

We and others have independently studied abnormality in primary cilia in the vascular and renal systems in PKD. We hypothesized that cilia in the vascular system play important roles in regulating blood pressure and vascular integrity through the expression of mechano- or chemosensory receptors. Supporting our hypothesis is that patients with abnormal cilia function (PKD) also show a greater incidence of hypertension and other cardiovascular problems. In theory, drugs that interfere or alter cilia sensory function could prevent or delay this high blood pressure increase. This idea is based on our most recent chemical-screening studies showing that dopamine receptor is localized in endothelial cilia and that this ciliary receptor has dual chemo and mechano-sensing roles in endothelial cells. We showed that "activated" dopamine receptor-type 5 in the cilia could switch its chemosensing function to mechanoreceptor, while "non-activated" receptor has a primary function as a chemoreceptor. Activation of ciliary dopamine receptor could bypass mechano-ciliary polycystin complex through a mechanism that increases the cilia length. The extension of cilia probably serves to increase the sensitivity of these sensory organelles to fluid flow, in which dopamine receptor-type 5 acts as the mechanoreceptor.

CONCLUSION

As more evidence is presented to support the direct involvement of primary cilia in the cardiovascular system, this necessitates large-scale screening studies for drugs to investigate whether targeting primary cilia function or structure towards hypertension results in better outcomes.

CONFLICT OF INTEREST

The author(s) confirm that this article content has no conflict of interest.

ACKNOWLEDGEMENTS

Authors would like to thank Charisse Montgomery for her editing service. Due to restricted space, the authors apologize to those whose work is not cited in this paper. Z. Saad's and A. Mohieldin's work partially fulfills the requirements for a Ph.D. degree in Experimental Therapeutics and Medicinal and Biological Chemistry degrees, respectively. A. Al-Omran's, A. Zarban's and H. Saternos's work fulfills the requirements for a Master's degree in Pharmacology. Work from our laboratory that is cited in this paper has been supported by grant from DOD (PR130153) to S.M.N. We are thankful to the University of Toledo research programs as part of this work is funded by The University of Toledo's intramural startup fund for W.A.A.

REFERENCES

[1] Wheatley DN. Landmarks in the first hundred years of primary (9+0) cilium research. Cell Biol Int 2005; 29(5): 333-9.

[2] Nauli SM, Alenghat FJ, Luo Y, *et al*. Polycystins 1 and 2 mediate mechanosensation in the primary cilium of kidney cells. Nat Genet 2003; 33(2): 129-37.

[3] Cano DA, Sekine S, Hebrok M. Primary cilia deletion in pancreatic epithelial cells results in cyst formation and pancreatitis. Gastroenterology 2006; 131(6): 1856-69.

[4] Masyuk AI, Masyuk TV, Splinter PL, Huang BQ, Stroope AJ, LaRusso NF. Cholangiocyte cilia detect changes in luminal fluid flow and transmit them into intracellular Ca2+ and cAMP signaling. Gastroenterology 2006; 131(3): 911-20.

[5] Nauli SM, Kawanabe Y, Kaminski JJ, Pearce WJ, Ingber DE, Zhou J. Endothelial cilia are fluid shear sensors that regulate calcium signaling and nitric oxide production through polycystin-1. Circulation 2008; 117(9): 1161-71.

[6] Van der Heiden K, Hierck BP, Krams R, *et al*. Endothelial primary cilia in areas of disturbed flow are at the base of atherosclerosis. Atherosclerosis 2008; 196(2): 542-50.

[7] AbouAlaiwi WA, Takahashi M, Mell BR, *et al*. Ciliary polycystin-2 is a mechanosensitive calcium channel involved in nitric oxide signaling cascades. Circ Res 2009; 104(7): 860-9.

[8] Nonaka S, Tanaka Y, Okada Y, *et al*. Randomization of left-right asymmetry due to loss of nodal cilia generating leftward flow of extraembryonic fluid in mice lacking KIF3B motor protein. Cell 1998; 95(6): 829-37.

[9] Nonaka S, Shiratori H, Saijoh Y, Hamada H. Determination of left-right patterning of the mouse embryo by artificial nodal flow. Nature 2002; 418(6893): 96-9.

[10] Essner JJ, Vogan KJ, Wagner MK, Tabin CJ, Yost HJ, Brueckner M. Conserved function for embryonic nodal cilia. Nature 2002; 418(6893): 37-8.

[11] McGrath J, Somlo S, Makova S, Tian X, Brueckner M. Two populations of node monocilia initiate left-right asymmetry in the mouse. Cell 2003; 114(1): 61-73.

[12] Karcher C, Fischer A, Schweickert A, *et al*. Lack of a laterality phenotype in Pkd1 knock-out embryos correlates with absence of polycystin-1 in nodal cilia. Differentiation 2005; 73(8): 425-32.

[13] Andrade YN, Fernandes J, Vazquez E, *et al*. TRPV4 channel is involved in the coupling of fluid viscosity changes to epithelial ciliary activity. J Cell Biol 2005; 168(6): 869-74.

[14] Teilmann SC, Byskov AG, Pedersen PA, Wheatley DN, Pazour GJ, Christensen ST. Localization of transient receptor potential ion channels in primary and motile cilia of the female murine reproductive organs. Mol Reprod Dev 2005; 71(4): 444-52.

[15] Teilmann SC, Christensen ST. Localization of the angiopoietin receptors Tie-1 and Tie-2 on the primary cilia in the female reproductive organs. Cell Biol Int 2005; 29(5): 340-6.

[16] Hearn T, Spalluto C, Phillips VJ, *et al*. Subcellular localization of ALMS1 supports involvement of centrosome and basal body dysfunction in the pathogenesis of obesity, insulin resistance, and type 2 diabetes. Diabetes 2005; 54(5): 1581-7.

[17] Winkelbauer ME, Schafer JC, Haycraft CJ, Swoboda P, Yoder BK. The C. elegans homologs of nephrocystin-1 and nephrocystin-4 are cilia transition zone proteins involved in chemosensory perception. J Cell Sci 2005; 118(Pt 23): 5575-87.

[18] Davenport JR, Watts AJ, Roper VC, *et al*. Disruption of intraflagellar transport in adult mice leads to obesity and slow-onset cystic kidney disease. Curr Biol 2007; 17(18): 1586-94.

[19] Shah AS, Ben-Shahar Y, Moninger TO, Kline JN, Welsh MJ. Motile cilia of human airway epithelia are chemosensory. Science 2009; 325(5944): 1131-4.

[20] Nishimura DY, Fath M, Mullins RF, *et al*. Bbs2-null mice have neurosensory deficits, a defect in social dominance, and retinopathy associated with mislocalization of rhodopsin. Proc Natl Acad Sci U S A 2004; 101(47): 16588-93.

[21] Moore A, Escudier E, Roger G, *et al*. RPGR is mutated in patients with a complex X linked phenotype combining primary ciliary dyskinesia and retinitis pigmentosa. J Med Genet 2006; 43(4): 326-33.

[22] Ghosh AK, Murga-Zamalloa CA, Chan L, Hitchcock PF, Swaroop A, Khanna H. Human retinopathy-associated ciliary protein retinitis pigmentosa GTPase regulator mediates cilia-dependent vertebrate development. Hum Mol Genet 2010; 19(1): 90-8.

[23] Kulaga HM, Leitch CC, Eichers ER, *et al*. Loss of BBS proteins causes anosmia in humans and defects in olfactory cilia structure and function in the mouse. Nat Genet 2004; 36(9): 994-8.

[24] Layman WS, McEwen DP, Beyer LA, *et al*. Defects in neural stem cell proliferation and olfaction in Chd7 deficient mice indicate a mechanism for hyposmia in human CHARGE syndrome. Hum Mol Genet 2009; 18(11): 1909-23.

[25] Moorman SJ, Shorr AZ. The primary cilium as a gravitational force transducer and a regulator of transcriptional noise. Dev Dyn 2008; 237(8): 1955-9.

[26] Christensen ST, Pedersen SF, Satir P, Veland IR, Schneider L. The primary cilium coordinates signaling pathways in cell cycle control and migration during development and tissue repair. Curr Top Dev Biol 2008; 85: 261-301.

[27] Han YG, Kim HJ, Dlugosz AA, Ellison DW, Gilbertson RJ, Alvarez-Buylla A. Dual and opposing roles of primary cilia in medulloblastoma development. Nat Med 2009; 15(9): 1062-5.

[28] Wong SY, Seol AD, So PL, *et al*. Primary cilia can both mediate and suppress Hedgehog pathway-dependent tumorigenesis. Nat Med 2009; 15(9): 1055-61.

[29] Salathe M. Regulation of mammalian ciliary beating. Annu Rev Physiol 2007; 69: 401-22.

[30] Zariwala MA, Knowles MR, Omran H. Genetic defects in ciliary structure and function. Annu Rev Physiol 2007; 69: 423-50.

[31] Brunner S, Colman D, Travis AJ, *et al*. Overexpression of RPGR leads to male infertility in mice due to defects in flagellar assembly. Biol Reprod 2008; 79(4): 608-17.

[32] Lee L, Campagna DR, Pinkus JL, *et al*. Primary ciliary dyskinesia in mice lacking the novel ciliary protein Pcdp1. Mol Cell Biol 2008; 28(3): 949-57.

[33] Imai H, Hakkaku N, Iwamoto R, *et al*. Depletion of selenoprotein GPx4 in spermatocytes causes male infertility in mice. J Biol Chem 2009; 284(47): 32522-32.

[34] Ibanez-Tallon I, Pagenstecher A, Fliegauf M, *et al*. Dysfunction of axonemal dynein heavy chain Mdnah5 inhibits ependymal flow and reveals a novel mechanism for hydrocephalus formation. Hum Mol Genet 2004; 13(18): 2133-41.

[35] Sawamoto K, Wichterle H, Gonzalez-Perez O, *et al*. New neurons follow the flow of cerebrospinal fluid in the adult brain. Science 2006; 311(5761): 629-32.

[36] Wodarczyk C, Rowe I, Chiaravalli M, Pema M, Qian F, Boletta A. A novel mouse model reveals that polycystin-1 deficiency in ependyma and choroid plexus results in dysfunctional cilia and hydrocephalus. PLoS One 2009; 4(9): e7137.

[37] Eddy CA, Pauerstein CJ. Anatomy and physiology of the fallopian tube. Clin Obstet Gynecol 1980; 23(4): 1177-93.

[38] Lyons RA, Saridogan E, Djahanbakhch O. The reproductive significance of human Fallopian tube cilia. Hum Reprod Update 2006; 12(4): 363-72.

[39] Littlewood Evans A, Muller U. Stereocilia defects in the sensory hair cells of the inner ear in mice deficient in integrin alpha8beta1. Nat Genet 2000; 24(4): 424-8.

[40] Grillet N, Kazmierczak P, Xiong W, *et al*. The mechanotransduction machinery of hair cells. Sci Signal 2009; 2(85): pt5.

[41] Grillet N, Schwander M, Hildebrand MS, *et al*. Mutations in LOXHD1, an evolutionarily conserved stereociliary protein, disrupt hair cell function in mice and cause progressive hearing loss in humans. Am J Hum Genet 2009; 85(3): 328-37.

[42] Nauli SM, Haymour HS, AbouAlaiwi WA, Lo ST, Nauli AM. Primary cilia are mechanosensory organelles in vestibular tissues. Mechanosensitivity and Mechanotransduction: Springer Netherlands; 2011. p. 317-50.

[43] Collin SP, Barry Collin H. Primary cilia in vertebrate corneal endothelial cells. Cell Biol Int 2004; 28(2): 125-30.

[44] Doughty MJ. Changes in cell surface primary cilia and microvilli concurrent with measurements of fluid flow across the rabbit corneal endothelium *ex vivo*. Tissue Cell 1998; 30(6): 634-43.

[45] Kojimahara M. Endothelial cilia in rat mesenteric arteries and intramyocardial capillaries. Z Mikrosk Anat Forsch 1990; 104(3): 412-6.

[46] Gallagher BC. Primary cilia of the corneal endothelium. Am J Anat 1980; 159(4): 475-84.

[47] Satir P, Christensen ST. Overview of structure and function of mammalian cilia. Annu Rev Physiol 2007; 69: 377-400.

[48] Hildebrandt F, Otto E. Cilia and centrosomes: a unifying pathogenic concept for cystic kidney disease? Nat Rev Genet 2005; 6(12): 928-40.

[49] Praetorius HA, Spring KR. A physiological view of the primary cilium. Annu Rev Physiol 2005; 67: 515-29.

[50] Berbari NF, Bishop GA, Askwith CC, Lewis JS, Mykytyn K. Hippocampal neurons possess primary cilia in culture. J Neurosci Res 2007; 85(5): 1095-100.

[51] Whitfield JF. The neuronal primary cilium--an extrasynaptic signaling device. Cell Signal 2004; 16(7): 763-7.

[52] Fuchs JL, Schwark HD. Neuronal primary cilia: a review. Cell Biol Int 2004; 28(2): 111-8.

[53] Handel M, Schulz S, Stanarius A, *et al*. Selective targeting of somatostatin receptor 3 to neuronal cilia. Neuroscience 1999; 89(3): 909-26.

[54] Malone AM, Anderson CT, Tummala P, *et al*. Primary cilia mediate mechanosensing in bone cells by a calcium-independent mechanism. Proc Natl Acad Sci U S A 2007; 104(33): 13325-30.

[55] Whitfield JF. The solitary (primary) cilium--a mechanosensory toggle switch in bone and cartilage cells. Cell Signal 2008; 20(6): 1019-24.

[56] Xiao Z, Zhang S, Magenheimer BS, Luo J, Quarles LD. Polycystin-1 regulates skeletogenesis through stimulation of the osteoblast-specific transcription factor RUNX2-II. J Biol Chem 2008; 283(18): 12624-34.

[57] Christensen ST, Voss JW, Teilmann SC, Lambert IH. High expression of the taurine transporter TauT in primary cilia of NIH3T3 fibroblasts. Cell Biol Int 2005; 29(5): 347-51.

[58] Schneider L, Clement CA, Teilmann SC, *et al*. PDGFRalphaalpha signaling is regulated through the primary cilium in fibroblasts. Curr Biol 2005; 15(20): 1861-6.

[59] Schroder JM, Schneider L, Christensen ST, Pedersen LB. EB1 is required for primary cilia assembly in fibroblasts. Curr Biol 2007; 17(13): 1134-9.

[60] Nauli SM, Haymour HS, Aboualaiwi WA, Lo ST, Nauli AM. Primary Cilia are Mechanosensory Organelles in Vestibular Tissues. In: A. Kamkin IK, editor. Mechanosensitivity and Mechanotransduction: Springer Science+Business Media; 2011. p. 317-50.

[61] Schwartz EA, Leonard ML, Bizios R, Bowser SS. Analysis and modeling of the primary cilium bending response to fluid shear. Am J Physiol 1997; 272(1 Pt 2): F132-8.

[62] Praetorius HA, Spring KR. Removal of the MDCK cell primary cilium abolishes flow sensing. J Membr Biol 2003; 191(1): 69-76.

[63] Praetorius HA, Spring KR. Bending the MDCK cell primary cilium increases intracellular calcium. J Membr Biol 2001; 184(1): 71-9.

[64] Kottgen M, Buchholz B, Garcia-Gonzalez MA, *et al*. TRPP2 and TRPV4 form a polymodal sensory channel complex. J Cell Biol 2008; 182(3): 437-47.

[65] Wang S, Zhang J, Nauli SM, *et al*. Fibrocystin/polyductin, found in the same protein complex with polycystin-2, regulates calcium responses in kidney epithelia. Mol Cell Biol 2007; 27(8): 3241-52.

[66] Hirokawa N, Tanaka Y, Okada Y, Takeda S. Nodal flow and the generation of left-right asymmetry. Cell 2006; 125(1): 33-45.

[67] Jain R, Pan J, Driscoll JA, *et al*. Temporal relationship between primary and motile ciliogenesis in airway epithelial cells. Am J Respir Cell Mol Biol 2010; 43(6): 731-9.

[68] Ally A. Ventrolateral medullary control of cardiovascular activity during muscle contraction. Neurosci Biobehav Rev 1998; 23(1): 65-86.

[69] Krimer LS, Muly EC, 3rd, Williams GV, Goldman-Rakic PS. Dopaminergic regulation of cerebral cortical microcirculation. Nat Neurosci 1998; 1(4): 286-9.

[70] Korner PI, Head GA, Badoer E, Bobik A, Angus JA. Role of brain amine transmitters and some neuromodulators in blood pressure, heart rate, and baroreflex control. J Cardiovasc Pharmacol 1987; 10(Suppl 12): S26-32.

[71] Taylor EW, Jordan D, Coote JH. Central control of the cardiovascular and respiratory systems and their interactions in vertebrates. Physiol Rev 1999; 79(3): 855-916.

[72] Greisen G. Autoregulation of cerebral blood flow in newborn babies. Early Hum Dev 2005; 81(5): 423-8.

[73] Bolz S, Pieperhoff S, De Wit C, Pohl U. Chronic increases in transmural pressure reduce NO-mediated dilations in isolated resistance arteries of the hamster. Acta Physiol Scand 2000; 168(1): 113-7.

[74] Rubanyi GM. Ionic mechanisms involved in the flow- and pressure-sensor function of the endothelium. Z Kardiol 1991; 80(Suppl 7): 91-4.

[75] Spurrell BE, Murphy TV, Hill MA. Intraluminal pressure stimulates MAPK phosphorylation in arterioles: temporal dissociation from myogenic contractile response. Am J Physiol Heart Circ Physiol 2003; 285(4): H1764-73.

[76] Pyke KE, Tschakovsky ME. The relationship between shear stress and flow-mediated dilatation: implications for the assessment of endothelial function. J Physiol 2005; 568(Pt 2): 357-69.

[77] Raitakari OT, Celermajer DS. Flow-mediated dilatation. Br J Clin Pharmacol 2000; 50(5): 397-404.

[78] Chien S. Mechanotransduction and endothelial cell homeostasis: the wisdom of the cell. Am J Physiol Heart Circ Physiol 2007; 292(3): H1209-24.

[79] Brown TD. Techniques for mechanical stimulation of cells *in vitro*: a review. J Biomech 2000; 33(1): 3-14.

[80] Stossel TP, Condeelis J, Cooley L, *et al*. Filamins as integrators of cell mechanics and signalling. Nat Rev Mol Cell Biol 2001; 2(2): 138-45.

[81] Janmey PA, McCulloch CA. Cell mechanics: integrating cell responses to mechanical stimuli. Annu Rev Biomed Eng 2007; 9: 1-34.

[82] Tarbell JM, Pahakis MY. Mechanotransduction and the glycocalyx. J Intern Med 2006; 259(4): 339-50.

[83] Feletou M, Vanhoutte PM. Endothelium-dependent hyperpolarizations: past beliefs and present facts. Ann Med 2007; 39(7): 495-516.

[84] Ignarro LJ, Cirino G, Casini A, Napoli C. Nitric oxide as a signaling molecule in the vascular system: an overview. J Cardiovasc Pharmacol 1999; 34(6): 879-86.

[85] Nakane M. Soluble guanylyl cyclase: physiological role as an NO receptor and the potential molecular target for therapeutic application. Clin Chem Lab Med 2003; 41(7): 865-70.

[86] Ong AC, Ward CJ, Butler RJ, *et al*. Coordinate expression of the autosomal dominant polycystic kidney disease proteins, polycystin-2 and polycystin-1, in normal and cystic tissue. Am J Pathol 1999; 154(6): 1721-9.

[87] Hateboer N, Veldhuisen B, Peters D, *et al*. Location of mutations within the PKD2 gene influences clinical outcome. Kidney Int 2000; 57(4): 1444-51.

[88] Prasad RM, Jin X, Aboualaiwi WA, Nauli SM. Real-time vascular mechanosensation through *ex vivo* artery perfusion. Biol Proced Online 2014; 16(1): 6.

[89] Van der Heiden K, Groenendijk BC, Hierck BP, *et al*. Monocilia on chicken embryonic endocardium in low shear stress areas. Dev Dyn 2006; 235(1): 19-28.

[90] Iomini C, Tejada K, Mo W, Vaananen H, Piperno G. Primary cilia of human endothelial cells disassemble under laminar shear stress. J Cell Biol 2004; 164(6): 811-7.

[91] Poole CA, Jensen CG, Snyder JA, Gray CG, Hermanutz VL, Wheatley DN. Confocal analysis of primary cilia structure and colocalization with the Golgi apparatus in chondrocytes and aortic smooth muscle cells. Cell Biol Int 1997; 21(8): 483-94.

[92] Wu J, Du H, Wang X, Mei C, Sieck GC, Qian Q. Characterization of primary cilia in human airway smooth muscle cells. Chest 2009; 136(2): 561-70.

[93] Wu G, Markowitz GS, Li L, *et al*. Cardiac defects and renal failure in mice with targeted mutations in Pkd2. Nat Genet 2000; 24(1): 75-8.

[94] Marszalek JR, Ruiz-Lozano P, Roberts E, Chien KR, Goldstein LS. Situs inversus and embryonic ciliary morphogenesis defects in mouse mutants lacking the KIF3A subunit of kinesin-II. Proc Natl Acad Sci U S A 1999; 96(9): 5043-8.

[95] Sang L, Miller JJ, Corbit KC, *et al*. Mapping the NPHP-JBTS-MKS protein network reveals ciliopathy disease genes and pathways. Cell 2011; 145(4): 513-28.

[96] Willaredt MA, Gorgas K, Gardner HA, Tucker KL. Multiple essential roles for primary cilia in heart development. Cilia 2012; 1(1): 23.

[97] Clement CA, Ajbro KD, Koefoed K, *et al*. TGF-beta signaling is associated with endocytosis at the pocket region of the primary cilium. Cell Rep 2013; 3(6): 1806-14.

[98] Kim K, Drummond I, Ibraghimov-Beskrovnaya O, Klinger K, Arnaout MA. Polycystin 1 is required for the structural integrity of blood vessels. Proc Natl Acad Sci U S A 2000; 97(4): 1731-6.

[99] Ecder T, Schrier RW. Cardiovascular abnormalities in autosomal-dominant polycystic kidney disease. Nat Rev Nephrol 2009; 5(4): 221-8.

[100] Griffin MD, Torres VE, Grande JP, Kumar R. Vascular expression of polycystin. J Am Soc Nephrol 1997; 8(4): 616-26.

[101] Dolan JM, Meng H, Singh S, Paluch R, Kolega J. High fluid shear stress and spatial shear stress gradients affect endothelial

proliferation, survival, and alignment. Ann Biomed Eng 2011; 39(6): 1620-31.
[102] Aboualaiwi WA, Muntean BS, Ratnam S, *et al*. Survivin-induced abnormal ploidy contributes to cystic kidney and aneurysm formation. Circulation 2014; 129(6): 660-72.
[103] AbouAlaiwi WA, Ratnam S, Booth RL, Shah JV, Nauli SM. Endothelial cells from humans and mice with polycystic kidney disease are characterized by polyploidy and chromosome segregation defects through survivin down-regulation. Hum Mol Genet 2011; 20(2): 354-67.
[104] Nazarewicz RR, Salazar G, Patrushev N, *et al*. Early endosomal antigen 1 (EEA1) is an obligate scaffold for angiotensin II-induced, PKC-alpha-dependent Akt activation in endosomes. J Biol Chem 2011; 286(4): 2886-95.
[105] Li W, Wang H, Kuang CY, *et al*. An essential role for the Id1/PI3K/Akt/NFkB/survivin signalling pathway in promoting the proliferation of endothelial progenitor cells *in vitro*. Mol Cell Biochem 2012; 363(1-2): 135-45.
[106] Lin J, Guan Z, Wang C, *et al*. Inhibitor of differentiation 1 contributes to head and neck squamous cell carcinoma survival *via* the NF-kappaB/survivin and phosphoinositide 3-kinase/Akt signaling pathways. Clin Cancer Res 2010; 16(1): 77-87.
[107] Chapman AB, Rubinstein D, Hughes R, *et al*. Intracranial aneurysms in autosomal dominant polycystic kidney disease. N Engl J Med 1992; 327(13): 916-20.
[108] Blitzer AL, Panagis L, Gusella GL, Danias J, Mlodzik M, Iomini C. Primary cilia dynamics instruct tissue patterning and repair of corneal endothelium. Proc Natl Acad Sci U S A 2011; 108(7): 2819-24.
[109] Luo N, Conwell MD, Chen X, *et al*. Primary cilia signaling mediates intraocular pressure sensation. Proc Natl Acad Sci U S A 2014; 111(35): 12871-6.
[110] Luo N, West CC, Murga-Zamalloa CA, *et al*. OCRL localizes to the primary cilium: a new role for cilia in Lowe syndrome. Hum Mol Genet 2012; 21(15): 3333-44.
[111] Owens GK. Regulation of differentiation of vascular smooth muscle cells. Physiol Rev 1995; 75(3): 487-517.
[112] Lu CJ, Du H, Wu J, *et al*. Non-random distribution and sensory functions of primary cilia in vascular smooth muscle cells. Kidney Blood Press Res 2008; 31(3): 171-84.
[113] Shi ZD, Tarbell JM. Fluid flow mechanotransduction in vascular smooth muscle cells and fibroblasts. Ann Biomed Eng 2011; 39(6): 1608-19.
[114] Fick GM, Johnson AM, Hammond WS, Gabow PA. Causes of death in autosomal dominant polycystic kidney disease. J Am Soc Nephrol 1995; 5(12): 2048-56.
[115] Guay-Woodford LM. Renal cystic diseases: diverse phenotypes converge on the cilium/centrosome complex. Pediatr Nephrol 2006; 21(10): 1369-76.
[116] Lilova MI, Petkov DL. Intracranial aneurysms in a child with autosomal recessive polycystic kidney disease. Pediatr Nephrol 2001; 16(12): 1030-2.
[117] Biagini A, Maffei S, Baroni M, *et al*. Familiar clustering of aortic dissection in polycystic kidney disease. Am J Cardiol 1993; 72(9): 741-2.
[118] Capisonda R, Phan V, Traubuci J, Daneman A, Balfe JW, Guay-Woodford LM. Autosomal recessive polycystic kidney disease: outcomes from a single-center experience. Pediatr Nephrol 2003; 18(2): 119-26.
[119] Gabow PA. Autosomal dominant polycystic kidney disease. N Engl J Med 1993; 329(5): 332-42.
[120] Roy S, Dillon MJ, Trompeter RS, Barratt TM. Autosomal recessive polycystic kidney disease: long-term outcome of neonatal survivors. Pediatr Nephrol 1997; 11(3): 302-6.
[121] Torres VE, Harris PC. Mechanisms of Disease: autosomal dominant and recessive polycystic kidney diseases. Nat Clin Pract Nephrol 2006; 2(1): 40-55; quiz.
[122] Nauli SM, Rossetti S, Kolb RJ, *et al*. Loss of polycystin-1 in human cyst-lining epithelia leads to ciliary dysfunction. J Am Soc Nephrol 2006; 17(4): 1015-25.
[123] AbouAlaiwi WA, Lo ST, Nauli SM. Primary Cilia: Highly Sophisticated Biological Sensors. Sensors 2009; 9(9): 7003-20.
[124] Clausen P, Feldt-Rasmussen B, Iversen J, Lange M, Eidemak I, Strandgaard S. Flow-associated dilatory capacity of the brachial artery is intact in early autosomal dominant polycystic kidney disease. Am J Nephrol 2006; 26(4): 335-9.
[125] Wang D, Strandgaard S, Borresen ML, *et al*. Asymmetric dimethylarginine and lipid peroxidation products in early autosomal dominant polycystic kidney disease. Am J Kidney Dis 2008; 51(2): 184-91.
[126] Gabow PA, Chapman AB, Johnson AM, *et al*. Renal structure and hypertension in autosomal dominant polycystic kidney disease. Kidney Int 1990; 38(6): 1177-80.
[127] Gonzalo A, Gallego A, Rivera M, Orte L, Ortuno J. Influence of hypertension on early renal insufficiency in autosomal dominant polycystic kidney disease. Nephron 1996; 72(2): 225-30.
[128] Chapman AB, Schrier RW. Pathogenesis of hypertension in autosomal dominant polycystic kidney disease. Semin Nephrol 1991; 11(6): 653-60.
[129] Ecder T, Schrier RW. Hypertension in autosomal-dominant polycystic kidney disease: early occurrence and unique aspects. J Am Soc Nephrol 2001; 12(1): 194-200.
[130] Kolb RJ, Nauli SM. Ciliary dysfunction in polycystic kidney disease: an emerging model with polarizing potential. Front Biosci 2008; 13: 4451-66.
[131] Abdul-Majeed S, Nauli SM. Calcium-mediated mechanisms of cystic expansion. Biochim Biophys Acta 2011; 1812(10): 1281-90.
[132] Chapman AB, Johnson A, Gabow PA, Schrier RW. The renin-angiotensin-aldosterone system and autosomal dominant polycystic kidney disease. N Engl J Med 1990; 323(16): 1091-6.
[133] Ecder T, Chapman AB, Brosnahan GM, Edelstein CL, Johnson AM, Schrier RW. Effect of antihypertensive therapy on renal function and urinary albumin excretion in hypertensive patients with autosomal dominant polycystic kidney disease. Am J Kidney Dis 2000; 35(3): 427-32.
[134] Ramunni A, Saracino A, Esposito T, Saliani MT, Coratelli P. Renal vascular resistance and renin-angiotensin system in the pathogenesis of early hypertension in autosomal dominant polycystic kidney disease. Hypertens Res 2004; 27(4): 221-5.
[135] Kaspareit-Rittinghausen J, Deerberg F, Rapp KG, Wcislo A. Renal hypertension in rats with hereditary polycystic kidney disease. Z Versuchstierkd 1990; 33(5): 201-4.
[136] Lavoie JL, Lake-Bruse KD, Sigmund CD. Increased blood pressure in transgenic mice expressing both human renin and angiotensinogen in the renal proximal tubule. Am J Physiol Renal Physiol 2004; 286(5): F965-71.
[137] Loghman-Adham M, Soto CE, Inagami T, Cassis L. The intrarenal renin-angiotensin system in autosomal dominant polycystic kidney disease. Am J Physiol Renal Physiol 2004; 287(4): F775-88.
[138] Mancia G, Dell'Oro R, Quarti-Trevano F, Scopelliti F, Grassi G. Angiotensin-sympathetic system interactions in cardiovascular and metabolic disease. J Hypertens Suppl 2006; 24(1): S51-6.
[139] van den Meiracker AH, Boomsma F. The angiotensin II-sympathetic nervous system connection. J Hypertens 2003; 21(8): 1453-4.
[140] Chapman AB, Gabow PA. Hypertension in autosomal dominant polycystic kidney disease. Kidney Int Suppl 1997; 61: S71-3.
[141] McPherson EA, Luo Z, Brown RA, *et al*. Chymase-like angiotensin II-generating activity in end-stage human autosomal dominant polycystic kidney disease. J Am Soc Nephrol 2004; 15(2): 493-500.
[142] Shiroyanagi Y, Tanabe K, Hashimoto Y, *et al*. Kidney transplantation in the recipient with autosomal-dominant polycystic kidney disease: a single center experience. Transplant Proc 2000; 32(7): 1841-3.
[143] Florijn KW, Chang PC, van der Woude FJ, van Bockel JH, van Saase JL. Long-term cardiovascular morbidity and mortality in autosomal dominant polycystic kidney disease patients after renal transplantation. Transplantation 1994; 57(1): 73-81.
[144] Patch C, Charlton J, Roderick PJ, Gulliford MC. Use of antihypertensive medications and mortality of patients with autosomal dominant polycystic kidney disease: a population-based study. Am J Kidney Dis 2011; 57(6): 856-62.
[145] Torres VE, Grantham JJ, Chapman AB, *et al*. Potentially modifiable factors affecting the progression of autosomal dominant

polycystic kidney disease. Clin J Am Soc Nephrol 2011; 6(3): 640-7.

[146] Torres VE, Bankir L, Grantham JJ. A case for water in the treatment of polycystic kidney disease. Clin J Am Soc Nephrol 2009; 4(6): 1140-50.

[147] Chapman AB, Gabow PA, Schrier RW. Reversible renal failure associated with angiotensin-converting enzyme inhibitors in polycystic kidney disease. Ann Intern Med 1991; 115(10): 769-73.

[148] Bursztyn M. Polycystic kidney disease and angiotensin-converting enzyme inhibitors. Ann Intern Med 1992; 117(1): 90.

[149] Nutahara K, Higashihara E, Horie S, *et al*. Calcium channel blocker versus angiotensin II receptor blocker in autosomal dominant polycystic kidney disease. Nephron Clin Pract 2005; 99(1): c18-23.

[150] Rahbari-Oskoui F, Williams O, Chapman A. Mechanisms and management of hypertension in autosomal dominant polycystic kidney disease. Nephrol Dial Transplant 2014; 29(12): 2194-201.

[151] Schrier RW, Abebe KZ, Perrone RD, *et al*. Blood Pressure in Early Autosomal Dominant Polycystic Kidney Disease. N Engl J Med 2014; 371(24): 2255-66.

[152] Abou Alaiwi WA, Lo ST, Nauli SM. Primary cilia: highly sophisticated biological sensors. Sensors (Basel) 2009; 9(9): 7003-20.

[153] Nauli SM, Jin X, Hierck BP. The mechanosensory role of primary cilia in vascular hypertension. Int J Vasc Med 2011; 2011: 376281.

Received: December 10, 2014 Revised: June 09, 2015 Accepted: June 09, 2015

Graphical Abstract

Current Hypertension Reviews, **2015**, *Vol. 11, No. 1* **00**

Vascular Endothelial Primary Cilia: Mechanosensation and Hypertension

Ashraf M. Mohieldin, Hossain Saad Md Zubayer, Alzahra J. Al Omran, Hannah C. Saternos, Ali Zarban, Surya M. Nauli and Wissam A. AbouAlaiwi*

Department of Pharmacology, University of Toledo Health Science Campus, Toledo, OH, USA

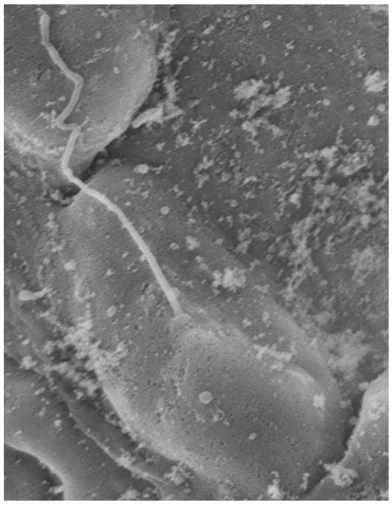

Primary cilia are mechanosensory organelles extending from the cell surface to sense cues in the extracellular environment and transduce signals into the cell producing a response that regulate a physiological phenomenon like blood pressure.

Research Article

pH sensors and ion Transporters: Potential therapeutic targets for acid-base disorders

Kimberly F. Atkinson, Surya M. Nauli*

Department of Biomedical & Pharmaceutical Sciences, Chapman University, Irvine, CA, USA.

ABSTRACT

Regulation of pH is critical for physiological processes. Maintenance of acid-base homeostasis is tightly regulated by the renal and respiratory systems. However, fluctuations in extracellular pH are also sensed by other organ systems. Ion transporter activity to modify the amount of acid (H^+ and CO_2) and bicarbonate HCO_3^- is therefore actively maintained within the kidney and lung. This review describes acid-base disorders (acidosis and alkalosis) and highlights the importance of pH sensors and ion transporters that may be potential therapeutic targets for treatment of acid-base disorders. Specifically, the renal pH sensors proline-rich tyrosine kinase-2 (Pyk2) and G-protein coupled receptor-4 (GPR4) are discussed here.

Keywords: pH sensor, acid-base disorder, acidosis, alkalosis, Pyk2, GPR4

Received 18 Feb 2016 Received in revised form 27 Mar 2016 Accepted 31 Mar 2016

***Address for correspondence**
Surya M. Nauli,
Department of Biomedical and Pharmaceutical Sciences, Chapman University, Irvine, CA, USA.
E-mail: nauli@chapman.edu; snauli@uci.edu

RESPIRATORY AND RENAL REGULATION OF ARTERIAL PH

Regulation of physiological pH is very important since most biochemical processes occur only within a narrow pH range. Typically, intracellular pH is about 7.2 and extracellular (or arterial) pH is between 7.36 and 7.44. pH fluctuation can occur in many organs and triggers a response in multiple cell types. pH can change as a result of ischemia, inflammation, exercise, musculoskeletal pain, and normal metabolic and neuronal activity [1]. Acid base homeostasis is primarily maintained by the renal and respiratory systems, but pH is also sensed by the epididymis, osteoclast, myocyte, neuron, and acid/base-producing cells in the kidney, gut, and pancreas, among others. Within the cell interior and in the blood, the carbonic acid-bicarbonate buffering system works to maintain pH homeostasis by adjusting the amount of hydrogen and bicarbonate ions present. The reaction of the CO_2/HCO_3^- buffering system, catalyzed by carbonic anhydrase (CA), is as follows: $CO_2 + H_2O \rightleftarrows H_2CO_3 \rightleftarrows H^+ + HCO_3^-$ [2]. CO_2 can readily diffuse through the membrane without the aid of a transporter. The lipid bilayer however is impermeable to charged H^+ and HCO_3^-, thereby requiring transport proteins to allow these ions to cross. Regulation of the acid or base transporters occurs through signaling transduction cascades initiated by a pH sensor, which is a protein directly activated by fluctuations in arterial or intracellular pH. This article focuses on the ion transporters that regulate pH and the putative pH sensors that control H^+ and HCO_3^- influx and efflux within a cell.

Acid loads occur regularly due to metabolism of protein from a Western diet. Normal physiology is therefore in place to prevent acidemia after ingestion of dietary acids including compensatory mechanisms of the renal and respiratory systems. Excessive drops in pH (<6.8) is termed acidosis, and can occur as a result of the loss of an alkali load via diarrhea or vomiting [3].The kidney can compensate for acid loads by increasing proximal tubule bicarbonate reabsorption, increasing distal acid secretion, and/or increasing ammonia excretion [4]. Hyperventilation is another way the body prevents acidosis by decreasing P_{CO2} [4]. Alkali loads can be metabolic, due to excessive excretion of urinary (or gastric) acid or respiratory; it can also due to hyperventilation, which lowers P_{CO2}. To maintain a normal pH, the proximal tubule compensates for an alkali load by decreasing bicarbonate reabsorption; the pH can also be lowered through hypoventilation [4].

The respiratory system regulates pH by altering the amount of CO_2 in the blood versus that exhaled through breathing. There are respiratory compensatory mechanisms triggered by decreased blood pH that results in greater diaphragm contraction, therefore more CO_2 gets exhaled [5]. The equilibrium between CO_2 (gas) ↔ CO_2 (dissolved) varies with partial pressure of CO_2, temperature, and pH [2]. Upon entering the low CO_2 concentration environment of the lungs, erythrocytes control the amount of CO_2 exhaled through regulation of the activity of CA and of ion transporter activity, specifically of AE1 (anion exchanger 1), which exchanges intracellular HCO_3^- for extracellular Cl^-. CA converts HCO_3^- to CO_2, which readily diffuses across the membrane and is exhaled [2]. This is shown in the diagram in (**Figure 1 and Panel B**). Anion exchangers (AEs) (AE1, AE2, AE3, and AE4) are important bicarbonate transporters in nearly all acid sensitive cells, as shown in (**Figure 1**). AE1 is a bicarbonate/chloride exchanger expressed in the erythrocyte and collecting duct (**Figure 1 and Panel D**). AE2 is another important bicarbonate/chloride exchanger expressed in gastric parietal cells and osteoclasts (**Figure 1 and Panel C**). AE3 is important in myocyte acidification. AE4, a sodium/bicarbonate cotransporter, is important in the brain (**Figure 1 and Panel A**) and in B-IC cells of the collecting duct (**Figure 1 and Panel D**). Other important bicarbonate transporters include NBCe1, Ndcbe, and Pendrin described in more detail in (**Table 1**).

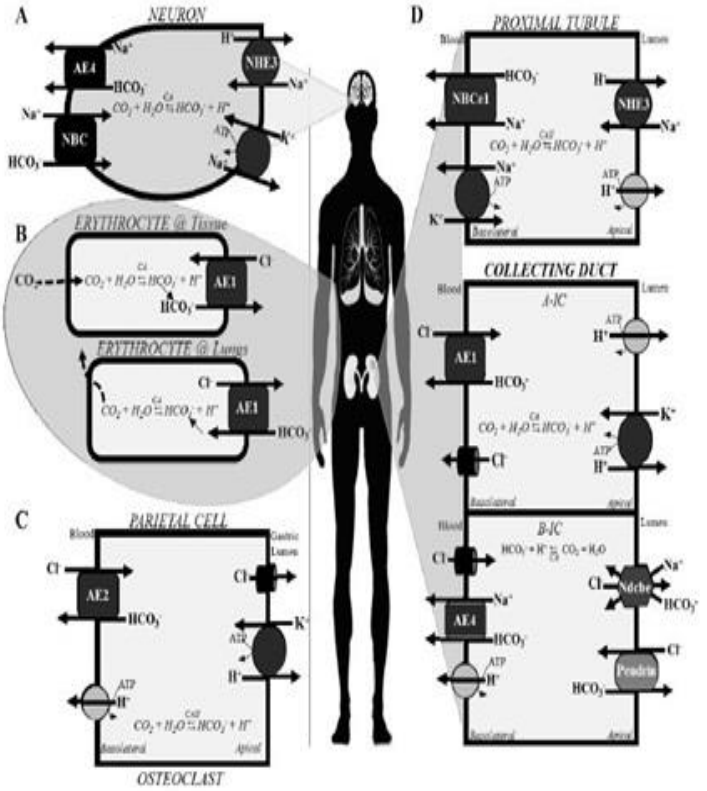

The diagram shows the main six cell types involved in pH sensing and/or regulation of arterial pH and the acid (H^+) and base (HCO_3^-) transporters expressed on the plasma membrane of each cell type. **(A)** The neuron senses and responds to changes in pH through regulation of bicarbonate transporters AE4 (HCO_3^- efflux) and NBC (HCO_3^- influx). **(B)** Respiratory regulation of pH occurs primarily through AE1 in erythrocytes, which interestingly reverses the direction of its normal HCO_3^-/Cl^- transport when in the lungs. Bicarbonate secretion occurs when the blood is at the body's tissues. When at the lungs, bicarbonate absorption occurs through AE1. Once inside the cell, bicarbonate is converted to CO2, diffuses through the membrane and is exhaled. **(C)** The gastric parietal cell and osteoclast exhibit similar ion transporter expression, with basolateral bicarbonate absorption through AE2 and proton extrusion through the basolateral H^+ ATPase and apical H^+,K^+-ATPase activity. **(D)** The three polarized epithelial cells diagramed on the right show renal acid- and base-secreting cells of the proximal tubule (top) and collecting duct (middle and bottom). Two types of intercalated cells are shown; Type A acid-secreting (A-IC) cells (middle) and type B bicarbonate-secreting (B-IC) cells (bottom). In the proximal tubule, basolateral bicarbonate reabsorption occurs via NBCe1 and apical acid secretion occurs via NHE3 and the H^+-ATPase. In A-ICs of the collecting duct, basolateral bicarbonate reabsorption occurs via AE1 and apical acid secretion occurs via H^+,K^+-ATPase and V-ATPase. In B-ICs of 15 the collecting duct, basolateral bicarbonate reabsorption occurs via AE4 and apical bicarbonate transport occurs via Ndcbe and Pendrin. Proton reabsorption also occurs in B-ICs across the basolateral membrane via active transport of the V-ATPase.

Figure 1: Cell-specific transporters involved in regulation of acid-base homeostasis.

Table 1: Transport proteins involved in pH regulation. The following transporters in the regulation of acid-base homeostasis are activated by changes in arterial pH. The cells expressing each protein and the function of each transporter are shown.

	Ion Transporter	Gene	Cell type	Ion efflux	Ion influx	Function	Refs
AE1	Anion exchanger 1; B and 3 protein	SLC4A1	Collecting duct (AIC)	Cl^-	HCO_3^-	Bicarbonate reabsorption (Cl^-/HCO_3^- exchanger)	[4]
AE2	Anion exchanger 2	SLC4A2	Gastric parietal cells and osteoclasts	Cl^-	HCO_3^-	Cl^-/HCO_3^- exchanger	[24]
AE3	Anion exchanger 3	SLC4A3	Cardiac myocyte	Cl^-	HCO_3^-	Myocyte acidification (Cl^-/HCO_3^- exchanger)	[2]
AE4	Anion exchanger 4	SLC4A9	Collecting duct (BIC) and Neuron	Na^+	HCO_3^-	Bicarbonate reabsorption	[4]
HKα1	α-subunit of gastric H^+,K^+-ATPase		Gastric parietal cells and Collecting duct (A-IC)	H^+	K^+	Urinary and intestinal acidification	
HKα2	α-subunit of colonic H^+,K^+-ATPase	ATP1A2	Colonic and Collecting duct (AIC)	H^+	K^+	Urinary and intestinal acidification	[8,2]
KCC4	KCl cotransporter	SLC12A7	Collecting duct	Cl^-	K^+	Urinary acidification	[4]
NBCe1	Sodium bicarbonate cotransporter-1	SLC4A4	Proximal tubule	HCO_3^-	Na^+	HCO_3^- absorption (Electrogenic Na^+/HCO_3^- cotransporter)	[4]
Ndcbe	Sodium-Driven Chloride/Bicarbonate Exchanger	SLC4A8	Collecting duct (B-IC)	Cl^-	Na^+ and HCO_3^-	HCO_3^- secretion (Na^+/HCO_3^- cotransporter)	[4]
NHE1	Na^+/H^+ exchanger 1		Cardiac myocyte Neuron	H^+	Na^+	Cardiac hypertrophy Epilepsy	[2]
NHE3	Na^+/H^+ exchanger 3		Proximal tubule and Neuron	H^+	Na^+	Urinary acidification	[26]
NHE6	Na^+/H^+ exchanger 6		Neuron	H^+	Na^+	Epilepsy and brain disorders	[19,26]
NHE9	Na^+/H^+ exchanger 9		Neuron	H^+	Na^+	ADHD	[26]
Pendrin			Collecting duct (B-IC)	HCO_3^-	Cl^-	Bicarbonate secretion	[4]
SLC26A7			Gastric parietal cells, CCD and OMCD	Cl^-	HCO_3^-	Basolateral HCO_3^- reabsorption (Cl^-/HCO_3^- exchanger)	[27]
V-ATPase	Vacuolar-type H^+-ATPase		Collecting duct and Epididymal clear cells	H^+		Urinary acidification	[8,13]

The kidneys are ultimately responsible for maintenance of acid base homeostasis through regulation of the HCO_3^- reabsorption and H^+ excretion into the urine. 90% of bicarbonate reabsorption occurs in the proximal tubule via transporters that are often Cl^- driven [6]. Acidification of the urine occurs primarily in the distal nephron via proton transporters that are often Na^+ or K^+ driven, such as the sodium/hydrogen exchangers (NHE) and Na^+, (H^+), K^+- ATPases. The apical membrane of the collecting duct is known to pump protons into the lumen via V-ATPases and H^+, K^+-ATPases to acidify the urine. The collecting duct (CD) is comprised of three segments, the cortical collecting duct (CCD), outer medullary collecting duct (OMCD), and inner medullary collecting duct (IMCD), each consisting of a different distribution of principal and intercalated cells. The three types of intercalated (IC) cells are acid-secreting Type A-ICs, bicarbonate-secreting Type B-ICs, and nonAnonB-ICs (not discussed in this article). (**Figure 1 and Panel D**) diagrams the transporters present in the apical and basolateral membranes of renal proximal tubule and intercalated cells. Many of the transporters responsible for the maintenance of pH are listed in (**Table 1**) along with the localization, physiological function, and ion specificity for each transporter.

CLINICAL MANIFESTATIONS AND PHARMACOLOGICAL IMPLICATIONS OF ACID-BASE DISORDERS

pH is indicative of acid-base status using the Henderson-Hasselbalch equation:

$$pH = pK + \log_{10} \frac{[Hco_3^-]}{Pco_2}$$

The acid dissociation constant is denoted as pK, bicarbonate concentration is in millimoles per liter and P_{CO2} is in millimeters of mercury [7]. Acid-base disorders involving abnormal CO_2 (changes in P_{CO2}) are termed respiratory disorders whereas those involving bicarbonate or acid are termed metabolic disorders [4]. Acidosis and alkalosis can each be either metabolic or respiratory. The methods for assessing acid-base disturbances depend on if the cause is respiratory or metabolic. Clinical evaluation includes analysis of any primary disease (pulmonary, cardiovascular, gastrointestinal) that may cause a secondary acid-base disturbance. Although these acid-base disorders are often due to genetic and/or physiological abnormalities, they can also be side-effects of certain medications or intoxications, as shown in (**Table 2**).

Table 2: Drug-induced acid-base disorders [6]. Acidosis (low pH) and alkalosis (high pH) can be due to dysregulation of H^+ or HCO_3^-, termed Metabolic, or due to abnormal CO_2 or P_{CO2}, termed Respiratory. These acid-base disorders can result from medications or intoxications.

	Metabolic		Respiratory
	Normal Anion Gap	**Elevated Anion Gap**	
Acidosis	Acetazolamide Topiramate Amphotericin B Ifosfamide	Linezolid Lorazepam Metformin Nitroprusside Nucleoside reverse transcriptase inhibitors Ethylene glycol Ethanol/Methanol	Opiates Benzodiazepines Propofol
Alkalosis	Diuretic therapy Bicarbonate administration Mineralocorticoids		Salicylates Nicotine Xanthine

Clinical evaluations of acid-base disorders involve measurement of blood pH, bicarbonate levels, and calculation of the urinary anion gap (AG), usually 10-12 mEq/L, and defined as follows:

$AG = Na^+ - (Cl^- + HCO_3^-)$. The AG is elevated in patients with metabolic acidosis (defined by arterial pH <7.35), which occurs due to excessive bicarbonate loss or acid loading. Symptoms of acidosis include weakness, headaches, shortness of breath, increased heart rate, nausea, vomiting, diarrhea, and sleepiness. Metabolic acidosis contributes to chronic kidney disease progression to end-stage renal disease [8]. Renal tubular acidosis (RTA) is a kidney disease that causes metabolic acidosis. Recent studies have shown that alkali treatment via sodium bicarbonate treatment slows the progression of CKD [9]. There are several types of RTA, including distal RTA (dRTA) and proximal RTA (pRTA), where distal and proximal refer to the segment of the nephron affected. Acid-base disorder treatment usually relies on treating the primary disease or problem that is contributing to the dysregulation of pH. In extreme cases of acidosis, bicarbonate infusions are used to regulate systemic pH. 7

pH SENSORS: REGULATION OF ION TRANSPORT

Regulation of the ion transporters that maintain pH homeostasis typically involves acid- or base activated signaling transduction mechanisms. Changes in pH may activate ion transporters directly, but more likely are sensed by an upstream pH sensor that regulates transporter activity, either directly or via a signaling cascade. Although a universal pH sensor has not been identified, several pH-sensitive signaling pathways that control acid-base transport have been elucidated. Putative pH sensors include pH-

sensitive G-protein coupled receptors (GPCRs) [10], H^+-sensing ion channels [11], alkali-sensing receptor tyrosine kinases (RTKs), soluble adenylyl cyclase (sAC) [12], cyclic nucleotides, and intracellular non-RTKs [12,13]. It is expected that there must be a pH sensor, a protein activated by changes in extracellular pH, such as a membrane-spanning GPCR, ion channel, or receptor tyrosine kinase. In the cardiovascular system, acid-sensing ion channels (ASICs), relatives of Epithelial Sodium Channel (ENaC), may be responsible for sensing changes in pH in the blood, as well as regulating blood pressure [14]. There are also four known acid-stimulated GPCRs activated by the protonation of extracellular histidine residues at low pH: GPR4 (G-protein coupled receptor-4) [3], OGR1 (ovarian cancer GPR1) aka GPR68 [15], TDAG8 (T Cell death-associated gene) aka GPR65 [16], and G2A aka GPR132 [10], shown in (**Table 3**). In the kidney, GPR4 is required for proper acid secretion [17]. GPR4-/- knockout mice develop metabolic acidosis due to reduced acid secretion, and also exhibit abnormal angiogenesis and increased insulin sensitivity [17]. GPR4 signals through a cAMP/PKA-mediated signaling mechanism and is required for H+, K+- ATPase activation in the CD [8]. Acid-sensing GPCRs have also been shown to be important in cancer cells, which often thrive in an acidic micro-environment [10].

Table 3: Putative Intracellular pH Sensors. The intracellular pH-sensitive proteins that have been identified are listed along with the particular cell types they are found, the downstream signaling proteins, and downstream targets.

Gene symbol	Protein Name	pH_o or pH_i	Localization	Signaling Mechanism	Target	Ref
Pyk2 (FAK)	Proline-rich tyrosine kinase-2 (Focal adhesion kinase)	pH_i	Proximal tubule collecting duct Osteoclast	Ca^{++} → ERK1/2	NHE3 V-ATPase	[13,18,19]
sAC	Soluble Adenylyl Cyclase	pH_i	Epididymis collecting duct	cAMP	V-ATPase ENaC	[22,23]
GPR4	G-protein coupled receptor-4	pH_o	Kidney, vasculature, pancreas	G_s →cAMP →PKA	AE1	[3,12,17]
OGR1 (GPR68)	Ovarian Cancer G-protein coupled receptor	pH_o	Bone, smooth muscle	G_q → PLC → Ca^{++}	V-ATPase	[15]
TDAG8 (GPR65)	T-Cell Death associated GPCR	pH_o	Immune and lymphoid cells	G_s → tmAC → cAMP → PKA	Inhibits MAPK	[16]

**tmAC – transmembrane adenylyl cyclase*

Intracellular pH sensors are localized inside the cell and activated by changes in intracellular pH (pH_i). Two potential intracellular pH sensors are proline-rich tyrosine kinase-2 (Pyk2) and sAC. Pyk2, an acid-activated non-RTK, is a putative intracellular pH sensor in the kidney that controls acid secretion through regulation of NHE3 and vacuolar V-ATPase activity in the proximal tubule and collecting duct, respectively [13,18,19]. In the case of Pyk2, mitogen-activated protein kinase (MAPK) signaling cascades involving extracellular signal-related kinase-1/2 (ERK1/2) control acid-activation of H+-secretion (via NHE3 and H^+-ATPase) during pH recovery after an acid load [13,20,21]. V-type H^+-ATPase mobilization is regulated by sAC, an intracellular CO_2/HCO_3^- sensor directly activated by increased intracellular calcium and/or bicarbonate ions [22]. sAC stimulates cAMP/cGMP release via phospholipase C (PLC) and protein kinase C (PKC)-mediated signaling pathways to regulate V-ATPase recycling in the epididymis and Na^+ reabsorption in the collecting duct [22,23]. Mineralocorticoids stimulate H^+-ATPase activity in the medullary collecting duct. Mutations in genes that encode the α4 and β1 Isoforms of the V-ATPase lead to dRTA [6]. The importance of V-ATPase activity in acid-base balance, especially its regulation in the

kidney, makes it a possible therapeutic target for controlling systemic pH. Pharmacologically, the transporters of the distal nephron and the pH sensors that regulate their activity would be good therapeutic targets for the treatment of acidosis.

PHYSIOLOGY OF ACID-BASE STUDIES

Renal micropuncture, nephron microperfusion and various molecular and biochemical techniques have greatly contributed to our current understanding on the acid-base regulation. The use of transgenic mice has also allowed us to further comprehend the physiological roles of acid-base transports. A mutation in acid-base transport can result in neonatal death [24-27]. However, it is important to note that these mice also have other severe phenotypes in addition to acid-base imbalance. Other phenotypes include growth retardation, pulmonary edema, electrolyte imbalance, anemia, intestinal obstruction, and other organ abnormalities, making it hard to discern the cause of death in these mice. Interestingly, administration of sodium bicarbonate in one of the mouse models prolonged survival rate, indicating that acid-base balance could dampen the progression of organ damage [26]. Physiologically, the acid-base homeostasis is also known to be a redundant process. To better understand this, we will use NHE3 as an example. In NHE3 mutant mice, NHE8 plays a compensatory role in renal acidification [27,28]. Both NHE2 and NHE3 also share a redundant function [29]. Although NHE3 mutant mice may present mild absorptive defects [30,31], the resulting hypovolemia does not help in understanding the specific effects of NHE3 deficiency on kidney function [32]. Furthermore, there is co-regulation between NHE3 with different NHE isoforms [33,34], denoting a highly complex acid-base regulation. Given the significance of acid-base regulation in all tissues, it is not surprising that we have a redundant physiological system to compensate any acid-base imbalance in our body. Nonetheless, transgenic mouse models have provided a plethora of knowledge on acid-base transport in vivo. This includes a better understanding that NHE3 plays an important role in fluid and bicarbonate reabsorption in the proximal convoluted tubule but does not play an important role in NH4 excretion [31].

Despite the significant physiological complexity, much has been learned about acid-base regulation in vivo through animal models, including the molecular mechanism of different transporters (**Table 1**). For more information about animal models used to study acid-base regulation, please refer to a recent comprehensive review [35-39].

SUMMARY

In summary, the regulation of systemic (or arterial) pH is highly complex and involves different mechanisms in multiple cell types, various transporters, and pH sensors. Recent advances using transgenic animal models suggest no single genetic knockout mouse has caused a major disruption in acid-base homeostasis, indicating it is a highly complex and redundant process. Pharmacological control of pH may be accomplished by targeting ion transporters, pH sensors, or signaling molecules that regulate acid-base homeostasis. We have discussed the putative pH sensors and ion transporters that need to be examined as therapeutic targets, including but not limited to Pyk2, sAC, and GPR4.

ACKNOWLEDGEMENTS

We would like to thank Rinzhin T. Sherpa for his technical support and contribution. We also thank Dr. Thomas D. DuBose, M.D, M.A.C.P at Wake Forest School of Medicine for his proofreading and advice. This work was supported in part by Congressionally Directed Medical Research Program PR130153.

REFERENCES

1. Abdelhamid RE, Sluka KA. ASICs Mediate Pain and Inflammation in Musculoskeletal Diseases. Physiology. 2015; 30(6): 449-459.
2. Casey JR. Why bicarbonate?. Biochemistry and Cell Biology. 2006; 84(6): 930-939.
3. Sun X, Stephens L, DuBose TD, Petrovic S. Adaptation by the collecting duct to an exogenous acid load is blunted by deletion of the proton-sensing receptor GPR4. Am. J. Physiol. Regul. Integr. Comp. Physiol. 2015; 309(2): F120-F136.
4. Hamm LL, Nakhoul N, Hering-Smith KS. Acid-Base Homeostasis. Clin. J. Am. Soc. Nephrol: CJASN. 2015; 10(12): 2232-2242.
5. Clancy J, Andrew M. Intermediate and long-term regulation of acid-base

homeostasis. Br. J. Nurs. 2007; 16(17): 1076-1079.
6. Ayers P, Dixon C, Mays A. Acid-Base Disorders: Learning the Basics. Nutrition in Clinical Practice. 2014; 30(1): 14-20.
7. Berend K, de Vries APJ, Gans ROB. Physiological Approach to Assessment of Acid-Base Disturbances. N. Engl. J. Med. 2014; 371(15): 1434-1445.
8. Codina J, Opyd TS, Powell ZB, Furdui CM, Petrovic S, Penn RB, et al. pHdependent regulation of the α-subunit of H+-K+-ATPase (HKα2). Am. J. Physiol. Renal. Physiol. 2011; 301(3): F536-F543.
9. Scialla JJ. The balance of the evidence on acid-base homeostasis and progression of chronic kidney disease. Kidney International. 2015; 88(1): 9-11.
10. Justus CR, Dong L, Yang LV. Acidic tumor microenvironment and pH-sensing G proteincoupled receptors. Frontiers in Physiology. 2013; 4: 354.
11. Liu S, Cheng X-Y, Wang F, Liu C-F. Acid-sensing ion channels: potential therapeutic targets for neurologic diseases. Translational Neurodegeneration. 2015; 4: 10.
12. Brown D, Wagner CA. Molecular Mechanisms of Acid-Base Sensing by the Kidney. Clin. J. Am. Soc. Nephrol. 2012; 23(5): 774-780.
13. Fisher KD, Codina J, Petrovic S, DuBose TD Pyk2 regulates H+-ATPase-mediated proton secretion in the outer medullary collecting duct via an ERK1/2 signaling pathway. Am J Physiol Renal Physiol. 2012; 303(9): F1353-F1362.
14. Lu Y, Ma X, Sabharwal R, Snitsarev V, Morgan D, Rahmouni K, et al. The Ion Channel ASIC2 is required for Baroreceptor and Autonomic Control of the Circulation. Neuron 2009; 64(6): 885-897.
15. Ludwig M-G, Vanek M, Guerini D, Gasser JA, Jones CE, Junker U, et al. Proton-sensing G-protein-coupled receptors. Nature. 2003; 425(6953): 93-98.
16. Ishii S, Kihara Y, Shimizu T. Identification of T Cell Death-associated Gene 8 (TDAG8) as a Novel Acid Sensing G-protein-coupled Receptor. J. Biol. Chem. 2005; 280(10): 9083-9087.
17. Sun X, Yang LV, Tiegs BC, Arend LJ, McGraw DW, Penn RB, et al. Deletion of the pH Sensor GPR4 Decreases Renal Acid Excretion. Clin. J. Am. Soc. Nephrol: JASN. 2009; 21(10): 1745-1755.
18. Li S, Sato S, Yang X, Preisig PA, Alpern RJ. Pyk2 activation is integral to acid stimulation of sodium/hydrogen exchanger 3. J. Clin. Invest. 2004; 114(12): 1782-1789.
19. Preisig PA. The acid-activated signaling pathway: Starting with Pyk2 and ending with increased NHE3 activity. Kidney Int. 2007; 72(11): 1324-1329.
20. Odunewu A, Fliegel L. Acidosis-mediated regulation of the NHE1 isoform of the Na+/H+ exchanger in renal cells. Am. J. Physiol. Renal. Physiol. 2014; 305(3): F370-F381.
21. Guan J, Wu X, Arons E, Christou H. The p38 Mitogen-Activated Protein kinase pathway is involved in the regulation of Heme Oxygenase-1 by acidic extracellular pH in aortic smooth muscle cells. J. Cell. Biochem. 2008; 105(5): 1298-1306.
22. Pastor-Soler N, Beaulieu Vr, Litvin TN, Da Silva N, Chen Y, Brown D, et al. Bicarbonate-regulated Adenylyl Cyclase (sAC) Is a Sensor That Regulates pH-dependent V-ATPase Recycling. J. Biol. Chem. 2003; 278(49): 49523-49529.
23. Hallows KR, Wang H, Edinger RS, Butterworth MB, Oyster NM, Li H, et al. Regulation of Epithelial Na(+) Transport by Soluble Adenylyl Cyclase in Kidney Collecting Duct Cells. J. Biol. Chem. 2009; 284(9): 5774-5783.
24. Hummler E, Barker P, Talbot C, Wang Q, Verdumo C, Grubb B, et al. A mouse model for the renal saltwasting syndrome pseudohypoaldosteronism. Proceedings of the National Academy of Sciences of the United States of America. 1997; 94(21): 11710-11715.
25. Gawenis LR, Bradford EM, Prasad V, Lorenz JN, Simpson JE, Clarke LL, et al. Colonic Anion Secretory Defects and Metabolic Acidosis in Mice Lacking the NBC1 Cotransporter. J. Biol. Chem. 2007; 282(12): 9042-9052.
26. Lo Y-F, Yang S-S, Seki G, Yamada H, Horita S, Yamazaki O, et al. Severe metabolic acidosis causes early lethality in NBC1 W516X knock-in mice as a model of human isolated proximal renal tubular acidosis. Kidney International. 2011; 79(7): 730-741.

27. Stehberger PA, Shmukler BE, Stuart-Tilley AK, Peters LL, Alper SL, Wagner CA. Distal Renal Tubular Acidosis in Mice Lacking the AE1 (Band3) Cl-/HCO3- Exchanger (slc4a1). Clin. J. Am. Soc. Nephrol. 2007; 18(5): 1408-1418.
28. Baum M, Twombley K, Gattineni J, Joseph C, Wang L, Zhang Q, et al. Proximal tubule Na+/H+ exchanger activity in adult NHE8-/-, NHE3-/-, and NHE3-/-/NHE8-/- mice. Am. J. Physiol. Renal. Physiol. 2012; 303(11): F1495-F1502.
29. Bailey MA, Giebisch G, Abbiati T, Aronson PS, Gawenis LR, Shull GE, et al. NHE2-mediated bicarbonate reabsorption in the distal tubule of NHE3 null mice. J. Physiol. 2004; 561: 765-775.
30. Schultheis PJ, Clarke LL, Meneton P, Miller ML, Soleimani M, Gawenis LR, et al. Renal and intestinal absorptive defects in mice lacking the NHE3 Na +/H+ exchanger. Nat. Genet. 1998; 19(3): 282-285.
31. Li HC, Du Z, Barone S, Rubera I, McDonough AA, Tauc M, et al. Proximal tubule specific knockout of the Na(+)/H(+) exchanger NHE3: effects on bicarbonate absorption and ammonium excretion. J. Mol. Med. (Berlin, Germany). 2013; 91(8): 951-963.
32. Noonan WT, Woo AL, Nieman ML, Prasad V, Schultheis PJ, Shull GE, et al. Blood pressure maintenance in NHE3-deficient mice with transgenic expression of NHE3 in small intestine. Am. J. Physiol. Regul. Integr. Comp. Physiol. 2005; 288(3): R685-R691.
33. Good DW, Watts BA, George T, Meyer JW, Shull GE. Transepithelial HCO3- absorption is defective in renal thick ascending limbs from Na+/H+ exchanger NHE1 null mutant mice. Am. J. Physiol. Regul. Integr. Comp. Physiol. 2004; 287(6): F1244-F1249.
34. Watts BA, George T, Good DW. The Basolateral NHE1 Na+/H+ Exchanger Regulates Transepithelial Absorption through Actin Cytoskeleton Remodeling in Renal Thick Ascending Limb. J. Biol. Chem. 2005; 280(12): 11439-11447.
35. Eladari D, Kumai Y. Renal acid-base regulation: new insights from animal models. Pflugers. Arch. 2015; 467(8): 1623-1641.
36. Gawenis LR, Ledoussal C, Judd LM, Prasad V, Alper SL, Stuart-Tilley A. Mice with a Targeted Disruption of the AE2 Exchanger Are Achlorhydric. J. Biol. Chem. 2004; 279(29): 30531-30539.
37. Bobulescu IA, Moe OW. Na(+)/H(+) Exchangers in Renal Regulation of Acid-Base Balance. Seminars in nephrology. 2006; 26(5): 334-344.
38. Zhao H, Carney KE, Falgoust L, Pan JW, Sun D, Zhang Z. Emerging roles of Na+/H+ exchangers in epilepsy and developmental brain disorders. Progress in Neurobiology. 2016; 138-140: 19-35.
39. Petrovic S, Barone S, Xu J, Conforti L, Ma L, Kujala M. SLC26A7: a basolateral Cl-/HCO3- exchanger specific to intercalated cells of the outer medullary collecting duct. Am. J. Physiol. Renal. Physiol. 2004; 286(1): F161-F169.

SciMedCentral

Annals of Clinical Cytology and Pathology

Case Report

Capillary Endothelia from Two ADPKD Patients are Polyploidy

Sarmed H. Kathem[1,2], Wissam A. AbouAlaiwi[3], Xiaolin Zi[2] and Surya M. Nauli[1,2]*

[1]Department of Biomedical & Pharmaceutical Sciences, Chapman University, USA
[2]Department of Urology, University of California, USA
[3]Department of Pharmacology and Experimental Therapeutics, University of Toledo, USA

*Corresponding author
Surya M. Nauli, Chapman University, Harry and Diane Rinker Health Science Campus, 9401 Jeronimo Road, Irvine, CA 92618-1908, USA, Tel: 714-516-5480; Fax: 714-516-5481; Email: nauli@chapman.edu, snauli@uci.edu

Submitted: 10 March 2016

Accepted: 31 April 2016

Published: 25 April 2016

Abstract

Bilateral renal cyst formation is the main feature of autosomal dominant polycystic kidney disease (ADPKD). We and other laboratories have previously shown that cyst-lining epithelia of kidneys from ADPKD patients are characterized by polyploidy. In this report, we show that endothelia from the renal capillary beds of two ADPKD patients are also polyploidy. Spectral karyotyping study further confirms our flow cytometry analyses. We suggest that polyploidy may be used as a potential cellular marker in ADPKD.

INTRODUCTION

Autosomal dominant polycystic kidney disease (ADPKD) is the most common life-threatening hereditary genetic disease. Although kidneys are the major sites of clinical disease, the prevalence of extra renal manifestations in ADPKD is very high. These extra renal manifestations include cyst formation in other ductal organs and various cardiovascular abnormalities [1-3]. Polycystic kidney has also been associated with polyploidy [4-7]. At the molecular level, vascular endothelia from ADPKD have been associated with dysfunctional primary cilia [8] Aberrant cell proliferation has been reported in cells with defective cilia [9,10]. We recently showed that cystic renal epithelia from patients are polyploidy, probably through abnormal regulation of chromosomal passenger complex. Abnormality of this protein complex has also been associated with aneurysm formation in vascular endothelia of mouse polycystic models [11,12]. However, the endothelia of renal capillary beds from ADPKD patients have never been previously studied.

CASE REPORT

Human kidney samples from three subjects were taken; two were from ADPKD patients (54-years-old female and 49-years-old male), and the other was from a non-ADPKD subject. The nephrectomy was done in both ADPKD patients, because these kidneys had reached the end-stage renal failure and were further complicated by infections. In general, ADPKD kidney has a grossly distorted architecture characterized by fluid-filled cysts (Figure 1). We isolated endothelia from the renal capillary beds. First branches of capillaries from interlobar arteries were pooled. Due to the nature of primary cells from the capillary beds, we were not able to purify these isolated endothelial cells. Successful cell isolation typically provides homogenous cell morphology based on the side scatter from the flow cytometry. Capillaries were then briefly rinsed with phosphate buffered saline (pH 7.4). To dissociate the endothelial cells, capillaries were subsequently incubated with trypsin for 20-30 minutes at 37ºC. Because capillaries contain mainly endothelia, the isolation typically provides relatively pure endothelial cells. Endothelial cells from the samples were then processed for flow cytometry and spectral karyotyping analysis to investigate cellular polyploidy. Propidium iodide (PI) and 5-bromodeoxyuridine (BrdU) staining were used to analyze cellular polyploidy from the samples. Generally, PI was used for DNA content quantification, while BrdU was used as a marker for cell division. Our flow cytometry analyses showed abnormal polyploidy peaks in both ADPKD samples but not in non-ADPKD sample (Figure 2). Cells with >2N represent

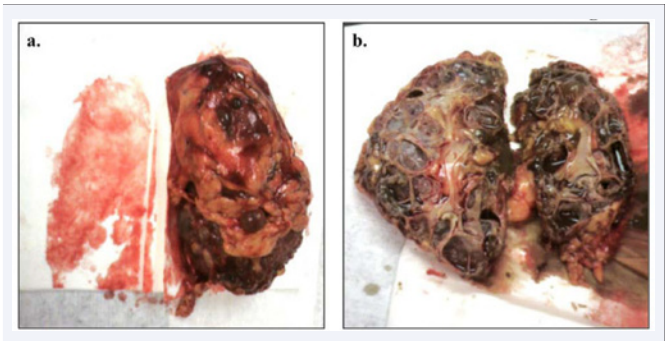

Figure 1 Autosomal dominant polycystic kidney a: Polycystic kidney is characterized by the grossly distorted and enlarged kidney. b: A polycystic kidney was cut in half, showing the presence of numerous fluid-filled cysts. Fluid accumulation in the cysts contributes to the heavy weight and large size of an ADPKD kidney.

polyploidy and have higher DNA content. In non-ADPKD, cells with >2N represent about 0.8%, while in ADPKD patients# 1 and 2 the polyploidy cells constitute of 16.5% and 8.2%, respectively. Interestingly, further analysis of PI and BrdU showed that the abnormal polyploidy cells retain their ability to undergo cell division. This result indicates that endothelia from ADPKD patients are associated with polyploidy and that those polyploidy cells could undergo cell division. Spectral karyotyping (SKY) was also used to confirm our flow cytometry results. Chromosomes from a single endothelium were differentially labeled with probes containing a mixture of fluorescent dyes (Rhodamine, Texas Red, Cy5, FITC and Cy5.5), as describe previously [13]. Unfortunately, we were not successful to karyotype endothelial sample from the second ADPKD patient. From the first ADPKD patient, a single ADPKD endothelium was analyzed, and it showed cellular tetraploidy (Figure 3).

DISCUSSION

We here report that endothelia from renal vascular of ADPKD patients are polyploidy. Those cells could potentially have abnormal cell division that may lead to vascular dysfunction. We previously reported that vascular endothelia from ADPKD patients are less sensitive to fluid-shear stress [8]. This report may thus associate the mechano-dysfunction and polyploidy in ADPKD endothelia. Independent studies have shown centrosomal over-amplification in polycystic kidneys from mice and human [4-7]. The abnormal centrosomal amplification was suggested to occur early in cystic kidney disease. Consequently, abnormal cell division and chromosomal segregation resulted from centrosomal over-duplication lead to polyploidy and genomic instability. Polyploidy has also been observed in vascular endothelial of polycystic kidney mouse models [11,12]. At least in the mice, it

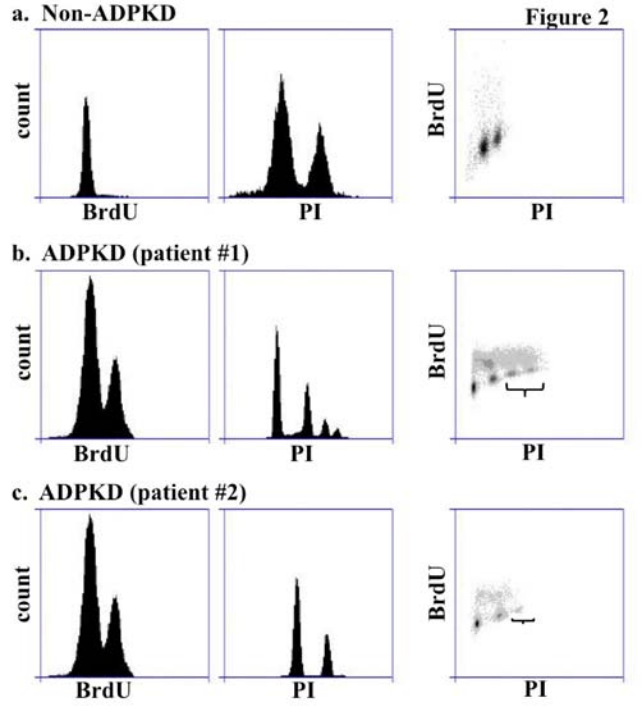

Figure 2 Flow cytometry analysis: Vascular endothelia were isolated from the renal capillary beds of non-APKD (a) and two independent ADPKD (b, c) kidneys. Cells were then labeled with propidium iodide (PI) and 5-bromodeoxyuridine (BrdU). PI and BrdU staining were analyzed individually and interdependently. Brackets indicate the presence of polyploidy cells.

Figure 3 Spectral Karyotype analysis Chromosomes from an endothelium were isolated and processed for labeling with fluorescence probes specific for each individual chromosome. A tetraploidy with a total of 92 chromosomes was observed in the sample obtained from a female ADPKD patient.

was postulated that polyploidy in endothelial cells could result in aneurysm formation, probably through abnormal chromosomal passenger complex. Our current study reinforces the previous findings that vascular endothelia and renal epithelia from polycystic mouse models and ADPKD patients are polyploidy.

CONCLUSION

Flow cytometry analyses using PI and BrdU indicate that ADPKD endothelia have higher DNA content and polyploidy. Analysis with spectral karyotyping further confirmed this result showing abnormal chromosomal number and tetraploidy. Our study is preliminary in nature, and a greater number of patients are needed for a future study. If confirmed in a larger scale study, this result might have an impact on the pathogenic event leading to the development of vascular abnormalities in ADPKD. We propose that polyploidy can be a broad cellular feature not only in the renal epithelia but also in vascular endothelia and that polyploidy may be used as a cellular marker to understand disease progression in ADPKD.

REFERENCES

1. Ecder T. Cardiovascular complications in autosomal dominant polycystic kidney disease. Curr Hypertens Rev. 2013; 9: 2-11.
2. Perrone RD, Malek AM, Watnick T. Vascular complications in autosomal dominant polycystic kidney disease. Nat Rev Nephrol. 2015; 11: 589-598.
3. Torres VE, Harris PC. Autosomal dominant polycystic kidney disease: the last 3 years. Kidney Int. 2009; 76: 149-168.
4. Jin X, Muntean BS, Aal-Aaboda MS, Duan Q, Zhou J, Nauli SM. L-type calcium channel modulates cystic kidney phenotype. Biochim Biophys Acta. 2014; 1842: 1518-1526.
5. Zhou X, Fan LX, Li K, Ramchandran R, Calvet JP, Li X. SIRT2 regulates ciliogenesis and contributes to abnormal centrosome amplification caused by loss of polycystin-1. Hum Mol Genet. 2014; 23: 1644-1655.
6. Burtey S, Riera M, Ribe E, Pennenkamp P, Rance R, Luciani J, et al. Centrosome overduplication and mitotic instability in PKD2 transgenic lines. Cell Biol Int. 2008; 32: 1193-1198.
7. Battini L, Macip S, Fedorova E, Dikman S, Somlo S, Montagna C, et al. Loss of polycystin-1 causes centrosome amplification and genomic instability. Hum Mol Genet. 2008; 17: 2819-2833.
8. AbouAlaiwi WA, Takahashi M, Mell BR, Jones TJ, Ratnam S, Kolb RJ, et al. Ciliary polycystin-2 is a mechanosensitive calcium channel involved in nitric oxide signaling cascades. Circ Res. 2009; 104: 860-869.
9. Jonassen JA, San Agustin J, Follit JA, Pazour GJ. Deletion of IFT20 in the mouse kidney causes misorientation of the mitotic spindle and cystic kidney disease. J Cell Biol. 2008; 183: 377-384.
10. Qin H, Wang Z, Diener D, Rosenbaum J. Intraflagellar transport protein 27 is a small G protein involved in cell-cycle control. Curr Biol. 2007; 17: 193-202.
11. Aboualaiwi WA, Muntean BS, Ratnam S, Joe B, Liu L, Booth RL, et al. Survivin-induced abnormal ploidy contributes to cystic kidney and aneurysm formation. Circulation. 2014; 129: 660-672.
12. AbouAlaiwi WA, Ratnam S, Booth RL, Shah JV, Nauli SM. Endothelial cells from humans and mice with polycystic kidney disease are characterized by polyploidy and chromosome segregation defects through survivin down-regulation. Hum Mol Genet. 2011; 20: 354-367.
13. AbouAlaiwi WA, Rodriguez I, Nauli SM. Spectral karyotyping to study chromosome abnormalities in humans and mice with polycystic kidney disease. J Vis Exp. 2012; 60.

Cite this article

Kathem SH, AbouAlaiwi WA, Zi X, Nauli SM (2016) Capillary Endothelia from Two ADPKD Patients are Polyploidy. Ann Clin Cytol Pathol 2(2): 1022.

PLOS | GENETICS

RESEARCH ARTICLE

Genetic Analysis Reveals a Hierarchy of Interactions between Polycystin-Encoding Genes and Genes Controlling Cilia Function during Left-Right Determination

Daniel T. Grimes[1¤a], Jennifer L. Keynton[1], Maria T. Buenavista[1,2,3¤b], Xingjian Jin[4¤c], Saloni H. Patel[1], Shinohara Kyosuke[5], Jennifer Vibert[1], Debbie J. Williams[1], Hiroshi Hamada[5], Rohanah Hussain[3], Surya M. Nauli[4], Dominic P. Norris[1]*

1 MRC Harwell, Harwell Science and Innovation Campus, Oxfordshire, United Kingdom, **2** School of Biological Sciences, University of Reading, Whiteknights, Reading, United Kingdom, **3** Diamond Light Source, Beamline B23, Chilton, Didcot, United Kingdom, **4** Chapman University and the University of California, Irvine, Irvine, California, United States of America, **5** Developmental Genetics Group, Graduate School of Frontier Biosciences, Osaka University and CREST, Japan Science and Technology Corporation (JST), Suita, Japan

¤a Current address: Molecular Biology Department, Princeton University, Princeton, New Jersey, United States of America
¤b Current address: National Foundation for Educational Research, The Mere, Upton Park, Slough, Berkshire, United Kingdom
¤c Current address: Washington University, Saint Louis, Missouri, United States of America
* d.norris@har.mrc.ac.uk

OPEN ACCESS

Citation: Grimes DT, Keynton JL, Buenavista MT, Jin X, Patel SH, Kyosuke S, et al. (2016) Genetic Analysis Reveals a Hierarchy of Interactions between Polycystin-Encoding Genes and Genes Controlling Cilia Function during Left-Right Determination. PLoS Genet 12(6): e1006070. doi:10.1371/journal.pgen.1006070

Editor: Gregory S. Barsh, Stanford University School of Medicine, UNITED STATES

Received: November 10, 2014

Accepted: April 30, 2016

Published: June 6, 2016

Data Availability Statement: All data are included within the manuscript.

Funding: This work was supported by awards from the Medical Research Council (http://www.mrc.ac.uk) to DPN (MC_U142670370), the National Institutes of Health (www.nih.gov/) to SMN (NIH-R01DK080640) and the US Department of Defense (http://cdmrp.army.mil/), Congressionally Directed Medical Research Program to SMN (PR130153). University of Reading, MRC Harwell and Diamond Light Source funded a studentship to MTB (MC_U142684171).

Abstract

During mammalian development, left-right (L-R) asymmetry is established by a cilia-driven leftward fluid flow within a midline embryonic cavity called the node. This 'nodal flow' is detected by peripherally-located crown cells that each assemble a primary cilium which contain the putative Ca^{2+} channel PKD2. The interaction of flow and crown cell cilia promotes left side-specific expression of *Nodal* in the lateral plate mesoderm (LPM). Whilst the PKD2-interacting protein PKD1L1 has also been implicated in L-R patterning, the underlying mechanism by which flow is detected and the genetic relationship between Polycystin function and asymmetric gene expression remains unknown. Here, we characterize a *Pkd1l1* mutant line in which *Nodal* is activated bilaterally, suggesting that PKD1L1 is not required for LPM Nodal pathway activation per se, but rather to restrict *Nodal* to the left side downstream of nodal flow. Epistasis analysis shows that *Pkd1l1* acts as an upstream genetic repressor of *Pkd2*. This study therefore provides a genetic pathway for the early stages of L-R determination. Moreover, using a system in which cultured cells are supplied artificial flow, we demonstrate that PKD1L1 is sufficient to mediate a Ca^{2+} signaling response after flow stimulation. Finally, we show that an extracellular PKD domain within PKD1L1 is crucial for PKD1L1 function; as such, destabilizing the domain causes L-R defects in the mouse. Our demonstration that PKD1L1 protein can mediate a response to flow coheres with a mechanosensation model of flow sensation in which the force of fluid flow drives asymmetric gene expression in the embryo.

The funders had no role in study design, data collection and analysis, decision to publish, or preparation of the manuscript.

Competing Interests: The authors have declared that no competing interests exist.

Author Summary

Vertebrates exhibit left-right (L-R) asymmetry in positioning and patterning their internal organs and associated vasculature; abnormal L-R asymmetry can result in birth defects such as congenital heart disease. The earliest known event in mammalian L-R patterning is a leftward fluid flow across a transient embryonic structure termed the node. This 'nodal flow' is driven by the action of motile cilia, hair-like organelles protruding from the cell surface within the node. Nodal flow is sensed by crown cells that surround the node; this requires immotile primary cilia and the putative cation channel Polycystin-2 (PKD2). A second Polycystin protein, PKD1L1, is implicated in this pathway. We describe two principle findings: a genetic hierarchy in cilia-motility genes act upstream of Polycystin-encoding genes and in which *Pkd1l1* acts upstream of, and likely represses *Pkd2*. We further demonstrate that PKD1L1 is sufficient to mediate a flow-induced Ca^{2+} response in cultured cells, and that an extracellular PKD domain is critical for both flow detection and proper L-R patterning. Together, these findings reveal a genetic pathway operating at the level of flow sensation and demonstrate that PKD1L1 is able to act to elicit flow-induced Ca^{2+} signals, thereby supporting the mechanosensation model of nodal flow sensation.

Introduction

The internal organs and vasculature of vertebrates are highly asymmetrical between left and right. For example, the heart and stomach become positioned towards the left side while the lungs undergo asymmetric branching, giving rise to different numbers of lobes on the left and right sides. Severe situs defects, such as the loss of concordance in positioning between different organs, called heterotaxia [1], are not usually compatible with survival. Moreover, situs defects frequently manifest as congenital heart malformations [2, 3] and therefore represent a major healthcare concern.

During mouse embryogenesis, left-right (L-R) symmetry is broken by leftward fluid flow across the surface of the node, a transient embryonic cavity filled with extracellular fluid [4, 5]. Leftward (or nodal) flow is generated by the clockwise motion (when viewed ventrally) of 200–300 motile monocilia, referred to here as nodal cilia. The core logic of this nodal flow model, that symmetry is broken by cilia-driven leftward flow, is now known to apply to other species including the teleost fish, zebrafish and medaka fish, as well as the frog *Xenopus laevis* [6].

As a result of nodal flow, asymmetries in gene expression emerge around the node in peripherally-located crown cells at the lateral edges of the pit. *Cerl2* (Mouse Genome Informatics–*Dand5*) becomes expressed in crown cells with a right-sided bias (R>L) by the late headfold (LHF) to early somite stages [7, 8]. CERL2 then asymmetrically represses Nodal signaling, resulting in an R<L asymmetry in crown cell NODAL activity [9]. This bias is transmitted to the lateral plate mesoderm (LPM) where a cascade consisting of NODAL, its' feedback repressor LEFTY2, and the transcription factor PITX2 (henceforth, the 'Nodal cascade') is established on the left side only [10, 11]. This left-restricted Nodal cascade is critical for proper organ L-R asymmetry and is highly conserved throughout vertebrates and some invertebrates [12]. Importantly, expression of *Lefty1* at the midline in the prospective floor plate (PFP) inhibits left-sided NODAL signals from spreading and activating the Nodal cascade on the right side of the mouse embryo [13, 14], thereby maintaining unilateral left-sided pathway activity.

How nodal flow in the node drives downstream gene expression asymmetries in crown cells has remained unanswered. Previous studies have suggested roles for Polycystin-2 (PC-2, PKD2 or TRPP2) and Polycystin 1-like 1 (PKD1L1) in the response to nodal flow [15–20]. PKD2 is a

six-pass transmembrane protein that acts as a non-selective cation channel [21], while PKD1L1 is an eleven-pass transmembrane protein which is argued to be sensory. PKD1L1 is expressed within the node and interacts with PKD2 [16, 17], leading to the notion that PKD1L1-PKD2 complexes within nodal cilia act as sensors of nodal flow [22]. However, the nature of the asymmetric signal that engages putative PKD1L1-PKD2 sensory complexes is not known. One proposal, the morphogen model, argues that the concentration of a chemical determinant becomes asymmetric in response to flow, thereby initiating a left-sided pathway [5, 23]. A second model, historically called the 'two-cilia hypothesis' (here referred to as the mechanosensation model), posits that the force of flow within the node is sensed on the left side, where it is likely to be stronger, thereby initiating events on the left that ultimately activate *Nodal* [18].

Polycystin-1 family members are known to bind to Polycystin-2 family members (TRPPs) and form receptor-channel complexes in contexts beyond L-R patterning. For example, PKD1 and PKD2 form complexes that are thought to sense urine flow and elicit downstream Ca^{2+} signals in the kidney; defects in this process may underlie autosomal dominant polycystic kidney disease (ADPKD) [24–27]. Moreover, the relative dosage of PKD1 and PKD2 influences the activity of stretch-activated ion channels (SACs) to regulate the sensation of pressure and control the arterial myogenic tone [28]. In this context, PKD1 and PKD2 act in an antagonistic fashion to control downstream events. Thus, diverse roles exist in the sensation of forces by PKD1/PKD2 in epithelial and endothelial cells. Polycystin complexes have also been documented to respond to other kinds of stimuli. PKD1L3/PKD2L1, for example, assemble to form an acid-sensing ion channel complex [29, 30] which plays a role in sour taste responses [31]. Thus, pairs of polycystin proteins sense a variety of stimuli via genetic and molecular mechanisms that are not well understood.

Here, we elaborate a genetic cascade acting downstream of nodal flow in L-R patterning that results in initiation of left-sided *Nodal*. We describe a *Pkd1l1* mutant in which the Nodal cascade is bilaterally activated, suggesting that *Pkd1l1* is required not for *Nodal* activation but to restrict *Nodal* to the left side. Moreover, *Pkd1l1* acts genetically upstream of *Pkd2* and downstream of flow; this regulates *Cerl2* asymmetry in a cilia-dependent fashion. Using artificial flow in a cell culture system, we find that PKD1L1 can mediate a response to fluid flow, initiating a Ca^{2+} signaling event upon the onset of flow. Finally, we demonstrate that an extracellular polycystic kidney disease (PKD) domain is critical for PKD1L1 function: a destabilizing mutation in the domain results in a lack of the flow-induced Ca^{2+} response in cultured cells and L-R patterning abnormalities in the mouse. This provides evidence that PKD1L1 mediates sensation of fluid flow in L-R patterning.

Results

We have previously analyzed a mouse *Pkd1l1* point mutant, called $Pkd1l1^{rks}$ (Fig 1A) [16]. $Pkd1l1^{rks/rks}$ homozygotes fail to activate the LPM Nodal cascade and exhibit morphological L-R defects similar to those displayed by both $Pkd2^{-/-}$ null mutants and $Pkd2^{lrm4/lrm4}$ point mutants (Fig 1A) [16, 19, 32]. However, since $Pkd1l1^{rks}$ is a point mutant, we set out to address the impact on L-R development of a distinct *Pkd1l1* allele, namely the targeted mutation $Pkd1l1^{tm1Lex}$ (here named $Pkd1l1^{tm1}$), which is likely a loss-of-function allele (S1 Fig) [33].

$Pkd1l1^{tm1/tm1}$ and $Pkd1l1^{rks/rks}$ Mutants Exhibit Discrete Abnormalities

When assessed on the same genetic background, $Pkd1l1^{tm1/tm1}$ and $Pkd1l1^{rks/rks}$ mutants exhibited distinct phenotypes. First, while the homozygous $Pkd1l1^{rks}$ mutation is lethal at embryonic day (E) 14.5–15.5 [16], we found that a proportion of $Pkd1l1^{tm1/tm1}$ mutants survived until

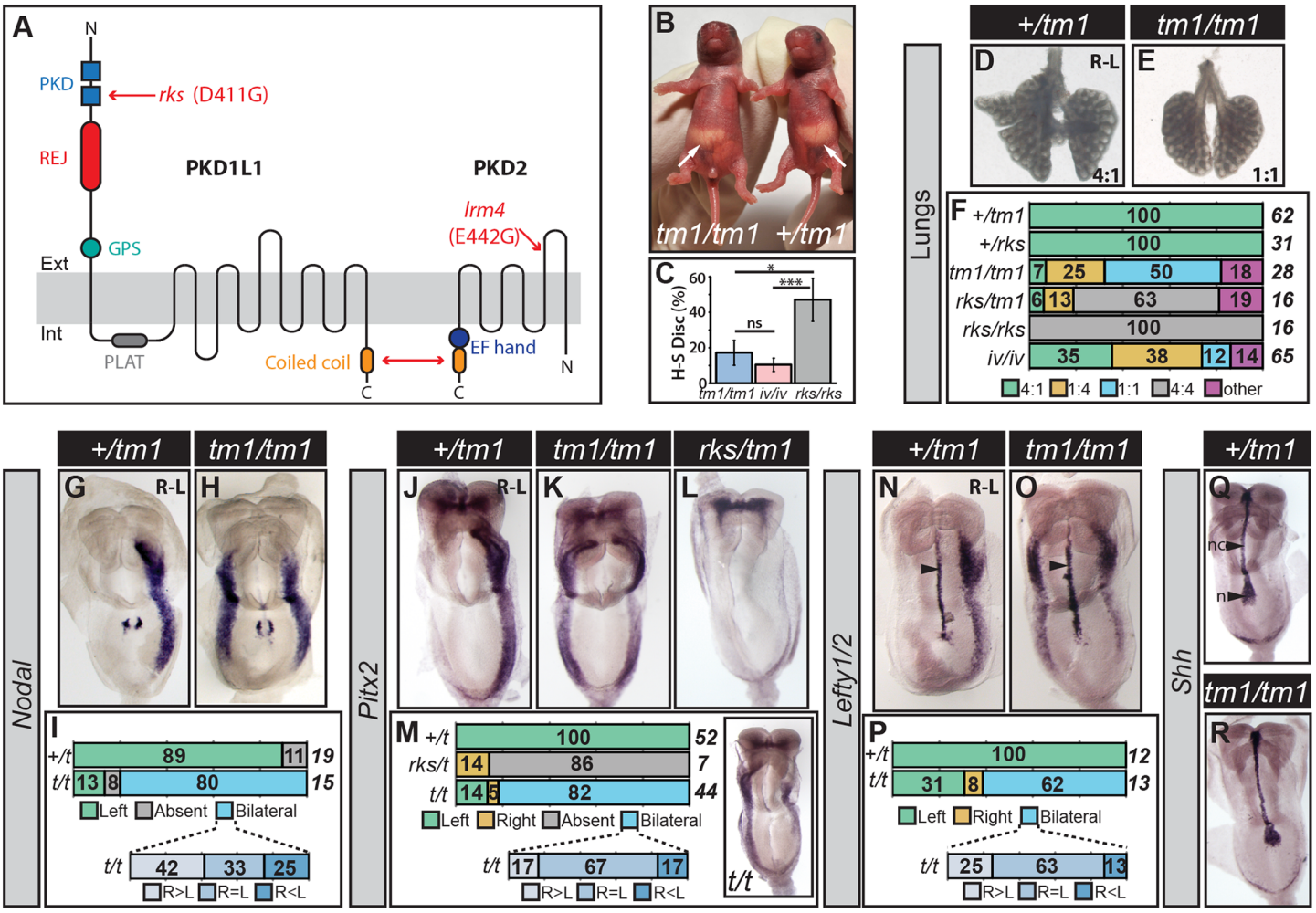

Fig 1. Phenotyping of *Pkd1l1*$^{tm1/tm1}$ Mutants. (A) Schematic diagram of PKD1L1 and PKD2 showing protein domains and the nature of the *Pkd1l1*^{rks} and *Pkd2*^{lrm4} point mutations. The double headed red arrow denotes the site of interaction between PKD1L1 and PKD2. PKD—Polycystic Kidney Disease; REJ—Receptor for Egg Jelly; GPS—G-protein Coupled Receptor Proteolytic Site; PLAT—Polycystin-1, Liopoxygenase, Alpha-Toxin. (B) *Pkd1l1*$^{tm1/tm1}$ and sibling control showing reversed and normal situs, respectively. White arrows indicate stomach position. (C) Heart-stomach discordance (H-S Disc.) in *Pkd1l1*$^{tm1/tm1}$, *Dnah11*$^{iv/iv}$ and *Pkd1l1*$^{rks/rks}$ mutants scored at E13.5. Normally, the heart apex and stomach are positioned to the left. H-S Disc. is defined as the heart apex and stomach being on opposite sides. ns—not significant; *—p<0.05; **—p<0.001, Fisher's Exact Test applied. (D-F) Lung situs assessed at E13.5 for embryos of the indicated genotypes with the ratio of lung lobes between left and right sides given. The percentage and total numbers of embryos showing each phenotype are indicated in *(F)*. (G-P) Expression patterns of *Nodal*, *Pitx2*, and *Lefty1/2* in embryos at E8.5 of the indicated genotypes, with the percentage number of embryos exhibiting each phenotype and the total number given. Embryos exhibiting bilateral marker expression are further categorized by whether they show equal or biased expression between the left and right sides. The inset in *(M)* shows a *Pkd1l1*$^{tm1/tm1}$ embryo with bilateral *Pitx2* expression but with a right-sided bias. Arrowheads in *(N)* and *(O)* indicate midline *Lefty1* expression. *t* is shorthand for *Pkd1l1*^{tm1}. (Q-R) Sonic hedgehog (*Shh*) expression in the node (n) and notochord (nc) at E8.5.

doi:10.1371/journal.pgen.1006070.g001

adulthood (S2A and S2B Fig). Surviving mutants either exhibited normal (57%) or reversed (43%) situs based on stomach position in neonates (Fig 1B). Second, though the laterality of heart and stomach was randomized in both *Pkd1l1*$^{tm1/tm1}$ and *Pkd1l1*$^{rks/rks}$ mutants at E13.5 (S2C–S2E Fig), the latter exhibited a significantly higher level of discordance between the two organs, reflecting a heterotaxic phenotype (Fig 1C). Third, whilst all *Pkd1l1*$^{rks/rks}$ mutants exhibited right lung isomerism, where four lung lobes develop on both the left and right sides [16], the majority of *Pkd1l1*$^{tm1/tm1}$ embryos displayed the complete opposite phenotype of bilaterally mono-lobed lungs, called left lung isomerism (Fig 1D–1F). This phenotype was not

completely penetrant; some *Pkd1l1*$^{tm1/tm1}$ mutants exhibited other lung lobation patterns, though never right isomerism (Fig 1F). In conclusion, the *Pkd1l1*^{tm1} allele has a strikingly different impact on both survival and L-R patterning compared to the *Pkd1l1*^{rks} point mutation.

Pkd1l1$^{tm1/tm1}$ Mutants Bilaterally Activate the Nodal Cascade

To pinpoint the molecular causes of the L-R defects in *Pkd1l1*$^{tm1/tm1}$ mutants, we examined L-R marker gene expression by mRNA whole mount in situ hybridization (WISH). In control embryos, *Nodal* was nearly always expressed in the left LPM between the 3–7 somite stages (ss) (Fig 1G and 1I), as expected. In contrast, *Nodal* was most often expressed bilaterally in *Pkd1l1*$^{tm1/tm1}$ mutants (Fig 1H and 1I). Similarly, *Pitx2* and *Lefty2*, both downstream targets of Nodal signaling in the LPM, were most frequently expressed bilaterally in *Pkd1l1*$^{tm1/tm1}$ embryos (Fig 1J, 1K, 1M and 1P). Of those embryos that exhibited bilateral activity of the Nodal cascade, most displayed similar levels and extents of *Nodal/Lefty2/Pitx2* expression on both sides, but some embryos exhibited a left or right bias (Fig 1I, 1M and 1P). Whilst the bilateral induction of the Nodal cascade in *Pkd1l1*$^{tm1/tm1}$ embryos explains the high level of left lung isomerism, the fact that some embryos exhibit slight, though randomized, asymmetries in this bilaterality might serve to explain why we find a relatively high incidence of normal, inverted, and other lung lobation patterns (50% in total; Fig 1F) that depart from the left isomerism predicted by truly bilateral Nodal signals. In summary, most *Pkd1l1*$^{tm1/tm1}$ mutant embryos exhibit bilateral activation of the Nodal cascade, representing another striking difference to *Pkd1l1*$^{rks/rks}$ mutants that display the opposite phenotypes of loss of LPM Nodal activity [16].

As a corollary of these results, we generated *Pkd1l1*$^{rks/tm1}$ trans-heterozygotes to further understand the differences between the *Pkd1l1*^{rks} and *Pkd1l1*^{tm1} alleles. The majority of *Pkd1l1*$^{rks/tm1}$ embryos exhibited right lung isomerism and loss of LPM *Pitx2* expression (Fig 1F, 1L and 1M), suggesting that the *Pkd1l1*^{rks} allele is dominant over *Pkd1l1*^{tm1}. We discuss the nature of the *Pkd1l1*^{rks} allele further in the **Discussion**.

Bilateral Nodal cascade activity in L-R mutants can result from midline defects [5, 34], including the failure to express *Lefty1* in the floor plate which constitutes a molecular 'midline barrier' [13]. The node and notochord were clearly specified in *Pkd1l1*$^{tm1/tm1}$ mutants, as evidenced by normal Sonic hedgehog (*Shh*) expression (n = 6/6 embryos) (Fig 1Q and 1R). *Lefty1* was also expressed at the midline of *Pkd1l1*$^{tm1/tm1}$ mutants; indeed *Lefty1* expression appeared more intense than in control embryos, perhaps owing to bilaterally high NODAL activity inducing *Lefty1* in both the left and right sides of the floor plate (Fig 1N and 1O). Thus, the *Lefty1* midline barrier is formed in *Pkd1l1*$^{tm1/tm1}$ mutants. Since *Pkd1l1*^{tm1} appears to be loss-of-function (hypomorphic or null), these data argue that rather than being required for activation of the LPM Nodal cascade, *Pkd1l1* is instead needed to restrict Nodal pathway activity to the left side of the embryo in a mechanism that is independent of the midline barrier.

Pkd1l1 Acts Downstream of Nodal Flow

Bilateral establishment of the Nodal cascade in both the right and left LPM can be caused by aberrant or absent nodal flow [35, 36]. We therefore imaged the node using differential interference contrast (DIC) microscopy and found that nodal cilia rotated normally, at around 12 Hz, in both *Pkd1l1*$^{tm1/tm1}$ mutants and wild-type controls (S3 Fig). We next assessed flow directly by immersing embryos in fluorescent beads, imaging the node cavity, then performing particle image velocimetry (PIV) analysis [37] to obtain a map of flow movements. This revealed that directional leftward flow was indeed generated both in control embryos and *Pkd1l1*$^{tm1/tm1}$ mutants (Fig 2A, 2B and S4 Fig). Thus, the Nodal cascade is induced bilaterally even in the presence of normal nodal flow in *Pkd1l1*$^{tm1/tm1}$ mutants.

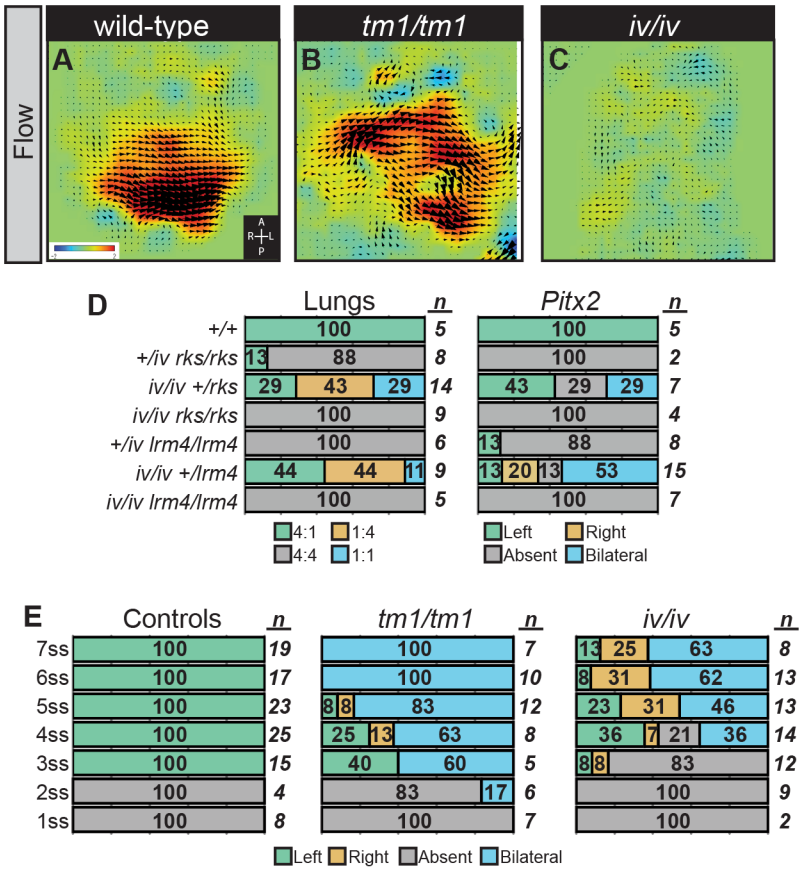

Fig 2. The Relationship Between Nodal Flow and *Pkd1l1*/*Pkd2* Function. (A-C) Nodal flow in embryos of indicated genotypes was examined at the 1–3 somite stages by means of PIV analysis. Flow was normal in *Pkd1l1*$^{tm1/tm1}$ mutants and wild-type controls but was absent in *Dnah11*$^{iv/iv}$ mutants. Black arrowheads denote the direction and speed of flow at that position while the false coloring indicates the direction and magnitude of the flow. Red indicates leftward and blue rightward fluid movements. (D) Lung situs (assessed at E13.5) and *Pitx2* expression (assessed at E8.5) for embryos of the indicated genotypes, with the percentage of embryos exhibiting each phenotype and the total number given. (E) *Pitx2* expression for *Pkd1l1*$^{tm1/tm1}$, *Dnah11*$^{iv/iv}$ and control embryos for each of the 1–7 somite stages. The onset of *Pitx2* expression is delayed in *Dnah11*$^{iv/iv}$ mutants but not in *Pkd1l1*$^{tm1/tm1}$ embryos.

doi:10.1371/journal.pgen.1006070.g002

Given that nodal flow is present in *Pkd1l1*$^{tm1/tm1}$ embryos while LPM *Nodal* expression is predominantly bilaterally activated, we predicted that *Pkd1l1* acts downstream of flow. Indeed, this would be expected for molecules required for flow-sensing. In order to determine the genetic control and the order of these events we assessed epistasis between *Pkd1l1*^{rks} and *Dnah11*^{iv}; *Dnah11*^{iv} disrupts an axonemal dynein heavy chain, resulting in immotile nodal cilia and loss of nodal flow (Fig 2C and S4 Fig) [35]. At E13.5 (lung situs assessed) and E8.5 (*Pitx2* expression assessed), *Pkd1l1*$^{rks/rks}$;*Dnah11*$^{iv/iv}$ double mutants exhibited right lung isomerism and loss of LPM *Pitx2*, respectively, and therefore phenocopied *Pkd1l1*$^{rks/rks}$ mutants rather than *Dnah11*$^{iv/iv}$ mutants (Fig 2D and S1 Table). This demonstrates that the *Pkd1l1*$^{rks/rks}$ phenotype still manifests in the absence of nodal flow. Similar results were obtained when we assessed epistasis between *Dnah11*^{iv} and *Pkd2*^{lrm4}; in this experiment, *Pkd2*$^{lrm4/lrm4}$;*Dnah11*$^{iv/iv}$ double mutants phenocopied *Pkd2*$^{lrm4/lrm4}$ and not *Dnah11*$^{iv/iv}$ (Fig 2D and S1 Table). Thus, genetically ablating flow, which is otherwise present, does not alter the L-R phenotype of either *Pkd1l1*$^{rks/rks}$ or *Pkd2*$^{lrm4/lrm4}$ embryos. This demonstrates that the roles of *Pkd1l1* and *Pkd2* are

downstream of nodal flow, supporting the notion that these genes mediate the sensation of flow. We did not generate *Pkd1l1*$^{tm1/tm1}$;*Dnah11*$^{iv/iv}$ double mutants because the phenotypes of the single mutants are highly similar (S2 Fig), so an analysis of double mutant embryos would be uninformative.

Induction of the Nodal Cascade Is Delayed in Embryos Lacking Flow but Not in *Pkd1l1*$^{tm1/tm1}$ Mutants

If the response to flow is mediated through PKD1L1, it might be expected that loss of nodal flow (*Dnah11*$^{iv/iv}$ mutants) and targeted mutation of the putative flow sensor (*Pkd1l1*$^{tm1/tm1}$ mutants) would result in the same phenotype. Indeed, at E13.5, the L-R defects of *Dnah11*$^{iv/iv}$ and *Pkd1l1*$^{tm1/tm1}$ embryos are highly similar (Fig 1C, 1F and S2E Fig). In wild-type embryos, *Nodal* is expressed in the left LPM for around 6–8 hours beginning at the 3 ss [38, 39]. However, we found that the timing of LPM Nodal cascade induction, assessed by WISH for *Pitx2*, was subtly different between *Dnah11*$^{iv/iv}$ and *Pkd1l1*$^{tm1/tm1}$ mutants. While *Pitx2* expression was evident at the 3 ss but not before in control embryos, loss of flow in *Dnah11*$^{iv/iv}$ mutants delayed the onset of *Pitx2* until the 4 ss (Fig 2E); a delay of around 2 hours, perhaps resulting from a slower and stochastic activation of the cascade in the absence of the flow signal [35]. No such delay was evident in *Pkd1l1*$^{tm1/tm1}$ mutants; 100% of 3 ss *Pkd1l1*$^{tm1/tm1}$ embryos exhibited LPM *Pitx2* expression, and a single embryo displayed expression at the 2 ss (Fig 2E). Coupled to the above findings, this favors a model wherein nodal flow drives the timely repression of *Pkd1l1* on the left side: when *Pkd1l1* function is perturbed in *Pkd1l1*$^{tm1/tm1}$ mutants, the Nodal cascade activates bilaterally without delay.

Pkd1l1 Acts Upstream of *Cerl2* Asymmetry during Left-Right Development

At the LHF to early somite stages, the action of nodal flow represses *Cerl2* in left-sided node crown cells, resulting in the R>L *Cerl2* expression bias [8, 40, 41]. We therefore assessed *Cerl2* asymmetry in *Pkd1l1*$^{tm1/tm1}$ mutants by WISH; we quantified *in situ* staining and then calculated the percentage of total stain that was present in right-sided crown cells. In order to control for observation bias, samples were processed together, scored for L-R expression and genotyped only after analysis. As expected, the percentage of *Cerl2* stain was greater on the right side than the left side in control embryos measured at the 1–3 ss when *Cerl2* asymmetry was obvious by inspection (Fig 3A and 3C). In contrast, *Cerl2* asymmetry failed to manifest in *Pkd1l1*$^{tm1/tm1}$ mutants, which instead exhibited a symmetrical pattern of *Cerl2* expression (Fig 3B and 3C). Consistent with this, most *Pkd1l1*$^{tm1/tm1}$ mutants exhibited symmetrical crown cell *Nodal* expression whereas *Nodal* showed the expected subtle R<L bias in control embryos (Fig 3D–3F). Thus, functional *Pkd1l1* is not required for crown cell *Cerl2* or *Nodal* expression *per se*, but it is needed for asymmetries in their expression to manifest downstream of nodal flow.

Close examination of stage-matched *Pkd1l1*$^{tm1/tm1}$ and control embryos stained for *Cerl2* under identical experimental conditions, revealed that the bilaterally symmetrical expression in mutants represents bilateral downregulation of *Cerl2*, rather than the left-side only downregulation observed in wild-type embryos (Fig 3A and 3B). All samples were scored before genotyping, in order to remove observer bias. We furthermore repeated this staining then genotyping procedure multiple times and obtained the same results from different litters, supporting the conclusions (S5 Fig). Thus, genetically, *Pkd1l1* normally acts to maintain high levels of *Cerl2*. In contrast, *Cerl2* levels remain bilaterally high (derepressed) in *Pkd1l1*$^{rks/rks}$ and *Pkd2*$^{lrm4/lrm4}$ embryos [16]; these differences in crown cell *Cerl2* levels between *Pkd1l1*$^{tm1/tm1}$ and *Pkd1l1*$^{rks/rks}$

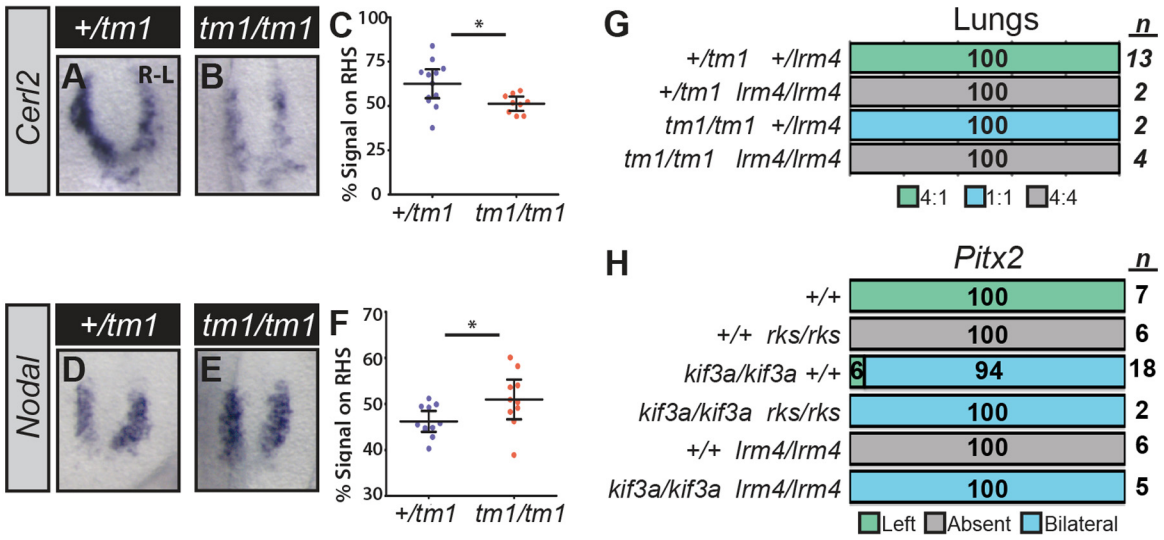

Fig 3. The Genetic Relationship between *Pkd1l1*, *Pkd2*, and Cilia. (A-F) *Cerl2* (*A-C*) and *Nodal* (*D-F*) expression at the node of *Pkd1l1*$^{tm1/tm1}$ and control embryos. Quantitation of *in situ* signal reveals expression of both genes to be more symmetrical in mutant embryos (*C*, *F*). *—p<0.05, unpaired *t*-test applied. Error bars represent 95% confidence intervals. (G-H) Lung situs *(G)* (assessed at E13.5) and *Pitx2* expression *(H)* (assessed at E8.5) for embryos of the indicated genotypes, with the percentage of embryos exhibiting each phenotype and the total number given.

doi:10.1371/journal.pgen.1006070.g003

embryos would be expected given the distinct LPM Nodal cascade activities found in these mutants.

The Genetic Relationship between *Pkd1l1*^{tm1} and *Pkd2*^{lrm4}

Since it has been hypothesized that PKD1L1 and PKD2 act as a flow-sensing complex, it is somewhat surprising that opposite phenotypes are present in *Pkd1l1*$^{tm1/tm1}$ (bilateral Nodal cascade) and *Pkd2*$^{lrm4/lrm4}$ (absent Nodal cascade) mutants. To understand the genetic relationship between the two, we generated *Pkd1l1*$^{tm1/tm1}$;*Pkd2*$^{lrm4/lrm4}$ double mutant embryos. At E13.5, all *Pkd1l1*$^{tm1/tm1}$;*Pkd2*$^{lrm4/lrm4}$ double mutants exhibited right lung isomerism (Fig 3G and S2 Table), thereby phenocopying *Pkd2*$^{lrm4/lrm4}$ single mutants and not *Pkd1l1*$^{tm1/tm1}$ embryos (Figs 1F, 3G and S2 Table). This shows that *Pkd2* is genetically epistatic to *Pkd1l1*.

The data described so far suggest a genetic pathway linking nodal flow to the emergence of gene asymmetries within crown cells in which flow impacts *Pkd1l1* which lies genetically upstream of *Pkd2*. *Pkd2* activity, in turn, influences crown cell *Cerl2* and *Nodal* expression and, ultimately, activation of the LPM Nodal cascade. In depth discussion of this genetic scheme and further interpretation of these results are included in the **Discussion**.

Pkd1l1 and *Pkd2* Require Cilia to Function

Immotile cilia found on crown cells are required for the sensation of nodal flow [42]. Since PKD1L1 and PKD2 localize to nodal cilia [17, 18], we asked whether cilia were required for *Pkd1l1* and/or *Pkd2* function *in vivo*. Loss of the anterograde intraflagellar transport motor component, KIF3A, results in a failure of ciliogenesis and bilateral induction of the LPM Nodal cascade (Fig 3H) [34, 43]. Both *Pkd1l1*$^{rks/rks}$;*Kif3a*$^{-/-}$ and *Pkd2*$^{lrm4/lrm4}$;*Kif3a*$^{-/-}$ double mutants exhibited bilateral *Pitx2* expression, the phenotype of *Kif3a*$^{-/-}$ single mutants, whereas *Pkd1l1*$^{rks/rks}$ and *Pkd2*$^{lrm4/lrm4}$ single mutants lacked LPM *Pitx2* expression (Fig 3H and S3 Table). The simplest explanation of this phenotype, that the *Pkd1l1*$^{rks/rks}$ and *Pkd2*$^{lrm4/lrm4}$

phenotypes can be suppressed by loss of cilia, suggests that *Pkd1l1* and *Pkd2* require cilia to function *in vivo*. This genetic evidence is backed up by the findings that PKD2 and PKD1L1 localize to cilia [16–18].

The *Pkd1l1*^{rks} Mutation Destabilizes an Extracellular PKD Domain

We next addressed how the *Pkd1l1*^{rks} mutation impacts PKD1L1 protein function. Our genetic experiments comparing the targeted allele *Pkd1l1*^{tm1} to *Pkd1l1*^{rks} had suggested that *Pkd1l1*^{rks} is a non-null allele (Fig 1F and 1M). The *Pkd1l1*^{rks} point mutation itself resides in the second of two polycystic kidney disease (PKD) domains within the extracellular N-terminal portion of the protein (Fig 1A) [16]. An NMR structure of the first PKD domain from human PKD1, a close homolog of PKD1L1, revealed the domain to be a ß-sandwich fold consisting of seven ß-strands (Fig 4A) [44]. By extending our previous fold recognition modeling approaches [16], we have predicted the second PKD domain of mouse PKD1L1 to have a similar fold topology (Fig 4B). To validate our model, we performed structural studies on PKD1L1 by synchrotron radiation circular dichroism (SRCD) spectroscopy [45]. Conformational studies in solution of the purified second PKD domain from mouse PKD1L1 showed the typical appearance of a ß-strand protein (Fig 4D) consisting of 44% ß-strand and 56% disordered (linkers and loops between strands) by Raussens algorithm [46], in agreement with our molecular model.

We then assessed the impact of the *Pkd1l1*^{rks} point mutation upon the structure of PKD1L1's second PKD domain. Solution studies by SRCD of *rks*-mutated purified PKD domains shifted the SRCD spectra, which now exhibited characteristics of increased disorder (Fig 4D), with structural content changed to being 31% ß-strand and 69% disordered. Thermal denaturation studies on both wild-type and *rks*-mutated PKD domains showed the wild-type domain to have a higher melting temperature (Tm) of 68.6°C, compared to 56.4°C for the *rks*-mutated domain (Fig 4E). Both of these lines of evidence support the notion that the *Pkd1l1*^{rks} point mutation destabilizes the extracellular PKD domain. Indeed, such a destabilization was also observed in our molecular models which predicted an increase in disorder reflected by a loss of secondary structure in the C' ß-strand in particular, marked by asterisks in Fig 4C (see [44] for PKD domain ß-strand nomenclature).

In *Pkd1l1*$^{rks/rks}$ mutants, it is possible that the point mutation causes a drastic inability of the protein to properly fold or be localized to the correct cellular compartment. Whilst we cannot fully rule out this possibility, it seems unlikely since the phenotype of *Pkd1l1*$^{rks/rks}$ mutants is very different to *Pkd1l1*$^{tm1/tm1}$. Moreover, *Pkd1l1*^{rks} is dominant over *Pkd1l1*^{tm1} whilst neither *Pkd1l1*^{rks} nor *Pkd1l1*^{tm1} exhibit phenotypes in the heterozygous state. Thus, we favour a model in which the PKD domain structural destabilization we have observed results in abrogated functionality of that domain within the protein, thereby implicating the PKD domain in PKD1L1 function in L-R patterning. It is worth noting that similar point mutations in PKD domains of PKD1 also impact the stability and mechanical properties of PKD domains [47].

PKD1L1 Mediates a Response to Artificial Fluid Flow

After establishing that *Pkd1l1* is necessary for L-R patterning, we then sought to test sufficiency of PKD1L1 in the response to flow in a context in which we can control fluid flow and assay the cells Ca^{2+} signal response. We therefore addressed this issue by asking the question: can PKD1L1 function in the cellular response to shear stress induced by fluid flow?

In vascular endothelial cells and kidney epithelial cells, flow-induced shear stress elicits a Ca^{2+} signaling response. This signaling event depends on primary cilia as well as the Polycystin protein PKD1; cells isolated from *Pkd1*$^{-/-}$ mice do not undergo flow-induced Ca^{2+} signaling (FICS) [48, 49]. We utilized this experimentally tractable system to ask how expression of

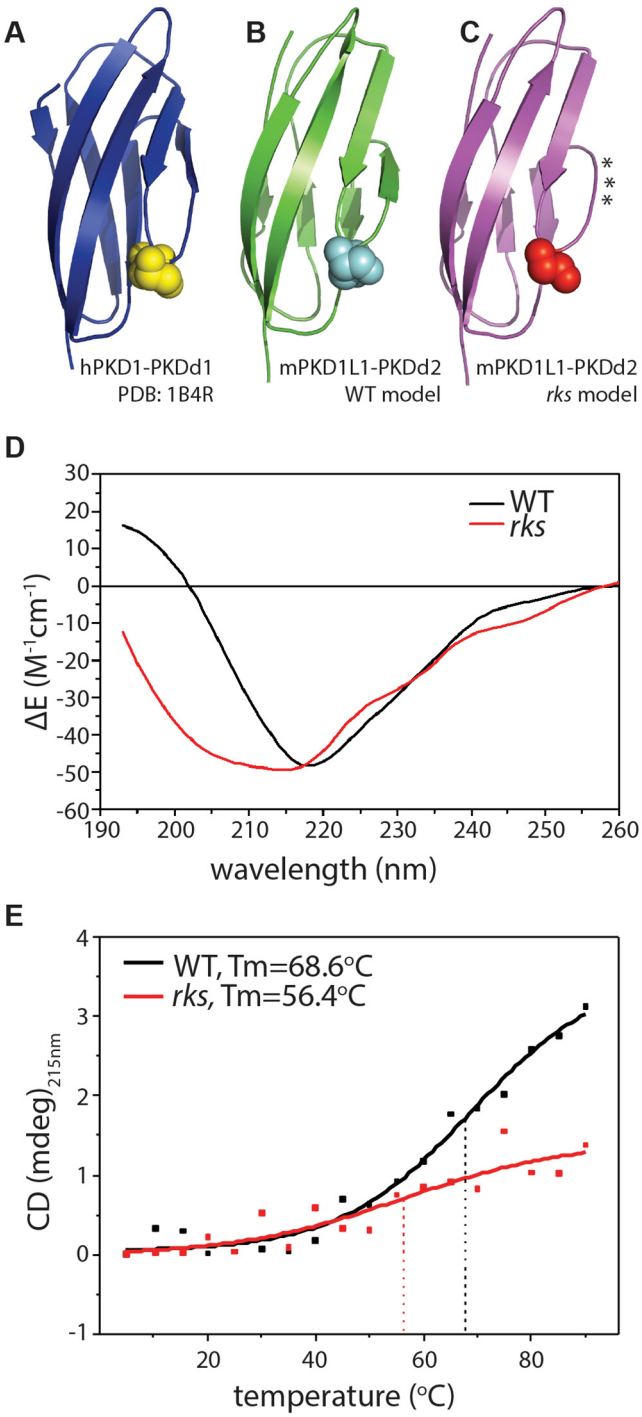

Fig 4. Destabilization of a PKD Domain by the *Pkd1l1*^{rks} Mutation. (A-C) Structure of human PKD1 PKD domain 1 (*A*) and models of mouse PKD1L1 PKD domain 2; wild-type (*B*) or *rks*-mutated (*C*). Domains are largely composed of β-sheets (block arrows). The aspartic acid mutated in *Pkd1l1*^{rks}, or its equivalent in PKD1, is shown in space-fill. The asterisks denote loss of secondary structure in the *rks*-mutated domain. (D) SRCD spectroscopy of mouse PKD1L1 PKD domain 2 for wild-type and *rks*-mutated domains. Spectra are consistent with decreased stability (decreased secondary structure) in mutated domains. (E) Thermal denaturation analysis of PKD1L1 PKD domain 2: a reduced melting temperature (Tm) of 56.4°C is evident in the *rks*-mutated domain; in wild-type controls a Tm of 68.6°C is detected.

doi:10.1371/journal.pgen.1006070.g004

PKD1L1 impacted FICS. We loaded ciliated endothelial cells with the Ca^{2+}-binding dye Fura2-AM, applied fluid flow at 7.2 dyne/cm^2, then recorded Ca^{2+} response by ratiometric fluorescence imaging. In Fig 5A and 5B we show representative images from selected time-points, whilst in Fig 5C and 5D we show averaged traces from multiple fields of view for the changes in intracellular Ca^{2+} after the onset of flow (arrows). Finally, the results of three independent transfections, with quantitation of 50 GFP+ and 50 GFP- cells per transfection, are collated in Fig 5E (see S5 Table for numerical results); statistical comparison among groups was performed using ANOVA followed by Tukey's posttest, with $p<0.05$ taken as statistically significant differences. In wild-type cells, a transient Ca^{2+} response upon the onset of fluid flow was observed (Fig 5A, 5C and 5E). As anticipated, loss of PKD1 in cells generated from *Pkd1*$^{-/-}$

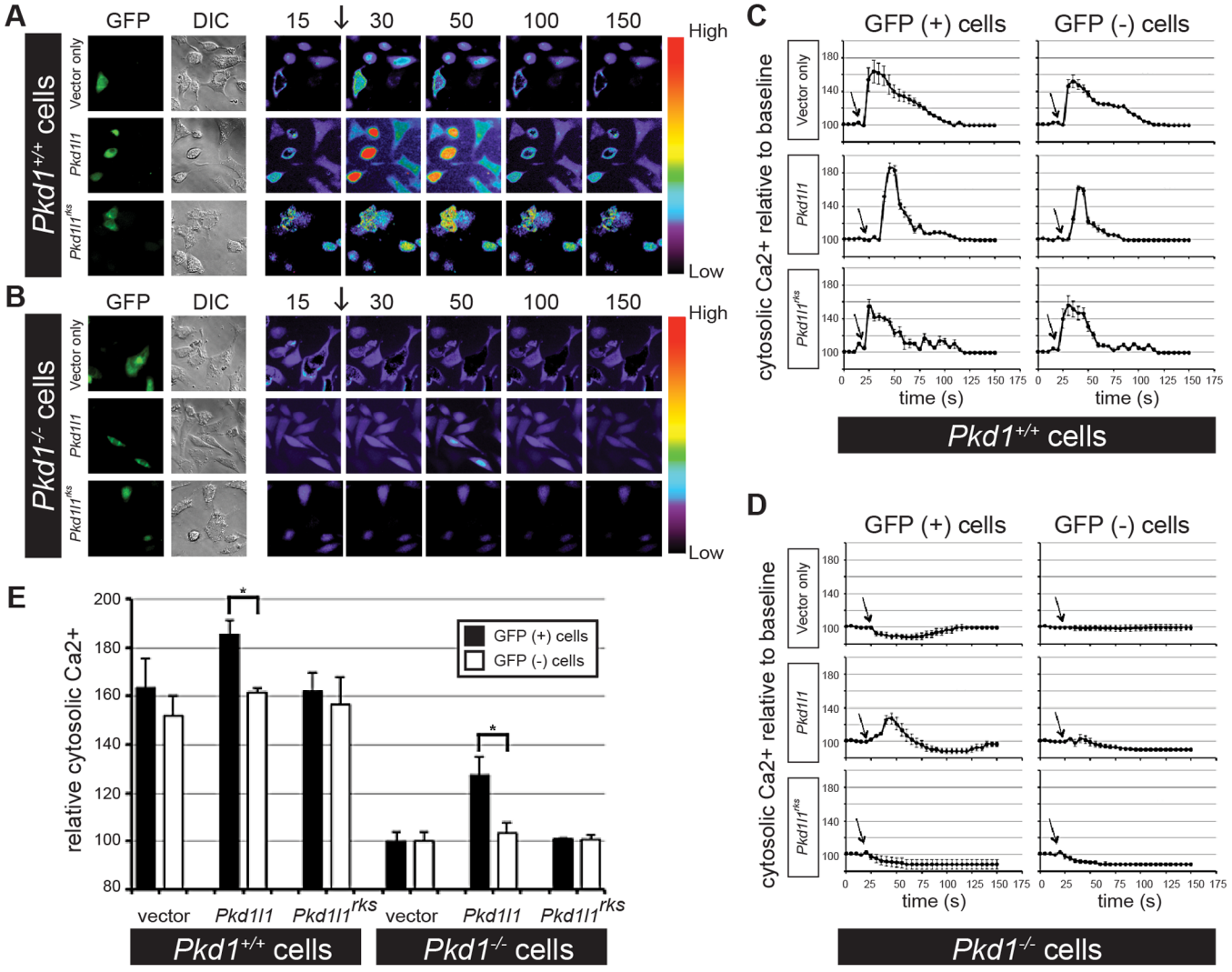

Fig 5. Flow-Induced Ca^{2+} Signaling Depends on PKD1L1. (A-B) *Pkd1*$^{+/+}$ *(A)* and *Pkd1*$^{-/-}$*(B)* cells were transfected with vector-GFP alone, PKD1L1-GFP or PKD1L1^{rks}-GFP. Successfully transfected cells had green fluorescence (GFP), and the entire cell population was observed by DIC. After baseline Ca^{2+} level was taken, fluid-shear stress was applied to cells (arrow). Numbers indicate time in seconds (s). Color bars indicate Ca^{2+} level (pseudocoloured), where black-purple and yellow-red represent low and high Ca^{2+} levels, respectively (C-D) Quantitation from independent experiments of *Pkd1*$^{+/+}$ *(C)* and *Pkd1*$^{-/-}$*(D)* cells was averaged and plotted in line graphs. Within the same cell population, successfully transfected (GFP+) and non-transfected (GFP-) cells were analyzed separately. Arrows indicate the start of fluid-shear stress. Time is indicated in seconds (s). (E) Statistical analysis was done by analyzing the peak changes of intracellular Ca^{2+}. While vector-GFP is used as a negative control, non-transfected cells (GFP-) were also used as an internal control. n = 150 cells for each group in three independent transfections. *—p<0.05.

doi:10.1371/journal.pgen.1006070.g005

mice abolished the FICS response (Fig 5B, 5D and 5E). Expression of a PKD1L1-GFP construct was able to restore FICS in *Pkd1*$^{-/-}$ cells and to increase the magnitude of the response in *Pkd1*$^{+/+}$ cells (Fig 5A–5E). Importantly, we did not see a restoration in either untransfected cells (GFP-negative) within the same sample or within separate samples that were transfected with GFP alone (Fig 5A–5E). These experiments demonstrate that PKD1L1 can mediate a Ca^{2+} response to fluid flow. In contrast to wild-type PKD1L1-GFP, expression of PKD1L1^{rks}-GFP protein did not rescue FICS in *Pkd1*$^{-/-}$ cells (Fig 5A–5E). Thus, in our cell line system, PKD1L1 restores FICS in the absence of PKD1. In the node, *Pkd1l1* acts downstream of flow and upstream of *Pkd2* and *Cerl2/Nodal* asymmetries in the sensation pathway.

Proper Localization of PKD2 to Nodal Cilia Requires PKD1L1

Finally, we turned our attention to the localization of PKD2 protein in the node. In contexts where PKD1 and PKD2 function together, PKD2 localization to cilia has been shown to depend on the presence of PKD1 [48]; this perhaps explains why PKD2 is not functional in the absence of PKD1 [50]. By contrast, we find bilateral *Nodal* expression in *Pkd1l1*$^{tm1/tm1}$ mutants, implying bilateral PKD2 activity in this *Pkd1l1* mutant background. Two possibilities that could explain this apparent contradiction are: (1) PKD2 localization to cilia is not required for its role in L-R patterning; or (2) PKD2 can still localize to cilia and signal in the *Pkd1l1*$^{tm1/tm1}$ mutant. We tested these by assessing PKD2 subcellular localization within the node of wild-type and mutant embryos at 8.0 dpc.

In wild-type control embryos, PKD2 localized to all nodal cilia (Fig 6A and 6B), as previously reported [18]. Most cilia showed continuous PKD2 staining along the ciliary axoneme,

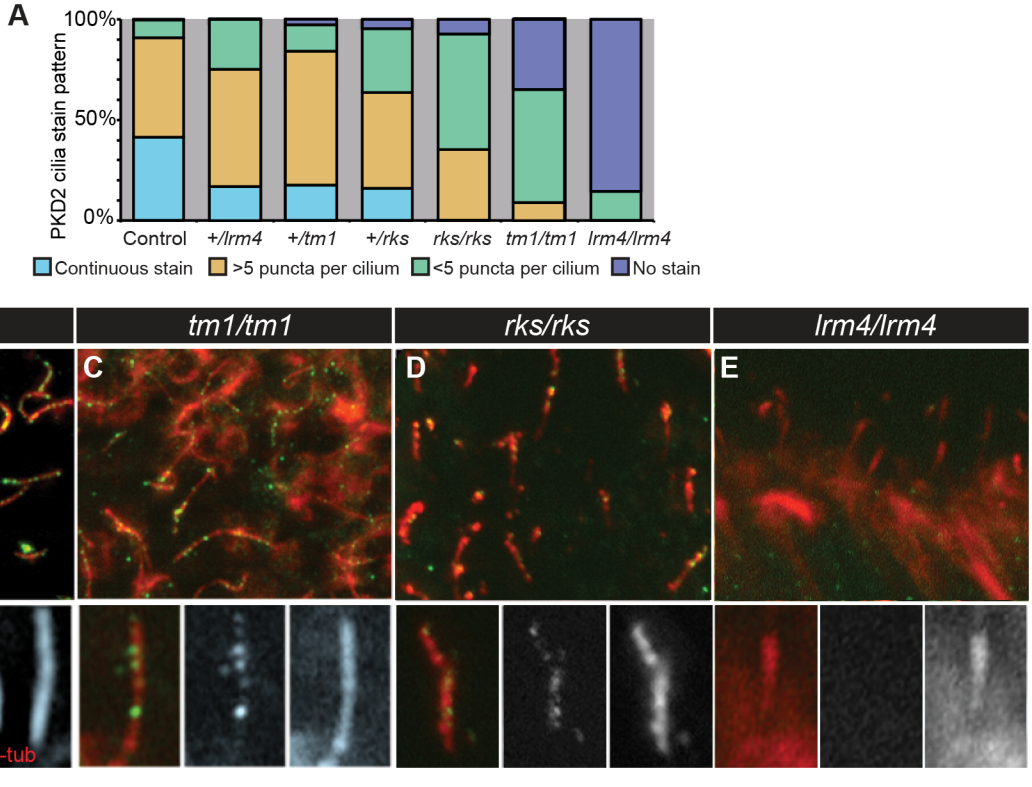

Fig 6. Cilia and PKD2 Localization and Function. (A-E) PKD2 localization in nodal cilia of embryos of the indicated genotype. Staining was divided into categories and quantitation is given in (*A*). In (*A*), all genotypes are statistically significantly different from each other ($p<0.001$) except for *Pkd2*$^{+/lrm4}$ and *Pkd1l1*$^{+/tm1}$ which are statistically not significantly different.

doi:10.1371/journal.pgen.1006070.g006

marked by acetylated α-tubulin, or greater than five PKD2 puncta per cilium (Fig 6A and 6B). By contrast, PKD2 was absent from the vast majority of cilia in *Pkd2*$^{lrm4/lrm4}$ mutants (Fig 6A and 6E), in agreement with the finding that the *lrm4* mutation prevents a PKD2-Venus fusion from localizing to nodal cilia in transient transgenic mouse embryos [51]. The *lrm4* point mutation changes a residue in the first extracellular loop of PKD2 (Fig 1A) [32], but does not affect its channel activity [51]. It is currently not known why PKD2^{lrm4} protein fails to properly localize to nodal cilia. Nevertheless, given the striking L-R defects of *Pkd2*$^{lrm4/lrm4}$ mutants, these data suggest a requirement for PKD2 protein localization to nodal cilia; without PKD2 in cilia, the downstream Nodal cascade is not activated on either the left or right sides, resulting in right isomerism in mutants.

In *Pkd1l1*$^{tm1/tm1}$ mutants, we observed reduced PKD2 ciliary levels compared to controls (Fig 6A and 6C), showing that proper levels of functional PKD1L1 are needed for the efficient import or retention of PKD2 in nodal cilia. *Pkd1l1*$^{+/tm1}$ heterozygous embryos exhibited reduced ciliary PKD2 (Fig 6A), suggesting that PKD2 levels within nodal cilia are controlled, at least in part, by the dosage of PKD1L1. Thus, whilst we do observe reduced PKD2 in the nodal cilia of *Pkd1l1*$^{tm1/tm1}$ mutants, this is not a complete loss of PKD2 as has been observed in distinct cell types when *Pkd1* is ablated [48]. An assessment of PKD1L1 localization and levels in these mutant backgrounds will require functional PKD1L1 antibodies, which are currently unavailable. Finally, we also assessed the PKD2 localization to nodal cilia in *Pkd1l1*$^{rks/rks}$ mutants and found that it was also reduced (albeit to a lesser extent than in *Pkd1l1*$^{tm1/tm1}$) in *Pkd1l1*$^{rks/rks}$ mutants (Fig 6A and 6D). Together, these data suggest that PKD2 localization to cilia does not depend entirely on functional PKD1L1.

Discussion

Addressing how nodal flow is sensed by the embryo to elicit downstream asymmetries in gene expression is critical if we are to understand the early phases of L-R patterning. We, and others, have previously implicated the Polycystin proteins PKD1L1 and PKD2 in the sensation of nodal flow. Here, we reveal that *Pkd1l1* acts in a genetic pathway at the level of flow sensation, placing *Pkd1l1* function between flow and *Pkd2*. Moreover, we demonstrate that PKD1L1 protein is sufficient to elicit a Ca^{2+} signal in response to artificial fluid flow.

A Genetic Repression Model of Nodal Flow Sensation

Our genetic experiments suggest a pathway in which flow acts upstream of *Pkd1l1* which, via *Pkd2* (that lies downstream on the pathway), signals to affect crown cell *Cerl2* and *Nodal* levels. The result of this pathway, initiated by nodal flow, is to increase left-sided crown cell NODAL signalling and thereby activate the Nodal pathway in the left LPM only.

We can further extend our genetic results to interpret the nature of the interactions between adjacent genes on the pathway (summarized in Fig 7). Since the *Pkd1l1*$^{tm1/tm1}$ is likely to be hypomorphic or null (S1 Fig) i.e. loss-of-function, and *Pkd1l1*$^{tm1/tm1}$ mutants exhibit bilateral LPM Nodal cascade activity, we suggest that *Pkd1l1* normally represses Nodal cascade activation and that this repression must be relieved by nodal flow on the left side only. Moreover, since *Pkd1l1*$^{tm1/tm1}$ and *Pkd2*$^{lrm4/lrm4}$ mutants have opposite crown cell *Cerl2* and *Nodal* phenotypes as well as distinct LPM *Nodal* phenotypes, and that the *Pkd2*$^{lrm4/lrm4}$ phenotype manifests in double mutants, we suggest that, genetically, *Pkd1l1* acts as an upstream repressor of *Pkd2*. Finally, *Pkd2* is known to act as a genetic repressor of *Cerl2* which itself is an antagonist of the Nodal pathway. This model, described pictorially in Fig 7A and 7B, coheres with the genetic tests we have performed in this study. It is worth noting that this interpretation of the data relies on *Pkd1l1*^{tm1} being a hypomorphic or null allele, something which is very likely (S1 Fig),

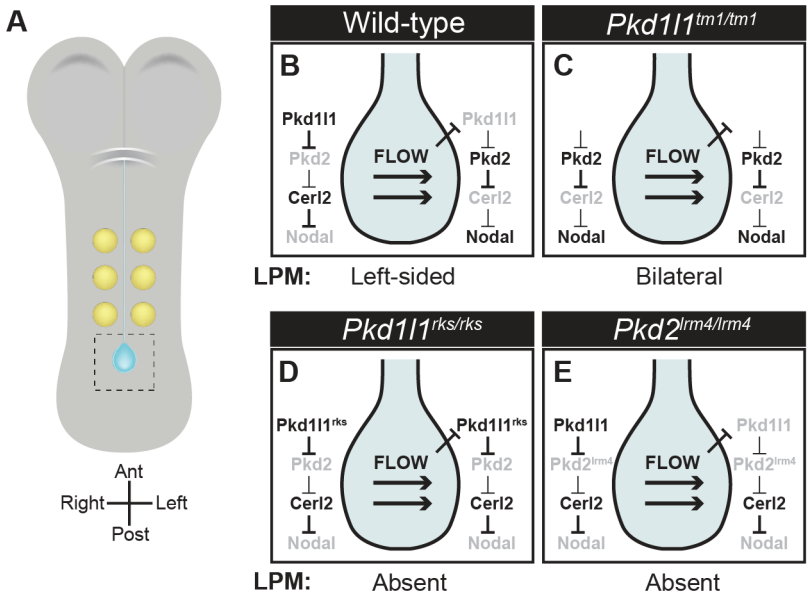

Fig 7. Multi-repression Model for L-R Asymmetry Determination in Crown Cells. (A) Schematic of a 3 ss flat-mounted mouse embryo showing somites (yellow), and node (blue). (B) Pictorial representation of the multi-repression model in which flow represses *Pkd1l1* on the left side, resulting in the derepression of *Pkd2*, inhibition of *Cerl2* and, as a result, higher NODAL activity on the left. (C-E) Predictions of the multi-repression model in various genetic mutants including the impact on the crown cell genetic pathway as well as the predicted LPM Nodal cascade activity.

doi:10.1371/journal.pgen.1006070.g007

but owing to the absence of functional PKD1L1 antibodies, not something we have formally tested at the protein level. It is formally possible that a cryptic initiation codon downstream of the deleted exons in *Pkd1l1*^{tm1} results in a portion of PKD1L1 being expressed in mutants, and our repression model must be considered with this caveat in mind. Nevertheless, the model predicts bilateral Nodal cascade activity in the absence of *Pkd1l1* (Fig 7C), something we do see in *Pkd1l1*$^{tm1/tm1}$ mutants, as well as absent Nodal cascade activity in loss-of-function *Pkd2* mutants like *Pkd2*$^{lrm4/lrm4}$ (Fig 7E), again in agreement with experiment. Moreover, it is worth emphasizing that this is a genetic model and that our study leaves open several possibilities regarding the nature of the molecular interactions between adjacent members of this genetic cascade. The genetic relationships uncovered here could manifest via direct molecular repression of PKD2 by PKD1L1 or more indirectly by the control of PKD1L1 and/or PKD2 localization.

Our multi-repression-based genetic model ascribes two functions to *Pkd1l1* in L-R patterning: (1) to mediate a flow-based signal (or, genetically, to receive a signal from *Dnahc11*, mutants of which we use in our genetic experiments to eliminate flow) and (2) to genetically repress *Pkd2* activity. In the absence of flow, *Pkd1l1* represses *Pkd2* in the node. The onset of flow (*Dnahc11* function) relieves this repression, causing *Pkd2* to activate and thereby initiates a cascade that results in left-sided Nodal signals. In the absence of *Pkd1l1*, repression of *Pkd2* is relieved and signals are activated bilaterally independently of flow (since the *Dnahc11*^{iv} mutation does not manifest in the presence of *Pkd1l1*^{rks}). By contrast, since *Pkd2* is required for *Cerl2* repression and *Nodal* activation, loss of *Pkd2* function results in bilateral absence of the Nodal cascade. The repression model provides an explanation for the previously published *Pkd1l1*^{rks} mutant phenotype since the *Pkd1l1*^{rks} mutation seems to uncouple the two functions of *Pkd1l1*. The *Pkd1l1*^{rks} mutation structurally disrupts an extracellular PKD domain, resulting

in PKD1L1^{rks} protein being unable to elicit Ca^{2+} signals downstream of artificial flow. Moreover, NODAL activity is bilaterally repressed in *Pkd1l1*$^{rks/rks}$ mutants, implying that *Pkd2* is inactive regardless of the presence of normal nodal flow in these mutants. This is consistent with the idea that the *Pkd1l1*^{rks} mutation is loss-of-function with respect to role (1), flow sensation, but, owing to its insensitivity to flow, it appears gain-of-function with respect to role (2), *Pkd2* inhibition (i.e. *Pkd2* remains inhibited regardless of the presence of the upstream activating signal, nodal flow) (Fig 7D).

Furthermore, the repression model coheres with the subtle phenotypic differences between *Pkd1l1*$^{tm1/tm1}$ and *Dnah11*$^{iv/iv}$ mutants. Though these two mutants exhibit overtly similar phenotypes, with high levels of left lung isomerism and bilateral Nodal cascade activity, it is noteworthy that these outcomes result from distinct mechanisms. In *Dnah11*$^{iv/iv}$ mutants, loss of flow results in stochastic (unbiased) Nodal pathway activation; crucially, initiation of the Nodal cascade in the LPM occurs with a delay of around 2 hours in the absence of flow. This is consistent with the repression model, since the pathway to activate Nodal robustly requires repression of *Pkd1l1* by flow; this would not occur in a timely fashion in the absence of flow. In stark contrast, the *Pkd1l1*^{tm1} allele leads to bilateral LPM Nodal pathway activity without delay, interpreted in our model as loss of *Pkd1l1* leading to the fast derepression of *Nodal*. Why the Nodal cascade activates at all in the absence of flow is an intriguing question and suggests that repression of *Pkd1l1* by flow is not absolutely required for *Nodal* activation but, rather, the repression is required for biased expression to manifest at the correct time. If this pathway is not activated in this way owing to lack of flow, stochastic changes in fluid movement, or other variations, followed by positive feedback loops operating at the node and LPM [14, 40] likely result in randomized or bilateral Nodal activity.

Pkd1l1, *Pkd2*, and Cilia

Our experiments, in which we generated *Pkd1l1*$^{rks/rks}$;*Kif3a*$^{-/-}$ and *Pkd2*$^{lrm4/lrm4}$;*Kif3a*$^{-/-}$ double mutants and found that they exhibited the same LPM Nodal pathway activity as *Kif3a*$^{-/-}$ mutants, show that cilia (or, strictly, *Kif3a*) are required for the manifestation of the *Pkd1l1* and *Pkd2* mutant phenotypes. A simple explanation of this finding is that PKD1L1 and PKD2 require cilia to function, in agreement with their sub-cellular localization to cilia [16–18, 42, 52]. However, this relatively complicated genetic interaction warrants further discussion. In *Kif3a*$^{-/-}$ mutants, the vast majority of nodal cilia are lost [34, 43] and the Nodal cascade is bilaterally activated. This suggests that cilia provide an inhibitory signal preventing LPM Nodal cascade activation. In contrast, loss of *Pkd2* results in the absence of LPM *Nodal*, implying that *Pkd2* acts to overcome this inhibition. In *Pkd2*$^{lrm4/lrm4}$;*Kif3a*$^{-/-}$ double mutants, the loss of cilia-mediated inhibition results in *Nodal* being activated (now bilaterally) independently of *Pkd2*. Therefore, loss of that cilia-based inhibition (in *Kif3a*$^{-/-}$) suppresses loss of *Pkd2*. However, since *Pkd1l1*^{tm1} does not suppress *Pkd2*^{lrm4}, it seems likely that the cilia-based inhibitory signal is not provided by *Pkd1l1*. These data speak to an apparent paradox in the field; since PKD2 acts to activate LPM *Nodal* and is thought to act in cilia, how can loss of cilia result in bilateral Nodal activity? One possibility is that Hedgehog signaling, which acts in the LPM bilaterally upstream of Nodal activation [53], could be augmented sufficiently to affect *Nodal* expression upon loss of cilia. Moreover, loss of *Kif3a* impacts both flow generation and sensation in the node [5, 18] and also affects midline structures resulting in barrier defects. Thus, the inhibitory signal (in terms of Nodal activation) provided by cilia independently of *Pkd1l1/Pkd2* function could be acting at the node, the LPM, the midline, or in a combination of these locations. However, the most important contribution likely comes from crown cell cilia since embryos expressing *Kif3a* solely in crown cells express *Nodal* exclusively in the left LPM following

application of leftward flow [42]. This result coheres with our interpretation of the *Pkd1l1*$^{rks/rks}$;*Kif3a*$^{-/-}$ and *Pkd2*$^{lrm4/lrm4}$;*Kif3a*$^{-/-}$ double mutant phenotypes because the cilia-based repressive signal, that cannot be overcome by mutation of *Pkd1l1* or *Pkd2*, appears to be acting most dominantly within the sensory cilia of the crown cells.

The finding that loss of cilia masks the *Pkd2*^{lrm4} mutant phenotype reinforces the idea that PKD2 must localize to nodal cilia to activate downstream Nodal signals [51], (and this manuscript). Others have demonstrated a requirement for PKD1 or PKD1L1 in the localization of PKD2 to cilia [16, 17, 48]. If PKD2 localization to cilia were entirely dependent on wild-type PKD1L1, we might expect no PKD2-mediated Nodal cascade activation in *Pkd1l1*$^{tm1/tm1}$ mutants, the opposite of the bilateral Nodal activity that we do see. However, our results show this clearly not to be the case; some PKD2 still localizes to nodal cilia in *Pkd1l1*$^{tm1/tm1}$ mutants. Although there is less PKD2 in the nodal cilia of *Pkd1l1*$^{tm1/tm1}$ mutants compared to wild-type, interpreting this result in light of our genetic model suggests this lower amount of PKD2 to be active in the absence of PKD1L1. These findings further suggest that PKD2 cannot respond to nodal flow in the *Pkd1l1*$^{tm1/tm1}$ mutant since in these mutants nodal flow is normal and some PKD2 localizes to cilia; however, we see no evidence for consistent lateralized downstream Nodal cascade activity, implying that no flow sensation is occurring.

PKD1L1 and the Response to Nodal Flow

Whether PKD1L1 is part of a pathway mediating sensation of an asymmetrically distributed chemical determinant positioned by nodal flow (chemosensation), or the force of flow itself (mechanosensation), remains a topic of debate [16, 22, 42, 54]. Here, we demonstrate that, in a tissue culture system where the onset of flow and the presence/absence of PKD1L1 is controlled, PKD1L1 cell autonomously mediates Ca^{2+} signaling downstream of fluid flow. Thus, our work favours a mechanosensation model of nodal flow sensation.

Left-biased Ca^{2+} signals have been observed around the node and thus correlate with left-sided Nodal activation [18, 36, 55]; these signals depend on both flow and PKD2. Thus, non-functional *Pkd2* alleles, such as *Pkd2*^{lrm4}, should abolish this Ca^{2+} signal and lead to loss of *Nodal* induction, a result we find in *Pkd2*$^{lrm4/lrm4}$ mutants. In *Pkd1l1*$^{tm1/tm1}$ mutants, we observe bilateral *Nodal*, suggesting bilateral Ca^{2+} signaling. Extrapolation of our genetic model, in which *Pkd1l1*$^{tm1/tm1}$ represents loss of *Pkd1l1*, into a simple molecular model can explain this: on the left side of the node, PKD2 repression by PKD1L1 is relieved by flow, resulting in the opening of PKD2 channels and activation of the Nodal cascade. In our tissue culture system, we do not see Ca^{2+} signals upon loss of the cells endogenous flow sensor, PKD1. Importantly, upon expression of PKD1L1 in this system, the cells again become competent to respond to flow, demonstrating that PKD1L1 can mediate flow sensation. PKD2 activity in *Pkd1l1*$^{tm1/tm1}$ mutant embryos could not be recapitulated in the cell line we used because PKD1, not PKD1L1, is the endogenous flow sensor. Thus, the two systems provide complementary information, but are not directly analogous. Of note is that either PKD1 or PKD1L1 can function independently to mediate flow sensation in our tissue culture flow chamber system. The embryonic system provides us with a genetic model that can explain the mouse mutant phenotypes, whereas the tissue culture experiments reveal PKD1L1 protein to be able to mediate a cellular response to flow sensation.

With this in mind, though our data supports the mechanosensation model, this study does not rule out the importance of asymmetrically distributed molecules in the node cavity. Modeling studies demonstrate the viability of the concept of L-R asymmetric morphogen gradients within the node [56]. Nodal vesicular parcels (NVPs), large membrane-encased vesicles, have been described transiting the node and opening on the left side [23] and these might

asymmetrically deliver a left-side determinant. Indeed, recently CERL2 protein has been demonstrated to transition from right-biased to left-biased in response to nodal flow; the timing of this event is notable in that left-biased localization is not detected until several hours after the establishment of L-R asymmetry at the node, when it functions to shut down NODAL activity and thereby lock in asymmetry [57]. Future study will determine whether flow-driven asymmetric distribution of molecules functions solely in this later event.

Nevertheless, other considerations favour the mechanosensation hypothesis. Firstly, the fact that the *Pkd1l1*^{rks} point mutation impacts one of two extracellular PKD domains implicates this domain in PKD1L1 function during L-R patterning. Interestingly, PKD domains are required in other contexts where mechanosensing occurs. For example, PKD1, which harbors fifteen PKD domains, is argued to act as a mechanosensor of fluid flow in the kidney [58]. However, this alone does not formally rule out a role for the PKD domain, or PKD1L1 in general, as a binding site for an unknown chemical determinant. Indeed, the Polycystin-1 family member PKD1L3 acts as a chemical receptor needed for sour taste perception [59], though it is noteworthy that PKD1L3 does not contain PKD domains.

Secondly, PKD domains exhibit remarkable mechanical strength along the N-to-C terminal axis [60, 61]. Some mutations in human PKD1 that cause ADPKD have been found within the PKD domains [47, 62]. An assessment of domain strength within these disease variants by atomic force microscopy found that many human disease associated point mutations caused a weakening of the PKD domains, suggesting that domain strength is critical for function [47]. Here, we found by molecular modeling, SRCD spectroscopy, and melting temperature analysis, that the *Pkd1l1*^{rks} point mutation structurally destabilizes the second PKD domain of PKD1L1. We thus hypothesize that such a destabilization leads to reduced domain strength and, therefore, the inability of PKD1L1^{rks} to transduce the force of nodal flow. This is corroborated by our finding that unlike PKD1L1, PKD1L1^{rks} protein does not mediate mechanosensation in response to fluid flow.

PKD1L1-PKD2L1 complexes in cilia of neural derived cells are known to facilitate a constitutive ciliary Ca^{2+} flux [52, 63], while a pressure clamp failed to induce signaling through PKD1L1-PKD2L1 complexes at physiological force levels. Whilst this somewhat contrasts with our data, it is worth noting that different cell types and a different PKD protein pair are examined in each study. Moreover, the nature of flow/force sensation by cilia will not necessarily translate to simple pressure upon the channel; cilia become deformed by motion within a flow leading to stresses along as well as perpendicular to the membrane. It is unclear to what extent all such forces will be modeled by pressure clamping.

The mechanistic details of how PKD1L1 mediates flow sensation in the node will require a multi-disciplinary approach combining structural biology, computational approaches, and genetics. Our finding that PKD1L1 and PKD2 function during L-R patterning requires primary cilia is intriguing; it has been argued that the bending of the ciliary membrane as a result of flow might be critical for mechanosensation by Polycystin proteins [48]. One possibility is that the N-terminus of PKD1L1 is tethered to the ciliary membrane so that PKD domains lie parallel to the membrane. Thus, when the membrane is bent by flow, the PKD domains would be placed under mechanical force along their N- to C-terminal axis, where they exhibit mechanical strength; this might aid in force transduction.

In summary, we reveal a genetic pathway for the early phases of L-R patterning which encompasses the generation of nodal flow, its' sensation, and subsequent downstream changes in gene expression. Moreover, in a tissue culture system we demonstrate that PKD1L1 can mediate the sensation of fluid flow to elicit Ca^{2+} signals. Finally, we implicate a PKD domain of PKD1L1 in the response to flow and L-R patterning.

Materials and Methods

Ethics Statement

All experiments were performed under the guidelines and approval of the Home Office, UK and the MRC Harwell, UK Ethics Committee; Euthanasia was by cervical dislocation of adults and decapitation of embryos.

Mice

The mouse lines used in this study are: *Pkd1l1*^{rks}; *Pkd1l1*^{tm1Lex} (*Pkd1l1*^{tm1}); *Pkd2*^{lrm4}; *Dnah11*^{iv}; *Kif3a*^{tm1Gsn} (*Kif3a*$^{-}$); *Pkd1*^{tm1Jzh} (*Pkd1*$^{-}$). All experiments were performed under the guidelines and approval of the Home Office, UK; Euthanasia was by cervical dislocation of adults and decapitation of embryos. *Pkd1l1*^{rks}, *Pkd2*^{lrm4}, and *Dnah11*^{iv} lines were congenic on C3H/HeH, while *Pkd1l1*^{tm1} and *Kif3a*$^{-}$ were only used for experiments after at least four and two back-crosses to C3H/HeH, respectively.

In Situ Hybridization

Whole mount in situ hybridization (WISH) was performed using digoxygenin-labeled riboprobes using standard procedures. Quantitation of crown cell gene expression was performed using ImageJ, NIH.

Analysis of Embryonic Nodes

To visualize nodal cilia rotation, embryos were mounted on slides with the node facing up. Differential interference contrast (DIC) microscopy was then performed using a Leica DM2500 compound microscope with a monochrome high-speed Hamamatsu camera attached. Quantitation was performed by counting cilia rotations from movies taken at approximately 100 frames per second for at least 10 cilia per embryo and at least 3 embryos per genotype. For detection of nodal flow, fluorescent beads (0.2 μm; Invitrogen F-8848) were diluted 1:10 with dissection medium supplemented with 2% fetal bovine serum and then placed over mounted embryos. The node was imaged using a Zeiss Axio Observer Z1 microscope with a VivaTome extension to allow for high-speed optical sectioning. Particle Image Velocimetry (PIV) analysis was performed as previously described [37].

Quantitative Reverse Transcription PCR (qRT-PCR)

RNA was extracted from single embryos using a Microplus kit (Qiagen) according to manufacturers' instructions. 500 ng of RNA was used for cDNA synthesis using a SuperScriptIII First-Strand Synthesis SuperMix for qRT-PCR kit (Invitrogen). qPCR was performed in triplicate on a 7900 Fast Machine (Life Technologies) using Fast SYBR Green Mastermix (Life Technologies) with 20 ng cDNA and 500 nM forward and reverse primers in a final 20 μl reaction volume (see S4 Table for primer sequences). Quantitation was relative to *Hprt* and fold changes were calculated using the $\Delta\Delta C_T$ method (7500 Software v2.0.6., Life Technologies).

Protein Expression and Purification

Both wild-type and *rks*-mutated versions of PKD domain 2 from mouse PKD1L1 were tagged at the N-terminus with His, expressed in *E. coli*, purified using a His column, refolded at decreasing urea concentration by affinity chromatography then vacufuged and dialysed. Protein concentration was calculated based on the measured ultraviolet (UV) absorbance (at 1 mm path length) at 280 nm on an Implen NanoPhotometer.

In Vitro Flow-Induced Ca^{2+} Signaling (FICS) Assessment

Vascular endothelial cells were extracted from wild-type or *Pkd1*$^{-/-}$ embryos as previously described [49]. Cells were cultured in permissive conditions (in the presence of interferon-γ at 33°C) to induce proliferation then transfected with 1 μg/mL pEGFP-N1 plasmid (Clontech Laboratories) containing EGFP only, PKD1L1-EGFP, or PKD1L1^{rks}-EGFP. To promote cell differentiation and cilia growth, cells were grown under non-permissive conditions (in the absence of interferon-γ at 39°C) to induce differentiation.

For FICS experiments we used previously described protocols [64]. Briefly, cells were loaded with 5 μM Fura2-AM (Invitrogen) for 30 minutes at 39°C. Basal fluorescence was measured for one minute before the onset of fluid flow using a Nikon TE2000 microscope with Metafluor software. A shear stress of 7.2 dyne/cm^2 was achieved in an FCS2 chamber with electrical enclosure heater (Biotechs, Inc.) at a flow rate of 550 μL/sec. Flow was then applied and fluorescence was monitored every 4 seconds. At the end of the experiment, minimum fluorescence measurements were obtained by treating cells with 2 mM EGTA and 10 μM ionomycin. After achieving the minimum signal, the maximum fluorescence was obtained by treating cells with excess calcium (10 mM). All fluorescence measurements were corrected for auto-fluorescence.

All quantifiable experimental values are expressed as mean +/- standard error of the mean (SEM), with values of $p<0.05$ being considered statistically significant. Data analysis was performed using SigmaPlot software Version 11 and comparisons among groups were done using ANOVA followed with Tukey's posttest.

Synchrotron Radiation Circular Dichroism (SRCD) Spectroscopy

Far UV SRCD experiments were performed using Module B of Beamline B23 at the Diamond Light Source (Didcot, Oxfordshire UK). Measurements of protein solutions were carried out in 20 mM Tris and 50 mM NaCl, pH8.5, at a concentration of 0.145 mg/ml (wild-type PKD domain) or 0.104 mg/ml (*rks*-mutated PKD domain). Four scans were taken at 20°C (1 nm increment, 1 s integration time and a scan rate of 38 nm/min) and averaged. Spectra of buffer alone were subtracted from the sample spectra. Secondary structure composition was calculated from the experimental spectra using Raussens algorithm [46].

Supporting Information

S1 Fig. Characterisation of the *Pkd1l1*^{tm1} allele. The *Pkd1l1*^{tm1} allele (*Pkd1l1*^{tm1Lex}; [33]) comprises a beta-galactosidase-neomycin fusion gene (beta-geo) inserted in place of exons 3, 4 and 5 (labelled 'LacZ' in the schematic given in D). Importantly, this insertion contains a stop codon and polyA signal at its 3' end. The data in this figure demonstrate that in *Pkd1l1*$^{tm1/tm1}$ mutants, the gene is disrupted either by splicing onto the beta-geo cassette or by splicing around the cassette in a fashion that introduces a premature stop codon which truncates the protein very early, suggesting that *Pkd1l1*^{tm1} is a null or strong hypomorph. (AA'-AG') Expression of *Pkd1l1* was assessed by LacZ staining, revealing that expression from the beta-geo reporter locus mirrors the endogenous expression pattern [16]. *Pkd1l1*$^{+/tm1}$ embryos that were phenotypically normal; 7.5 dpc (AA'-AB'), 8.5 dpc (AC'-AE'), and 9.5 dpc (AF'-AG') embryos were assessed. (B) WISH analysis of *Pkd1l1* expression in *Pkd1l1*$^{+/tm1}$ and *Pkd1l1*$^{tm1/tm1}$ embryos at 8.5 dpc. If all transcripts splice into beta-geo, then we would predict there to be no mRNA present for 3' portions of *Pkd1l1*. However, WISH revealed equivalent expression patterns in both wild-type and mutant embryos (assessed with a probe covering exons 20–24); expression in the *Pkd1l1*$^{tm1/tm1}$ embryos appears slightly reduced. (C) A proportion of *Pkd1l1*^{tm1} transcripts splice from exon 2 to exon 6, skipping the beta-geo insertion. It is documented that a proportion of gene trap alleles produce novel splice products that 'jump over' the gene trap. We therefore investigated whether

the message detected by WISH *(B)* might result from such a splicing event around the targeted insertion. cDNA was prepared from wild-type, *Pkd1l1*$^{+/tm1}$ and *Pkd1l1*$^{tm1/tm1}$ 8.5 dpc embryos. PCR primers in exons 1 (5'-TTGGCAGGTGCAACTACTGT-3') and 6 (5'-CCCATGTTCTT-CACTGGGGG-3') were used to amplify the intervening region. This resulted in a band of the predicted size (~800bp) in wild-type and *Pkd1l1*$^{+/tm1}$ samples and a smaller band (~350 bp) in *Pkd1l1*$^{+/tm1}$ and *Pkd1l1*$^{tm1/tm1}$ samples (gel on right; *t* refers to *tm1*). The wild-type band was missing from the *Pkd1l1*$^{tm1/tm1}$ samples. The smaller band is of the size predicted for a splicing event between exons 2 and 6, as confirmed by Sanger sequencing. The resulting message in *Pkd1l1*$^{tm1/tm1}$ is out of frame such that any resulting protein would truncate within 18 amino acids of the exon 2-exon 6 splicing event. This would lead to a very small product, lacking all characterised protein domains including having no transmembrane domains. Thus, in *Pkd1l1*$^{tm1/tm1}$ embryos, the second exon of *Pkd1l1* either splices onto the beta-geo cassette (which harbours a polyA and stop codon) or splices from exon 2-exon 6 producing an out of frame transcript which contains a stop codon after 18 amino acids. (D) Quantitative analysis of *Pkd1l1* transcripts reveals that the level of transcript detected in 3' potions of the locus in *Pkd1l1*$^{tm1/tm1}$ is equivalent to the level of transcript that splices exons 2–6 in *Pkd1l1*$^{tm1/tm1}$ embryos. Only single long *Pkd1l1* Havana-curated transcripts exist in both mouse and humans. To test whether additional start sites might exist we utilised quantitative reverse transcription PCR (qRT-PCR) to measure the expression levels of different regions of the transcript. The following assays were used:

- Exon 1–2 assesses expression from the known start site of the locus. Surprisingly, this revealed a 2-fold upregulation of *Pkd1l1* in *Pkd1l1*$^{tm1/tm1}$ embryos, suggesting that a negative feedback loop controls *Pkd1l1* expression.
- Exon 2–3 and Exon 5–6 assess wild-type expression. As exon 3, 4 and 5 are absent from the *Pkd1l1*$^{tm1/tm1}$ allele, as expected, no expression in this region of the transcript is evident in *Pkd1l1*$^{tm1/tm1}$ mutants.
- Exon 2-LacZ assesses the splicing from exon 2 into the beta-geo insertion; the predicted splice product. As predicted, this product is present in both *Pkd1l1*$^{+/tm1}$ and *Pkd1l1*$^{tm1/tm1}$ and is approximately twice as highly expressed in the mutant relative to the heterozygous state.
- Exon 2–6 assesses splicing around the beta-geo insertion, which is predominant in *Pkd1l1*$^{tm1/tm1}$ and *Pkd1l1*$^{+/tm1}$ samples. We also observed a very small amount of exon 2–6 splicing in wild-type samples in this assay. However, additional analysis suggests this low level of expression to be an artefact of the qPCR assay and not a biologically meaningful splice variant.
- Exon 21–22 assesses expression of a 3' region of the locus. This product overlaps the WISH probe used above *(B)*.

(E) The relative levels of the exon 2–6 versus exon 2-LacZ were calculated, revealing that exon 2–6 splicing occurs at ~35% of the level for exon 2-LacZ splicing in both the *Pkd1l1*$^{+/tm1}$ and *Pkd1l1*$^{tm1/tm1}$ embryos. In combination with the doubled level of transcription of the *Pkd1l1* locus in *Pkd1l1*$^{tm1/tm1}$ embryos, this explains the level of transcript that we detect by exon 21–22 qRT-PCR. For all experiments, error bars show the RQ_{min} and RQ_{max} when confidence levels are set at 95%.
(DOCX)

S2 Fig. Pkd1l1$^{tm1/tm1}$ mutants exhibit variable times of death and gross heart and stomach situs defects that are similar to Pkd1l1$^{rks/rks}$ and Dnah11$^{iv/iv}$ mutants. (A-B) Charts showing the observed (Obs) and expected (Exp) frequencies of *Pkd1l1* genotype for embryos dissected at E13.5 *(A)* or recovered as surviving adults *(B)*. There is a statistically significant loss of *Pkd1l1$^{tm1/tm1}$* mutants at these time points (chi-square test applied). When dissected at E13.5, 32% of *Pkd1l1$^{tm1/tm1}$* (n = 13/41) had already arrested *in utero* (at various times between E9.5-E12.5). Approximately 35% of the expected number of homozygotes survived until adulthood. (C-D) Examples of reversed heart (H) and stomach (S) laterality in *Pkd1l1$^{tm1/tm1}$* embryos *(D)* compared to a control *(C)* at E13.5. Normally, the heart apex and stomach are positioned to the left of the body cavity, but this is reversed in a proportion of *Pkd1l1$^{tm1/tm1}$* mutants. R-L refers to right-left. (E) Heart and stomach laterality scored at E13.5 for *Pkd1l1$^{tm1/tm1}$*, *Dnah11$^{iv/iv}$* and *Pkd1l1$^{rks/rks}$* mutants. The percentage of embryos showing each phenotype and the total number of embryos examined is given. *t* refers to *Pkd1l1^{tm1}*.
(DOCX)

S3 Fig. Quantitation of nodal cilia rotation frequency in *Pkd1l1$^{tm1/tm1}$* and control embryos. Cilia rotation fequency for *Pkd1l1$^{tm1/tm1}$* mutants and wild-type controls. At least three embryos of each genotype were assessed and analysis was performed blind to genotype. Error bars represent standard error of the mean. No statistically significant difference (ns) was found between the two genotypes, Student *t*-test applied.
(DOCX)

S4 Fig. PIV analysis of nodal flow. PIV analysis was conducted on of wild-type (WT), *Pkd1l1$^{tm1/tm1}$*, *Pkd2$^{lrm4/lrm4}$*, *Pkd1l1$^{rks/rks}$* and *Dnah11$^{iv/iv}$* 8.5 dpc embryos. Examples of PIV analysis at different somite stages (ss) are shown. Flow was present and leftward at all stages assessed in all genotypes except *Dnah11$^{iv/iv}$* which exhibited absence of flow.
(DOCX)

S5 Fig. Overall *Cerl2* levels are decreased in *Pkd1l1$^{tm1/tm1}$* mutants compared to control embryos. *Cerl2* expression at the node of *Pkd1l1$^{tm1/tm1}$* mutants and control embryos at the 1–3 somite stage from three separate litters. In each case, expression is more symmetrical and expression levels are lower in *Pkd1l1$^{tm1/tm1}$* embryos than in controls. Embryos from the same litter were treated identically throughout the procedure and scoring of expression was performed prior to genotyping.
(DOCX)

S1 Table. Genetic interaction between *Dnah11^{iv}* and *Pkd1l1^{rks}* or *Pkd2^{lrm4}*. n, number; NS, normal situs; RS, reversed situs; RI, right isomerism; LI, left isomerism; PI, partial isomerism; L, left; R, right; B, bilateral; A, absent. Lung situs was scored at 13.5 dpc, while LPM *Pitx2* expression was determined by WISH at 8.5 dpc.
(DOCX)

S2 Table. Genetic interaction between *Pkd1l1^{tm1}* and *Pkd2^{lrm4}*. n, number; NS, normal situs; RS, reversed situs; RI, right isomerism; LI, left isomerism; PI, partial isomerism. Lung situs was scored at 13.5 dpc.
(DOCX)

S3 Table. Genetic interaction between *Kif3a^{-}* and *Pkd1l1^{rks}* or *Pkd2^{lrm4}*. n, number; L, left; R, right; B, bilateral; A, absent. LPM *Pitx2* expression was determined by WISH at 8.5 dpc.
(DOCX)

S4 Table. *Pkd1l1*^{tm1} primers used for qRT-PCR.
(DOCX)

S5 Table. Numerical results of flow chamber experiments.
(DOCX)

Acknowledgments

We thank Joe Holmes, Jackie Harrison, and Sara Wells (Mary Lyon Centre, Harwell) for animal husbandry; Jeremy Sanderson, Michelle Simon, Will Letton, Chris Esapa, Helen Hilton, and George Nicholson (Medical Research Council, Harwell) for technical assistance and advice; the Diamond Light Source for B23 beamtime (SM7560 and SM8084).

Author Contributions

Conceived and designed the experiments: DTG DPN. Performed the experiments: DTG JLK MTB XJ SHP DJW. Analyzed the data: DTG JLK KS HH RH SMN DPN DJW JV. Wrote the paper: DTG DPN. Analyzed nodal flow movies: KS JV HH. Performed SRCD experiments: MTB RH. Performed the Ca2+ experiments: XJ SMN.

References

1. Peeters H, Devriendt K. Human laterality disorders. European journal of medical genetics. 2006; 49 (5):349–62. PMID: 16461029.
2. Ramsdell AF. Left-right asymmetry and congenital cardiac defects: getting to the heart of the matter in vertebrate left-right axis determination. Developmental biology. 2005; 288(1):1–20. PMID: 16289136.
3. Li Y, Klena NT, Gabriel GC, Liu X, Kim AJ, Lemke K, et al. Global genetic analysis in mice unveils central role for cilia in congenital heart disease. Nature. 2015; 521(7553):520–4. Epub 2015/03/26. doi: 10.1038/nature14269 PMID: 25807483.
4. Nonaka S, Shiratori H, Saijoh Y, Hamada H. Determination of left-right patterning of the mouse embryo by artificial nodal flow. Nature. 2002; 418(6893):96–9. PMID: 12097914.
5. Nonaka S, Tanaka Y, Okada Y, Takeda S, Harada A, Kanai Y, et al. Randomization of left-right asymmetry due to loss of nodal cilia generating leftward flow of extraembryonic fluid in mice lacking KIF3B motor protein. Cell. 1998; 95(6):829–37. PMID: 9865700.
6. Blum M, Weber T, Beyer T, Vick P. Evolution of leftward flow. Semin Cell Dev Biol. 2009; 20(4):464–71. Epub 2008/12/06. doi: 10.1016/j.semcdb.2008.11.005 PMID: 19056505.
7. Pearce JJ, Penny G, Rossant J. A mouse cerberus/Dan-related gene family. Dev Biol. 1999; 209 (1):98–110. PMID: 10208746.
8. Marques S, Borges AC, Silva AC, Freitas S, Cordenonsi M, Belo JA. The activity of the Nodal antagonist Cerl-2 in the mouse node is required for correct L/R body axis. Genes Dev. 2004; 18(19):2342–7. PMID: 15466485.
9. Kawasumi A, Nakamura T, Iwai N, Yashiro K, Saijoh Y, Belo JA, et al. Left-right asymmetry in the level of active Nodal protein produced in the node is translated into left-right asymmetry in the lateral plate of mouse embryos. Developmental biology. 2011; 353(2):321–30. PMID: 21419113. doi: 10.1016/j.ydbio.2011.03.009
10. Shiratori H, Hamada H. The left-right axis in the mouse: from origin to morphology. Development. 2006; 133(11):2095–104. PMID: 16672339.
11. Norris DP. Cilia, calcium and the basis of left-right asymmetry. BMC biology. 2012; 10:102. Epub 2012/12/22. doi: 10.1186/1741-7007-10-102 PMID: 23256866; PubMed Central PMCID: PMC3527145.
12. Namigai EK, Kenny NJ, Shimeld SM. Right across the tree of life: The evolution of left-right asymmetry in the Bilateria. Genesis. 2014. Epub 2014/02/11. doi: 10.1002/dvg.22748 PMID: 24510729.
13. Meno C, Shimono A, Saijoh Y, Yashiro K, Mochida K, Ohishi S, et al. lefty-1 is required for left-right determination as a regulator of lefty-2 and nodal. Cell. 1998; 94(3):287–97. PMID: 9708731.
14. Nakamura T, Mine N, Nakaguchi E, Mochizuki A, Yamamoto M, Yashiro K, et al. Generation of robust left-right asymmetry in the mouse embryo requires a self-enhancement and lateral-inhibition system. Dev Cell. 2006; 11(4):495–504. PMID: 17011489.

15. Bisgrove BW, Snarr BS, Emrazian A, Yost HJ. Polaris and Polycystin-2 in dorsal forerunner cells and Kupffer's vesicle are required for specification of the zebrafish left-right axis. Dev Biol. 2005; 287 (2):274–88. PMID: 16216239.

16. Field S, Riley KL, Grimes DT, Hilton H, Simon M, Powles-Glover N, et al. Pkd1l1 establishes left-right asymmetry and physically interacts with Pkd2. Development. 2011; 138(6):1131–42. PMID: 21307093. doi: 10.1242/dev.058149

17. Kamura K, Kobayashi D, Uehara Y, Koshida S, Iijima N, Kudo A, et al. Pkd1l1 complexes with Pkd2 on motile cilia and functions to establish the left-right axis. Development. 2011; 138(6):1121–9. Epub 2011/02/11. doi: 10.1242/dev.058271 PMID: 21307098.

18. McGrath J, Somlo S, Makova S, Tian X, Brueckner M. Two populations of node monocilia initiate left-right asymmetry in the mouse. Cell. 2003; 114(1):61–73. PMID: 12859898.

19. Pennekamp P, Karcher C, Fischer A, Schweickert A, Skryabin B, Horst J, et al. The ion channel polycystin-2 is required for left-right axis determination in mice. Curr Biol. 2002; 12(11):938–43. PMID: 12062060.

20. Schottenfeld J, Sullivan-Brown J, Burdine RD. Zebrafish curly up encodes a Pkd2 ortholog that restricts left-side-specific expression of southpaw. Development. 2007; 134(8):1605–15. PMID: 17360770.

21. Koulen P, Cai Y, Geng L, Maeda Y, Nishimura S, Witzgall R, et al. Polycystin-2 is an intracellular calcium release channel. Nat Cell Biol. 2002; 4(3):191–7. PMID: 11854751.

22. Norris DP, Grimes DT. Developmental biology. Cilia discern left from right. Science. 2012; 338 (6104):206–7. Epub 2012/10/16. doi: 10.1126/science.1230401 PMID: 23066068.

23. Tanaka Y, Okada Y, Hirokawa N. FGF-induced vesicular release of Sonic hedgehog and retinoic acid in leftward nodal flow is critical for left-right determination. Nature. 2005; 435(7039):172–7. PMID: 15889083.

24. Patel A. The primary cilium calcium channels and their role in flow sensing. Pflugers Arch. 2015; 467 (1):157–65. doi: 10.1007/s00424-014-1516-0 PMID: 24764075.

25. Nauli SM, Rossetti S, Kolb RJ, Alenghat FJ, Consugar MB, Harris PC, et al. Loss of polycystin-1 in human cyst-lining epithelia leads to ciliary dysfunction. J Am Soc Nephrol. 2006; 17(4):1015–25. doi: 10.1681/ASN.2005080830 PMID: 16565258.

26. Hanaoka K, Qian F, Boletta A, Bhunia AK, Piontek K, Tsiokas L, et al. Co-assembly of polycystin-1 and -2 produces unique cation-permeable currents. Nature. 2000; 408(6815):990–4. doi: 10.1038/35050128 PMID: 11140688.

27. Patel A, Honore E. Polycystins and renovascular mechanosensory transduction. Nat Rev Nephrol. 2010; 6(9):530–8. doi: 10.1038/nrneph.2010.97 PMID: 20625375.

28. Sharif-Naeini R, Folgering JH, Bichet D, Duprat F, Lauritzen I, Arhatte M, et al. Polycystin-1 and -2 dosage regulates pressure sensing. Cell. 2009; 139(3):587–96. doi: 10.1016/j.cell.2009.08.045 PMID: 19879844.

29. Yu Y, Ulbrich MH, Li MH, Dobbins S, Zhang WK, Tong L, et al. Molecular mechanism of the assembly of an acid-sensing receptor ion channel complex. Nature communications. 2012; 3:1252. doi: 10.1038/ncomms2257 PMID: 23212381; PubMed Central PMCID: PMCPMC3575195.

30. Ishii S, Kurokawa A, Kishi M, Yamagami K, Okada S, Ishimaru Y, et al. The response of PKD1L3/PKD2L1 to acid stimuli is inhibited by capsaicin and its pungent analogs. FEBS J. 2012; 279(10):1857–70. doi: 10.1111/j.1742-4658.2012.08566.x PMID: 22420714; PubMed Central PMCID: PMCPMC3492849.

31. Horio N, Yoshida R, Yasumatsu K, Yanagawa Y, Ishimaru Y, Matsunami H, et al. Sour taste responses in mice lacking PKD channels. PLoS One. 2011; 6(5):e20007. doi: 10.1371/journal.pone.0020007 PMID: 21625513; PubMed Central PMCID: PMCPMC3098277.

32. Ermakov A, Stevens JL, Whitehill E, Robson JE, Pieles G, Brooker D, et al. Mouse mutagenesis identifies novel roles for left-right patterning genes in pulmonary, craniofacial, ocular, and limb development. Dev Dyn. 2009; 238(3):581–94. PMID: 19235720. doi: 10.1002/dvdy.21874

33. Vogel P, Read R, Hansen GM, Freay LC, Zambrowicz BP, Sands AT. Situs inversus in Dpcd/Poll-/-, Nme7-/-, and Pkd1l1-/- mice. Veterinary pathology. 2010; 47(1):120–31. PMID: 20080492. doi: 10.1177/0300985809353553

34. Takeda S, Yonekawa Y, Tanaka Y, Okada Y, Nonaka S, Hirokawa N. Left-right asymmetry and kinesin superfamily protein KIF3A: new insights in determination of laterality and mesoderm induction by kif3A-/- mice analysis. J Cell Biol. 1999; 145(4):825–36. PMID: 10330409.

35. Okada Y, Nonaka S, Tanaka Y, Saijoh Y, Hamada H, Hirokawa N. Abnormal nodal flow precedes situs inversus in iv and inv mice. Mol Cell. 1999; 4(4):459–68. PMID: 10549278.

36. Song H, Hu J, Chen W, Elliott G, Andre P, Gao B, et al. Planar cell polarity breaks bilateral symmetry by controlling ciliary positioning. Nature. 2010; 466(7304):378–82. PMID: 20562861. doi: 10.1038/nature09129

37. Hashimoto M, Shinohara K, Wang J, Ikeuchi S, Yoshiba S, Meno C, et al. Planar polarization of node cells determines the rotational axis of node cilia. Nature cell biology. 2010; 12(2):170–6. PMID: 20098415. doi: 10.1038/ncb2020

38. Collignon J, Varlet I, Robertson EJ. Relationship between asymmetric nodal expression and the direction of embryonic turning. Nature. 1996; 381(6578):155–8.

39. Lowe LA, Supp DM, Sampath K, Yokoyama T, Wright CV, Potter SS, et al. Conserved left-right asymmetry of nodal expression and alterations in murine situs inversus. Nature. 1996; 381(6578):158–61. PMID: 8610013.

40. Nakamura T, Saito D, Kawasumi A, Shinohara K, Asai Y, Takaoka K, et al. Fluid flow and interlinked feedback loops establish left-right asymmetric decay of Cerl2 mRNA. Nature communications. 2012; 3:1322. Epub 2012/12/29. doi: 10.1038/ncomms2319 PMID: 23271656.

41. Schweickert A, Vick P, Getwan M, Weber T, Schneider I, Eberhardt M, et al. The nodal inhibitor Coco is a critical target of leftward flow in Xenopus. Curr Biol. 2010; 20(8):738–43. PMID: 20381352. doi: 10.1016/j.cub.2010.02.061

42. Yoshiba S, Shiratori H, Kuo IY, Kawasumi A, Shinohara K, Nonaka S, et al. Cilia at the Node of Mouse Embryos Sense Fluid Flow for Left-Right Determination via Pkd2. Science (New York, NY. 2012. PMID: 22983710.

43. Marszalek JR, Ruiz-Lozano P, Roberts E, Chien KR, Goldstein LS. Situs inversus and embryonic ciliary morphogenesis defects in mouse mutants lacking the KIF3A subunit of kinesin-II. Proc Natl Acad Sci U S A. 1999; 96(9):5043–8. PMID: 10220415.

44. Bycroft M, Bateman A, Clarke J, Hamill SJ, Sandford R, Thomas RL, et al. The structure of a PKD domain from polycystin-1: implications for polycystic kidney disease. Embo J. 1999; 18(2):297–305. PMID: 9889186.

45. Hussain R, Javorfi T, Siligardi G. Circular dichroism beamline B23 at the Diamond Light Source. Journal of synchrotron radiation. 2012; 19(Pt 1):132–5. doi: 10.1107/S0909049511038982 PMID: 22186655.

46. Raussens V, Ruysschaert JM, Goormaghtigh E. Protein concentration is not an absolute prerequisite for the determination of secondary structure from circular dichroism spectra: a new scaling method. Analytical biochemistry. 2003; 319(1):114–21. PMID: 12842114.

47. Ma L, Xu M, Forman JR, Clarke J, Oberhauser AF. Naturally occurring mutations alter the stability of polycystin-1 polycystic kidney disease (PKD) domains. J Biol Chem. 2009; 284(47):32942–9. PMID: 19759016. doi: 10.1074/jbc.M109.021832

48. Nauli SM, Alenghat FJ, Luo Y, Williams E, Vassilev P, Li X, et al. Polycystins 1 and 2 mediate mechanosensation in the primary cilium of kidney cells. Nat Genet. 2003; 33(2):129–37. PMID: 12514735.

49. Nauli SM, Kawanabe Y, Kaminski JJ, Pearce WJ, Ingber DE, Zhou J. Endothelial cilia are fluid shear sensors that regulate calcium signaling and nitric oxide production through polycystin-1. Circulation. 2008; 117(9):1161–71. doi: 10.1161/CIRCULATIONAHA.107.710111 PMID: 18285569; PubMed Central PMCID: PMC3071982.

50. Nauli SM, Zhou J. Polycystins and mechanosensation in renal and nodal cilia. Bioessays. 2004; 26(8):844–56. Epub 2004/07/27. doi: 10.1002/bies.20069 PMID: 15273987.

51. Yoshiba S, Shiratori H, Kuo IY, Kawasumi A, Shinohara K, Nonaka S, et al. Cilia at the node of mouse embryos sense fluid flow for left-right determination via Pkd2. Science. 2012; 338(6104):226–31. Epub 2012/09/18. doi: 10.1126/science.1222538 PMID: 22983710.

52. DeCaen PG, Delling M, Vien TN, Clapham DE. Direct recording and molecular identification of the calcium channel of primary cilia. Nature. 2013; 504(7479):315–8. Epub 2013/12/18. doi: 10.1038/nature12832 PMID: 24336289.

53. Tsiairis CD, McMahon AP. An Hh-dependent pathway in lateral plate mesoderm enables the generation of left/right asymmetry. Curr Biol. 2009; 19(22):1912–7. PMID: 19879143. doi: 10.1016/j.cub.2009.09.057

54. Hirokawa N, Tanaka Y, Okada Y. Cilia, KIF3 molecular motor and nodal flow. Curr Opin Cell Biol. 2012. PMID: 22285930.

55. Yuan S, Zhao L, Brueckner M, Sun Z. Intraciliary calcium oscillations initiate vertebrate left-right asymmetry. Curr Biol. 2015; 25(5):556–67. Epub 2015/02/11. doi: 10.1016/j.cub.2014.12.051 PMID: 25660539.

56. Okada Y, Takeda S, Tanaka Y, Izpisua Belmonte JC, Hirokawa N. Mechanism of nodal flow: a conserved symmetry breaking event in left-right axis determination. Cell. 2005; 121(4):633–44. PMID: 15907475.

57. Inacio JM, Marques S, Nakamura T, Shinohara K, Meno C, Hamada H, et al. The dynamic right-to-left translocation of Cerl2 is involved in the regulation and termination of Nodal activity in the mouse node. PloS one. 2013; 8(3):e60406. doi: 10.1371/journal.pone.0060406 PMID: 23544137; PubMed Central PMCID: PMC3609817.

58. Harris PC, Torres VE. Polycystic kidney disease. Annual review of medicine. 2009; 60:321–37. PMID: 18947299. doi: 10.1146/annurev.med.60.101707.125712

59. Ishimaru Y, Inada H, Kubota M, Zhuang H, Tominaga M, Matsunami H. Transient receptor potential family members PKD1L3 and PKD2L1 form a candidate sour taste receptor. Proc Natl Acad Sci U S A. 2006; 103(33):12569–74. PMID: 16891422.

60. Forman JR, Yew ZT, Qamar S, Sandford RN, Paci E, Clarke J. Non-native interactions are critical for mechanical strength in PKD domains. Structure. 2009; 17(12):1582–90. PMID: 20004162. doi: 10.1016/j.str.2009.09.013

61. Forman JR, Qamar S, Paci E, Sandford RN, Clarke J. The remarkable mechanical strength of polycystin-1 supports a direct role in mechanotransduction. Journal of molecular biology. 2005; 349(4):861–71. PMID: 15894330.

62. Norris DP, Grimes DT. Mouse models of ciliopathies: the state of the art. Disease models & mechanisms. 2012; 5(3):299–312. Epub 2012/05/09. doi: 10.1242/dmm.009340 PMID: 22566558; PubMed Central PMCID: PMC3339824.

63. Delling M, DeCaen PG, Doerner JF, Febvay S, Clapham DE. Primary cilia are specialized calcium signalling organelles. Nature. 2013; 504(7479):311–4. Epub 2013/12/18. doi: 10.1038/nature12833 PMID: 24336288.

64. AbouAlaiwi WA, Takahashi M, Mell BR, Jones TJ, Ratnam S, Kolb RJ, et al. Ciliary polycystin-2 is a mechanosensitive calcium channel involved in nitric oxide signaling cascades. Circulation research. 2009; 104(7):860–9. doi: 10.1161/CIRCRESAHA.108.192765 PMID: 19265036; PubMed Central PMCID: PMC3085025.

Calcium channels in primary cilia

Surya M. Nauli, Rajasekharreddy Pala, and Steven J. Kleene

Purpose of review
Primary cilia have become important organelles implicated in embryonic development, organogenesis, health, and diseases. Although many studies in cell biology have focused on changes in ciliary length or ciliogenesis, the most common readout for evaluating ciliary function is intracellular calcium.

Recent findings
Recent tools have allowed us to examine intracellular calcium in more precise locations, that is, the cilioplasm and cytoplasm. Advances in calcium imaging have also allowed us to identify which cilia respond to particular stimuli. Furthermore, direct electrophysiological measurement of ionic currents within a cilium has provided a wealth of information for understanding the sensory roles of primary cilia.

Summary
Calcium imaging and direct measurement of calcium currents demonstrate that primary cilia are sensory organelles that house several types of functional calcium channels. Although intracellular calcium now allows a functional readout for primary cilia, discussions on the relative contributions of the several channel types have just begun. Perhaps, all of these calcium channels are required and necessary to differentiate stimuli in different microenvironments.

Keywords
cilium, imaging, patch clamping

INTRODUCTION

Cilia are sensory organelles that project from the apical membrane in many cell types. Based on their axonemal structure, cilia can be divided into '9+0' or '9+2' types. However, a general classification of cilia is more complex because of the discoveries of a '9+4' axonemal structure in Hensen's node of rabbit [1] and a '3+0' structure in a protozoan [2]. Primary cilia are usually considered to be nonmotile, solitary structures with a '9+0' axoneme, although some are in fact motile. They were first described in the 1800s [3]. In 1997, Schwartz *et al.* [4] showed that a nonmotile primary cilium could easily be deflected by fluid movement surrounding the cell. This is probably the first suggestion of a sensory role for primary cilia; it offered a physiological function for primary cilia in sensing fluid flow. Since then, nonmotile cilia have been proposed to have broad and complex sensory roles (Table 1).

PRIMARY CILIA AND INTRACELLULAR READOUT

The most commonly used readout of ciliary function is the concentration of intracellular calcium. In the 2000s, the laboratories of Spring and Zhou independently demonstrated that primary cilia play a crucial role in sensing mechanical fluid shear stress [30,31]. Both laboratories showed that bending primary cilia with a micropipette or with fluid flow activates the cilium and increases cytoplasmic calcium in renal epithelial cells. Since then, other laboratories have utilized intracellular calcium as a readout to understand the functions of primary cilia in vascular endothelial cells [32▪,33], renal epithelial cells [34–36], eye trabecular meshwork cells [37], nodal cells [19,21], hepatocytes [17,22], osteocytes [38], and chondrocytes [39].

A recent advance is the use of genetically encoded calcium-sensitive proteins targeted to the cilium. This technique allows differentiation of intracellular calcium signaling between cilioplasm and cytoplasm. Independent studies from the Nauli, Jacobs, Inoue, and Sun laboratories have detected

Department of Biomedical and Pharmaceutical Sciences, Chapman University, Irvine, California and Department of Molecular and Cellular Physiology, University of Cincinnati, Cincinnati, Ohio, USA

Correspondence to Surya M. Nauli, Harry and Diane Rinker Health Science Campus, Chapman University, 9401 Jeronimo Road, Irvine, CA 92618-1908, USA. Tel: +1 714 516 5480; fax: +1 714 516 5481; e-mail: nauli@chapman.edu; snauli@uci.edu

Curr Opin Nephrol Hypertens 2016, 25:452–458
DOI:10.1097/MNH.0000000000000251

KEY POINTS

- Different calcium channels in a cilium may have different cellular functions.
- Simultaneous measurement of single currents and concurrent imaging of cilioplasmic and cytoplasmic calcium are probably the best ways to resolve the controversies in fluid flow-induced intracellular calcium changes.
- Although the mechanisms of calcium signaling are controversial, there is a consensus that primary cilia are mechanosensory organelles.

calcium changes within primary cilia in response to fluid flow [40▪▪–43▪▪]. As discussed below, Clapham's group argues that these changes do not result from calcium crossing the ciliary membrane [44▪▪].

In vascular endothelial cells, a nitric oxide readout has also been used to understand primary ciliary function [45]. Protein modification, cleavage, and proteomic studies have also been used for this purpose [45,46]. Cell morphology may be another potential readout of ciliary function [47].

DIRECT MEASUREMENT OF IONIC CURRENTS IN THE PRIMARY CILIUM

The first direct electrophysiological evidence for the presence of single channel currents in a cilium was provided by Cantiello's group [48]. In 2005, they demonstrated a transmembrane cation-conducting channel of 156 pS in artificial bilayers that included cilia from renal epithelial cells. This channel was inhibited by an antibody against polycystin-2 [transient receptor potential cation channel, subfamily P, member 2 (TRPP2)], suggesting that TRPP2 contributed to the channels seen. When normalized to total protein, ciliary membrane was found to have 400 times more channel current, compared with plasma membrane.

In a subsequent study, Cantiello's group learned that vasopressin further increases cationic channel activity in cilia [48]. Due in part to electrophysiological evidence, it was proposed that primary cilia have a 3′,5′-cyclic adenosine monophosphate (cAMP)-dependent second-messenger signaling mechanism whose function includes the modulation of ciliary TRPP2 channel activity [49]. TRPP2 activity is thought to modulate calcium level in the cilioplasm. This regulatory pathway may also provide a molecular mechanism for microtubule regulation by calcium channel function, which in turn may help modulate ciliary length and function [50].

Direct electrophysiological measurement in a single cilium is challenging, due in part to the tiny size of the cilium (diameter ~200 nm). In addition, the cilium in a typical cell monolayer is oriented perpendicular to (above) the cell surface, which makes the cilium difficult to resolve. Kleene's laboratory circumvented this problem by growing adherent cells on small, spherical beads that could be easily moved within the recording chamber. With this technique, an entire cilium can be pulled into a recording microelectrode from the side of the bead, allowing sensitive, repeatable electrical recordings from the cilium [51]. This method has allowed identification of a ciliary transient receptor potential cation channel, subfamily M, member 4 (TRPM4), which can be activated by high cilioplasmic calcium [52]. This channel does not conduct calcium, and its physiological significance is not yet understood. However, the concentration of cilioplasmic calcium is expected to influence its

Table 1. Sensory roles of solitary nonmotile primary cilia

Function	Disease relevance	References
Chemosensor	Diabetes; obesity; and polycystic liver	[5–9]
Developmental regulator	Abnormal development and cancer	[10–12]
Gravitational sensor	Potential osteoporosis or chondroporosis	[13]
Light sensor	Retinitis pigmentosa and blindness	[14,15]
Mechanosensor	Polycystic kidney, liver, and pancreas	[16–18]
Nodal flow sensor	Situs inversus; situs ambiguus; and situs isomerism	[19–21]
Osmosensor	Unknown; detect changes in composition and tonicity of ductal bile	[22]
Shear stress sensor	Hypertension, aneurysm, and atherosclerosis	[23–26]
Smell sensor	Anosmia and hyposmia	[27,28]
Thermosensor	Abnormal thermal hyperalgesia	[29]

activity. In 2013, Clapham's laboratory also developed a means of directly recording from the ciliary membrane and discovered a ciliary polycystic kidney disease 1 like 1 (PKD1L1)/transient receptor potential cation channel, subfamily P, member 3 (TRPP3) channel, which is described below [53].

CILIARY CALCIUM CHANNELS

The primary cilium incorporates several types of calcium-conducting channel in its membrane. These channels may facilitate the cilium's role as a polymodal sensory antenna.

Transient receptor potential cation channel, subfamily C, member 1

It is generally thought that transient receptor potential cation channel, subfamily C, member 1 (TRPC1) mediates calcium entry into the cell in response to the depletion of endoplasmic calcium stores or activation of receptors coupled to the phospholipase C system [54]. Cantiello's laboratory demonstrated by immunocytochemistry that TRPC1 is present in the primary cilia of renal epithelia [48]. Interestingly, it has also been reported that TRPP2 can form a channel in combination with TRPC1 [55]. Heteromultimers of TRPP2 and TRPC1 were found to have a single-channel conductance, amiloride sensitivity, and ion permeability that are distinct from those of TRPP2 or TRPC1 alone. This channel assembly was found in the renal epithelial cilia and could be activated by a G protein-coupled receptor. It was further proposed that a TRPP2/TRPC1 complex plays a role in the mechanosensory function to initiate calcium signaling at the base of the cilium [55]. This view is consistent with the idea that TRPC1 itself is a stretch-activated calcium channel [56].

Transient receptor potential cation channel, subfamily P, member 2

Several laboratories have independently shown that TRPP2 [also known as polycystin-2, PC2, or polycystic kidney disease 2 (PKD2)] contributes to responses to fluid flow in cholangiocytes [17], embryonic node [19,21,43▪▪], left–right organizer of zebrafish [43▪▪], osteocytes [57], renal epithelia [29,30,58,59], smooth muscle cells [60], and vascular endothelia [24].

Fluid shear force causes bending of primary cilia and activates a polycystin-1/TRPP2 complex [30]. TRPP2 conducts calcium and is linked to polycystin-1, which exhibits a remarkable mechanical strength, supporting a role in mechanotransduction [61]. The calcium signal through this mechanical fluid activation is then amplified by calcium release from stores modulated by the ryanodine receptor. The mechanosensitivity of the polycystin-1/TRPP2 complex has been confirmed directly; the ratio of polycystin-1/TRPP2 plays an important role in the cell mechanics of mechanosensation [62]. This model supports the idea that normal expression levels of polycystin-1 and TRPP2 are important to suppress the cystic kidney phenotype [63–65].

Among calcium channels, TRPP2 probably has the earliest functional role during embryogenesis in establishing the left–right asymmetry of the visceral organs [19–21]. TRPP2 regulates embryonic nodal gene expression at the left side of the embryonic endodermal node. TRPP2 functions in mechanosensation by increasing internal calcium in response to the leftward nodal flow. Norris' laboratory further showed that polycystin-1L1 (PKD1L1) is the interacting flow sensor and is required to regulate the TRPP2 channel within the embryonic endodermal node [20].

Transient receptor potential cation channel, subfamily P, member 3

TRPP3, also called polycystin-L [polycystic kidney disease 2-like (PKDL)] or polycystin-2L1 [polycystic kidney disease 2-like 1 ((PKD2L1)], is localized to primary cilia [53,66] and the centrosome [67]. TRPP3 is a calcium channel with a high homology with TRPP2 [68]. TRPP3 is regulated by calcium, exhibiting both calcium-dependent activation and calcium-dependent inactivation [69]. This indicates that TRPP3 may act as a transducer of calcium-mediated signaling.

While directly recording from the primary cilia of several cell types, Clapham's laboratory found a large, outwardly rectifying, current [53]. Because knocking down either PKD1L1 or TRPP3 abolished this current, it is likely caused by a PKD1L1/TRPP3 complex. The current is cation-nonselective, with similar permeabilities for calcium and barium ions [53], and is inactivated by high internal ciliary calcium [inhibitory concentration at 50% inhibition (IC_{50}) = 445 nmol/l] [70]. Coexpression of PKD1L1 and TRPP3 yielded calcium-permeable channels of 103 pS. It is further proposed that the PKD1L1/TRPP3 heteromeric channel establishes the cilium as a unique calcium compartment within cells that modulates Hedgehog signaling pathways [53].

A very recent study by Zhou's group indicates that TRPP3 in the neuronal primary cilium regulates neuronal excitability and susceptibility to pentylenetetrazol-induced seizure in mice [66]. The group

showed that TRPP3 interacts with the β2 adrenergic receptor and that the receptor–channel complex regulates cAMP response element-binding protein. This functional interaction plays a crucial role in chronic seizure disorder and epilepsy.

Transient receptor potential cation channel, subfamily V, member 4

The primary cilium forms a calcium microdomain that is influenced by calcium entry through transient receptor potential cation channel, subfamily V, member 4 (TRPV4) [40▪▪]. It was shown that TRPV4 mediates flow-induced ciliary calcium increases. Thus, it is proposed that TRPV4 has a role in mechanotransduction in the primary cilium. Although TRPV4 is involved in the flow-induced calcium transient, interestingly, the association of TRPC1 with TRPV4 prolongs the flow-induced calcium influx [71]. It has also been shown that TRPV4 interacts with TRPP2 to form a channel complex. The TRPP2/TRPV4 complex has distinct biophysical, pharmacological, and regulatory profiles compared with either TRPP2 or TRPV4 channels [72]. Furthermore, TRPV4 interacts with oculocerebrorenal syndrome of Lowe (OCRL), an inositol polyphosphate 5-phosphatase. This interaction is required for primary cilia to sense changes in pressure and subsequently regulates calcium influx in response to pressure stimulation [37].

Aside from mechanosensing, the TRPP2/TRPV4 complex forms a thermosensitive molecular sensor in primary cilia [29]. Consistent with this view, it has been shown that prolonged cold preservation of an organ could cause irreversible pathological changes in the primary cilia [73]. LaRusso's group has also shown that the ciliary TRPV4 can sense changes in osmolality [22]. It is proposed that localization of TRPV4 in primary cilia is required to sense tonicity in the microenvironment.

Other calcium channels in the primary cilia

Nauli's laboratory has recently shown that the L-type calcium channel modulates cystic kidney phenotype, hydrocephalus, and left–right asymmetry defects [74,75]. L-type calcium channel knockdown in zebrafish facilitates the formation of these ciliopathic phenotypes. The L-type calcium channel is present in renal epithelial cilia, as judged by immunocytochemistry [41▪▪]. Although it is unclear if this channel has any role in the mechanosensation mediated by primary cilia, it does play an important role in an agonist-induced calcium response measured in the cilia [41▪▪]. This further reiterates the importance of calcium signaling in the chemosensory roles of primary cilia. The primary cilium also regulates L-type calcium channel expression through wingless-related integration site (Wnt) signaling [75]. Suppressed Wnt signaling prevents calcium channel, voltage-dependent 1.2 expression, ultimately resulting in the phenotypes of polycystic kidney disease.

Surprisingly, proteomic screening of mammalian primary cilia has not shown strong evidence of other calcium channels [76,77]. The screening shows mainly signaling proteins. However, recent functional screening indicates that the following calcium channels may regulate ciliogenesis: inositol 1,4,5-trisphosphate receptor, type 3 (Itpr3), calcium voltage-gated channel, subunit alpha 1 (Cacna1d), calcium channel, voltage-dependent, subunit beta 2 (Cacnb2), and cation channel, sperm associated 4 (Catsper4) [78]. Unfortunately, it is unclear if any of these channels are localized to primary cilia.

ACTIVATION OF CILIARY CALCIUM CHANNELS

A critical remaining issue is to identify stimuli that cause the various ciliary calcium channels to open. Studies intended to relate these channels to ciliary mechanosensitivity have revealed the difficulty of the problem. In cells derived from renal epithelium, it is clear that deflection of the cilium leads to an increase in calcium in the cell body [30,31]. This response requires the cilium, external calcium, and two calcium-conducting channels (TRPP2 and TRPV4) [29,30,79]. These channels are found on the cilium (although not exclusively), so it has seemed plausible that ciliary deflection might open ciliary calcium channels. Calcium in the cilium might then initiate the cytoplasmic response (although probably not by simple diffusion [70]). To test whether flow increases ciliary calcium in renal epithelial cells, Su *et al.* [42▪▪] targeted a calcium-sensitive fluorescent protein to the cilium and deflected the cilium with fluid flow. This caused a slow increase in ciliary calcium. Whether cytoplasmic calcium also changed was not determined. The researchers took care to test for a possible artifact: changes of fluorescence because of movement of the cilium relative to the focal plane during flow. With a calcium-insensitive fluorophore, there was no significant change in fluorescence during flow, suggesting that the calcium increase initially observed was not because of a motion artifact. Cilia in this study were viewed from above (end on).

Using a similar targeted sensor in renal epithelial cells, but viewing the cilia from the side, Jin *et al.* [41▪▪] also reported flow-induced increases in ciliary calcium and, under some but not all conditions, also

measured an increase in cytoplasmic calcium. The ciliary response almost always peaked before the cytoplasmic response. Using a fluorescence resonance energy transfer-based calcium sensor, Lee *et al.* [40▪▪] also reported flow-induced calcium increases in osteocyte primary cilia and in the cytoplasm. On an individual cell basis, about 60% of calcium peaks occurred in the primary cilium prior to the cytoplasm of the same cell. However, the authors could not conclude whether the ciliary response preceded the cytoplasmic response.

To further understand the role of ciliary calcium in an in-vivo model, Yuan *et al.* [43▪▪] studied ciliary calcium in live zebrafish embryos, and, in particular in the left–right organizer. This organizer (analogous to the embryonic node in mouse) initiates left–right asymmetry during embryonic development. A calcium-sensitive fluorophore was targeted to the cilia, and a calcium-insensitive ciliary fluorophore allowed correction for motion artifacts. Ciliary calcium oscillations were observed, particularly along the left side of the organizer. The oscillations were substantially reduced when ciliary motility was impaired, suggesting that the oscillations may be a consequence of ciliary motility. The oscillations were reduced when TRPP2 expression was decreased. In some cells, the increase in ciliary calcium preceded a cytoplasmic calcium wave. In those cells, accumulation of ciliary calcium may be required for generation of a robust cytoplasmic calcium signal. In a recent study by Delling *et al.* [44▪▪], however, deflection of cilia in cells from murine embryonic node caused no detectable elevation of intraciliary calcium, and there was no difference in cytoplasmic calcium oscillation between left-side and right-side embryonic node.

Delling *et al.* [44▪▪] recently concluded that flow-induced changes in the fluorescence of ciliary calcium sensors are often artifactual. In contrast to Su *et al.* [42▪▪], Delling *et al.* [44▪▪] did observe a small motion artifact, which was shown to be significant when the cilia were viewed from above. After correcting for this ciliary motion, no ciliary Ca^{2+} responses to flow were detected in a variety of primary cilia or in the kinocilia of the inner ear. When no ciliary calcium response is observed, one must consider whether the calcium indicator is sensitive across the range of cilioplasmic calcium concentrations expected. Resting ciliary calcium can be as high as 742 nmol/l [70]. In the study that found no ciliary calcium responses, the sensitivity of the indicator to calcium was carefully measured [44▪▪]. Given that reported sensitivity, the fluorescent signal would already reach ~90% at 742 nmol/l, and any additional increase in ciliary calcium would cause only a slight increase in fluorescence. However, increasing cilioplasmic calcium by membrane permeabilization in the presence of external calcium (>1 mM) showed directly that the calcium sensor was responsive in the cell [44▪▪].

Delling *et al.* also note that even a true increase in ciliary calcium should not be taken to imply the opening of ciliary channels. Instead, it was shown that calcium can first be generated in the cytoplasm and then simply diffuse into the cilium [44▪▪]. The rates of flow used to increase ciliary calcium create a shear stress on the plasma membrane of 0.3–1.0 dyn/cm^2 [41▪▪,42▪▪]. Such a shear stress can increase cytoplasmic calcium [35,36,40▪▪,58,59]. Although most organelles are separated from the cytoplasm by enclosing membranes, there is direct passage between cilioplasm and cytoplasm at the ciliary base (necklace). Thus, some increases in ciliary calcium may occur via diffusion of calcium from the cell body [44▪▪]. This cannot account for a situation where ciliary calcium increases but cytoplasmic calcium does not [41▪▪]. In some circumstances, there is no increase in cytosolic calcium unless the cilium is present [79].

CONCLUSION

Advances in microscopic technique have allowed us to differentiate cytoplasmic and ciliary calcium signaling. The ability to patch-clamp one cilium has permitted us to study single calcium currents from an excised or intact primary cilium. Although current studies have provided important information on primary cilia, it may be unsettling to know the complexity of the cilium. Perhaps the question becomes why the cell needs so many different calcium channels in this tiny organelle? It is still a matter of some judgment whether deflection of a primary cilium causes calcium to enter across the ciliary membrane. At this point, our questions greatly outnumber our answers.

Acknowledgements

None.

Financial support and sponsorship

Work from the Nauli laboratory that is cited in this chapter has been supported by grants from the DoD (PR130153) and Chapman University. S.J.K. received support from National Institutes of Health (NIH) grant R21 DK091917 and the University Research Council of the University of Cincinnati.

Conflicts of interest

There are no conflicts of interest.

REFERENCES AND RECOMMENDED READING

Papers of particular interest, published within the annual period of review, have been highlighted as:

- ■ of special interest
- ■■ of outstanding interest

1. Feistel K, Blum M. Three types of cilia including a novel 9+4 axoneme on the notochordal plate of the rabbit embryo. Dev Dyn 2006; 235:3348–3358.
2. Prensier G, Vivier E, Goldstein S, Schrevel J. Motile flagellum with a "3 + 0" ultrastructure. Science 1980; 207:1493–1494.
3. Bloodgood RA. From central to rudimentary to primary: the history of an underappreciated organelle whose time has come. The primary cilium. Methods Cell Biol 2009; 94:3–52.
4. Schwartz EA, Leonard ML, Bizios R, Bowser SS. Analysis and modeling of the primary cilium bending response to fluid shear. Am J Physiol 1997; 272:F132–F138.
5. Kathem SH, Mohieldin AM, Abdul-Majeed S, *et al.* Ciliotherapy: a novel intervention in polycystic kidney disease. J Geriatr Cardiol 2014; 11:63–73.
6. Abdul-Majeed S, Nauli SM. Dopamine receptor type 5 in the primary cilia has dual chemo- and mechano-sensory roles. Hypertension 2011; 58:325–331.
7. Masyuk AI, Gradilone SA, Banales JM, *et al.* Cholangiocyte primary cilia are chemosensory organelles that detect biliary nucleotides via P2Y12 purinergic receptors. Am J Physiol Gastrointest Liver Physiol 2008; 295:G725–G734.
8. Davenport JR, Watts AJ, Roper VC, *et al.* Disruption of intraflagellar transport in adult mice leads to obesity and slow-onset cystic kidney disease. Curr Biol 2007; 17:1586–1594.
9. Winkelbauer ME, Schafer JC, Haycraft CJ, *et al.* The C. elegans homologs of nephrocystin-1 and nephrocystin-4 are cilia transition zone proteins involved in chemosensory perception. J Cell Sci 2005; 118:5575–5587.
10. Wong SY, Seol AD, So PL, *et al.* Primary cilia can both mediate and suppress Hedgehog pathway-dependent tumorigenesis. Nat Med 2009; 15:1055–1061.
11. Han YG, Kim HJ, Dlugosz AA, *et al.* Dual and opposing roles of primary cilia in medulloblastoma development. Nat Med 2009; 15:1062–1065.
12. Christensen ST, Pedersen SF, Satir P, *et al.* The primary cilium coordinates signaling pathways in cell cycle control and migration during development and tissue repair. Curr Top Dev Biol 2008; 85:261–301.
13. Moorman SJ, Shorr AZ. The primary cilium as a gravitational force transducer and a regulator of transcriptional noise. Dev Dyn 2008; 237:1955–1959.
14. Moore A, Escudier E, Roger G, *et al.* RPGR is mutated in patients with a complex X linked phenotype combining primary ciliary dyskinesia and retinitis pigmentosa. J Med Genet 2006; 43:326–333.
15. Nishimura DY, Fath M, Mullins RF, *et al.* Bbs2-null mice have neurosensory deficits, a defect in social dominance, and retinopathy associated with mislocalization of rhodopsin. Proc Natl Acad Sci U S A 2004; 101:16588–16593.
16. Cano DA, Sekine S, Hebrok M. Primary cilia deletion in pancreatic epithelial cells results in cyst formation and pancreatitis. Gastroenterology 2006; 131:1856–1869.
17. Masyuk AI, Masyuk TV, Splinter PL, *et al.* Cholangiocyte cilia detect changes in luminal fluid flow and transmit them into intracellular Ca2+ and cAMP signaling. Gastroenterology 2006; 131:911–920.
18. Nauli SM, Rossetti S, Kolb RJ, *et al.* Loss of polycystin-1 in human cyst-lining epithelia leads to ciliary dysfunction. J Am Soc Nephrol 2006; 17:1015–1025.
19. Yoshiba S, Shiratori H, Kuo IY, *et al.* Cilia at the node of mouse embryos sense fluid flow for left-right determination via Pkd2. Science 2012; 338:226–231.
20. Field S, Riley KL, Grimes DT, *et al.* Pkd1l1 establishes left-right asymmetry and physically interacts with Pkd2. Development 2011; 138:1131–1142.
21. McGrath J, Somlo S, Makova S, *et al.* Two populations of node monocilia initiate left-right asymmetry in the mouse. Cell 2003; 114:61–73.
22. Gradilone SA, Masyuk AI, Splinter PL, *et al.* Cholangiocyte cilia express TRPV4 and detect changes in luminal tonicity inducing bicarbonate secretion. Proc Natl Acad Sci U S A 2007; 104:19138–19143.
23. Aboualaiwi WA, Muntean BS, Ratnam S, *et al.* Survivin-induced abnormal ploidy contributes to cystic kidney and aneurysm formation. Circulation 2014; 129:660–672.
24. AbouAlaiwi WA, Takahashi M, Mell BR, *et al.* Ciliary polycystin-2 is a mechanosensitive calcium channel involved in nitric oxide signaling cascades. Circ Res 2009; 104:860–869.
25. Nauli SM, Kawanabe Y, Kaminski JJ, *et al.* Endothelial cilia are fluid shear sensors that regulate calcium signaling and nitric oxide production through polycystin-1. Circulation 2008; 117:1161–1171.
26. Van der Heiden K, Hierck BP, Krams R, *et al.* Endothelial primary cilia in areas of disturbed flow are at the base of atherosclerosis. Atherosclerosis 2008; 196:542–550.
27. Layman WS, McEwen DP, Beyer LA, *et al.* Defects in neural stem cell proliferation and olfaction in Chd7 deficient mice indicate a mechanism for hyposmia in human CHARGE syndrome. Hum Mol Genet 2009; 18:1909–1923.
28. Kulaga HM, Leitch CC, Eichers ER, *et al.* Loss of BBS proteins causes anosmia in humans and defects in olfactory cilia structure and function in the mouse. Nat Genet 2004; 36:994–998.
29. Kottgen M, Buchholz B, Garcia-Gonzalez MA, *et al.* TRPP2 and TRPV4 form a polymodal sensory channel complex. J Cell Biol 2008; 182:437–447.
30. Nauli SM, Alenghat FJ, Luo Y, *et al.* Polycystins 1 and 2 mediate mechanosensation in the primary cilium of kidney cells. Nat Genet 2003; 33:129–137.
31. Praetorius HA, Spring KR. Bending the MDCK cell primary cilium increases intracellular calcium. J Membr Biol 2001; 184:71–79.
32. ■ Atkinson KF, Kathem SH, Jin X, *et al.* Dopaminergic signaling within the primary cilia in the renovascular system. Front Physiol 2015; 6:103.

This is an extension study showing changes in cilioplasmic calcium in response to dopaminergic agonist.

33. Upadhyay VS, Muntean BS, Kathem SH, *et al.* Roles of dopamine receptor on chemosensory and mechanosensory primary cilia in renal epithelial cells. Front Physiol 2014; 5:72.
34. Rydholm S, Zwartz G, Kowalewski JM, *et al.* Mechanical properties of primary cilia regulate the response to fluid flow. Am J Physiol Renal Physiol 2010; 298:F1096–F1102.
35. Xu C, Shmukler BE, Nishimura K, *et al.* Attenuated, flow-induced ATP release contributes to absence of flow-sensitive, purinergic Cai2+ signaling in human ADPKD cyst epithelial cells. Am J Physiol Renal Physiol 2009; 296:F1464–F1476.
36. Rohatgi R, Battini L, Kim P, *et al.* Mechanoregulation of intracellular Ca2+ in human autosomal recessive polycystic kidney disease cyst-lining renal epithelial cells. Am J Physiol Renal Physiol 2008; 294:F890–F899.
37. Luo N, Conwell MD, Chen X, *et al.* Primary cilia signaling mediates intraocular pressure sensation. Proc Natl Acad Sci U S A 2014; 111:12871–12876.
38. Malone AM, Anderson CT, Tummala P, *et al.* Primary cilia mediate mechanosensing in bone cells by a calcium-independent mechanism. Proc Natl Acad Sci U S A 2007; 104:13325–13330.
39. Wann AK, Zuo N, Haycraft CJ, *et al.* Primary cilia mediate mechanotransduction through control of ATP-induced Ca2+ signaling in compressed chondrocytes. FASEB J 2012; 26:1663–1671.
40. ■■ Lee KL, Guevarra MD, Nguyen AM, *et al.* The primary cilium functions as a mechanical and calcium signaling nexus. Cilia 2015; 4:7.

This study demonstrates that fluid flow-induced calcium increase in primary cilia of osteocyte requires TRPV4. In many cells, fluid flow induces an increase in ciliary calcium followed by cytosolic calcium increase.

41. ■■ Jin X, Mohieldin AM, Muntean BS, *et al.* Cilioplasm is a cellular compartment for calcium signaling in response to mechanical and chemical stimuli. Cell Mol Life Sci 2014; 71:2165–2178.

This study demonstrates that fluid flow-induced calcium increase in renal primary cilia requires polycystin-2.

42. ■■ Su S, Phua SC, DeRose R, *et al.* Genetically encoded calcium indicator illuminates calcium dynamics in primary cilia. Nat Methods 2013; 10:1105–1107.

This study shows that fluid-flow evokes calcium signals in cilioplasm.

43. ■■ Yuan S, Zhao L, Brueckner M, Sun Z. Intraciliary calcium oscillations initiate vertebrate left-right asymmetry. Curr Biol 2015; 25:556–567.

Without any artificial fluid flow, calcium oscillation is detected in the primary cilia of the embryonic nodes, and polycystin-2 is required for this cilioplasmic calcium oscillation.

44. ■■ Delling M, Indzhykulian AA, Liu X, *et al.* Primary cilia are not calcium-responsive mechanosensors. Nature 2016; 531:656–660.

With artificial fluid flow, no calcium changes are observed in the primary cilia of nodal, ear, bone, or kidney cells.

45. Nauli SM, Jin X, AbouAlaiwi WA, *et al.* Non-motile primary cilia as fluid shear stress mechanosensors. Methods Enzymol 2013; 525:1–20.
46. Low SH, Vasanth S, Larson CH, *et al.* Polycystin-1, STAT6, and P100 function in a pathway that transduces ciliary mechanosensation and is activated in polycystic kidney disease. Dev Cell 2006; 10:57–69.
47. Boehlke C, Kotsis F, Patel V, *et al.* Primary cilia regulate mTORC1 activity and cell size through Lkb1. Nat Cell Biol 2010; 12:1115–1122.
48. Raychowdhury MK, McLaughlin M, Ramos AJ, *et al.* Characterization of single channel currents from primary cilia of renal epithelial cells. J Biol Chem 2005; 280:34718–34722.
49. Raychowdhury MK, Ramos AJ, Zhang P, *et al.* Vasopressin receptor-mediated functional signaling pathway in primary cilia of renal epithelial cells. Am J Physiol Renal Physiol 2009; 296:F87–F97.
50. Abdul-Majeed S, Moloney BC, Nauli SM. Mechanisms regulating cilia growth and cilia function in endothelial cells. Cell Mol Life Sci 2012; 69:165–173.
51. Kleene NK, Kleene SJ. A method for measuring electrical signals in a primary cilium. Cilia 2012; 1:17.
52. Flannery RJ, Kleene NK, Kleene SJ. A TRPM4-dependent current in murine renal primary cilia. Am J Physiol Renal Physiol 2015; 309:F697–F707.
53. DeCaen PG, Delling M, Vien TN, Clapham DE. Direct recording and molecular identification of the calcium channel of primary cilia. Nature 2013; 504:315–318.
54. Huang GN, Zeng W, Kim JY, *et al.* STIM1 carboxyl-terminus activates native SOC, I(crac) and TRPC1 channels. Nat Cell Biol 2006; 8:1003–1010.

55. Bai CX, Giamarchi A, Rodat-Despoix L, *et al.* Formation of a new receptor-operated channel by heteromeric assembly of TRPP2 and TRPC1 subunits. EMBO Rep 2008; 9:472–479.

56. Maroto R, Raso A, Wood TG, *et al.* TRPC1 forms the stretch-activated cation channel in vertebrate cells. Nat Cell Biol 2005; 7:179–185.

57. Xu H, Guan Y, Wu J, *et al.* Polycystin 2 is involved in the nitric oxide production in responding to oscillating fluid shear in MLO-Y4 cells. J Biomech 2014; 47:387–391.

58. Du J, Wong WY, Sun L, *et al.* Protein kinase G inhibits flow-induced Ca2+ entry into collecting duct cells. J Am Soc Nephrol 2012; 23:1172–1180.

59. Wang S, Zhang J, Nauli SM, *et al.* Fibrocystin/polyductin, found in the same protein complex with polycystin-2, regulates calcium responses in kidney epithelia. Mol Cell Biol 2007; 27:3241–3252.

60. Narayanan D, Bulley S, Leo MD, *et al.* Smooth muscle cell transient receptor potential polycystin-2 (TRPP2) channels contribute to the myogenic response in cerebral arteries. J Physiol 2013; 591:5031–5046.

61. Forman JR, Qamar S, Paci E, *et al.* The remarkable mechanical strength of polycystin-1 supports a direct role in mechanotransduction. J Mol Biol 2005; 349:861–871.

62. Sharif-Naeini R, Folgering JH, Bichet D, *et al.* Polycystin-1 and -2 dosage regulates pressure sensing. Cell 2009; 139:587–596.

63. Gainullin VG, Hopp K, Ward CJ, *et al.* Polycystin-1 maturation requires polycystin-2 in a dose-dependent manner. J Clin Invest 2015; 125:607–620.

64. Pritchard L, Sloane-Stanley JA, Sharpe JA, *et al.* A human PKD1 transgene generates functional polycystin-1 in mice and is associated with a cystic phenotype. Hum Mol Genet 2000; 9:2617–2627.

65. Ma M, Tian X, Igarashi P, *et al.* Loss of cilia suppresses cyst growth in genetic models of autosomal dominant polycystic kidney disease. Nat Genet 2013; 45:1004–1012.

66. Yao G, Luo C, Harvey M, *et al.* Disruption of polycystin-L causes hippocampal and thalamocortical hyperexcitability. Hum Mol Genet 2016; 25:448–458.

67. Bui-Xuan EF, Li Q, Chen XZ, *et al.* More than colocalizing with polycystin-1, polycystin-L is in the centrosome. Am J Physiol Renal Physiol 2006; 291:F395–F406.

68. Nomura H, Turco AE, Pei Y, *et al.* Identification of PKDL, a novel polycystic kidney disease 2-like gene whose murine homologue is deleted in mice with kidney and retinal defects. J Biol Chem 1998; 273:25967–25973.

69. Chen XZ, Vassilev PM, Basora N, *et al.* Polycystin-L is a calcium-regulated cation channel permeable to calcium ions. Nature 1999; 401:383–386.

70. Delling M, DeCaen PG, Doerner JF, *et al.* Primary cilia are specialized calcium signalling organelles. Nature 2013; 504:311–314.

71. Ma X, Qiu S, Luo J, *et al.* Functional role of vanilloid transient receptor potential 4-canonical transient receptor potential 1 complex in flow-induced Ca2+ influx. Arterioscler Thromb Vasc Biol 2010; 30:851–858.

72. Zhang ZR, Chu WF, Song B, *et al.* TRPP2 and TRPV4 form an EGF-activated calcium permeable channel at the apical membrane of renal collecting duct cells. PLoS One 2013; 8:e73424.

73. Lu H, Dong J, Zhang Y, *et al.* Pathological changes in primary cilia: a novel mechanism of graft cholangiopathy caused by prolonged cold preservation in a rat model of orthotopic liver transplantation. Biosci Trends 2014; 8:206–211.

74. Jin X, Muntean BS, Aal-Aaboda MS, *et al.* L-type calcium channel modulates cystic kidney phenotype. Biochim Biophys Acta 2014; 1842:1518–1526.

75. Muntean BS, Jin X, Williams FE, Nauli SM. Primary cilium regulates CaV1.2 expression through Wnt signaling. J Cell Physiol 2014; 229:1926–1934.

76. Mick DU, Rodrigues RB, Leib RD, *et al.* Proteomics of primary cilia by proximity labeling. Dev Cell 2015; 35:497–512.

77. Ishikawa H, Thompson J, Yates JR 3rd, Marshall WF. Proteomic analysis of mammalian primary cilia. Curr Biol 2012; 22:414–419.

78. Slaats GG, Wheway G, Foletto V, *et al.* Screen-based identification and validation of four new ion channels as regulators of renal ciliogenesis. J Cell Sci 2015; 128:4550–4559.

79. Praetorius HA, Spring KR. Removal of the MDCK cell primary cilium abolishes flow sensing. J Membr Biol 2003; 191:69–76.